

2015

Development of New Linking Chemistry with the fac- $\{\text{Re}(\text{CO})_3\}^+$ Core for Eventual Applications in Radiopharmaceuticals in Imaging and Therapy

Aponsu Meregnna Pramuditha Lakmi Abhayawardhana

Louisiana State University and Agricultural and Mechanical College, prammj@gmail.com

Follow this and additional works at: https://digitalcommons.lsu.edu/gradschool_dissertations



Part of the [Chemistry Commons](#)

Recommended Citation

Abhayawardhana, Aponsu Meregnna Pramuditha Lakmi, "Development of New Linking Chemistry with the fac- $\{\text{Re}(\text{CO})_3\}^+$ Core for Eventual Applications in Radiopharmaceuticals in Imaging and Therapy" (2015). *LSU Doctoral Dissertations*. 1150.
https://digitalcommons.lsu.edu/gradschool_dissertations/1150

This Dissertation is brought to you for free and open access by the Graduate School at LSU Digital Commons. It has been accepted for inclusion in LSU Doctoral Dissertations by an authorized graduate school editor of LSU Digital Commons. For more information, please contact gradetd@lsu.edu.

DEVELOPMENT OF NEW LINKING CHEMISTRY WITH THE *fac*- $\{\text{Re}^{\text{I}}(\text{CO})_3\}^+$ CORE FOR
EVENTUAL APPLICATIONS IN RADIOPHARMACEUTICALS IN IMAGING AND
THERAPY

A Dissertation

Submitted to the Graduate Faculty of the
Louisiana State University and
Agricultural and Mechanical College
in partial fulfillment of the
requirements for the degree of
Doctor of Philosophy

in

The Department of Chemistry

by
Aponsu Meregnna Pramuditha Lakmi Abhayawardhana
B.Sc. University of Colombo, Sri Lanka, 2006
December 2015

Dedicated with love to my family

ACKNOWLEDGMENT

I would like to extend my deepest gratitude to my advisor, Dr. Luigi G. Marzilli for his outstanding supervision, excellent mentorship, and support throughout my graduate career. His unique perspective on research and his sharp insight on almost any issue have immensely helped me to expand my subject knowledge, independent thinking as well as writing skills. I am deeply appreciative of the effort he has taken to help me both academically and emotionally through the rough road to finish this dissertation. I am particularly indebted to Dr. Patricia Marzilli not only for her careful reading of my drafts and endless help with the work in this dissertation, but also for her invaluable advice, warm-hearted support, and for being there to care for me and my family throughout the past six years.

I further extend sincere thanks to my committee members, Dr. Carol Taylor, Dr. Graca Vicente, and Dr. Andrew Maverick for their continuous support and constructive advice whenever needed and for always helping me to stay strong and positive. I am honored and grateful to have such wonderful professors on my committee. I thank Dr. Richard Oberlin and Dr. Guan Jia for serving on my committee and for being very helpful. I also thank Dr. William Crowe and Dr. Evgueni Nesterov for offering their expertise through valuable discussions. I am grateful to Dr. Doug Gilman for the encouragement and help given to me in various ways since the beginning of this journey.

I greatly appreciate the friendship, and support of my labmates Chase Andrepont, Kokila Ranasinghe, and Arielle Nabatilan. Also, my warmest thanks go to Nerissa Lewis for being there to listen, cheer me up, and always reaching out to help. I am also deeply thankful to my former labmate, Dr. Theshini Perera who is like my sister, for warmly welcoming me to Marzilli lab, for all the good times we shared and for being behind my success from start to end. A special word of thanks should go to Dr. Nalin de Silva, Dr. Rohini de Silva, Dr. S. Hewage, and Mr. W.

Pathirana for being sources of inspiration and encouraging me to continue with my graduate studies.

I thank late Dr. Dale Treleaven, Dr. Thomas Weldeghiorghis, and Dr. Frank Fronczek, not only for their expertise with NMR spectroscopy and X-ray structure determination, but also for the willingness to help me at all times, their friendship and the words of encouragement. I sincerely acknowledge Dr. Svetlana Pakhomova for the various crystal structure determinations. I am grateful to Ms. Kim Mollere for helping me with all the paper work and for her kind support to me and my family.

I thank all my friends, relatives, and teachers for the support and well wishes. To my sister, I express my warmest thanks for always being there for me and for taking such great care of my parents when I'm not there to do so. I am indebted to my parents, Rani and Sunil Abhayawardhana who are the pillars of my life. They have worked hard day and night to support my education and bring me this far. I am thankful for the unconditional love and everything they have done for me. I also thank my husband's parents who are always supporting me and encouraging me with their best wishes. I could not have managed to complete my dissertation without the love and blessings from all four of these amazing parents.

I thank our baby, Senaya (who did forty weeks of research with me) for being a source of unending joy and bringing a smile to our lives no matter how rough things have been. My husband and I have realized what a miracle life is since the day she came into our lives. Lastly, my husband, Manjula, with his endless love, unending encouragement, patience and support has been the bedrock upon which the past few years of my life has been built. No words could ever express my appreciation for the sacrifices he has made for me and to make this dream possible. It has been such a blessing to share my life with him and our baby.

TABLE OF CONTENTS

DEDICATION	ii
ACKNOWLEDGMENTS	iii
LIST OF TABLES	vii
LIST OF FIGURES.....	ix
LIST OF ABBREVIATIONS.....	xiii
ABSTRACT.....	xv
CHAPTER 1. INTRODUCTION	1
1.1. The Role of Technetium and Rhenium in Imaging and Therapy.....	1
1.2. Conjugation of the <i>fac</i> -[M ^I (CO) ₃] ⁺ (M = ^{99m} Tc, Re) Core with Biomolecules	3
1.3. References.....	6
CHAPTER 2. A New Series of Complexes Possessing Rare “Tertiary” Sulfonamide Nitrogen-to-Metal Bonds of Normal Length: <i>fac</i> -[Re(CO) ₃ (N(SO ₂ R)DIEN)]PF ₆ Complexes with Hydrophilic Sulfonamide Ligands.	9
2.1. Introduction.....	9
2.2. Experimental Section.....	11
2.3. Results and Discussion	18
2.4. Conclusions.....	36
2.5. References.....	37
CHAPTER 3. New Monodentate Amidine Superbasic Ligands with a Single Configuration in <i>fac</i> -[Re(CO) ₃ (5,5'- or 6,6'-Me ₂ bipyridine)(amidine)] BF ₄ Complexes	41
3.1. Introduction.....	41
3.2. Experimental Section.....	44
3.3. Results and Discussion	53
3.4. Conclusions.....	73
3.5. References.....	74
CHAPTER 4. X-RAY STRUCTURAL, AND NMR SPECTRAL FEATURES OF <i>fac</i> -[Re(CO) ₃ (L)(HNC(CH ₃)N(CH ₂) _x)]BF ₄ AMIDINE COMPLEXES (L = 5,5'-Me ₂ BIPY OR 6,6'-Me ₂ BIPY AND x = 3 OR 4) AND EVALUATION OF A NEW EFFICIENT METHOD FOR SYNTHESIZING <i>fac</i> -[Re(CO) ₃ (L)(AMIDINE)]BF ₄ COMPLEXES.....	77
4.1. Introduction.....	77
4.2. Experimental Section.....	84
4.3. Results and Discussion	95
4.4. Conclusions.....	126
4.5. References.....	127
CHAPTER 5. CONCLUSIONS	129

APPENDIX A. SUPPLEMENTARY MATERIAL FOR CHAPTER 2	131
APPENDIX B. SUPPLEMENTARY MATERIAL FOR CHAPTER 3.....	142
APPENDIX C. SUPPLEMENTARY MATERIAL FOR CHAPTER 4.....	145
APPENDIX D. PERMISSION	156
VITA	158

LIST OF TABLES

Table 2.1. Crystal Data and Structure Refinement for $[\text{Re}(\text{CO})_3(\text{N}(\text{SO}_2\text{Me})\text{dien})]\text{PF}_6$ (4) and $[\text{Re}(\text{CO})_3(\text{N}(\text{SO}_2\text{tol})\text{dien})]\text{PF}_6$ (6).....	20
Table 2.2. Selected Bond Distances (Å) and Angles (deg) for $[\text{Re}(\text{CO})_3(\text{N}(\text{SO}_2\text{Me})\text{dien})]\text{PF}_6$ (4) and $[\text{Re}(\text{CO})_3(\text{N}(\text{SO}_2\text{tol})\text{dien})]\text{PF}_6$ (6).....	21
Table 2.3. ^1H NMR Shifts (ppm) of <i>exo</i> - and <i>endo</i> -NH and <i>exo</i> - and <i>endo</i> -CH Signals for $[\text{Re}(\text{CO})_3(\text{N}(\text{SO}_2\text{R})\text{dien})]\text{PF}_6$ Complexes in Various Solvents at 25 °C.....	29
Table 3.1. Crystal Data and Structural Refinement for Complexes Having the General Formula, $[\text{Re}(\text{CO})_3(5,5'\text{-Me}_2\text{bipy})(\text{HNC}(\text{CH}_3)\text{N}(\text{CH}_2\text{CH}_2)_2\text{Y})]\text{BF}_4$	46
Table 3.2. Crystal Data and Structural Refinement for Complexes Having the General Formula, $[\text{Re}(\text{CO})_3(6,6'\text{-Me}_2\text{bipy})(\text{HNC}(\text{CH}_3)\text{N}(\text{CH}_2\text{CH}_2)_2\text{Y})]\text{BF}_4$	47
Table 3.3. Selected Bond Distances (Å) and Angles (deg) for Complexes Having the General Formula, $[\text{Re}(\text{CO})_3(5,5'\text{-Me}_2\text{bipy})(\text{HNC}(\text{CH}_3)\text{N}(\text{CH}_2\text{CH}_2)_2\text{Y})]\text{BF}_4$	59
Table 3.4. Selected Bond Distances (Å) and Angles (deg) for Complexes Having the General Formula, $[\text{Re}(\text{CO})_3(6,6'\text{-Me}_2\text{bipy})(\text{HNC}(\text{CH}_3)\text{N}(\text{CH}_2\text{CH}_2)_2\text{Y})]\text{BF}_4$	60
Table 3.5. ^1H NMR Shifts (ppm) for L, N ₃ H, and C _{am} CH ₃ in $[\text{Re}(\text{CO})_3(\text{L})(\text{HNC}(\text{CH}_3)\text{N}(\text{CH}_2\text{CH}_2)_2\text{Y})]\text{BF}_4$ Complexes (Acetonitrile- <i>d</i> ₃ , 25 °C).....	68
Table 3.6. Times for Complete Reaction of $[\text{Re}(\text{CO})_3(\text{L})(\text{CH}_3\text{CN})]\text{BF}_4$ Complexes with Heterocyclic Amines (HN(CH ₂ CH ₂) ₂ Y) to Form $[\text{Re}(\text{CO})_3(\text{L})(\text{HNC}(\text{CH}_3)\text{N}(\text{CH}_2\text{CH}_2)_2\text{Y})]\text{BF}_4$ Complexes ^a	70
Table 4.1. ^1H NMR Shifts (ppm) for $[\text{Re}(\text{CO})_3(\text{L})(\text{HNC}(\text{CH}_3)\text{N}(\text{CH}_2)_x)]\text{BF}_4$ Complexes (CDCl ₃ , 27 °C).....	86
Table 4.2. ^1H NMR Shifts (ppm) for $[\text{Re}(\text{CO})_3(\text{L})(\text{HNC}(\text{C}_6\text{H}_5)\text{N}(\text{CH}_2)_x)]\text{BF}_4$ Complexes in CDCl ₃ at 27 °C.....	87
Table 4.3. ^{13}C NMR Shifts (ppm) for $[\text{Re}(\text{CO})_3(\text{L})(\text{HNC}(\text{CH}_3)\text{N}(\text{CH}_2)_x)]\text{BF}_4$ Complexes in CDCl ₃ at 27 °C.....	88
Table 4.4. ^{13}C NMR Shifts (ppm) for $[\text{Re}(\text{CO})_3(\text{Me}_2\text{bipy})(\text{HNC}(\text{C}_6\text{H}_5)\text{N}(\text{CH}_2)_x)]\text{BF}_4$ Complexes in CDCl ₃ at 27 °C.....	89
Table 4.5. Times (min) for Complete Reaction of $[\text{Re}(\text{CO})_3(5,5'\text{-Me}_2\text{bipy})(\text{RCN})]\text{BF}_4$ Complexes with Amines to Form $[\text{Re}(\text{CO})_3(5,5'\text{-Me}_2\text{bipy})(\text{amidine})]\text{BF}_4$ Complexes.....	96

Table 4.6. Crystal Data and Structural Refinement for $[\text{Re}(\text{CO})_3(5,5'\text{-Me}_2\text{bipy})(\text{HNC}(\text{CH}_3)\text{N}(\text{CH}_2)_3)]\text{BF}_4$ (1), $[\text{Re}(\text{CO})_3(6,6'\text{-Me}_2\text{bipy})(\text{HNC}(\text{CH}_3)\text{N}(\text{CH}_2)_3)]\text{BF}_4$ (2), $[\text{Re}(\text{CO})_3(5,5'\text{-Me}_2\text{bipy})(\text{HNC}(\text{CH}_3)\text{N}(\text{CH}_2)_4)]\text{BF}_4$ (3), and $[\text{Re}(\text{CO})_3(6,6'\text{-Me}_2\text{bipy})(\text{HNC}(\text{CH}_3)\text{N}(\text{CH}_2)_4)]\text{BF}_4$ (4).....98

Table 4.7. Crystal Data and Structural Refinement for $[\text{Re}(\text{CO})_3(5,5'\text{-Me}_2\text{bipy})(\text{HNC}(\text{C}_6\text{H}_5)\text{N}(\text{CH}_2)_3)]\text{BF}_4$ (5), $[\text{Re}(\text{CO})_3(6,6'\text{-Me}_2\text{bipy})(\text{HNC}(\text{C}_6\text{H}_5)\text{N}(\text{CH}_2)_3)]\text{BF}_4$ (6), $[\text{Re}(\text{CO})_3(5,5'\text{-Me}_2\text{bipy})(\text{HNC}(\text{C}_6\text{H}_5)\text{N}(\text{CH}_2)_4)]\text{BF}_4$ (7), $[\text{Re}(\text{CO})_3(6,6'\text{-Me}_2\text{bipy})(\text{HNC}(\text{C}_6\text{H}_5)\text{N}(\text{CH}_2)_4)]\text{BF}_4$ (8), $[\text{Re}(\text{CO})_3(5,5'\text{-Me}_2\text{bipy})(\text{HNC}(\text{C}_6\text{H}_5)\text{N}(\text{CH}_2)_5)]\text{BF}_4$ (9), and $[\text{Re}(\text{CO})_3(6,6'\text{-Me}_2\text{bipy})(\text{HNC}(\text{C}_6\text{H}_5)\text{N}(\text{CH}_2)_5)]\text{BF}_4$ (10).....99

Table 4.8. Selected Bond Distances (Å) and Angles (deg) for $[\text{Re}(\text{CO})_3(5,5'\text{-Me}_2\text{bipy})(\text{HNC}(\text{CH}_3)\text{N}(\text{CH}_2)_3)]\text{BF}_4$ (1), $[\text{Re}(\text{CO})_3(6,6'\text{-Me}_2\text{bipy})(\text{HNC}(\text{CH}_3)\text{N}(\text{CH}_2)_3)]\text{BF}_4$ (2), $[\text{Re}(\text{CO})_3(5,5'\text{-Me}_2\text{bipy})(\text{HNC}(\text{CH}_3)\text{N}(\text{CH}_2)_4)]\text{BF}_4$ (3), and $[\text{Re}(\text{CO})_3(6,6'\text{-Me}_2\text{bipy})(\text{HNC}(\text{CH}_3)\text{N}(\text{CH}_2)_4)]\text{BF}_4$ (4).....104

Table 4.9. Selected Bond Distances (Å) and Angles (deg) for $[\text{Re}(\text{CO})_3(5,5'\text{-Me}_2\text{bipy})(\text{HNC}(\text{C}_6\text{H}_5)\text{N}(\text{CH}_2)_3)]\text{BF}_4$ (5), $[\text{Re}(\text{CO})_3(6,6'\text{-Me}_2\text{bipy})(\text{HNC}(\text{C}_6\text{H}_5)\text{N}(\text{CH}_2)_3)]\text{BF}_4$ (6), $[\text{Re}(\text{CO})_3(5,5'\text{-Me}_2\text{bipy})(\text{HNC}(\text{C}_6\text{H}_5)\text{N}(\text{CH}_2)_4)]\text{BF}_4$ (7), $[\text{Re}(\text{CO})_3(6,6'\text{-Me}_2\text{bipy})(\text{HNC}(\text{C}_6\text{H}_5)\text{N}(\text{CH}_2)_4)]\text{BF}_4$ (8), $[\text{Re}(\text{CO})_3(5,5'\text{-Me}_2\text{bipy})(\text{HNC}(\text{C}_6\text{H}_5)\text{N}(\text{CH}_2)_5)]\text{BF}_4$ (9), and $[\text{Re}(\text{CO})_3(6,6'\text{-Me}_2\text{bipy})(\text{HNC}(\text{C}_6\text{H}_5)\text{N}(\text{CH}_2)_5)]\text{BF}_4$ (10).....105

LIST OF FIGURES

Figure 1.1. Representation of the <i>fac</i> -[M(CO) ₃] ⁺ core with three ligands depicted by L.....	3
Figure 1.2. Schematic representation of the bifunctional chelate strategy	4
Figure 2.1. General reaction scheme for the synthesis of <i>N</i> (SO ₂ R)dien ligands (<i>top</i>) and [Re(CO) ₃ (<i>N</i> (SO ₂ R)dien)] ⁺ complexes (<i>bottom</i>).....	18
Figure 2.2. ORTEP plots of the cations in [Re(CO) ₃ (<i>N</i> (SO ₂ Me)dien)]PF ₆ (4) (<i>left</i>) and Re(CO) ₃ (<i>N</i> (SO ₂ tol)dien)]PF ₆ (6) (<i>right</i>). Thermal ellipsoids are drawn with 50% probability	19
Figure 2.3. Overlay of Re, C1, C2, and C3 atoms of [Re(CO) ₃ (<i>N</i> (SO ₂ tol)dien)]PF ₆ (6) (<i>blue</i>) and [Re(CO) ₃ (<i>N</i> (SO ₂ tol)dpa)]PF ₆ ³⁵ (<i>magenta</i>) complexes. (The SO ₂ R groups have been omitted for clarity).....	23
Figure 2.4. ¹ H NMR spectra of [Re(CO) ₃ (<i>N</i> (SO ₂ R)dien)]PF ₆ complexes (4–6) in acetone- <i>d</i> ₆ at 25 °C.....	26
Figure 2.5. ¹ H NMR spectra of [Re(CO) ₃ (<i>N</i> (SO ₂ tol)dien)]PF ₆ (6), illustrating the relative position of NH signals observed at 25 °C in a) acetonitrile- <i>d</i> ₃ , b) acetone- <i>d</i> ₆ , and c) DMSO- <i>d</i> ₆	30
Figure 2.6. ¹ H- ¹ H ROESY spectrum of [Re(CO) ₃ (<i>N</i> (SO ₂ tol)dien)]PF ₆ (6) in acetone- <i>d</i> ₆ at 25 °C. An expanded version of this figure is in Supporting Information (Figure S6.. ..	31
Figure 3.1. The four conceivable [Re(CO) ₃ (5,5'-Me ₂ bipy)HNC(CH ₃)NHR)] ⁺ isomers, in which N–N denotes the 5,5'-Me ₂ bipy ligand. The isomers with the <i>E'</i> and <i>Z</i> configurations are typically abundant. The isomer with the <i>Z'</i> configuration is unstable and not observed. ²⁵ The isomer with the <i>E</i> configuration is known, but its abundance is usually too low to allow detection. However, as illustrated here, the pathway between the <i>E'</i> and <i>Z</i> configurations undoubtedly passes through the <i>E</i> configuration and not the <i>Z'</i> configuration	43
Figure 3.2. Reactions forming [Re(CO) ₃ (L)(HNC(CH ₃)N(CH ₂ CH ₂) ₂ Y)] ⁺ complexes observed upon treatment of [Re(CO) ₃ (L)(CH ₃ CN)] ⁺ complexes with heterocyclic amines (HN(CH ₂ CH ₂) ₂ Y) in acetonitrile at 25 °C.	54
Figure 3.3. ORTEP plots of the cations in [Re(CO) ₃ (5,5'-Me ₂ bipy)(HNC(CH ₃)N(CH ₂ CH ₂) ₂ CH ₂)]BF ₄ (3), [Re(CO) ₃ (5,5'-Me ₂ bipy)(HNC(CH ₃)N(CH ₂ CH ₂) ₂ (CH ₂) ₂)]BF ₄ (4), [Re(CO) ₃ (5,5'-Me ₂ bipy)(HNC(CH ₃)N(CH ₂ CH ₂) ₂ (CH ₂) ₃)]BF ₄ (5), [Re(CO) ₃ (5,5'-Me ₂ bipy)(HNC(CH ₃)N(CH ₂ CH ₂) ₂ NH)]BF ₄ (6), and [Re(CO) ₃ (5,5'-Me ₂ bipy)(HNC(CH ₃)N(CH ₂ CH ₂) ₂ O)]BF ₄ (7). Thermal ellipsoids are drawn with 50% probability.....	55

Figure 3.4. ORTEP plots of the cations in $[\text{Re}(\text{CO})_3(6,6'\text{-Me}_2\text{bipy})(\text{HNC}(\text{CH}_3)\text{N}(\text{CH}_2\text{CH}_2)_2\text{CH}_2)]\text{BF}_4$ (8), $[\text{Re}(\text{CO})_3(6,6'\text{-Me}_2\text{bipy})(\text{HNC}(\text{CH}_3)\text{N}(\text{CH}_2\text{CH}_2)_2(\text{CH}_2)_2)]\text{BF}_4$ (9), $[\text{Re}(\text{CO})_3(6,6'\text{-Me}_2\text{bipy})(\text{HNC}(\text{CH}_3)\text{N}(\text{CH}_2\text{CH}_2)_2(\text{CH}_2)_3)]\text{BF}_4$ (10), $[\text{Re}(\text{CO})_3(6,6'\text{-Me}_2\text{bipy})(\text{HNC}(\text{CH}_3)\text{N}(\text{CH}_2\text{CH}_2)_2\text{NH})]\text{BF}_4$ (11), and $[\text{Re}(\text{CO})_3(6,6'\text{-Me}_2\text{bipy})(\text{HNC}(\text{CH}_3)\text{N}(\text{CH}_2\text{CH}_2)_2\text{O})]\text{BF}_4$ (12). Thermal ellipsoids are drawn with 50% probability. For 10, both conformations of the disordered 8-membered ring are shown, and H atoms are not illustrated, except for N-H.....56

Figure 3.5. Views of piperidinylamidine complexes, $[\text{Re}(\text{CO})_3(\text{L})(\text{HNC}(\text{CH}_3)\text{N}(\text{CH}_2\text{CH}_2)_2\text{CH}_2)]\text{BF}_4$, depicted with the C13–Re–C14 equatorial plane perpendicular to the plane of the paper. Shown at *left* and *middle* are front and side views, respectively, of complex 8 with L = 6,6'-Me₂bipy. Pictured at *right* is a side view of complex 3 with L = 5,5'-Me₂bipy.....64

Figure 3.6. Ranking of increasingly unfavorable total steric repulsive interactions (each double-headed arrow indicates an interaction) in $[\text{Re}(\text{CO})_3(\text{Me}_2\text{bipy})(\text{HNC}(\text{CH}_3)\text{OCH}_3)]^+$, $[\text{Re}(\text{CO})_3(\text{L})\text{HNC}(\text{CH}_3)\text{NHR}]^+$, and $[\text{Re}(\text{CO})_3(\text{L})(\text{HNC}(\text{CH}_3)\text{N}(\text{CH}_2\text{CH}_2)_2\text{Y})]^+$ complexes [N–N denotes the 5,5'- or 6,6'-Me₂bipy ligands, and Y = CH₂, (CH₂)₂, (CH₂)₃, NH, or O].65

Figure 3.7. Aromatic region of the ¹H NMR spectra in acetonitrile at 25 °C of the reaction of $[\text{Re}(\text{CO})_3(5,5'\text{-Me}_2\text{bipy})(\text{CH}_3\text{CN})]\text{BF}_4$ (1) with morpholine to form $[\text{Re}(\text{CO})_3(5,5'\text{-Me}_2\text{bipy})(\text{HNC}(\text{CH}_3)\text{N}(\text{CH}_2\text{CH}_2)_2\text{O})]\text{BF}_4$ (7).....71

Figure 4.1. Four conceivable isomers of *fac*- $[\text{Re}(\text{CO})_3(5,5'\text{-Me}_2\text{bipy})(\text{HNC}(\text{CH}_3)\text{NHR})]^+$ N–N denotes a C₂-symmetrical bidentate N-donor ligand. Note that the *Z'* isomer was not detected. ..79

Figure 4.2. Synthetic scheme for *fac*- $[\text{Re}(\text{CO})_3(\text{Me}_2\text{bipy})(\text{HNC}(\text{CH}_3)\text{N}(\text{CH}_2)_2\text{Y})]\text{BF}_4$ complexes,¹⁹ showing numbering system for discussion of NMR data (N–N denotes the Me₂bipy ligand).80

Figure 4.3. Conceivable isomers of *fac*- $[\text{Re}(\text{CO})_3(\text{Me}_2\text{bipy})(\text{HNC}(\text{R})\text{N}(\text{CH}_2)_2\text{Y})]\text{BF}_4$ complexes; R = CH₃ or C₆H₅. N–N = 5,5'-Me₂bipy or 6,6'-Me₂bipy ligand; double-headed arrows indicate steric interactions between groups, and arrow thickness reflects predicted qualitative severity of the steric repulsions.....81

Figure 4.4. Comparisons of Methods A and B used to synthesize *fac*- $[\text{Re}(\text{CO})_3(5,5'\text{-Me}_2\text{bipy})(\text{HNC}(\text{CH}_3)\text{N}(\text{CH}_2)_3)]\text{BF}_4$, illustrated for azetidine.82

Figure 4.5. Synthesis of *fac*- $[\text{Re}(\text{CO})_3(\text{Me}_2\text{bipy})(\text{HNC}(\text{C}_5\text{H}_6)\text{N}(\text{CH}_2)_2\text{Y})]\text{BF}_4$ complexes, showing the numbering system for discussing the phenyl ring NMR signals. N–N denotes the Me₂bipy ligand.....83

Figure 4.6. Stack plot of ¹H NMR spectra (CDCl₃, 27 °C) obtained to monitor steps 1 and 2 of Method B. Spectra chosen for the figure to illustrate the NMR data for Method B are from reaction of piperidine to form $[\text{Re}(\text{CO})_3(5,5'\text{-Me}_2\text{bipy})(\text{HNC}(\text{CH}_3)\text{N}(\text{CH}_2)_5)]\text{BF}_4^2$ because slow

enough to obtain intermediate spectra for step 2. Also, the salt is NaBF₄ because crystals could be obtained. Signals of starting 5,5'-Me₂bipy are labeled with •. Signals for [Re(CO)₃(5,5'-Me₂bipy)(CH₃CN)]BF₄ are labeled with * in the 10-min step 1 and step 2 traces and with assignments in the step 1 30-min trace. Signals for the final [Re(CO)₃(5,5'-Me₂bipy)(HNC(CH₃)N(CH₂)₅)]BF₄ product are labeled with □ in the step 2 10-min trace and with assignments in the step 2 30-min trace.93

Figure 4.7. ORTEP plots of the cations of [Re(CO)₃(5,5'-Me₂bipy)(HNC(CH₃)N(CH₂)₃)]BF₄ (1), [Re(CO)₃(6,6'-Me₂bipy)(HNC(CH₃)N(CH₂)₃)]BF₄ (2), [Re(CO)₃(5,5'-Me₂bipy)(HNC(CH₃)N(CH₂)₄)]BF₄ (3), and [Re(CO)₃(6,6'-Me₂bipy)(HNC(CH₃)N(CH₂)₄)]BF₄ (4). Thermal ellipsoids are drawn with 50% probability.101

Figure 4.8. ORTEP plots of the cations of [Re(CO)₃(5,5'-Me₂bipy)(HNC(C₆H₅)N(CH₂)₃)]BF₄ (5), [Re(CO)₃(5,5'-Me₂bipy)(HNC(C₆H₅)N(CH₂)₄)]BF₄ (7), and [Re(CO)₃(5,5'-Me₂bipy)(HNC(C₆H₅)N(CH₂)₅)]BF₄ (9). Thermal ellipsoids are drawn with 50% probability..102

Figure 4.9. ORTEP plots of the cations of [Re(CO)₃(6,6'-Me₂bipy)(HNC(C₆H₅)N(CH₂)₃)]BF₄ (6), [Re(CO)₃(6,6'-Me₂bipy)(HNC(C₆H₅)N(CH₂)₄)]BF₄ (8), and [Re(CO)₃(6,6'-Me₂bipy)(HNC(C₆H₅)N(CH₂)₅)]BF₄ (10). Thermal ellipsoids are drawn with 50% probability.103

Figure 4.10. View from top of [Re(CO)₃(5,5'-Me₂bipy)(HNC(CH₃)N(CH₂)₅)]BF₄ (*left*) and [Re(CO)₃(5,5'-Me₂bipy)(HNC(C₆H₅)N(CH₂)₅)]BF₄ (*right*) complexes with the mean plane of the 5,5'-Me₂bipy rings oriented parallel to the plane of the paper. The heterocyclic CH₂ groups were deleted for clarity107

Figure 4.11. Designation of the N-CH₂ *endo* and N-CH₂ *exo* groups, illustrated for the structure of *fac*-[Re(CO)₃(5,5'-Me₂bipy)(HNC(CH₃)N(CH₂)₄)]BF₄ (3).....109

Figure 4.12. Stack plot of a selected region of the ¹H NMR spectra (CD₃CN, 27 °C) of [Re(CO)₃(5,5'-Me₂bipy)(HNC(CH₃)N(CH₂)_x)]BF₄ complexes.....110

Figure 4.13. Stack plot of a selected region of the ¹H NMR spectra (CDCl₃, 27 °C) of [Re(CO)₃(5,5'-Me₂bipy)(HNC(C₆H₅)N(CH₂)_x)]BF₄ complexes. Diethyl ether signals are marked with an asterisk111

Figure 4.14. Selected region of the ROESY spectrum (CDCl₃, 27 °C) of Re(CO)₃(5,5'-Me₂bipy)(HNC(CH₃)N(CH₂)₃)]BF₄ (1).113

Figure 4.15. Selected region of the ROESY spectrum (CDCl₃, 27 °C) of Re(CO)₃(5,5'-Me₂bipy)(HNC(CH₃)N(CH₂)₄)]BF₄ (3).113

Figure 4.16. ROESY spectrum (CDCl₃, 27 °C) of [Re(CO)₃(5,5'-Me₂bipy)(HNC(C₆H₅)N(CH₂)₄)]BF₄ (7). Diethyl ether signals are marked with an asterisk.114

Figure 4.17. ^1H NMR stack plot of $[\text{Re}(\text{CO})_3(5,5'\text{-Me}_2\text{bipy})(\text{HNC}(\text{CH}_3)\text{N}(\text{CH}_2)_3)]\text{BF}_4$ (*bottom*) and $[\text{Re}(\text{CO})_3(5,5'\text{-Me}_2\text{bipy})(\text{HNC}(\text{C}_6\text{H}_5)\text{N}(\text{CH}_2)_3)]\text{BF}_4$ (*top*) in CDCl_3 at $27\text{ }^\circ\text{C}$116

Figure 4.18. ^1H NMR stack plot of $[\text{Re}(\text{CO})_3(5,5'\text{-Me}_2\text{bipy})(\text{HNC}(\text{CH}_3)\text{N}(\text{CH}_2)_5)]\text{BF}_4$ in CDCl_3 at $-13\text{ }^\circ\text{C}$ (*blue*) and $27\text{ }^\circ\text{C}$ (*red*). Diethyl ether signals are marked with an asterisk.....125

LIST OF ABBREVIATIONS

<u>Abbreviation</u>	<u>Definition</u>
^{99m}Tc	metastable nuclear isomer of technetium-99
NMR	nuclear magnetic resonance
ROESY	rotating-frame overhauser effect spectroscopy
NOESY	nuclear overhauser effect spectroscopy
COSY	correlation spectroscopy
EXSY	exchange spectroscopy
HSQC	heteronuclear single quantum correlation
HMBC	heteronuclear multiple-bond correlation
ESI	electrospray ionization
MALDI	matrix-assisted laser desorption ionization
TOF	time of flight
min	minutes
h	hours
Hz	hertz
MHz	megahertz
ppm	parts per million
mM	milimolar
μM	micromolar
μL	microliter
mmol	milimoles
J	coupling constant
d	doublet

s	singlet
m	multiplet
b or br	broad signal
equiv	equivalent
TMS	trimethylsilane
DMSO	dimethyl sulfoxide
OTf	trifluoromethanesulfonate anion
1D	one-dimensional
2D	two-dimensional
M	metal
L	ligand

ABSTRACT

The facile labeling of biomolecules with a radionuclide is a key goal in radiopharmaceutical development. This study explores two different ligand systems for *fac*-[Re(CO)₃L]⁺ complexes, that could be used in bioconjugation.

The first approach uses a tridentate ligand having a sulfonamide linkage and modeled on previously evaluated *fac*-[Re(CO)₃(N(SO₂R)dpa)]PF₆ complexes. The present goal was to develop new related sulfonamide complexes with more hydrophilic ligands designed to avoid the bioavailability problems that would plague the N(SO₂R)dpa ligand system. A series of *fac*-[Re(CO)₃(N(SO₂R)dien)]PF₆ complexes with different R groups linked to the central nitrogen of a symmetric tridentate sulfonamides were synthesized with the aim of improving the favorable *in vivo* bioavailability. These compounds are characterized by NMR spectroscopy and by X-ray crystallography.

The second approach using monodentate ligands led to the synthesis of several amidine complexes. The challenge of avoiding isomers of amidine complexes was overcome by using C₂-symmetrical heterocyclic secondary amines with 6-membered and larger rings to create an amidine substituent bulkier than the amidine CCH₃ group. Treatment of *fac*-[Re(CO)₃(Me₂bipy)(CH₃CN)] BF₄ with these amines in organic solvents yielded novel *fac*-[Re(CO)₃(Me₂bipy)(HNC(CH₃)N(CH₂)₂Y)]BF₄ complexes having only one isomer with the *E* configuration as established by solid-state and ¹H NMR spectroscopic data. The combination of the high steric bulk and the C₂-symmetry of the amidine substituents favors the *E* configuration exclusively.

I extended the chemistry to smaller heterocyclic amines with 4- and 5-membered rings and found amidine formation reactions were faster. Moreover, I also showed that the amidine formation reactions were faster when the methyl group of *fac*-[Re(CO)₃(Me₂bipy)(CH₃CN)]BF₄

was replaced by a phenyl group. A series of *fac*-[Re(CO)₃(Me₂bipy)(HNC(C₆H₅)N(CH₂)_x)]⁺ complexes were synthesized, characterized and used in the comparison with the analogous *fac*-[Re(CO)₃(Me₂bipy)(HNC(CH₃)N(CH₂)_x)]⁺ complexes in order to understand the properties of amidine complexes and to correlate the structural features with their behavior in solution. Furthermore, a new method employing the *fac*-[Re(CO)₃(H₂O)₃]⁺ precursor successfully demonstrated the synthesis of *fac*-[Re(CO)₃(Me₂bipy)(amidine)]⁺ complexes in more aqueous conditions. This new method holds promise for use in biomedical studies.

CHAPTER 1

INTRODUCTION

The non-invasive nature and the ability to function as a technique for dynamic imaging make nuclear medicine a powerful diagnostic and therapeutic tool. Procedures in nuclear medicine provide the ability to view metabolic activity and physiological function, thus playing an important role in obtaining useful information about the function of certain organs and tissues.¹ Radiopharmaceuticals are pharmaceutical preparations of radioisotopes which are safe for human administration for the purpose of diagnosing or treating diseases. The widespread utilization of radiopharmaceuticals and the challenges in diagnostic and therapeutic procedures create a growing demand for the development of specific radiopharmaceuticals. Thus, much research is employed in order to identify better agents with the ability to specifically target different locations in the body to produce images with better resolution as well as to treat specific cells, organs, or tissues.²⁻⁴

1.1 The Role of Technetium and Rhenium in Imaging and Therapy

Technetium-99m (^{99m}Tc) is the most widely used radioisotope in diagnostic nuclear medicine, with over 80% of the nuclear medicine studies performed every year utilizing it.³⁻⁸ The availability of the short-lived ^{99m}Tc ($t_{1/2} = 6 \text{ h}$) is one of the major factors that has promoted the universal use of ^{99m}Tc . The parent nucleus, molybdenum-99 (^{99}Mo) decays to ^{99m}Tc through beta decay with a half-life of 66 h. Moreover, ^{99m}Tc emits 140 keV gamma rays with sufficiently high energy to be useful for clinical imaging and sufficiently low energy to prevent a high radiation risk to the patient. ^{99m}Tc also has an ideal half-life that is long enough for pharmaceutical preparation, accumulation in the target tissues, and clinical investigations, yet short enough to reduce excessive radiation exposure to the patient.^{2,3,7} Early studies in the development of various ^{99m}Tc complexes takes advantage of physiological processes in the body (e.g., absorption,

distribution, metabolism, and excretion) for imaging different organs. However, over the years research has led to the discovery of careful design of novel ^{99m}Tc complexes with the ability to efficiently and accurately diagnose many diseases at earlier stages and follow up with the response to treatment.^{4,7}

Radionuclide therapy employing radiopharmaceuticals labeled with beta-emitting radionuclides is emerging as an important part of nuclear medicine. $^{186/188}\text{Re}$ isotopes are being used as beta emitters in therapeutic applications.⁷ Both ^{186}Re ($E = 1.1 \text{ MeV}$, $t_{1/2} = 89.2 \text{ h}$) and ^{188}Re ($E = 2.1 \text{ MeV}$, $t_{1/2} = 16.9 \text{ h}$) possess favorable nuclear properties that make them capable of delivering therapeutic doses of radiation to cancerous tissue.⁷ Furthermore, complexes containing the $^{186/188}\text{Re}$ isotopes have been developed to target specific tissues without causing adverse effects on normal tissue.^{9,10} Radionuclide therapy, in addition to the management of thyroid cancer, is utilized for bone pain palliation and for the treatment of joint pain, as in rheumatoid arthritis. Some other recent research areas include treatment of non-resectable liver cancer, non-melanoma skin cancer, and inhibition of arterial restenosis following balloon angioplasty.^{11,12}

Rhenium and technetium, which are members of the same group of the periodic table, share similar chemical properties. Non-radioactive Re is frequently used as a model for studying the initial properties and behavior of clinically useful agents with radioactive ^{99m}Tc . A ligand suitable for technetium chelation is usually also suitable for rhenium chelation. This possibility of radiolabeling molecules of medicinal interest with diagnostic or therapeutic radionuclides by the same chemical approach has recently received considerable interest. The diverse chemistry of technetium and rhenium has led the way to the discovery of many complexes with different coordination numbers and geometries. This study is mainly aimed at exploiting the chemistry of new complexes with the versatile tricarbonyl core : *fac*- $[\text{M}(\text{CO})_3]^+$ ($\text{M} = ^{99m}\text{Tc}^I, ^{186/188}\text{Re}^I$).

1.2 Conjugation of the fac - $[M^I(CO)_3]^+$ ($M = {}^{99m}\text{Tc}$, Re) Core with Biomolecules

Among several other ${}^{99m}\text{Tc}$ or Re -incorporated cores used in current studies and applications, the fac - $[M(CO)_3]^+$ core possesses promise for developing useful clinical agents owing to its many attractive properties. This core contains three facile CO ligands which are tightly coordinated to the metal center, thus stabilizing the low +1 oxidation state (Figure 1.1). Complexes of the fac - $[M(CO)_3]^+$ core have a low-spin d^6 configuration, hence, exhibit a high in vivo robustness, an essential for medical applications.¹³

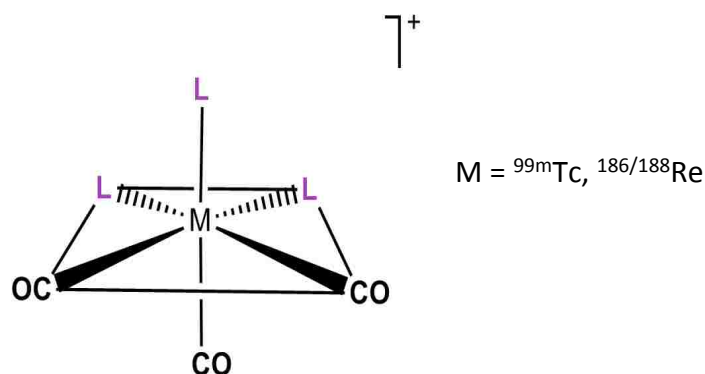


Figure 1.1. Representation of the fac - $[M(CO)_3]^+$ core with three ligands depicted by L

Octahedral complexes of $[M(CO)_3]^+$ are generally smaller than complexes of the corresponding metals in higher oxidation states with other cores and are therefore considered less likely to impact important characteristics of molecules to which they are conjugated.^{4,7,13} The low molecular weight of the fac - $[M^I(CO)_3]^+$ core therefore permits the labeling of low molecular weight biomolecules while retaining their high specificity.⁶ The precursor complex, fac - $[M^I(CO)_3(\text{H}_2\text{O})]^+$, is soluble in aqueous media and is readily accessible in aqueous-based kit formulations.⁶ The three water molecules in this precursor can be readily replaced by mono-, bi-, and tridentate ligand systems, or a combination of them. Numerous ligand systems and their coordination with the fac - $[M(CO)_3]^+$ core have been investigated. In particular, tridentate

chelators containing N-, S-, or O-donors have been shown to provide well-defined, kinetically inert and stable organometallic complexes which are suitable for application in vivo^{9,14-17}. Many studies of *fac*-Re(CO)₃L complexes (L = a facially coordinated tridentate ligand), including those from our laboratory, have aided in developing a better understanding of NMR spectral features of *fac*-Re(CO)₃L complexes having simple donor ligands.¹⁸⁻²¹

Owing to the broad applicability of the *fac*-[M^I(CO)₃]⁺ core, many molecules such as peptides, antibodies, glucose and certain receptor ligands have been labeled.⁴ At present, great interest surrounds the concept of combining ^{99m}Tc and ^{188/186}Re with biomolecules in order to selectively target specific locations and biological processes.^{4,6,7,22-27} Introduction of a suitable chain of bridging atoms (linker) into a basic ligand framework or into a functional group allows coupling of the *fac*-[M^I(CO)₃] core to the biomolecule (Figure 1.2).²⁸

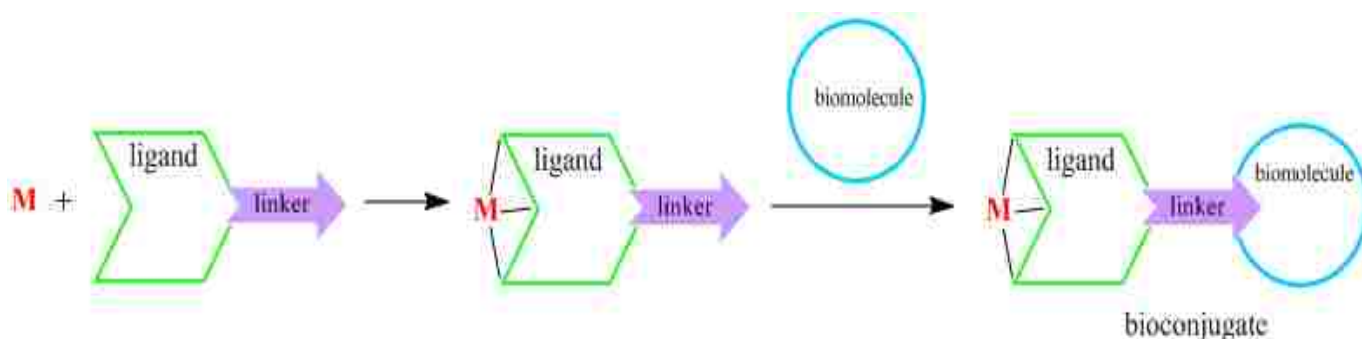


Figure 1.2. Schematic representation of the bifunctional chelate strategy

When medically interesting molecules are radiolabeled with the *fac*-[M(CO)₃]⁺ core, usually a post-labeling approach with bifunctional chelating agents is employed.^{6,29} These agents enable the covalent linkage to a biomolecule as well as the coordination of the radiometal. Different functional groups such as amines, thiols, and carboxylates have been used to

functionalize many of the ligand systems that are used to chelate the $fac-[M(CO)_3]^+$ core.⁸ However, despite the success of these complexes with the metal tricarbonyl core, there is still a need for novel and innovative strategies for bioconjugation techniques and radiolabeling procedures in order to expedite the development of radiotracers with the $fac-[M(CO)_3]^+$ core. The specific theme of the present study is to explore two new possible approaches of bioconjugation: $fac-[Re^I(CO)_3L]^n$ complexes with a tridentate sulfonamide linker and with a monodentate amidine linker.

The first part of this work describes the synthesis of new $fac-[Re(CO)_3(N(SO_2R)(CH_2Z)_2)]PF_6$ complexes ($Z = CH_2NH_2$; $R = Me, dmb, \text{ or } tol$) in aqueous medium and detailed analysis of the structure and solution behavior of these complexes. Our recent discovery of the rare sulfonamide nitrogen-to-metal bonds of normal length, in $fac-[Re(CO)_3(N(SO_2R)(CH_2Z)_2)]^n$ complexes with $N(SO_2R)dpa$ ligands derived from di-(2-picolyl)amine ($N(H)dpa$) ($Z = 2\text{-pyridyl}$) showed the potential of the sulfonamide bond as a linking method of targeting moieties to the $fac-[M(CO)_3]^+$ core.³⁰ However, the planar, electron-withdrawing 2-pyridyl groups of $N(SO_2R)dpa$ destabilize the ligand to base and create relatively rigid chelate rings. Moreover, the hydrophobic 2-pyridyl groups could cause undesirable accumulation in the liver, limiting future use in radiopharmaceuticals. To overcome these problems, a robust, hydrophilic, and flexible $N(CH_2Z)_2$ chelate framework was synthesized by using new C_2 -symmetric ligands, $N(SO_2R)(CH_2Z)_2$ with.

The second part discusses how treatment of the organic precursors, $fac-[Re(CO)_3(L)(CH_3CN)]BF_4$ [$L = 5,5'$ -dimethyl-2,2'-bipyridine (5,5'-Me₂bipy) and 6,6'-dimethyl-2,2'-bipyridine (6,6'-Me₂bipy)], with five C_2 -symmetrical saturated heterocyclic amines yielded new amidine complexes, $fac-[Re(CO)_3(L)(HNC(CH_3)N(CH_2CH_2)_2Y)]BF_4$ [$Y = CH_2, (CH_2)_2, (CH_2)_3, NH \text{ or } O$] possessing the novel feature of having only one isomer.³¹ In contrast to the

closely related amidine complexes with primary amines, which had isomers owing to the double-bond character of the amidine ($C_{am}-N_3$) bond,³² the presence of only the *E* isomer of the *fac*- $[Re(CO)_3(L)(HNC(CH_3)N(CH_2CH_2)_2Y)]BF_4$ was established by crystallographic and 1H NMR spectroscopic methods.³¹ The absence of other isomers is undoubtedly attributable to the unfavorable clashes between the equatorial ligands and the bulky $N(CH_2CH_2)_2Y$ ring moiety of the axial amidine ligand. Moreover, the rate of amidine formation was found to be faster when the size of the saturated heterocyclic amine ring was getting smaller. Thus, further studies were employed using smaller heterocyclic rings and important NMR spectral features have been investigated. Because this new linking chemistry offers promise as a suitable method for preparing isomerically pure conjugated *fac*- $[^{99m}Tc(CO)_3L]^{n+/-}$ imaging agents, a new method in more aqueous media was utilized as the next step. The new method evaluates the ability to utilize the *fac*- $[Re(CO)_3(H_2O)_3]^+$ precursor in the amidine synthesis. The promising results of this study starting with the *fac*- $[M(CO)_3(H_2O)_3]^+$ precursor encouraged us to demonstrate further the applicability of the Re amidine chemistry. Thus, amidine complexes with different drug analogues were synthesized and characterized as a preliminary step before ^{99m}Tc labeling and biological studies of these complexes.

1.3 References

- (1) *Advances in medical radiation imaging for cancer diagnosis and treatment*, Nuclear Technology Review **2006**, International Atomic Energy Agency, 110-127.
- (2) Schubiger, P. A.; Alberto, R.; Smith, A. *Bioconjugate Chem.* **1996**, *7*, 165-179.
- (3) Dilworth, J. R.; Parrot, S. J. *Chem. Soc. Rev.* **1998**, *27*, 43-55.
- (4) Alberto, R. In *Technetium-99m radiopharmaceuticals : status and trends*; International Atomic Energy Agency: Vienna, 2009, p 19-40.
- (5) Schwochau, K. *Angew. Chem. Int. Ed. Engl.* **1994**, *33*, 2258-2267.
- (6) Bartholomä, M.; Valliant, J.; Maresca, K. P.; Babich, J.; Zubieta, J. *Chem. Commun. (Cambridge, U.K.)* **2009**, 493-512.

- (7) Abram, U.; Alberto, R. *J. Braz. Chem. Soc.* **2006**, *17*, 1486-1500.
- (8) Liu, S. *Chem. Soc. Rev.* **2004**, *33*, 445-461.
- (9) Schibli, R.; Bella, R.; Alberto, R.; Garcia-Garayoa, E.; Ortner, K.; Abram, U.; Schubiger, A. *P. Bioconjugate Chem.* **2000**, *11*, 34-351.
- (10) Volkert, W. A.; Hoffman, T. J. *Chem. Rev.* **1999**, *99*, 2269-2292.
- (11) Gunderson, L. L.; Tepper, J. E. *Clinical Radiation Oncology*; Second Edition ed.; Elsevier Health Sciences, **2007**.
- (12) Wöhrle, J.; Krause, B. J.; Nusser, T.; Mottaghy, F. M.; Habig, T.; Kochs, M.; Kotzerke, J.; Reske, S. N.; Hombach, V.; Höher, M. *Eur. J. Nucl. Med. Mol. Imaging* **2006**, *33*, 1314-1320.
- (13) Mindt, T.; Struthers, H.; García-Garayoa, E.; Desbouis, D.; Schibli, R. *Chimia* **2007**, *61*, 725-731.
- (14) Alberto, R.; Pak, J. K.; van Staveren, D.; Mundwiler, S.; Benny, P. *Biopolymers* **2004**, *76*, 324-333.
- (15) Desbouis, D.; Struthers, H.; Spiwok, V.; Küster, T.; Schibli, R. *J. Med. Chem.* **2008**, *51*, 6689-6698.
- (16) Wei, L.; Babich, J. W.; Ouellette, W.; Zubieta, J. *Inorg. Chem.* **2006**, *45*, 3057-3066.
- (17) Schibli, R.; Schubiger, P. A. *Eur. J. Nucl. Med. Mol. Imaging* **2002**, *29*, 1529-1542.
- (18) Christoforou, A. M.; Marzilli, P. A.; Fronczek, F. R.; Marzilli, L. G. *Inorg. Chem.* **2007**, *46*, 11173-11182.
- (19) Lipowska, M.; Cini, R.; Tamasi, G.; Xu, X.; Taylor, A. T.; Marzilli, L. G. *Inorg. Chem.* **2004**, *43*, 7774-7783.
- (20) Banerjee, S. R.; Maresca, K. P.; Francesconi, L.; Valliant, J.; Babich, J. W.; Zubieta, J. *Nucl. Med. Biol.* **2005**, *32*, 1-20.
- (21) Christoforou, A. M.; Fronczek, F. R.; Marzilli, P. A.; Marzilli, L. G. *Inorg. Chem.* **2007**, *46*, 6942-6949.
- (22) Alberto, R.; Schibli, R.; Abram, U.; Egli, A.; Knapp, F. F.; Schubiger, P. A. *Radiochim. Acta* **1997**, *79*, 99-103.
- (23) Alberto, R.; Schibli, R.; Schubiger, P. A.; Abram, U.; Pietzsch, H. J.; Johannsen, B. *J. Am. Chem. Soc.* **1999**, *121*, 6076-6077.
- (24) Murray, A.; Simms, M. S.; Scholfield, D. P.; Vincent, R. M.; Denton, G.; Bishop, M. C.; Price, M. R.; Perkins, A. C. *J. Nucl. Med.* **2001**, *42*, 726-732.

- (25) Schibli, R.; Schwarzbach, R.; Alberto, R.; Ortner, K.; Schmalle, H.; Dumas, C.; Egli, A.; Schubiger, P. A. *Bioconjugate Chem.* **2002**, *13*, 750-756.
- (26) Agorastos, N.; Borsig, L.; Renard, A.; Antoni, P.; Viola, G.; Springler, B.; Kurz, P.; Alberto, R. *Chem. Eur. J.* **2007**, *13*, 3842-3852.
- (27) Cyr, J. E.; Pearson, D. A.; Wilson, D. M.; Nelson, C. A.; Guaraldi, M.; Azure, M. T.; Lister-James, J.; Dinkelborg, L. M.; Dean, R. T. *J. Med. Chem.* **2007**, *50*, 1354-1364.
- (28) Alberto, R. *Eur. J. Nucl. Med. Mol. Imaging* **2003**, *30*, 1299-1302.
- (29) Kluba, C. A.; Mindt, T. L. *Molecules* **2013**, *18*, 3206-3226.
- (30) Perera, T.; Abhayawardhana, P.; Marzilli, P. A.; Fronczek, F. R.; Marzilli, L. G. *Inorg. Chem.* **2013**, *52*, 2412-2421.
- (31) Abhayawardhana, P.; Marzilli, P. A.; Perera, T.; Fronczek, F. R.; Marzilli, L. G. *Inorg. Chem.* **2012**, *51*, 7271-7283.
- (32) Perera, T.; Fronczek, F. R.; Marzilli, P. A.; Marzilli, L. G. *Inorg. Chem.* **2010**, *49*, 7035-7045.

CHAPTER 2

COMPLEXES POSSESSING RARE “TERTIARY” SULFONAMIDE NITROGEN-TO-METAL BONDS OF NORMAL LENGTH: *fac*-[Re(CO)₃(N(SO₂R)DIEN)]PF₆ COMPLEXES WITH HYDROPHILIC SULFONAMIDE LIGANDS

2.1 Introduction

Many *fac*-[^{99m}Tc(CO)₃L]ⁿ imaging agents with facially coordinated tridentate ligands (L) have been studied¹⁻⁸ because of the convenient generation of the *fac*-[^{99m}Tc(CO)₃(H₂O)₃]⁺ precursor.^{9,10} Some of these imaging agents have exhibited satisfactory results in human volunteers and in early patient studies.^{4,7,8} Such *fac*-[^{99m}Tc(CO)₃L]ⁿ agents are more robust and have better pharmacokinetic properties than agents with bidentate ligands.¹¹ The γ -emitting ^{99m}Tc radionuclide has ideal nuclear properties^{12,13} for diagnostic applications in nuclear medicine.^{1,14-17}

The development of ^{99m}Tc radiopharmaceutical agents benefits from an understanding of the chemistry of their Re analogues. The discovery of a straightforward preparation of the *fac*-[Re(CO)₃(H₂O)₃]⁺ precursor¹⁸ has led to significantly improved aqueous synthetic methods for *fac*-[M(CO)₃L]ⁿ agents (M = various isotopes of Tc and Re).^{3,16,17,19-21} *fac*-[Re(CO)₃L]ⁿ complexes serve as excellent structural models for *fac*-[^{99m}Tc(CO)₃L]ⁿ imaging agents.^{4,22-27} Moreover, *fac*-[^{186/188}Re(CO)₃L]ⁿ agents themselves are emerging as promising radiopharmaceuticals, owing to their potential usefulness in radiotherapy.^{1,12,20,28}

New types of tridentate ligands and ligand conjugation methods will expand the likelihood of developing useful new agents with the *fac*-[M^I(CO)₃]⁺ core (M = ^{99m}Tc, ^{186/188}Re).^{10,29,30} Meeting such goals requires the identification of suitable linker systems with hi-

*Reproduced with permission from American Chemical Society: Abhayawardhana, P. L.; Marzilli, P. A.; Perera, T.; Fronczek, F. R.; Marzilli, L. G. “Complexes Possessing Rare “Tertiary” Sulfonamide Nitrogen-to-Metal Bonds of Normal Length: *fac*-[Re(CO)₃(N(SO₂R)dien)]PF₆ Complexes with Hydrophilic Sulfonamide Ligands”. *Inorg. Chem.* **2013**, 53, 1144–1155. Copyright 2015 American Chemical Society.

-gh stability, small size, and core ligands having a tridentate donor framework that does not increase the number of isomers.³¹⁻³⁴ Symmetrical linear tridentate ligands with linkage at the center donor are thus suitable candidates because the generation of racemic or diastereoisomeric mixtures of radiopharmaceuticals can be avoided.³⁵ Recent studies have reported promising biomedical properties for *fac*-[Re(CO)₃L]ⁿ complexes bearing a tridentate L with three N donors having a substituent replacing the proton at the central sp³ N.^{16,29,36,37} However, the conjugation of biologically important groups in these complexes was limited to groups attached via an N–C bond to the central N of ligands with the N(CH₂Z)₂ tridentate ligand framework. Z is commonly an N donor (e.g., 2-pyridyl)^{16,36} or a carboxyl group.³ The use of a biologically compatible linking group that did not create an N–C bond would greatly increase the chances of discovering useful agents.

Molecules containing a sulfonamide represent a very important class of biologically active molecules with a wide variety of applications.³⁹⁻⁴⁵ Therefore, we previously set out to explore conjugation that utilizes an N–S bond with the central N being the sulfonamide N.³⁵ The reaction of various sulfonyl chlorides (RSO₂Cl) with di-(2-picolyl)amine (*N*(H)dpa) afforded *N*(SO₂R)dpa ligands.³⁵ [Note that we use the normal convention: an *N* (italic N) designates a substituent location on nitrogen in the name of a compound. In this article, *N* designates a substituent located on the central or anchoring nitrogen atom of a tridentate ligand.] These *N*(SO₂R)dpa ligands readily added to *fac*-[Re(CO)₃(H₂O)₃]⁺ to form *fac*-[Re(CO)₃(*N*(SO₂R)dpa)]PF₆ (or BF₄) complexes. We learned that these were the only examples of structurally characterized bearing an N-bound, open-chain tertiary sulfonamide linkage with a normal M–N bond length. These *fac*-[Re(CO)₃(*N*(SO₂R)dpa)]PF₆ complexes were the first examples of such structurally characterized complexes with a neutral tertiary sulfonamide donor bound not only to the *fac*-[Re^l(CO)₃]⁺ core but to any metal center.³⁵ Although the results in that

report appeared to serve as proof of principle, the tridentate framework, $N(\text{CH}_2\text{Z})_2$ with $Z = 2$ -pyridyl, is relatively rigid and the resulting geometric constraints could possibly account for the observation of the $M\text{--}N(\text{sulfonamide})$ bond of normal length, as found in cases when complicated ligand ring structures fix the bond lengths.³⁵ Thus, the study of *fac*- $[\text{Re}(\text{CO})_3(N(\text{SO}_2\text{R})(\text{CH}_2\text{Z})_2)]^n$ complexes with more flexible chelate rings is of fundamental importance to coordination chemistry.

The new *fac*- $[\text{Re}(\text{CO})_3(N(\text{SO}_2\text{R})\text{dpa})]\text{X}$ complexes revealed the feasibility of having a tridentate ligand anchored by a central tertiary sulfonamide N. However, the two 2-pyridyl rings in a potential *fac*- $[\text{M}(\text{CO})_3(N(\text{SO}_2\text{R})\text{dpa})]^n$ imaging agent are hydrophobic, an undesirable property in an imaging agent because it is expected to promote liver uptake.¹² Also, the 2-pyridyl groups are electron withdrawing, facilitating decomposition of coordinated $N(\text{SO}_2\text{R})\text{dpa}$ ligands by strong base.³⁵

With the goals of exploring fundamental coordination chemistry of sulfonamides and of identifying ligands for use in imaging agents, we have now explored a more hydrophilic and more flexible ligand system that is suitable for our new conjugation method. Here we employ a prototypical triamine ligand framework based on diethylenetriamine ($N(\text{H})\text{dien}$).⁴⁶ In the new $N(\text{SO}_2\text{R})\text{dien}$ ligands, the aromatic 2-pyridyl groups of the *dpa* moiety are replaced with hydrophilic $\text{--CH}_2\text{NH}_2$ groups. The new ligands are stable to base and have the advantage of being small in size, a feature considered to be desirable for bioconjugates.^{32,34} All of the new complexes discussed below have the facial geometry, and thus from this point onward we omit the *fac*- designation when discussing specific compounds.

2.2 Experimental Section

Starting Materials. Methanesulfonyl chloride (MeSO_2Cl), 3,5-dimethylbenzenesulfonyl chloride (dmbSO_2Cl), 4-methylbenzenesulfonyl chloride (tolSO_2Cl), N,N,N -triethylamine,

trifluoroacetic acid (TFA), *N*(H)dien, 2-(*tert*-butoxycarbonyloxyimino)-2-(phenylacetonitrile), 4-dimethylaminopyridine, and $\text{Re}_2(\text{CO})_{10}$ were used as received from Aldrich. Aqueous $[\text{Re}(\text{CO})_3(\text{H}_2\text{O})_3]\text{OTf}$ (OTf = trifluoromethanesulfonate) was prepared by a known method.¹⁸

NMR Measurements. ^1H NMR and ^{13}C NMR spectra were recorded on a 400 MHz Bruker spectrometer. Peak positions are relative to TMS or to solvent residual peak, with TMS as reference. All NMR data were processed with TopSpin and MestReNova software. NMR data not presented in the Experimental Section can be found in the Results Section or in Supporting Information.

Mass Spectrometric Measurements. High resolution mass spectra were recorded on a Bruker Ultraflex MALDI TOF TOF mass spectrometer and an Agilent 6210 ESI TOF LCMS mass spectrometer.

X-ray Data Collection and Structure Determination. Intensity data were collected at low temperature on a Bruker Kappa Apex-II DUO CCD diffractometer fitted with an Oxford Cryostream cooler with graphite-monochromated $\text{Mo K}\alpha$ ($\lambda = 0.71073 \text{ \AA}$) radiation. Data reduction included absorption corrections by the multiscan method, with SADABS.⁴⁷ The structures were determined by direct methods and difference Fourier techniques and refined by full-matrix least squares using SHELXL-97.⁴⁸ All non-hydrogen atoms were refined anisotropically. All H atoms were visible in difference maps, but were placed in idealized positions, except for N–H hydrogen atoms, for which coordinates were refined. A torsional parameter was refined for each methyl group. Compound 6 has two independent formula units in the asymmetric unit.

Synthesis of *N,N'*-Bis(*tert*-butoxycarbonyl)diethylenetriamine (*N*(H)dien(Boc)₂). The *N*(H)dien(Boc)₂ ligand was prepared in 96% yield by a known method.⁴⁹ ^1H NMR signals (ppm)

in CDCl₃: 4.89 (br s, 1H, NH), 3.20 (m, 4H, 2CH₂), 2.72 (t, 4H, 2CH₂), 1.44 (s, 18H, 6CH₃). These ¹H NMR chemical shifts matched the previously reported values.⁴⁹

General Synthesis of *N*(SO₂R)dien. The following general procedure was employed to obtain the [*N*(SO₂Me)dienH₂](CF₃CO₂)₂ (1) and *N*(SO₂R)dien (R = dmb (2), R = tol (3)) ligands: a solution of the sulfonyl chloride (2 mmol) in 30 mL of dioxane was added dropwise over 2 h to a solution of *N*(H)dien(Boc)₂ (0.61 g, 2 mmol) and triethylamine (0.28 mL, 2 mmol) in dioxane (100 mL) at room temperature. The reaction mixture was stirred at room temperature for 20 h and filtered to remove any precipitate. The solvent was completely removed by rotary evaporation, water (50 mL) was added to the resulting oil, and the product was extracted into CH₂Cl₂ (2 × 25 mL). The CH₂Cl₂ extracts were combined and washed again with water (2 × 25 mL) at pH ~6. The organic layer was dried with anhydrous Na₂SO₄, and the CH₂Cl₂ was removed by rotary evaporation to yield an off-white solid. The Boc-protected diensulfonamide, *N*(SO₂R)dien(Boc)₂, was purified if necessary by column chromatography (silica gel column and a mixture of ethyl acetate/hexane). After characterization by ¹H NMR spectroscopy, this *N*(SO₂R)dien(Boc)₂ product was then deprotected by dropwise addition of trifluoroacetic acid (0.16–0.24 mL, 2–3 mmol) to a CH₂Cl₂ solution (at ~0 °C) of the compound (5 mL, 1 mmol). The reaction mixture was allowed to warm to room temperature, stirred for 16 h at room temperature, and then filtered; the filtrate was taken to dryness by rotary evaporation. Water at pH ~8–9 (50 mL) was added to the residue, and the product was extracted into CHCl₃ (2 × 25 mL). The combined CHCl₃ extracts were dried over anhydrous Na₂SO₄, and the solvent was removed by rotary evaporation, leaving a white/off-white powder or, when R = Me, a yellow oil.

General Synthesis of [Re(CO)₃(*N*(SO₂R)dien)]PF₆. A solution of the *N*(SO₂R)dien ligand (0.1 mmol) in methanol (2 mL) was added to an aqueous solution of [Re(CO)₃(H₂O)₃]OTf

(5 mL, 0.1 mmol). Methanol (1–2 mL) was added to dissolve any precipitate that formed. The pH of the reaction mixture was adjusted to ~6–7 with 0.5 M NaOH if necessary, and the clear reaction mixture was heated at reflux for 24 h. An excess (0.16 g, 1 mmol) of NaPF₆ was added to the clear solution, and the precipitate that formed within ~30 min was collected on a filter, washed with water, and air dried.

Synthesis of $[N(\text{SO}_2\text{Me})\text{dienH}_2](\text{CF}_3\text{CO}_2)_2$ ($[\text{1H}_2](\text{CF}_3\text{CO}_2)_2$). The use of MeSO₂Cl (0.16 mL, 2 mmol) in the general method described above yielded crude $N(\text{SO}_2\text{Me})\text{dien}(\text{Boc})_2$ as a brown oil (0.65 g, 85% yield). ¹H NMR signals (ppm) in DMSO-*d*₆: 6.92 (br s, 2H, 2NH), 3.14 (m, 4H, 2CH₂), 3.06 (m, 4H, 2CH₂), 2.89 (s, 3H, CH₃), 1.37 (s, 18H, 6CH₃).

The deprotection process described in the general method above afforded $N(\text{SO}_2\text{Me})\text{dien}$ (**1**) as a pale-yellow, oily substance (yield: 0.004 g, 18%). ¹H NMR signals (ppm) in CDCl₃: 3.25 (t, *J* = 6.3 Hz, 4H, 2CH₂), 2.93 (s, 3H, CH₃), 2.90 (t, *J* = 6.4 Hz, 4H, 2CH₂); in acetonitrile-*d*₃: 3.14 (t, *J* = 6.5 Hz, 4H, 2CH₂), 2.86 (s, 3H, CH₃), 2.76 (t, *J* = 6.5 Hz, 4H, 2CH₂); in DMSO-*d*₆: 3.08 (broad t, 4H, 2CH₂), 2.91 (s, 3H, CH₃), 2.67 (broad t, 4H, 2CH₂). ¹³C NMR signals (ppm) in CDCl₃: 51.59 (C5/6), 40.70 (C4/7), 37.60 (CH₃).

Compared to ligands with other R groups, isolation for R = Me produced a low yield, owing to the more hydrophilic nature of $N(\text{SO}_2\text{Me})\text{dien}$. To increase the amount of material available for synthesis of the complex, the general deprotection process was modified by adding a slight excess of trifluoroacetic acid to obtain the protonated ligand $[N(\text{SO}_2\text{Me})\text{dienH}_2](\text{CF}_3\text{CO}_2)_2$ ($[\text{1H}_2](\text{CF}_3\text{CO}_2)_2$). A mixture of $N(\text{SO}_2\text{Me})\text{dien}(\text{Boc})_2$ (0.38 g, 1 mmol) and trifluoroacetic acid (0.24 mL, 3 mmol) was stirred at room temperature for 16 h, and the resulting mixture was filtered; the white precipitate that was collected on a filter paper was washed several times with CH₂Cl₂ and air dried. The precipitate was then dissolved in methanol

(3 mL), and the solution was filtered. CH₂Cl₂ (~10 mL) was added to the filtrate until cloudiness was observed. After 24 h the undisturbed solution yielded thin, colorless, needle-like crystals of the trifluoroacetate salt of the protonated ligand [*N*(SO₂Me)dienH₂](CF₃CO₂)₂ ([1H₂](CF₃CO₂)₂) (0.29 g, 72% yield). ¹H NMR signals (ppm) in DMSO-*d*₆: 7.81 (br s, 6H, 2⁺NH₃), 3.37 (t, *J* = 6.2 Hz, 4H, 2CH₂), 3.04 (s, 3H, CH₃), 3.00 (t, *J* = 6.3 Hz, 4H, 2CH₂). ESI-MS: *m/z* calcd for C₅H₁₅O₂N₃S [*M* + H]⁺: 182.0958; found 182.0957.

Synthesis of *N*(SO₂dmb)dien (2). The use of dmbSO₂Cl (0.40 g, 2 mmol) according to the general synthetic procedure above yielded a pale yellow oil, which was purified by dissolving the oil in a minimum (~1 mL) of ethyl acetate and loading the solution onto a silica gel column. A 1:5 mixture of ethyl acetate:hexane was used to elute the remaining dmbSO₂Cl starting material (UV-vis). The product (UV-vis) was then eluted with a 2:3 (v:v) mixture of ethyl acetate/hexane. Thin-layer chromatography was used to determine the progress of separation. Removal of solvent by rotary evaporation yielded *N*(SO₂dmb)dien(Boc)₂ as a pale yellow powder (0.87 g, 92% yield). ¹H NMR signals (ppm) in CDCl₃: 7.65 (s, 2H, H₂/6), 7.21 (s, H, H₄), 5.19 (br s, 2H, NH), 3.32 (m, 4H, 2CH₂), 3.18 (m, 4H, 2CH₂), 2.38 (s, 6H, 2CH₃), 1.45 (s, 18H, 6CH₃).

Deprotection of *N*(SO₂dmb)dien(Boc)₂ (0.47 g, 1 mmol) with trifluoroacetic acid (0.16 mL, 2 mmol), by the procedure described above, afforded *N*(SO₂dmb)dien (2) as a white powder (0.26 g, 98% yield). ¹H NMR signals (ppm) in CDCl₃: 7.42 (s, 2H, H₂/6), 7.20 (s, H, H₄), 3.15 (t, *J* = 6.4 Hz 4H, 2CH₂), 2.91 (t, *J* = 6.4 Hz, 4H, 2CH₂), 2.38 (s, 6H, 2CH₃). ESI-MS: *m/z* calcd for C₁₂H₂₁O₂N₃S [*M* + H]⁺: 272.1427; found 272.1431.

Synthesis of *N*(SO₂tol)dien (3). The general procedure using tolSO₂Cl (0.44 g, 2 mmol) yielded *N*(SO₂tol)dien(Boc)₂ as a pale yellow oil (0.78 g, 86% yield). ¹H NMR signals (ppm) in

CDCl₃: 7.67 (d, *J* = 8.3 Hz, 2H, H2/6), 7.31 (d, *J* = 8.1 Hz, 2H, H3/5), 5.18 (br s, 2H, NH), 3.32 (m, 4H, 2CH₂), 3.17 (m, 4H, 2CH₂), 2.43 (s, 3H, CH₃), 1.45 (s, 18H, 6CH₃).

Deprotection of *N*(SO₂tol)dien(Boc)₂ (0.45 g, 1 mmol) with trifluoroacetic acid (0.16 mL, 2 mmol) afforded *N*(SO₂tol)dien (3) as a white powder (0.23 g, 92% yield). ¹H NMR signals (ppm) in CDCl₃: 7.70 (d, *J* = 8.2 Hz, 2H, H2/6), 7.31 (d, *J* = 8.0 Hz, 2H, H3/5), 3.15 (t, *J* = 6.4 Hz, 4H, 2CH₂), 2.91 (t, *J* = 6.4 Hz, 4H, 2CH₂), 2.43 (s, 3H, CH₃); in acetonitrile-*d*₃: 7.69 (d, *J* = 8.4 Hz, 2H, H2/6), 7.39 (d, *J* = 7.9 Hz, 2H, H3/5), 3.07 (t, *J* = 6.4 Hz, 4H, 2CH₂), 2.79 (t, *J* = 6.5 Hz, 4H, 2CH₂), 2.41 (s, 3H, CH₃). ESI-MS: *m/z* calcd for C₁₁H₁₉O₂N₃S [*M* + H]⁺: 258.1271; found 258.1277.

Synthesis of [Re(CO)₃(*N*(SO₂Me)dien)]PF₆ (4). The general method above, with the [1H₂](CF₃CO₂)₂ ligand (0.04 g, 0.1 mmol) and [Re(CO)₃(H₂O)₃]OTf (5 mL, 0.1 mmol), afforded [Re(CO)₃(*N*(SO₂Me)dien)]PF₆ (4) as a white crystalline precipitate (0.036 g, 60% yield) after the addition of NaPF₆ (~16 mg). (The pH of the acidic reaction mixture was adjusted to ~7 with 0.5 M NaOH before the solution was heated at reflux.) ¹H NMR signals (ppm) in DMSO-*d*₆: 5.65 (m, 2H, NH), 4.27 (m, 2H, NH), 3.57 (s, 3H, CH₃), 3.45 (m, 2H, CH₂), 3.22 (m, 2H, CH₂), 3.10 (m, 2H, CH₂), 2.97 (m, 4H, 2CH₂). ¹H NMR signals (ppm) of the R group in acetone-*d*₆: 3.62 (s, 3H, CH₃); in acetonitrile-*d*₃: 3.33 (s, 3H, CH₃). Chelate ring ¹H NMR signals for 4-6 in these solvents are reported in the Results Section. ¹³C NMR signals (ppm) in DMSO-*d*₆: 55.91 (C5/6), 44.86 (C4/7), 32.50 (CH₃). ¹³C NMR signals (ppm) in acetone-*d*₆: 55.11 (C5/6), 44.46 (C4/7), 30.97(CH₃). MALDI-TOF: *m/z* calcd for C₈H₁₅O₅N₃SRe [*M*⁺]: 452.029; found: 452.158.

Synthesis of [Re(CO)₃(*N*(SO₂dmb)dien)]PF₆ (5). The use of the general procedure with *N*(SO₂dmb)dien (2) (0.03 g, 0.1 mmol) afforded [Re(CO)₃(*N*(SO₂dmb)dien)]PF₆ (5) as a white precipitate (0.047 g, 69% yield) after the addition of NaPF₆ (~16 mg). ¹H NMR signals (ppm) in DMSO-*d*₆: 7.72 (s, 2H, H2/6), 7.57 (s, H, H4), 5.72 (m, 2H, NH), 4.28 (m, 2H, NH), 3.41 (m,

2H, CH₂), 3.14 (m, 2H, CH₂), 3.00 (m, 2H, CH₂), 2.65 (m, 2H, CH₂), 2.42 (s, 6H, 2CH₃). ¹H NMR signals (ppm) of the R group in acetone-*d*₆: 7.77 (s, 2H, H2/6), 7.60 (s, H, H4), 2.46 (s, 6H, 2CH₃); in acetonitrile-*d*₃: 7.65 (s, 2H, H2/6), 7.55 (s, H, H4), 2.44 (s, 6H, 2CH₃). ¹³C NMR signals (ppm) in acetone-*d*₆: 142.30 (dmb ring C1), 139.54 (dmb ring C4), 130.93 (dmb ring C2/6), 126.71(dmb ring C3/5), 57.83 (C5/6), 46.93 (C4/7), 22.09 (2CH₃). MALDI-TOF: *m/z* calcd for C₁₅H₂₁O₅N₃SRe [*M*⁺]: 542.076; found: 542.155.

Synthesis of [Re(CO)₃(N(SO₂tol)dien)]PF₆ (6). The use of *N*(SO₂tol)dien (3) (0.02 g, 0.1 mmol) as described in the general synthesis afforded [Re(CO)₃(*N*(SO₂tol)dien)]PF₆ (6) as a white precipitate (0.056 g, 84% yield) after the addition of NaPF₆ (~16 mg). Slow evaporation of a solution of the compound in acetone produced colorless, X-ray quality, needle-shaped crystals. ¹H NMR signals (ppm) in DMSO-*d*₆: 7.99 (d, *J* = 8.5 Hz, 2H, H2/6), 7.61 (d, *J* = 8.1 Hz, 2H, H3/5), 5.70 (m, 2H, NH), 4.28 (m, 2H, NH), 3.40 (m, 2H, CH₂), 3.14 (m, 2H, CH₂), 3.01 (m, 2H, CH₂), 2.66 (m, 2H, CH₂), ~2.5, overlapped (s, 3H, CH₃). ¹H NMR signals (ppm) of the R group in acetone-*d*₆: 8.05 (d, 2H, H2/6), 7.65 (d, 2H, H3/5), 2.53 (s, 3H, CH₃); in acetonitrile-*d*₃: 7.91(d, 2H, H2/6), 7.58 (d, 2H, H3/5), 2.51 (s, 3H, CH₃). ¹³C NMR signals (ppm) in DMSO-*d*₆: 147.80 (tol ring C4), 132.07 (tol ring C2/6), 131.00 (tol ring C3/5), 125.98 (tol ring C1), 56.20 (C5/6), 44.80 (C4/7), 21.69 (CH₃). ¹³C NMR signals (ppm) in acetone-*d*₆: 148.88 (tol ring C4), 132.70 (tol ring C2/6), 131.58 (tol ring C3/5), 127.05 (tol ring C1), 56.94 (C5/6), 46.00 (C4/7), 21.74 (CH₃). MALDI-TOF: *m/z* calcd for C₁₄H₁₉O₅N₃SRe [*M*⁺]: 528.060; found: 528.001.

Challenge Reactions of [Re(CO)₃(N(SO₂tol)dien)]PF₆ (6). Two 5 mM solutions of 6 in DMSO-*d*₆ (500 μL) were treated separately with 10 molar equiv (0.6 μL, 50 mM) or 2 molar equiv (0.12 μL, 10 mM) of diethylenetriamine and monitored over time by ¹H NMR spectroscopy. Another challenge experiment was carried out with a 5 mM solution of 6 in

DMSO-*d*₆ by first adding 1 molar equiv of 4-dimethylaminopyridine (4-Me₂Npy) and then increasing the 4-Me₂Npy to 10 molar equiv.

2.3 Results and Discussion

Synthesis of *N*(SO₂R)dien and [Re(CO)₃(*N*(SO₂R)dien)]PF₆. *N*(SO₂Me)dien (1), *N*(SO₂dmb)dien (2), and *N*(SO₂tol)dien (3) were synthesized by coupling *N*(H)dien with the respective sulfonyl chloride (Figure 2.1). In this case, unlike in the synthesis of *N*(SO₂R)dpa ligands,³⁵ additional steps are required to synthesize the *N*(SO₂R)dien ligands (1–3), owing to the possibility of attack by the terminal *N*(H)dien amino groups on the sulfur atom of the sulfonyl chloride. Thus, the *N*(H)dien terminal amine groups were protected with Boc groups. The products were obtained in good yield and purity, as indicated by ¹H NMR spectral data. Reaction of the deprotected ligands with an aqueous solution of [Re(CO)₃(H₂O)₃]OTf afforded [Re(CO)₃(*N*(SO₂Me)dien)]PF₆ (4), [Re(CO)₃(*N*(SO₂dmb)dien)]PF₆ (5), and [Re(CO)₃(*N*(SO₂tol)dien)]PF₆ (6) in 60–84% yields. All three complexes were characterized by ¹H and ¹³C NMR spectroscopy and by mass spectrometry (Experimental Section).

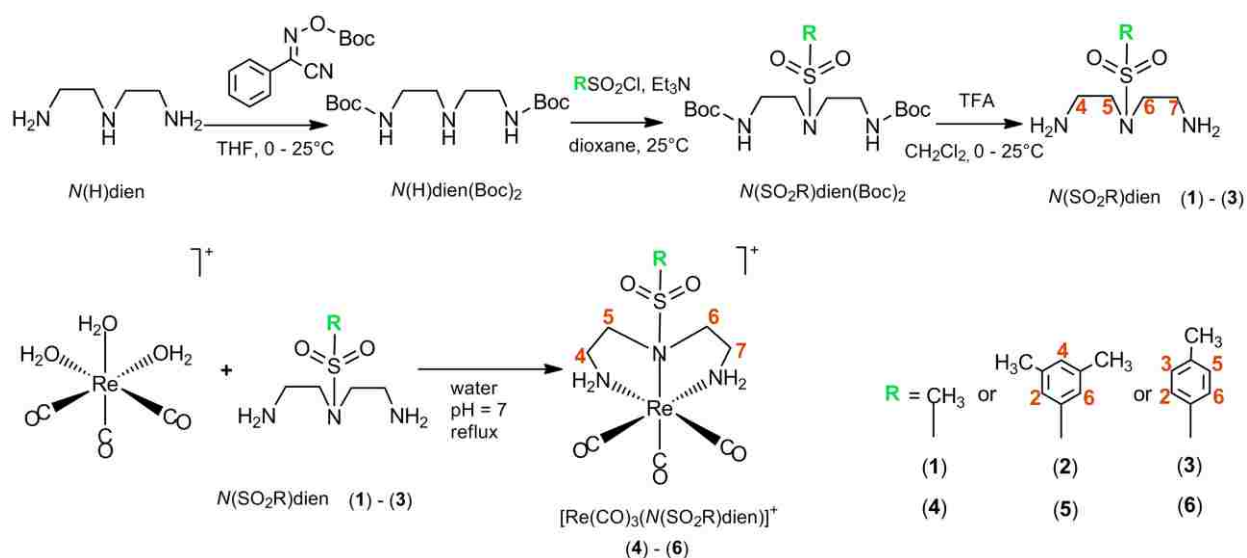


Figure 2.1. General reaction scheme for the synthesis of *N*(SO₂R)dien ligands (*top*) and [Re(CO)₃(*N*(SO₂R)dien)]⁺ complexes (*bottom*).

X-ray quality crystals of 4 and 6 were grown by slowly cooling a 5 mM solution of the compound in warm water. Crystals of 5 (grown by slow evaporation of a 5 mM acetone solution) suffered from twinning, space-group ambiguity, and disorder problems in the molecule, which prevented refinement within acceptable values. However, the structural characterization of 5 (using the same procedures as for 4 and 6) confirmed that all three N atoms of *N*(SO₂dmb)dien are coordinated to Re.

Structural Results. Crystal data and structural refinement details for [Re(CO)₃(*N*(SO₂Me)dien)]PF₆ (4) and [Re(CO)₃(*N*(SO₂tol)dien)]PF₆ (6) are summarized in Table 2.1, and the ORTEP plots appear in Figure 2.2 (see Figure 2.1 for the numbering scheme used to describe the solid-state data). Both 4 and 6 exhibit a pseudo octahedral structure, with the three carbonyl ligands occupying one face; the remaining three coordination sites are occupied by the three nitrogen atoms of the tridentate ligand.

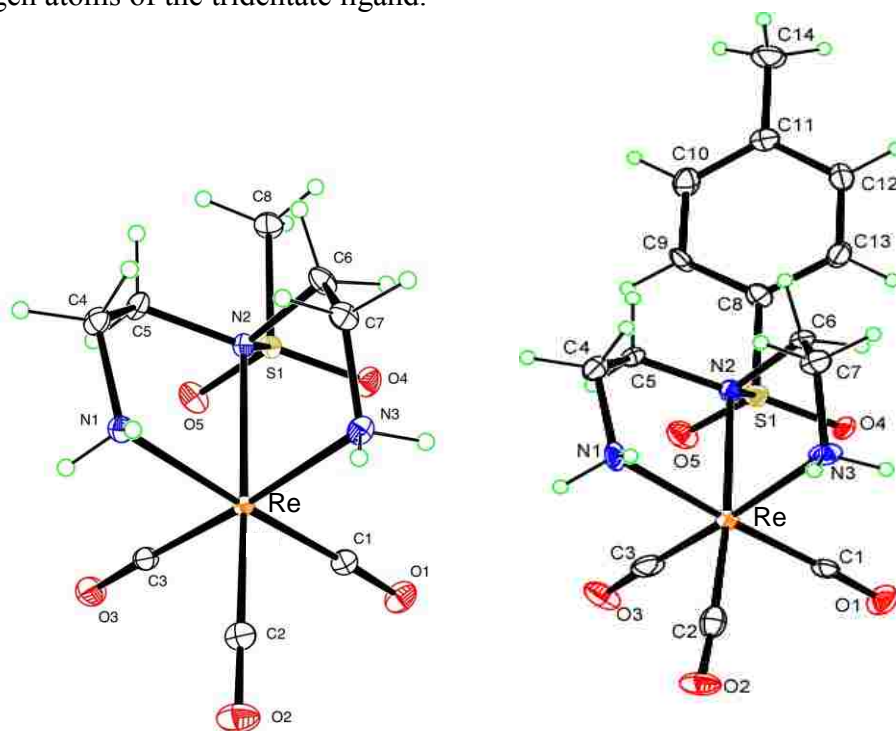


Figure 2.2. ORTEP plots of the cations in [Re(CO)₃(*N*(SO₂Me)dien)]PF₆ (4) (*left*) and [Re(CO)₃(*N*(SO₂tol)dien)]PF₆ (6) (*right*). Thermal ellipsoids are drawn with 50% probability.

Table 2.1. Crystal Data and Structure Refinement for [Re(CO)₃(N(SO₂Me)dien)]PF₆ (4) and [Re(CO)₃(N(SO₂tol)dien)]PF₆ (6)

	4	6
empirical formula	C ₈ H ₁₅ N ₃ O ₅ ReS·PF ₆	C ₁₄ H ₁₉ N ₃ O ₅ ReS·PF ₆
fw	596.46	672.55
crystal system	monoclinic	monoclinic
space group	<i>P2₁/c</i>	<i>P2₁/c</i>
unit cell dimensions		
<i>a</i> (Å)	12.822(3)	26.0233(14)
<i>b</i> (Å)	8.8089(19)	13.0607(7)
<i>c</i> (Å)	14.026(3)	12.2147(7)
<i>β</i> (deg)	94.373(10)	95.831(3)
<i>V</i> (Å ³)	1579.6(6)	4130.1(4)
<i>T</i> (K)	100	100
<i>Z</i>	4	8
ρ_{calc} (Mg/m ³)	2.508	2.163
abs coeff (mm ⁻¹)	8.02	6.15
2 θ_{max} (°)	70	71.2
<i>R</i> indices ^a	0.018	0.029
wR2 = [<i>I</i> > 2 σ (<i>I</i>)] ^b	0.044	0.055
data collected, R _{int}	28379, 0.034	51479, 0.033
data/param	6953/239	18802/585

^a $R = (\sum||F_o| - |F_c||)/\sum|F_o|$; ^bwR2 = $[\sum[w(F_o^2 - F_c^2)^2]/\sum[w(F_o^2)^2]]^{1/2}$, in which $w = 1/[\sigma^2(F_o^2) + (dP)^2 + (eP)]$ and $P = (F_o^2 + 2F_c^2)/3$.

Selected bond distances and angles of complexes 4 and 6 are presented in Table 2.2. The Re–C bond distance of the CO group trans to the sulfonamide group is not significantly different from those of the two cis Re–CO bonds, indicating the absence of any trans influence. All Re–N

Table 2.2. Selected Bond Distances (Å) and Angles (deg) for [Re(CO)₃(N(SO₂Me)dien)]PF₆ (4) and [Re(CO)₃(N(SO₂tol)dien)]PF₆ (6)

	4	6		4	6
bond distance			bond angle		
Re–N1	2.2377(14)	2.221(2)	N1–Re–N2	77.07(5)	77.54(7)
Re–N2	2.2763(14)	2.2686(19)	N1–Re–N3	86.53(6)	85.83(8)
Re–N3	2.2072(15)	2.216(2)	N2–Re–N3	77.80(5)	77.86(7)
Re–C1	1.9128(16)	1.913(2)	C2–Re–N1	95.72(6)	92.70(9)
Re–C2	1.9109(18)	1.911(2)	C3–Re–N1	92.31(6)	94.99(9)
Re–C3	1.9136(19)	1.917(3)	C2–Re–N3	96.60(7)	98.29(9)
S1–O5	1.4273(13)	1.4280(18)	C1–Re–N3	93.12(6)	91.92(9)
S1–O4	1.4324(13)	1.4339(17)	Re–N2–S1	111.07(7)	111.35(9)
S1–N2	1.7434(13)	1.759(2)	Re–N2–C5	105.93(9)	106.14(13)
			Re–N2–C6	110.01(10)	109.86(13)
non-bonded distance			S1–N2–C5	109.13(10)	108.82(14)
N1–N3	3.046(2)	3.021(3)	S1–N2–C6	108.52(10)	108.18(13)
N1–N2	2.812(2)	2.812(3)	C5–N2–C6	112.19(13)	112.52(18)
N2–N3	2.816(2)	2.818(3)	C1–Re–N2	99.98(6)	100.55(8)
			C3–Re–N2	97.91(6)	96.81(8)
deviation of N2 ^a	0.513(1)	0.514(2)	C1–Re–C2	87.25(7)	89.08(10)
			C3–Re–C2	87.62(7)	87.29(10)
			C1–Re–C3	87.83(7)	87.10(10)

^a Distance to the sulfonamide N from the plane defined by the S and the two C atoms attached to N2 (average of two independent molecules for 6).

bond distances in 6 are generally similar to the Re–N(sp³) distances observed in [Re(CO)₃L]⁺ complexes with prototypical NNN donor ligands, which range from ~2.21 to 2.29 Å as the bulk of substituents on the N atoms increases.^{46,50} However, the distances from Re to the central N2 (2.2763(14) Å in 4 and 2.2686(19) Å in 6) are significantly longer than the Re–N1 distances (2.2377(14) Å for 4 and 2.221(2) Å for 6) and Re–N3 distances (2.2072(15) Å for 4 and 2.216(2) Å for 6) (Table 2.2). These Re–N2 distances in 4 and 6 are significantly longer than the Re–N2 distance in [Re(CO)₃(N(H)dien)]PF₆⁴⁶ (2.201(3) Å), but they are comparable to the Re–N2 distance of [Re(CO)₃(N(Me)dien)]PF₆.⁴⁶ The Re–N2 distance in the latter complex (2.250(4) Å) is not statistically different from the Re–N2 distance in [Re(CO)₃(N(SO₂tol)dien)]PF₆ (6, Table 2.2), suggesting that the bond lengthening in 6 is caused chiefly by steric effects, not electronic effects. Furthermore, the good overlap of the three donor N atoms observed when the three carbonyl carbon (C1, C2 and C3) and Re atoms in the structure of 6 are superimposed with the corresponding atoms in [Re(CO)₃(N(Me)dien)]PF₆⁴⁶ (Supporting Information) demonstrates the lack of any large effect of having a tertiary sulfonamide nitrogen instead of a typical sp³ nitrogen serve as the central anchor of the tridentate ligand.

The lengthening of the Re–N2 bond in 4 and 6 versus [Re(CO)₃(N(H)dien)]PF₆ is similar to that observed in [Re(CO)₃(N(SO₂R)dpa)]PF₆ complexes (e.g., R = Me and tol) versus the parent [Re(CO)₃(N(H)dpa)]Br complex.^{30,35} The similarity of the central Re–N bond distances of the analogous [Re(CO)₃(N(SO₂R)dpa)]PF₆ complexes (average = ~2.277 Å) and in 4 and 6 (average = ~2.272 Å) indicates that the donating ability of the sulfonamide N is similar for both ligands.³⁵ Furthermore, all three donor N atoms show good overlap when the C1, C2, C3, and Re atoms in [Re(CO)₃(N(SO₂tol)dien)]PF₆ and [Re(CO)₃(N(SO₂tol)dpa)]PF₆ are superimposed (Figure 2.3). The central Re–N bond distance of the [Re(CO)₃(N(SO₂Me)dpa)]PF₆ complex

(2.2826(16) Å) is not significantly different from this distance in 4. Thus, the normal length of the Re–N(sulfonamide) bonds in $[\text{Re}(\text{CO})_3(\text{N}(\text{SO}_2\text{R})\text{dpa})]\text{PF}_6$ complexes is not a consequence of the rigidity of the 5-membered dpa chelate rings.

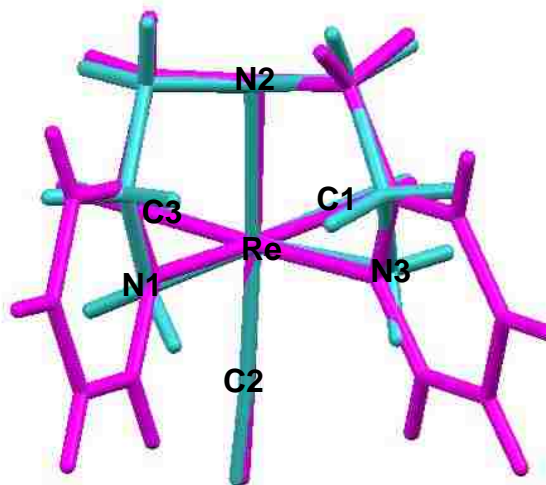


Figure 2.3. Overlay of Re, C1, C2, and C3 atoms of $[\text{Re}(\text{CO})_3(\text{N}(\text{SO}_2\text{tol})\text{dien})]\text{PF}_6$ (6) (blue) and $[\text{Re}(\text{CO})_3(\text{N}(\text{SO}_2\text{tol})\text{dpa})]\text{PF}_6$ ³⁵ (magenta) complexes. (The SO_2R groups have been omitted for clarity).

The sulfonamide nitrogen of the $\text{N}(\text{SO}_2\text{tol})\text{dpa}$ ligand in a Pd^{II} complex is not bound to Pd^{II} and all bond angles around the sulfonamide nitrogen of the $\text{N}(\text{SO}_2\text{tol})\text{dpa}$ ligand in the bidentate binding mode are close to 120° , indicating sp^2 hybridization for this N atom.⁵² In contrast, in 4 and 6, all bond angles around the sulfonamide N (N2) are $\sim 109^\circ$ (Table 2.2). This observation, which is consistent with data for $[\text{Re}(\text{CO})_3(\text{N}(\text{SO}_2\text{R})\text{dpa})]\text{PF}_6$ complexes,³⁵ indicates that the sulfonamide nitrogen changes from sp^2 to sp^3 hybridization upon tridentate binding to Re^{I} .³⁵ This conclusion is confirmed by the fact that the C5–N2 (average = 1.511 Å) and C6–N2 (average = 1.512 Å) bond distances are longer than an average C–N(sp^2) distance (~ 1.28 Å).⁵³ Data for all of the bond angles and distances involving the sulfonamide N indicate that it is sp^3 hybridized.

In $[\text{Re}(\text{CO})_3(\text{N}(\text{SO}_2\text{R})\text{dpa})]\text{PF}_6$ and other complexes that have metal-bound tertiary sulfonamide groups, the distance to the sulfonamide N from the plane defined by the S and the two C atoms attached to N typically ranges from 0.47–0.52 Å.³⁵ Such values are larger than those for the corresponding distance in complexes with an unbound sulfonamide N atom (0.06–0.26 Å).³⁵ In the new complexes, $[\text{Re}(\text{CO})_3(\text{N}(\text{SO}_2\text{Me})\text{dien})]\text{PF}_6$ (4) and $[\text{Re}(\text{CO})_3(\text{N}(\text{SO}_2\text{tol})\text{dien})]\text{PF}_6$ (6), this distance (Table 2.2) is in the range characteristic of a M–N bond.

Most of the known complexes with tertiary sulfonamide ligands exhibit relatively long M–N(sulfonamide) bond distances and short S–N distances, features attributed to the resonance contribution of the lone pair on the sulfonamide N and to the poor electron donation of the sulfonamide N to the metal.^{54,55} Thus, both the comparatively short Re–N(sulfonamide) bond distance [2.2763(14) for 4 and 2.2686(19) Å for 6] and the long S–N bond distance in these complexes [1.7434(13) for 4 and 1.759(2) Å for 6] indicate that the sulfonamide N is a relatively strong donor.

Only one other structurally characterized complex in which a diethylenetriamine derivative is bound to a metal (La^{III}) via a sulfonamide bond through the N has been reported;⁵⁶ the sulfonamide group in that complex, however, is part of a cyclic heptadentate ligand. Thus, the sulfonamide complexes reported here are the first structurally characterized metal complexes in which the metal is coordinated by the central tertiary sulfonamide N in a linear, highly flexible tridentate ligand.

We have previously discussed at length chelate ring pucker λ or δ chirality and the consequences on structure and NMR spectra of $[\text{Re}(\text{CO})_3(\text{polyamine})]\text{X}$ complexes.^{38,46,50} The cation of $[\text{Re}(\text{CO})_3(\text{N}(\text{SO}_2\text{Me})\text{dien})]\text{PF}_6$ (4) and one of the cations of $[\text{Re}(\text{CO})_3(\text{N}(\text{SO}_2\text{tol})\text{dien})]\text{PF}_6$ (6) (the one shown in Figure 2.2) have five-membered chelate

rings of different chirality (λ or δ). However, the other independent cation in the asymmetric unit of 6 (not shown) has chelate rings of the same chirality. The relative frequency of observing the same or different chiralities in the two chelate rings with a central tertiary sulfonamide N donor (4 and 6) suggests that structures in which the chirality of the rings differs may be slightly more stable than structures having rings of the same chirality. Thus, our finding agrees with cases in which the central N is a classical sp^3 N donor, namely that examples in which the chirality of the rings in a given structure differs ($\lambda\delta$ or $\delta\lambda$) occur more frequently than those in which the chirality is the same ($\lambda\lambda$ or $\delta\delta$).⁴⁶

NMR Spectroscopy. The $N(\text{SO}_2\text{R})\text{dien}$ ligands and the $[\text{Re}(\text{CO})_3(N(\text{SO}_2\text{R})\text{dien})]\text{PF}_6$ complexes reported here were characterized by ^1H NMR (1–6) and ^{13}C NMR (1, 3–6) spectroscopy, usually in one or more of several solvents (CDCl_3 , acetone- d_6 , acetonitrile- d_3 and DMSO- d_6). NMR signals were assigned by analyzing the splitting pattern, integration, and data from 2D NMR experiments.

The two methylene ^1H NMR signals in $N(\text{SO}_2\text{R})\text{dien}$ ligands (1–3) are triplets integrating to four protons in CDCl_3 (Experimental Section and Supporting Information). Selected data were obtained in acetonitrile- d_3 or in DMSO- d_6 (Experimental Section and Supporting Information). The C(5/6) H_2 triplet for 2 (R = dmb) and for 3 (R = tol) is slightly upfield from the C(5/6) H_2 triplet for 1 (R = Me) in CDCl_3 (Supporting Information). Shift values for the C(4/7) H_2 triplet are similar for all three ligands. These observations are attributed to the anisotropic sulfonamide aromatic groups, which are close to the C(5/6) H_2 groups but far from the C(4/7) H_2 groups. Similar results were obtained for 1 and 3 in acetonitrile- d_3 . The two protons in each methylene group are not sterically similar because the sulfonamide N lies out of the plane defined by the S and the two C atoms attached to N; the apparent magnetic equivalence in the NMR spectra

indicates that inversion at the sulfonamide nitrogen leads to time averaging, as discussed previously for the $N(\text{SO}_2\text{R})\text{dpa}$ ligands.³⁵

The spectra of the respective complexes, on the other hand, are consistent with each of the four protons in the chelate ring giving rise to a multiplet. For example, the methylene group ^1H NMR signals observed in acetonitrile- d_3 changed from two triplets (at 3.07 and 2.79 ppm) for the $N(\text{SO}_2\text{tol})\text{dien}$ ligand (3) to four multiplets [at 3.51, 3.16 (two overlapped), and 2.59 ppm; see Experimental Section and Supporting Information] for $[\text{Re}(\text{CO})_3(N(\text{SO}_2\text{tol})\text{dien})]\text{PF}_6$ (6). The least amount of overlap of the multiplets for complexes 4–6 was found in acetone- d_6 (Figure 2.4).

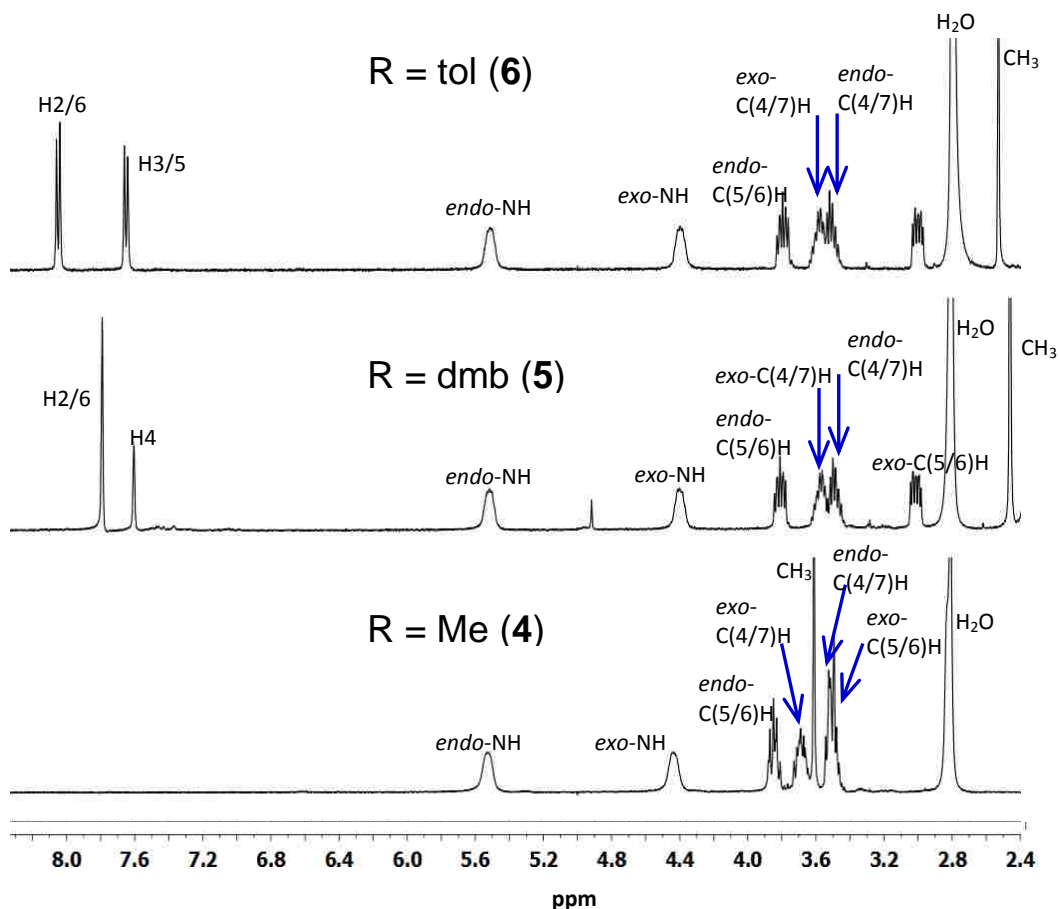


Figure 2.4. ^1H NMR spectra of $[\text{Re}(\text{CO})_3(N(\text{SO}_2\text{R})\text{dien})]\text{PF}_6$ complexes (4–6) in acetone- d_6 at 25 $^\circ\text{C}$.

Thus, as expected, the apparent magnetic equivalence of methylene protons in the free ligands is lost in 4–6. Similar changes in signals for methylene protons upon coordination of ligands have been reported for $[\text{Re}(\text{CO})_3(\text{N}(\text{SO}_2\text{R})\text{dpa})]\text{PF}_6$ complexes³⁵ and for $[\text{Re}(\text{CO})_3(\text{N}(\text{H})\text{dien})]\text{PF}_6$.⁴⁶

We designate the magnetically distinct protons in $-\text{CH}_2-$ or $-\text{NH}_2$ groups as *endo*-H or *exo*-H protons, on the basis of the orientation of the proton either toward (*endo*) or away (*exo*) from the carbonyl ligands (Chart 2.1). Note that the chelate rings in these complexes are puckered, and the corresponding protons in the two chelate rings are not equivalent in the solid state. However, the chelate rings are fluxional, and time averaging leads to only one signal for each type of CH or NH proton, or six ^1H NMR signals for the $\text{N}(\text{C}(5/6)\text{H}_2-\text{C}(4/7)\text{H}_2-\text{NH}_2)_2$ tridentate framework moiety.

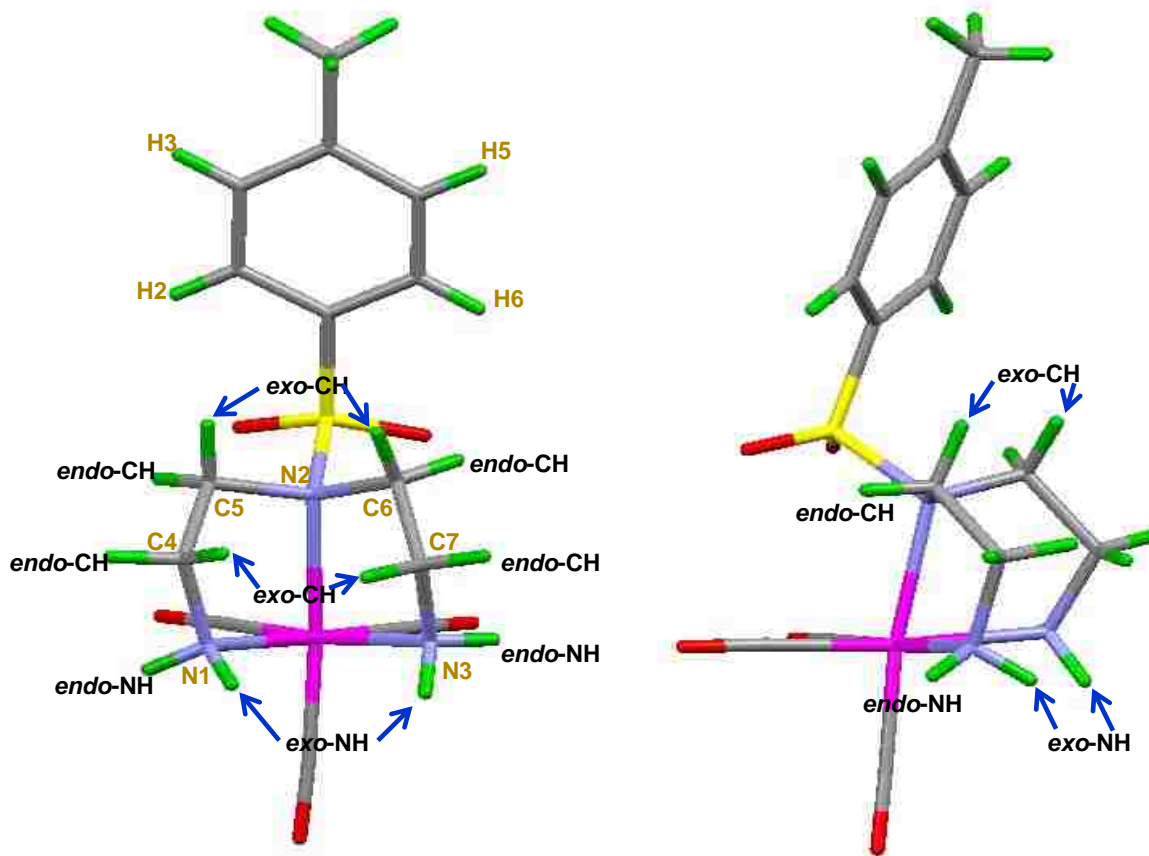


Chart 2.1. Front (*left*) and side (*right*) views of $[\text{Re}(\text{CO})_3(\text{N}(\text{SO}_2\text{tol})\text{dien})]\text{PF}_6$ (**6**), showing the designation of *endo*- and *exo*-CH and *endo*- and *exo*-NH protons.

¹H NMR Assignments. ¹H NMR signals of the protons in the terminal NH₂ groups of previously reported [Re(CO)₃(L)]ⁿ compounds (L = simple tridentate ligands similar to diethylenetriamine with two terminal –NH₂ groups)^{46,50} are well resolved. The *endo*-NH signal has a more downfield chemical shift than the *exo*-NH signal; solvent has access to the exposed *endo*-NH protons, but solvent access to the *exo*-NH protons is impeded by the chelate rings.^{46,50} The signal of the exposed *endo*-NH protons is shifted downfield by NH-solvent H-bonding. Both the shifts and the characteristic shift separation between these signals ($\Delta = \sim 1.5$ ppm in DMSO-*d*₆) are useful for assigning such NH NMR signals.^{46,50}

In this work, two broad ¹H NMR signals of [Re(CO)₃(*N*(SO₂tol)dien)]PF₆ (6) (5 mM) in DMSO-*d*₆ at 4.28 and 5.70 ppm decreased in size when D₂O was added, indicating that they are NH signals. The signals are connected by a strong COSY cross-peak, as expected for an NH₂ group (Supporting Information). The downfield signal at 5.70 ppm and the relatively upfield signal at 4.28 ppm, each integrating to two protons with $\Delta = \sim 1.5$ ppm, can be assigned as *endo*-NH and *exo*-NH signals, respectively.^{46,50}

Similar Δ values of ~ 1.5 ppm (DMSO-*d*₆), ~ 1.1 ppm (acetone-*d*₆), and ~ 1.0 ppm (acetonitrile-*d*₃) were observed between the downfield and upfield NH signals for all three complexes studied here (Table 2.3). This consistency aided in assigning the *endo*-NH and *exo*-NH signals in complexes 4–6 (Table 2.3, Figure 2.4). Although X-ray quality crystals for compound 5 have not been isolated, the ¹H NMR patterns and shifts of its chelate ring signals in all solvents used match the corresponding ¹H NMR data for the crystallographically characterized compound 6 (Table 2.3 and Figure 2.4). These ¹H NMR chemical shifts provide strong evidence that 5 has a structure very similar to that of 6. The NH signals of 6 in different solvents (Figure 2.5) are shifted downfield as the H-bonding ability of the solvent increases.

Table 2.3. ¹H NMR Shifts (ppm) of *exo*- and *endo*-NH and *exo*- and *endo*-CH Signals for [Re(CO)₃(N(SO₂R)dien)]PF₆ Complexes in Various Solvents at 25 °C

signal	R = Me (4)	R = dmb (5)	R = tol (6)
DMSO- <i>d</i> ₆			
<i>exo</i> -NH	4.27	4.28	4.28
<i>endo</i> -NH	5.65	5.72	5.70
<i>endo</i> -C(5/6)H	3.45	3.41	3.42
<i>exo</i> -C(4/7)H	3.23	3.14	3.14
<i>endo</i> -C(4/7)H	3.10	3.00	3.01
<i>exo</i> -C(5/6)H	2.97	2.65	2.66
acetone- <i>d</i> ₆			
<i>exo</i> -NH	4.45	4.40	4.40
<i>endo</i> -NH	5.54	5.52	5.51
<i>endo</i> -C(5/6)H	3.85	3.81	3.81
<i>exo</i> -C(4/7)H	3.69	3.58	3.55
<i>endo</i> -C(4/7)H	~3.50	3.50	3.52
<i>exo</i> -C(5/6)H	~3.50	3.02	3.02
acetonitrile- <i>d</i> ₃			
<i>exo</i> -NH	3.44	3.41	3.37
<i>endo</i> -NH	4.46	4.52	4.51
<i>endo</i> -C(5/6)H	3.50	3.52	3.51
<i>exo</i> -C(4/7)H	~3.18	~3.16	~3.16
<i>endo</i> -C(4/7)H	~3.18	~3.16	~3.16
<i>exo</i> -C(5/6)H	3.00	2.60	2.59

Thus, significant downfield chemical shifts are observed in acetone-*d*₆ and DMSO-*d*₆, in contrast to the relatively upfield chemical shifts observed in acetonitrile-*d*₃ (Table 2.3 and Figure 2.5),

owing to the weak interactions of that solvent with the NH groups. The highest Δ value (~ 1.5 ppm) occurs in DMSO- d_6 because it has the greatest H-bonding ability among the three solvents.

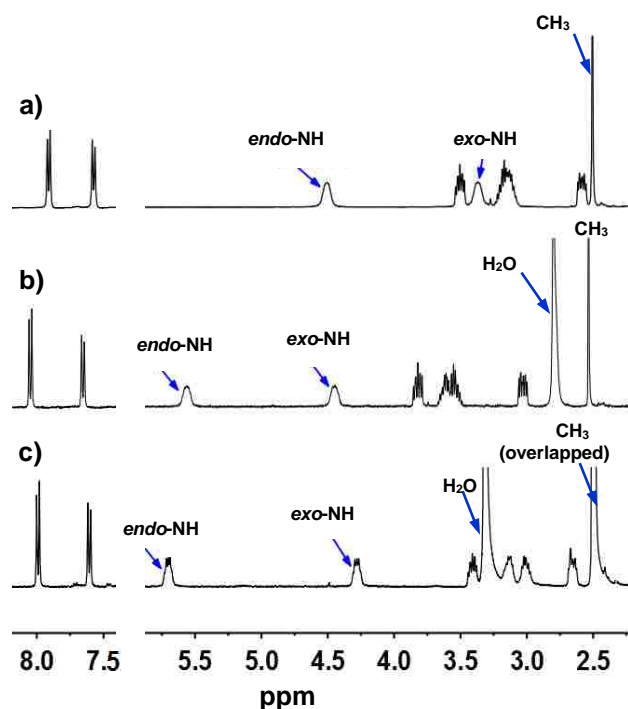


Figure 2.5. ^1H NMR spectra of $[\text{Re}(\text{CO})_3(\text{N}(\text{SO}_2\text{tol})\text{dien})]\text{PF}_6$ (6), illustrating the relative position of NH signals observed at 25 $^\circ\text{C}$ in a) acetonitrile- d_3 , b) acetone- d_6 , and c) DMSO- d_6 .

The *endo*-NH and *exo*-NH ^1H NMR signals assignments provide a starting point that allows us to exploit our structural data to achieve complete and unambiguous assignment of the ethylene ^1H NMR signals, which are rarely well resolved for coordinated ligands having such chelate rings.⁵⁰ To demonstrate our assignment strategy of assigning the multiplets to a specific *endo*-CH or *exo*-CH proton (Chart 2.1), we use $[\text{Re}(\text{CO})_3(\text{N}(\text{SO}_2\text{tol})\text{dien})]\text{PF}_6$ (6) in acetone- d_6 because of the low degree of overlap of signals for the ethylene group (Figure 2.4). The atom numbering system used in this discussion appears in Figure 2.1. Cross-peaks in COSY spectra (Supporting Information) and ROESY spectra (Figure 2.6 and Supporting Information) identify a multiplet as a C(4/7)H or C(5/6)H signal. In the solid state, the *endo*-NH protons have a shorter average distance to the *endo*-C(4/7)H protons (2.20 \AA) than to the *exo*-C(4/7)H protons (2.71 \AA),

and the *exo*-NH protons have a shorter average distance to the *exo*-C(4/7)H protons (2.22 Å) than to the *endo*-C(4/7)H protons (2.43 Å). Thus, from NH-CH NOE cross-peak intensities, the CH

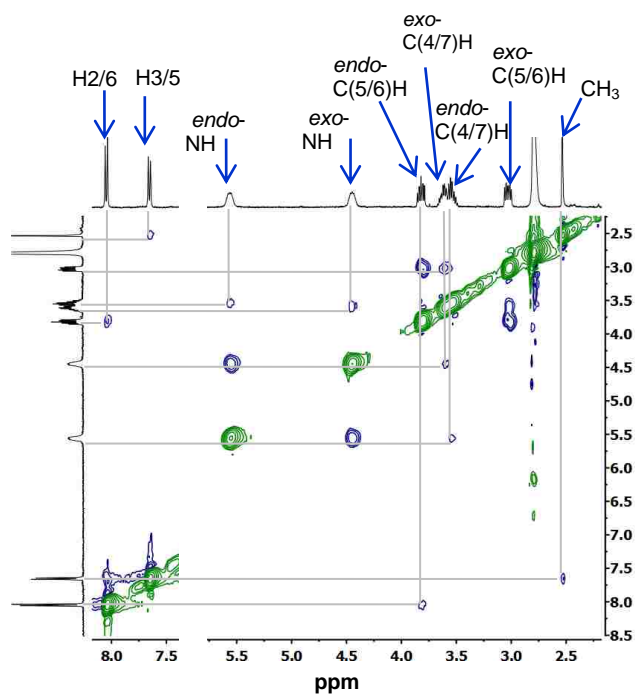


Figure 2.6. ^1H - ^1H ROESY spectrum of $[\text{Re}(\text{CO})_3(\text{N}(\text{SO}_2\text{tol})\text{dien})]\text{PF}_6$ (**6**) in acetone- d_6 at 25 °C. An expanded version of this figure is in Supporting Information.

multiplets at 3.52 ppm and 3.55 ppm are assigned to the *endo*- and *exo*-C(4/7)H protons, respectively. The average distance from the *exo*-C(4/7)H protons is shorter to the *exo*-C(5/6)H protons (2.30 Å) than to the *endo*-C(5/6)H protons (2.85 Å). In the ROESY spectrum, a strong NOE cross-peak from the *exo*-C(4/7)H multiplet to the most upfield multiplet at 3.02 ppm thus assigns the multiplet to the *exo*-C(5/6)H protons. Similarly, an NOE cross-peak from the *endo*-C(4/7)H multiplet to the most downfield multiplet at 3.81 ppm assigns this multiplet to the *endo*-C(5/6)H protons. The tosyl methyl singlet (2.53 ppm) of **6** has an NOE cross-peak to the tosyl doublet at 7.65 ppm, unambiguously assigning it to the tosyl H3/5 protons and the other tosyl doublet to H2/6. The latter is more downfield (8.05 ppm), consistent with the proximity of the H2/6 protons to the sulfonamide group, shown in previous work on the

[Re(CO)₃(N(SO₂tol)dpa)]PF₆ analogue to have an electron-withdrawing inductive effect.³⁵ A strong H2/6-to-*endo*-C(5/6)H NOE cross-peak and a very weak H2/6-to-*exo*-C(5/6)H cross-peak is consistent with the shorter H2/6-to-*endo*-C(5/6)H average distance (2.60 Å) compared to the H2/6-to-*exo*-C(5/6)H average distance (2.81 Å), thus confirming the assignment of the *endo*-C(5/6)H and *exo*-C(5/6)H signals (Table 2.3).

¹H NMR Shift Interpretation. The *exo*-C(5/6)H signal is more upfield for 5 and 6 than for 4 in acetone-*d*₆ (Figure 2.4). In 6 (Figure 2.2 and Chart 2.1), the relative average distance from the centroid of the tosyl ring to the *exo*-C(5/6)H protons (which point toward the center of the ring) is shorter (3.45 Å) than the distance (4.09 Å) to the *endo*-C(5/6)H protons (Chart 2.1). Thus, the anisotropic effect of the aromatic ring of the R group explains the unusually upfield shift of the *exo*-C(5/6)H multiplet at 3.02 ppm in acetone-*d*₆ for 5 and 6. This explanation is supported by the fact that the *exo*-C(5/6)H signal is not so upfield for 4, a complex in which R lacks an aromatic ring. This same trend, with the methylene *endo*-CH signal downfield from the *exo*-CH signal and the latter signal appearing more upfield when R has an aromatic ring (tol) than when R = Me, was reported for the [Re(CO)₃(N(SO₂R)dpa)]X complexes.³⁵

Coordination of a ligand normally leads to downfield ¹H NMR shift changes attributable to the metal inductive effect. Upon coordination to Re^I of the free N(SO₂R)dien ligands 1 and 3 in acetonitrile-*d*₃, the downfield shift for signals of the C4/7 protons is ~ 0.4 ppm. For example, the C(4/7)H₂ triplet for 1 shifts from 2.76 ppm downfield to ~3.18 ppm for the overlapping C(4/7)H signals of [Re(CO)₃(N(SO₂Me)dien)]PF₆ (4). A corollary of the relationships of the distance of the *exo*-C(5/6)H protons to the aromatic groups mentioned above for 6 is that the *endo*-C(5/6)H protons are farther from R, and the shift of the *endo*-C(5/6)H signal for 4 and 6 is not influenced by the R group. Hence, compared to the C(5/6)H₂ triplets of 1 and 3, the *endo*-C(5/6)H signals of 4 and 6 are shifted downfield (~0.4 ppm to ~3.5 ppm in acetonitrile-*d*₃).

Remarkably, upon coordination of $N(\text{SO}_2\text{Me})\text{dien}$ to form 4, the *exo*-C(5/6)H signal (expected to shift downfield by ~ 0.4 ppm owing to inductive effects) is shifted slightly upfield (0.14 ppm) compared to the free ligand triplet, even though $R = \text{Me}$ is not anisotropic. Presently there are not enough other complexes with assigned signals for us to interpret the factors influencing shift, but the upfield shift may be caused by the SO_2 group anisotropy. Also, although the reaction of free amines with acetone prevents comparison using acetone- d_6 , in DMSO- d_6 (the other solvent rather different from acetonitrile- d_3 that we used for the complexes) the same pattern of shift changes was observed upon coordination of 1 to form 4, including the slight upfield shift of the *exo*-C(5/6)H signal (Supporting Information). Thus, solvent effects are probably not causing the unexpected upfield shift.

The methyl ^1H NMR signal of $N(\text{SO}_2\text{Me})\text{dien}$ (1) shifted downfield upon coordination of 1 to form $[\text{Re}(\text{CO})_3(N(\text{SO}_2\text{Me})\text{dien})]\text{PF}_6$ (4) in both acetonitrile- d_3 (0.47 ppm) and DMSO- d_6 (0.66 ppm) (Experimental Section and Supporting Information). These downfield shifts can be attributed to the Re^{I} inductive effect. We previously attributed a similar downfield shift (~ 0.76 ppm) observed for $[\text{Re}(\text{CO})_3(N(\text{SO}_2\text{Me})\text{dpa})]\text{PF}_6$ to the Re^{I} inductive effect.³⁵ A slightly greater downfield shift (~ 1.03 ppm) relative to the free ligand reported for the $[\text{Re}(\text{CO})_3(N(\text{Me})\text{dien})]\text{PF}_6$ complex in DMSO- d_6 ⁴⁶ can be explained by the transmission of the inductive effect through just two bonds (N–C and C–H) versus three bonds in 4 (N–S, S–C, and C–H).

^{13}C NMR Shift Interpretation. Unlike ^1H NMR signals, the shifts of ^{13}C NMR signals are not very dependent on solvent effects (e.g., as discussed for the NH signals) or on aromatic ring anisotropic effects (e.g., as discussed for *exo*-C(5/6)H signals). Instead, ^{13}C NMR signals are influenced more significantly by other factors, with signals of aliphatic carbons most frequently being shifted downfield by metal inductive effects. Analysis of ^{13}C NMR shifts can often provide insight into the effect of a diamagnetic metal center on the ligand. Therefore, we undertook the

unambiguous assignment of the ^{13}C NMR signals of selected ligands and complexes as described in Supporting Information. The ^{13}C NMR signals of the chelate ring carbons shift downfield, as expected, by 4 to 5 ppm upon coordination of the tridentate ligands 1 and 3 to form complexes 4 and 6, and the shifts for the C4/7 and C5/6 signals of 4 are very similar to the shifts for these signals of 6 (data for acetonitrile- d_3 are reported in Supporting Information).

The methyl group ^{13}C NMR signal for the free $N(\text{SO}_2\text{Me})\text{dien}$ ligand (1) appears at 37.87 ppm, but it is shifted considerably *upfield* for $[\text{Re}(\text{CO})_3(N(\text{SO}_2\text{Me})\text{dien})]\text{PF}_6$ (4) (33.02 ppm, Supporting Information). The almost 5 ppm upfield change in shift when 1 forms 4 is unusual in that ^{13}C NMR shifts are influenced mainly by through-bond effects, such as the metal inductive effect expected to produce a downfield shift. For example, a significant ~ 14 ppm downfield ^{13}C NMR shift was observed for the methyl group of $[\text{Re}(\text{CO})_3(N(\text{Me})\text{dien})]\text{PF}_6$ (56.48 ppm) compared to the methyl group in the free $N(\text{Me})\text{dien}$ ligand (42.72 ppm) in acetonitrile- d_3 .⁵¹ Because of the unexpected upfield direction of the shift change of the methyl ^{13}C NMR signal of 4, we measured the ^{13}C NMR shift of the methyl signal of $[\text{Re}(\text{CO})_3(N(\text{SO}_2\text{Me})\text{dpa})]\text{PF}_6$ in DMSO- d_6 (32.88 ppm), a value ~ 6.5 ppm upfield compared to the methyl signal in the free $N(\text{SO}_2\text{Me})\text{dpa}$ ligand (39.24 ppm).⁵¹ We attribute the observed unusual upfield shift for 4 to the fact that the sulfonamide N undergoes an sp^2 -to- sp^3 rehybridization upon coordination to Re^{I} in both 4 and $[\text{Re}(\text{CO})_3(N(\text{SO}_2\text{Me})\text{dpa})]\text{PF}_6$.

Challenge Reactions of $[\text{Re}(\text{CO})_3(N(\text{SO}_2\text{tol})\text{dien})]\text{PF}_6$ (6) in DMSO- d_6 . No change was observed in the ^1H NMR signals of **6** (5 mM), even after six months, indicating that **6** is robust. However, addition of diethylenetriamine to 5 mM solutions of **6** to create solutions that were 50 mM or 10 mM in diethylenetriamine led to the elimination of all peaks for **6** by the next day and after about 6 days ($t_{1/2} \sim 28$ h), respectively. In both cases, the final ^1H NMR spectrum exhibits peaks for the $N(\text{SO}_2\text{tol})\text{dien}$ ligand (3) and for the known $[\text{Re}(\text{CO})_3(N(\text{H})\text{dien})]\text{PF}_6$ complex.⁴⁶

No signals indicating any intermediates were observed. The complete displacement of the coordinated $N(\text{SO}_2\text{tol})\text{dien}$ ligand of **6** by 10 mM diethylenetriamine establishes that although the Re–N bonds involving the central donor of $N(\text{SO}_2\text{R})\text{dien}$ ligands have normal lengths, the donor ability of the central sulfonamide nitrogen atom is lower than that of the central nitrogen atom of diethylenetriamine.

A related study³⁸ was reported for the neutral $\text{Re}(\text{CO})_3(\text{tmbSO}_2\text{-dien})$ complex. The coordinated unsymmetrical monoanionic NNN donor ligand, $\text{tmbSO}_2\text{-dien}^-$ (Chart 2.2), employed in that study has a 2,4,6-trimethylbenzenesulfonyl (tmbSO_2) group linked to one of the terminal N atoms of diethylenetriamine. The terminal donor of the free ligand prior to coordination is a secondary sulfonamide of the type $(\text{RSO}_2)\text{R}'\text{NH}$. When 10 molar equiv of diethylenetriamine was added to a solution of $\text{Re}(\text{CO})_3(\text{tmbSO}_2\text{-dien})$ (3 mM, $\text{DMSO-}d_6$), no coordinated $\text{tmbSO}_2\text{-dien}^-$ ligand was displaced, even after the solution was heated at $\sim 60^\circ\text{C}$.³⁸ Thus, the deprotonated monoanionic $\text{tmbSO}_2\text{-dien}^-$ ligand is clearly a better ligand than neutral $N(\text{SO}_2\text{tol})\text{dien}$.

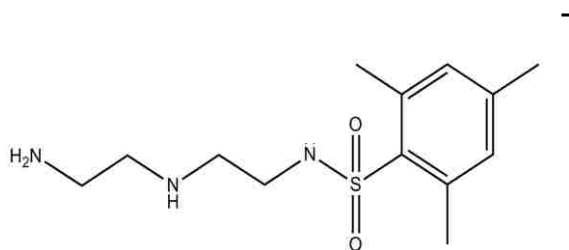


Chart 2.2. The $\text{tmbSO}_2\text{-dien}^-$ monoanionic ligand.³⁸

If the central tertiary sulfonamide donor in $N(\text{SO}_2\text{tol})\text{dien}$ were coordinated weakly enough to the Re in $[\text{Re}(\text{CO})_3(N(\text{SO}_2\text{R})\text{dien})]\text{PF}_6$ complexes, a good monodentate ligand might be able to substitute for the coordinated sulfonamide group. Therefore, we conducted a challenge experiment in which the strongly basic, potentially monodentate 4- Me_2Npy ligand was added to

$[\text{Re}(\text{CO})_3(\text{N}(\text{SO}_2\text{tol})\text{dien})]\text{PF}_6$ (**6**). No ^1H NMR spectral changes were observed over many days, even with a tenfold excess of 4-Me₂Npy. Such evidence indicates that the central sulfonamide bond is strong enough to stay coordinated to Re, even in the presence of an excess of a strong monodentate ligand. Also, the results show that the $[\text{Re}(\text{CO})_3(\text{N}(\text{SO}_2\text{tol})\text{dien})]\text{PF}_6$ complex is resistant to strong base, an advantage over $[\text{Re}(\text{CO})_3(\text{N}(\text{SO}_2\text{Me})\text{dpa})]\text{PF}_6$, which decomposes readily in the presence of base.³⁵

Solubility of $[\text{Re}(\text{CO})_3(\text{N}(\text{SO}_2\text{tol})\text{dien})]\text{PF}_6$ (6**) in Water.** A mixture of 5 mg of $[\text{Re}(\text{CO})_3(\text{N}(\text{SO}_2\text{tol})\text{dien})]\text{PF}_6$ (**6**) and 450 μL of D₂O gave a clear solution when heated in a boiling water bath for 30 min. The ^1H NMR spectrum of this solution, which compares favorably with spectra of **6** in other solvents (Figure 2.4), has four methylene multiplets, whereas the *N*(SO₂tol)dien ligand has two methylene triplets in D₂O. These results established that **6** dissolved unchanged to an extent much greater than is required for radiopharmaceuticals and that **6** is robust even in a hot aqueous solution. Furthermore, another experiment conducted using 5 mg of **6** also showed complete dissolution (observed visibly and by ^1H NMR spectroscopy) of **6** in a 450 μL :20 μL of D₂O:DMSO mixture (95.7%:4.3%). In contrast, similar NMR experiments carried out using the previously reported $[\text{Re}(\text{CO})_3(\text{N}(\text{SO}_2\text{Me})\text{dpa})]\text{PF}_6$ complex³⁵ show that even the $[\text{Re}(\text{CO})_3(\text{N}(\text{SO}_2\text{R})\text{dpa})]\text{PF}_6$ complex having the smallest R group is insoluble in D₂O or in D₂O:DMSO (95.7%:4.3%).

2.4 Conclusions

From the present results with $[\text{Re}(\text{CO})_3(\text{N}(\text{SO}_2\text{R})\text{dien})]\text{PF}_6$ complexes, in which the chelate rings are less rigid, we conclude that the M–N bond of normal length observed was not a result of the rigid tridentate framework in the $[\text{Re}(\text{CO})_3(\text{N}(\text{SO}_2\text{R})\text{dpa})]\text{X}^{35}$ complexes. In both series of complexes, the methyl ^{13}C NMR signal of the R = Me member of the series exhibited a very unusual *upfield* shift for an aliphatic carbon signal upon coordination of the ligand. This

result, attributed to the similar sp^2 -to- sp^3 rehybridization of the sulfonamide N upon coordination to Re^I in both series of complexes, further establishes that coordination of the sulfonamide N is not influenced by the rigidity of the $N(SO_2R)dpa$ chelate rings. The decomposition of the $[Re(CO)_3(N(SO_2R)dpa)]X$ complexes by base³⁵ led us to hypothesize that base was attacking the coordinated $N(SO_2R)dpa$ ligand, most likely by deprotonating the CH_2 group, and that the low electrophilicity of the $Z = CH_2NH_2$ group of the $N(CH_2CH_2NH_2)_2$ framework would confer stability toward base. The stability of the new $[Re(CO)_3(N(SO_2R)dien)]PF_6$ complexes toward base supports these hypotheses and allowed us to conduct a challenge reaction study with the basic $N(H)dien$ ligand. $N(H)dien$ replaced the coordinated $N(SO_2tol)dien$ ligand in $[Re(CO)_3(N(SO_2tol)dien)]PF_6$, indicating that the neutral sulfonamide N central donor in $N(SO_2tol)dien$ is a somewhat weaker donor than the central traditional sp^3 N donor in $N(H)dien$. Nevertheless, the new $[Re(CO)_3(N(SO_2R)dien)]PF_6$ complexes are long lived, even in the presence of base, and are relatively robust to heat treatment. As expected, the moderately hydrophilic character of the $Z = CH_2NH_2$ group of the $N(CH_2CH_2NH_2)_2$ framework also confers water solubility on the $[Re(CO)_3(N(SO_2R)dien)]PF_6$ complexes. The aqueous solubility of the new ligands and complexes is much higher than necessary for radiopharmaceutical kit formulation. Also, there are perceived advantages in using small chelate ligands when constructing bioconjugates, and the $N(CH_2CH_2NH_2)_2$ framework is relatively small. Thus, the results obtained here suggest that $N(SO_2R)dien$ ligands should be explored in the development of radiopharmaceuticals, including bioconjugates.

2.5 References

- (1) Schibli, R.; Schubiger, A. P. *Eur. J. Nucl. Med. Mol. Imaging* **2002**, *29*, 1529-1542.
- (2) Liu, S. *Chem. Soc. Rev.* **2004**, *33*, 445-461.
- (3) Lipowska, M.; Marzilli, L. G.; Taylor, A. T. *J. Nucl. Med.* **2009**, *50*, 454-460.

- (4) Lipowska, M.; He, H.; Malveaux, E.; Xu, X.; Marzilli, L. G.; Taylor, A. T. *J. Nucl. Med.* **2006**, *47*, 1032-1040.
- (5) Maresca, K. P.; Marquis, J. C.; Hillier, S. M.; Lu, G.; Femia, F. J.; Zimmerman, C. N.; Eckelman, W. C.; Joyal, J. L.; Babich, J. *Bioconjugate Chem.* **2010**, *21*, 1032-1042.
- (6) Alberto, R.; N'Dongo, H. P.; Clericuzio, M.; Bonetti, S.; Gabano, E.; Cassino, C.; Ravera, M.; Osella, D. *Inorg. Chim. Acta* **2009**, *362*, 4785-4790.
- (7) Taylor, A. T.; Lipowska, M.; Marzilli, L. G. *J. Nucl. Med.* **2010**, *51*, 391-396.
- (8) Taylor, A. T.; Lipowska, M.; Cai, H. *J. Nucl. Med.* **2013**, *54*, 578-584.
- (9) Alberto, R.; Schibli, R.; Egli, A.; Schubiger, A. P.; Abram, U.; Kaden, T. A. *J. Am. Chem. Soc.* **1998**, *120*, 7987-7988.
- (10) Alberto, R.; Ortner, K.; Wheatley, N.; Schibli, R.; Schubiger, A. P. *J. Am. Chem. Soc.* **2001**, *123*, 3135-3136.
- (11) Schibli, R.; Bella, R. L.; Alberto, R.; Garcia-Garayoa, E.; Ortner, K.; Abram, U.; Schubiger, A. P. *Bioconjugate Chem.* **2000**, *11*, 345-351.
- (12) Abram, U.; Alberto, R. *J. Braz. Chem. Soc.* **2006**, *17*, 1486-1500.
- (13) Duatti, A. In *Technetium-99m radiopharmaceuticals : status and trends*; International Atomic Energy Agency: Vienna, 2009, p 7-17.
- (14) Alberto, R. *Eur. J. Nucl. Med. Mol. Imaging* **2003**, *30*, 1299-1302.
- (15) Banerjee, S. R.; Maresca, K. P.; Francesconi, L.; Valliant, J.; Babich, J. W.; Zubieta, J. *Nucl. Med. Biol.* **2005**, *32*, 1-20.
- (16) Bartholomä, M.; Valliant, J.; Maresca, K. P.; Babich, J.; Zubieta, J. *Chem. Commun. (Cambridge, U.K.)* **2009**, 493-512.
- (17) Alberto, R. In *Technetium-99m radiopharmaceuticals : status and trends*; International Atomic Energy Agency: Vienna, 2009, p 19-40.
- (18) He, H.-Y.; Lipowska, M.; Xu, X.; Taylor, A. T.; Carlone, M.; Marzilli, L. G. *Inorg. Chem.* **2005**, *44*, 5437-5446.
- (19) Wei, L.; Babich, J. W.; Ouellette, W.; Zubieta, J. *Inorg. Chem.* **2006**, *45*, 3057-3066.
- (20) Desbouis, D.; Struthers, H.; Spiwok, V.; Küster, T.; Schibli, R. *J. Med. Chem.* **2008**, *51*, 6689-6698.
- (21) Lipowska, M.; He, H.; Xu, X.; Taylor, A. T.; Marzilli, P. A.; Marzilli, L. G. *Inorg. Chem.* **2010**, *49*, 3141-3151.
- (22) Alberto, R.; Schibli, R.; Schubiger, A. P.; Abram, U.; Pietzsch, H. J.; Johannsen, B. *J. Am. Chem. Soc.* **1999**, *121*, 6076-6077.

- (23) He, H.-Y.; Lipowska, M.; Xu, X.; Taylor, A. T.; Marzilli, L. G. *Inorg. Chem.* **2007**, *46*, 3385-3394.
- (24) He, H.-Y.; Lipowska, M.; Christoforou, A. M.; Marzilli, L. G.; Taylor, A. T. *Nucl. Med. Biol.* **2007**, *34*, 709-716.
- (25) Kyprianidou, P.; Tsoukalas, C.; Chiotellis, A.; Papagiannopolu, D.; Raptopoulou, C. P.; Terzis, A.; Pelecanou, M.; Papadopoulos, M.; Pirmettis, I. *Inorg. Chim. Acta* **2011**, *370*, 236-242.
- (26) Boros, E.; Häfeli, U. O.; Patrick, B. O.; Adam, M. J.; Orvig, C. *Bioconjugate Chem.* **2009**, *20*, 1002-1009.
- (27) Klenc, J.; Lipowska, M.; Marzilli, L. G.; Taylor, A. T. *Eur. J. Inorg. Chem.* **2012**, 4334-4344.
- (28) Schibli, R.; Schwarzbach, R.; Alberto, R.; Ortner, K.; Schmalte, H.; Dumas, C.; Egli, A.; Schubiger, P. A. *Bioconjugate Chem.* **2002**, *13*, 750-756.
- (29) Xia, J.; Wang, Y.; Li, G.; Yu, J.; Yin, D. *J. Radioanal. Nucl. Chem.* **2009**, *279*, 245-252.
- (30) Banerjee, S. R.; Levadala, M. K.; Lazarova, N.; Wei, L.; Valliant, J. F.; Stephenson, K. A.; Babich, J. W.; Maresca, K. P.; Zubieta, J. *Inorg. Chem.* **2002**, *41*, 6417-6425.
- (31) Pietzsch, H. J.; Gupta, A.; Reisgys, M.; Drews, A.; Seifert, S.; Syhre, R.; Spies, H.; Alberto, R.; Abram, U.; Schubiger, P. A.; Johannsen, B. *Bioconjugate Chem.* **2000**, *11*, 414-424.
- (32) Schubiger, P. A.; Alberto, R.; Smith, A. *Bioconjugate Chem.* **1996**, *7*, 165-177.
- (33) Hom, R.; Katzenellenbogen, J. *Nucl. Med. Biol.* **1997**, *24*, 485-498.
- (34) Dilworth, J. R.; Parrot, S. *Chem. Soc. Rev.* **1998**, *27*, 43-55.
- (35) Perera, T.; Abhayawardhana, P.; Marzilli, P. A.; Fronczek, F. R.; Marzilli, L. G. *Inorg. Chem.* **2013**, *52*, 2412-2421.
- (36) Storr, T.; Fisher, C. L.; Mikata, Y.; Yano, S.; Adam, M. J.; Orvig, C. *Dalton Trans.* **2005**, 654-655.
- (37) Alberto, R. *Top. Organomet. Chem.* **2010**, *32*, 219-246.
- (38) Christoforou, A. M.; Fronczek, F. R.; Marzilli, P. A.; Marzilli, L. G. *Inorg. Chem.* **2007**, *46*, 6942-6949.
- (39) Supuran, C. T.; Casini, A.; Scozzafava, A. *Med. Res. Rev.* **2003**, *23*, 535-558.
- (40) Drew, J. *Science* **2000**, *287*, 1960-1964.
- (41) Epstein, M. E.; Amodio-Groton, M.; Sadick, N. S. *J. Am. Acad. Dermatol.* **1997** *37*, 365-381.

- (42) Gadad, A. K.; Mahajanshetti, C. S.; Nimbalkar, S.; Raichurkar, A. *Eur. J. Med. Chem.* **2000**, *35*, 853-857.
- (43) Li, J. J.; Anderson, D. G.; Burton, E. G.; Cogburn, J. N.; Collins, J. T.; Garland, D. J.; Gregory, S. A.; Huang, H.-C.; Isakson, P. C.; Koboldt, C. M.; Logusch, E. W.; Norton, M. B.; Perkins, W. E.; Reinhard, E. J.; Seibert, K.; Veenhuizen, A. W.; Zang, Y.; Reitz, D. B. *J. Med. Chem.* **1995**, *38*, 4570-4578.
- (44) Maren, T. H. *Annu. Rev. Pharmacol. Toxicol.* **1976**, *16*, 309-327.
- (45) Renzi, G.; Scozzafava, A.; Supuran, C. T. *Bioorg. Med. Chem. Lett.* **2000**, *10*, 673-676.
- (46) Christoforou, A. M.; Marzilli, P. A.; Fronczek, F. R.; Marzilli, L. G. *Inorg. Chem.* **2007**, *46*, 11173-11182.
- (47) Otwinowski, Z.; Minor, W. *Macromolecular Crystallography, Part A, Methods in Enzymology*; New York Academic Press: New York, 1997; Vol. 276, pp. 307-326.
- (48) Sheldrick, G. *SADABS*, **2004**, University of Göttingen, Germany.
- (49) Lane, S. R.; Veerendra, B.; Rold, T. L.; Sieckman, G. L.; Hoffman, T. J.; Jurisson, S. S.; Smith, C. J. *Nucl. Med. Biol.* **2008**, *35*, 263-272.
- (50) Perera, T.; Marzilli, P. A.; Fronczek, F. R.; Marzilli, L. G. *Inorg. Chem.* **2010**, *49*, 5560-5572.
- (51) Perera, T.; Abhayawardhana, P.; Louisiana State University, Baton Rouge, LA. Unpublished work, 2013.
- (52) Canovese, L.; Visentin, F.; Chessa, G.; Uguagliati, P.; Levi, C.; Dolmella, A.; Bandoli, G. *Organometallics* **2006**, *25*, 5355-5365.
- (53) Perera, T.; Fronczek, F. R.; Marzilli, P. A.; Marzilli, L. G. *Inorg. Chem.* **2010**, *49*, 7035-7045.
- (54) Veltzé, S.; Egdal, R. K.; Johansson, F. B.; Bond, A. D.; McKenzie, C. J. *Dalton Trans.* **2009**, 10495-10504.
- (55) Lee, W.; Tseng, H.; Kuo, T. *Dalton Trans.* **2007**, 2563-2570.
- (56) Gunnlaugsson, T.; Leonard, J.; Mulready, S.; Nieuwenhuyzen, M. *Tetrahedron* **2004**, *60*, 105-113.
- (57) Rodriguez, V.; Gutierrez-Zorrilla, J. M.; Vitoria, P.; Luque, A.; Roman, P.; Martinez-Ripoll, M. *Inorg. Chim. Acta* **1999**, *290*, 57-63.
- (58) Orpen, A. G. *Chem. Soc. Rev.* **1993**, *22*, 191-197.
- (59) Harris, S. E.; Pascual, I.; Orpen, A. G. *J. Chem. Soc., Dalton Trans.* **2001**, 2996-3009.

CHAPTER 3

NEW MONODENTATE AMIDINE SUPERBASIC LIGANDS WITH A SINGLE CONFIGURATION IN *fac*-[Re(CO)₃(5,5'- OR 6,6'-Me₂BIPYRIDINE)(AMIDINE)]BF₄ COMPLEXES

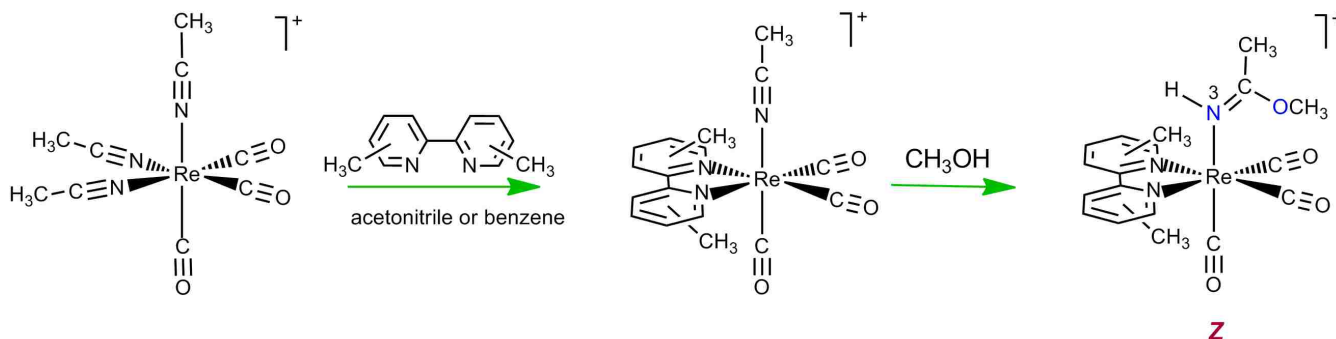
3.1 Introduction

Owing to the many ideal properties of the *fac*-[M^I(CO)₃] core in radiopharmaceuticals, *fac*-[M^I(CO)₃L]ⁿ (M = various isotopes of Tc and Re) complexes have recently been receiving much attention.¹⁻⁷ Some *fac*-[^{99m}Tc^I(CO)₃L]ⁿ imaging agents have undergone evaluation in humans,⁸⁻⁹ and *fac*-[^{186/188}Re^I(CO)₃L]ⁿ agents are emerging as being among the most promising radionuclides for therapeutic applications.^{2,10-11} At present, great interest surrounds the concept of combining ^{99m}Tc and ^{186/188}Re with biomolecules in order to produce selective targeting agents.^{5-6,11-17} *fac*-[Re^I(CO)₃L]ⁿ complexes prepared with natural-abundance rhenium are excellent models for the short-lived *fac*-[M^I(CO)₃L]ⁿ radiopharmaceuticals and are almost non-radioactive. Thus, the investigation of *fac*-[Re^I(CO)₃L]ⁿ complexes both aids in interpreting the chemistry of the radiopharmaceuticals and offers the potential for the discovery of new chemistry, some of which could be applied to radiopharmaceutical development.¹⁸⁻¹⁹

Our objectives are aimed at expanding the known chemistry of complexes with the *fac*-[Re^I(CO)₃] core.^{7,20-21} Syntheses in aqueous media carried out with the commonly used precursor, aqueous *fac*-[Re^I(CO)₃(H₂O)₃]⁺,²² have some limitations.²³ Thus, we have recently investigated the suitability of *fac*-[Re(CO)₃(CH₃CN)₃]X (X = PF₆ or BF₄) as a precursor for the synthesis of new complexes in organic solvents.²³ Treatment of *fac*-[Re(CO)₃(CH₃CN)₃]X with

*Reproduced with permission from American Chemical Society: Abhayawardhana, P.; Marzilli, P. A.; Perera, T.; Fronczek, F. R.; Marzilli, L. G. "New Monodentate Amidine Superbasic Ligands with a Single Configuration in *fac*-[Re(CO)₃(5,5'- or 6,6'-Me₂bipyridine)(amidine)]BF₄ Complexes". *Inorg. Chem.* **2012**, 51, 7271–7283. Copyright 2015 American Chemical Society.

bidentate aromatic sp^2 N-donor bipyridine-type L in either acetonitrile or benzene as solvent produced the desired *fac*-[Re(CO)₃(L)(CH₃CN)]X complexes in excellent yield [e.g., when L = 2,2'-bipyridine (bipy) or a dimethyl-2,2'-bipyridine (Me₂bipy), Scheme 3.1].²⁴ However, a recent study revealed that reactions to form these complexes in methanol instead led to addition of solvent to bound acetonitrile, forming iminoether complexes, *fac*-[Re(CO)₃(Me₂bipy)(HNC(CH₃)OCH₃)]BF₄.²³ The original acetonitrile carbon with a triple bond to the rhenium-bound nitrogen (N3) is converted in the reaction to an iminoether carbon (C_{ie}), and N3 adds a proton and rehybridizes from sp to sp^2 (Scheme 3.1). The C_{ie}-N3 bond has double-bond character, and the iminoether ligand potentially can have *E* and *Z* configurations. However, the *Z* isomer (Scheme 3.1) is favored exclusively because the axial iminoether ligand steric repulsions with the equatorial ligands (the two CO's and the Me₂bipy) are lower for the *Z* configuration than for the *E* configuration.²³



Scheme 3.1. General reaction scheme for the synthesis of [Re(CO)₃(L)(CH₃CN)]⁺ starting material²⁴ and for the formation of [Re(CO)₃(Me₂bipy)(HNC(CH₃)OCH₃)]⁺ (iminoether) complexes.²³

The reactions of *fac*-[Re(CO)₃(5,5'-Me₂bipy)(CH₃CN)]⁺ (1) with alcohols to form iminoethers were slow.²³ On the other hand, the related reactions of primary amines with 1 to form amidine complexes, *fac*-[Re(CO)₃(5,5'-Me₂bipy)(HNC(CH₃)NHR)]⁺, were more rapid.²⁵

However, these amidine complexes exist as mixtures of isomers. In the $\text{HNC}(\text{CH}_3)\text{NHR}$ ligands, both C–N bonds involving the amidine carbon (C_{am}), $\text{C}_{\text{am}}\text{--N}_3$ and $\text{C}_{\text{am}}\text{--N}_4$, have double-bond character. This situation raises the possibility that four configurations (E , E' , Z and Z') of the amidine ligands could exist (Figure 3.1). In fact, three configurations (E , E' , and Z) were found.²⁵ The isomers are named using these configurations. As illustrated and discussed below, steric effects strongly influence the relative abundance of the isomers.

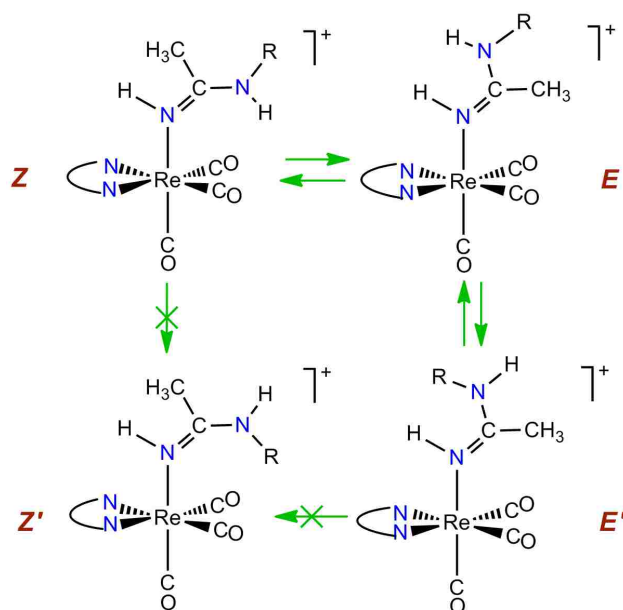


Figure 3.1. The four conceivable $[\text{Re}(\text{CO})_3(5,5'\text{-Me}_2\text{bipy})\text{HNC}(\text{CH}_3)\text{NHR}]^+$ isomers, in which N–N denotes the 5,5'-Me₂bipy ligand. The isomers with the E' and Z configurations are typically abundant. The isomer with the Z' configuration is unstable and not observed.²⁵ The isomer with the E configuration is known, but its abundance is usually too low to allow detection. However, as illustrated here, the pathway between the E' and Z configurations undoubtedly passes through the E configuration and not the Z' configuration.

The amidine group, such as that present in $\text{fac-}[\text{Re}(\text{CO})_3(5,5'\text{-Me}_2\text{bipy})(\text{HNC}(\text{CH}_3)\text{NHR})]\text{BF}_4$ complexes,²⁵ has the potential to serve as a linking group in the conjugation of the $\text{fac-}[\text{M}(\text{CO})_3]^+$ core ($\text{M} = {}^{99\text{m}}\text{Tc}$ and ${}^{186/188}\text{Re}$ radionuclides) with biomedical targeting moieties. The nitrogen donor group in amidine (and iminoether) ligands is superbasic.^{23,25} However, the finding of isomers of these complexes (Figure 3.1) complicates the

development of agents useful for biomedical imaging. Therefore, we now explore amidine ligands with a C_2 -symmetrical NR_2 substituent in place of the NHR substituent. This change eliminates the possibility of two configurations about the $C_{am}-N_4$ bond, restricting the number of conceivable isomers to two (with E or Z configurations about the $C_{am}-N_3$ bond). Furthermore, we expected that a large difference in substituent bulk (NR_2 vs. CH_3) on C_{am} should favor the E isomer exclusively.

We chose C_2 -symmetrical saturated heterocyclic secondary amines in our synthetic strategy because many related symmetric heterocyclic amine derivatives are present in ^{99m}Tc and $^{186/188}Re$ agents^{13,26-31} and in successful drugs.³¹⁻³² Because their use as ubiquitous building blocks in the synthesis of pharmaceuticals³¹ has provided information on the synthesis and properties of such amines, these amines are particularly desirable candidates for study. Indeed, a modified arylpiperazine was employed in one of the earliest examples of a *fac*- $[^{99m}Tc(CO)_3]^+$ -containing agent linked to a targeting biomolecule.¹³ All of the new complexes discussed below have the facial geometry, and thus from this point onward we omit the *fac*- designation when discussing specific compounds.

3.2 Experimental Section

Starting Materials. $Re(CO)_5Br$ was synthesized as described in the literature.³³ $Re_2(CO)_{10}$, 5,5'-dimethyl-2,2'-bipyridine (5,5'-Me₂bipy), 6,6'-dimethyl-2,2'-bipyridine (6,6'-Me₂bipy), piperidine, homopiperidine, heptamethyleneimine, morpholine, piperazine, and $AgBF_4$ were obtained from Aldrich. $[Re(CO)_3(CH_3CN)_3]BF_4$ (prepared by a slight modification of a known procedure³⁴) was used to prepare $[Re(CO)_3(5,5'$ - or $6,6'$ -Me₂bipy)(CH₃CN)]BF₄.²⁴

NMR Measurements. 1H NMR spectra were recorded on a 400 MHz Bruker spectrometer. Peak positions are relative to TMS or to solvent residual peak, with TMS as reference. All NMR data were processed with TopSpin and Mestre-C software.

X-ray Data Collection and Structure Determination. Intensity data were collected at low temperature on a Nonius Kappa CCD diffractometer fitted with an Oxford Cryostream cooler with graphite-monochromated Mo K α ($\lambda = 0.71073 \text{ \AA}$) radiation. Data reduction included absorption corrections by the multi-scan method, with HKL SCALEPACK.³⁵ All X-ray structures were determined by direct methods and difference Fourier techniques and refined by full-matrix least squares by using SHELXL-97.³⁶ All non-hydrogen atoms were refined anisotropically. All H atoms were visible in difference maps, but were placed in idealized positions, except for N-H hydrogen atoms, for which coordinates were refined. A torsional parameter was refined for each methyl group. For compounds 4, 5, and 9, the BF₄⁻ site was shared by a few percent bromide, and the occupancies of the two anions were constrained to sum to unity in the refinement. In compound **10**, the BF₄⁻ is disordered into two orientations and the 8-membered ring is disordered into two conformations. The occupancies refined to 0.891(5):0.109(5) for the anion and 0.521(6):0.479(6) for the 8-membered ring. Crystal data and details of refinements are listed in Tables 3.1 and 3.2.

General Synthesis of Amidine Complexes. An acetonitrile solution (6 mL) of [Re(CO)₃(5,5'-Me₂bipy)(CH₃CN)]BF₄ (1) or [Re(CO)₃(6,6'-Me₂bipy)(CH₃CN)]BF₄ (2) (40 mg, 0.06 mmol) was treated with an amine (0.60 mmol), and the reaction mixture was stirred at room temperature for 30 min or as specified. The volume was reduced to ~1 mL by rotary evaporation. Addition of diethyl ether to the point of cloudiness (~10-200 mL) produced a yellow crystalline material that was collected on a filter, washed with diethyl ether, and dried. All ¹H NMR spectra recorded both immediately upon dissolution of the products (3 to 12) and subsequently showed signals for one isomer.

Table 3.1. Crystal Data and Structural Refinement for Complexes Having the General Formula, $[\text{Re}(\text{CO})_3(5,5'\text{-Me}_2\text{bipy})(\text{HNC}(\text{CH}_3)\text{N}(\text{CH}_2\text{CH}_2)_2\text{Y})]\text{BF}_4$

Y =	CH ₂	(CH ₂) ₂	(CH ₂) ₃	NH	O
Complex	3	4	5	6	7
empirical formula	C ₂₂ H ₂₆ N ₄ O ₃ Re·BF ₄	C ₂₃ H ₂₈ N ₄ O ₃ Re·0.95(BF ₄)·0.05(Br)	C ₂₄ H ₃₀ N ₄ O ₃ Re·0.96(BF ₄)·0.04(Br)	C ₂₁ H ₂₅ N ₅ O ₃ Re·BF ₄	C ₂₁ H ₂₄ N ₄ O ₄ Re·BF ₄
Fw	667.48	681.16	695.50	668.47	669.45
crystal system	monoclinic	monoclinic	monoclinic	monoclinic	monoclinic
space group	<i>P</i> 2 ₁ / <i>n</i>	<i>P</i> 2 ₁ / <i>n</i>	<i>P</i> 2 ₁ / <i>n</i>	<i>P</i> 2 ₁ / <i>n</i>	<i>P</i> 2 ₁ / <i>n</i>
<i>a</i> (Å)	11.4576(10)	13.3550(15)	13.7247 (14)	11.6155(10)	11.3847(9)
<i>b</i> (Å)	13.4757(15)	13.2081(14)	11.1284 (10)	12.9640(14)	13.3112(10)
<i>c</i> (Å)	15.9875(15)	14.7562(18)	18.141 (2)	15.8176(11)	15.7988(15)
<i>β</i> (deg)	97.502(5)	105.347(6)	109.392 (3)	97.341(6)	97.843(6)
<i>V</i> (Å ³)	2447.3(4)	2510.1(5)	2613.6 (5)	2362.3(4)	2371.8(3)
<i>T</i> (K)	200	150	95	95	90
<i>Z</i>	4	4	4	4	4
ρ_{calc} (Mg/m ³)	1.812	1.802	1.768	1.880	1.875
abs coeff (mm ⁻¹)	5.03	4.98	4.78	5.21	5.19
2 θ_{max} (°)	60.2	61.0	72.6	68.4	70.0
<i>R</i> [<i>I</i> > 2 σ (<i>I</i>)] ^a	0.032	0.032	0.029	0.032	0.033
wR2 ^b	0.073	0.075	0.060	0.067	0.075
<i>w</i> scheme d,e	0.0315, 2.4602	0.0343, 3.5449	0.0230, 1.6351	0.0252, 1.6969	0.0354, 0
data/param	7180/323	7045/344	12259/345	9257/326	10062/323
Res. dens (eÅ ⁻³)	1.23, -1.23	1.08, -1.85	1.16, -1.54	1.37, -1.72	1.46, -1.70

^a $R = (\sum||F_o| - |F_c||) / \sum|F_o|$. ^b $wR2 = [\sum[w(F_o^2 - F_c^2)^2] / \sum[w(F_o^2)^2]]^{1/2}$, in which $w = 1/[\sigma^2(F_o^2) + (dP)^2 + (eP)]$ and $P = (F_o^2 + 2F_c^2)/3$.

Table 3.2. Crystal Data and Structural Refinement for Complexes Having the General Formula, $[\text{Re}(\text{CO})_3(6,6'\text{-Me}_2\text{bipy})(\text{HNC}(\text{CH}_3)\text{N}(\text{CH}_2\text{CH}_2)_2\text{Y})]\text{BF}_4$

Y =	CH ₂	(CH ₂) ₂	(CH ₂) ₃	NH	O
Complex	8	9	10	11	12
empirical formula	C ₂₂ H ₂₆ N ₄ O ₃ Re·BF ₄	C ₂₃ H ₂₈ N ₄ O ₃ Re·0.97(BF ₄)·0.03(Br)	C ₂₄ H ₃₀ N ₄ O ₃ Re·BF ₄	C ₂₁ H ₂₅ N ₅ O ₃ Re·BF ₄	C ₂₁ H ₂₄ N ₄ O ₄ Re·BF ₄
Fw	667.48	681.31	695.53	668.47	669.45
crystal system	monoclinic	monoclinic	monoclinic	monoclinic	monoclinic
space group	<i>P2₁/n</i>	<i>P2₁/n</i>	<i>P2₁/c</i>	<i>P2₁/n</i>	<i>P2₁/n</i>
<i>a</i> (Å)	8.9242(5)	11.4040(10)	12.5348(10)	12.401(2)	15.6441(15)
<i>b</i> (Å)	21.862(2)	17.724(2)	10.8431(9)	14.221(3)	9.3838(10)
<i>c</i> (Å)	12.3282(10)	12.3056(11)	19.692(2)	13.630(2)	16.1555(12)
β (deg)	95.358(4)	98.914(5)	105.942(4)	100.750(9)	91.294(4)
<i>V</i> (Å ³)	2394.7(3)	2457.2(4)	2573.5(4)	2361.5(7)	2371.0(4)
<i>T</i> (K)	90	100	90	95	90
<i>Z</i>	4	4	4	4	4
ρ_{calc} (Mg/m ³)	1.851	1.842	1.795	1.880	1.875
abs coeff (mm ⁻¹)	5.14	5.05	4.79	5.21	5.19
$2\theta_{\text{max}}$ (°)	72.0	69.8	68.0	65.2	71.4
<i>R</i> [<i>I</i> > 2 σ (<i>I</i>)] ^a	0.031	0.031	0.030	0.037	0.029
wR2 ^b	0.074	0.068	0.070	0.097	0.069
<i>w</i> scheme d,e	0.0349, 0	0.0271, 2.2079	0.0307, 2.8985	0.0575, 0.7244	0.0349, 1.1307
Data/param	10749/323	10050/333	9861/388	8537/326	10909/323
Res. dens (eÅ ⁻³)	1.59, -2.07	1.35, -1.99	1.83, -1.58	4.45, -2.55	2.22, -1.69

^a $R = (\sum||F_o| - |F_c||) / \sum|F_o|$. ^b $wR2 = [\sum[w(F_o^2 - F_c^2)^2] / \sum[w(F_o^2)^2]]^{1/2}$, in which $w = 1/[\sigma^2(F_o^2) + (dP)^2 + (eP)]$ and $P = (F_o^2 + 2F_c^2)/3$.

The ^1H NMR spectrum of all crystals described below was identical to that of the product obtained by this procedure. In order to study the progress of the amidine formation reactions, a 10 mM solution of 1 or 2 was prepared in 600 μL of acetonitrile- d_3 . We refer to such a solution as the 10 mM solution. An excess of amine (100 mM) was added to the 10 mM solution, and the reaction was monitored by NMR spectroscopy. In all cases, the only signals observed for products were those expected from the isolated products.

Synthesis of $[\text{Re}(\text{CO})_3(5,5'\text{-Me}_2\text{bipy})(\text{HNC}(\text{CH}_3)\text{N}(\text{CH}_2\text{CH}_2)_2\text{CH}_2)]\text{BF}_4$ (3). The use of this general method in the reaction of 1 with piperidine (59 μL , 0.60 mmol) afforded 30 mg (74% yield) of yellow crystalline material. ^1H NMR signals (ppm) in acetonitrile- d_3 : 8.85 (s, 2H, H6/6'), 8.26 (d, $J = 8.4$ Hz, 2H, H3/3'), 8.04 (d, $J = 8.4$ Hz, 2H, H4/4'), 4.78 (b, 1H, NH), 3.01 (m, 4H, 2CH₂), 2.48 (s, 6H, 5/5'-2CH₃), 2.10 (s, 3H, CCH₃), 1.48 (m, 2H, CH₂), 1.28 (m, 4H, 2CH₂).

X-ray quality crystals of 3 (*E* isomer) were produced upon slow evaporation of a solution of the crystalline material (5 mg/6 mL) in a 1/5 (v/v) mixture of acetonitrile/diethyl ether. The ^1H NMR spectrum of the crystals dissolved in acetonitrile- d_3 was identical to that of the bulk product.

Monitoring the progress of the reaction of 1 with piperidine (5.9 μL) as described above indicated that no signals for 1 remained after 5 min, and signals for 3 were the only product signals present.

Synthesis of $[\text{Re}(\text{CO})_3(5,5'\text{-Me}_2\text{bipy})(\text{HNC}(\text{CH}_3)\text{N}(\text{CH}_2\text{CH}_2)_2(\text{CH}_2)_2)]\text{BF}_4$ (4). The use of the general method in the reaction of 1 with homopiperidine (60 μL , 0.60 mmol) produced 33 mg (80% yield) of yellow crystalline material. ^1H NMR signals (ppm) in acetonitrile- d_3 : 8.87 (s, 2H, H6/6'), 8.27 (d, $J = 8.6$ Hz, 2H, H3/3'), 8.05 (d, $J = 8.1$ Hz, 2H, H4/4'), 4.52 (b, 1H, NH),

3.30 (b, m, 2H, CH₂), 2.96 (b, m, 2H, CH₂), 2.48 (s, 6H, 5/5'-2CH₃), 2.10 (s, 3H, CCH₃), 1.46 (b, m, 2H, CH₂), 1.31 (b, m, 2H, CH₂), 1.15 (b, m, 2H, CH₂), 0.96 (b, m, 2H, CH₂).

X-ray quality crystals of 4 (*E* isomer) grew upon slow evaporation of a solution of the crystalline material (5 mg/4 mL) in a 1/3 (v/v) mixture of acetonitrile/diethyl ether. The ¹H NMR spectrum of the crystals dissolved in acetonitrile-*d*₃ was identical to that of the bulk product.

Monitoring the progress of the reaction of 1 with homopiperidine (6 μL) as described above indicated that no signals for 1 remained after ~8 min.

Synthesis of [Re(CO)₃(5,5'-Me₂bipy)(HNC(CH₃)N(CH₂CH₂)₂(CH₂)₃)]BF₄ (5). The use of the general method in the reaction of 1 with heptamethyleneimine (76 μL, 0.60 mmol), but stirring for 8 h, yielded 13 mg (32%) of yellow crystalline material. ¹H NMR signals (ppm) in acetonitrile-*d*₃: 8.87 (s, 2H, H6/6'), 8.27 (d, *J* = 8.3 Hz, 2H, H3/3'), 8.04 (d, *J* = 8.0 Hz, 2H, H4/4'), 4.49 (b 1H, NH), 3.25 (b, 2H, CH₂), 3.05 (b, 2H, CH₂), 2.48 (s, 6H, 5/5'-2CH₃), 2.12 (s, 3H, CCH₃), 1.50 (b, m, 2H, CH₂), 1.39 (b, m, 2H, CH₂), 1.18 (b, m, 2H, CH₂), 0.96 (b, m, 2H, CH₂), 0.71 (b, m, 2H, CH₂).

X-ray quality crystals of 5 (*E* isomer) grew upon slow evaporation of a solution of the crystalline material (10 mg/~200 mL) in a 1/200 (v/v) mixture of acetonitrile/diethyl ether. The ¹H NMR spectrum of the crystals dissolved in acetonitrile-*d*₃ was identical to that of the bulk product.

Monitoring the progress of the reaction of 1 with heptamethyleneimine (7.6 μL) as described above indicated that no signals for 1 remained after 6 h.

Synthesis of [Re(CO)₃(5,5'-Me₂bipy)(HNC(CH₃)N(CH₂CH₂)₂NH)]BF₄ (6). The general synthetic reaction of 1 with piperazine (52 mg, 0.60 mmol) yielded 34 mg (84%) of yellow crystalline material. ¹H NMR signals (ppm) in acetonitrile-*d*₃: 8.85 (s, 2H, H6/6'), 8.26 (d,

$J = 8.4$ Hz, 2H, H3/3'), 8.04 (d, $J = 8.4$ Hz, 2H, H4/4'), 4.84 (b, 1H, NH), 2.95 (m, 4H, 2CH₂), 2.53 (m, 4H, 2CH₂), 2.48 (s, 6H, 5/5'-2CH₃), 2.12 (s, 3H, CCH₃).

X-ray quality crystals of 6 (*E* isomer) formed upon slow evaporation of a 16 mL solution of the crystalline material (5 mg) in a 1/15 (v/v) mixture of acetonitrile/diethyl ether. The ¹H NMR spectrum of the crystals dissolved in acetonitrile-*d*₃ was identical to that of the bulk product.

Monitoring the progress of the reaction of 1 with piperazine (5.2 mg) as described above indicated that no signals for 1 remained after 20 min.

Synthesis of [Re(CO)₃(5,5'-Me₂bipy)(HNC(CH₃)N(CH₂CH₂)₂O)]BF₄ (7). The general synthetic reaction of 1 with morpholine (53 μL, 0.60 mmol) (stirring time, 6 h) yielded 33 mg (83%) of yellow crystalline material. ¹H NMR signals (ppm) in acetonitrile-*d*₃: 8.85 (s, 2H, H6/6'), 8.26 (d, $J = 8.4$ Hz, 2H, H3/3'), 8.05 (d, $J = 8.1$ Hz, 2H, H4/4'), 4.94 (b, 1H, NH), 3.45 (m, 2H, CH₂), 3.00 (m, 2H, CH₂), 2.48 (s, 6H, 5/5'-2CH₃), 2.14 (s, 3H, CCH₃).

X-ray quality crystals of 7 (*E* isomer) grew upon slow evaporation of a 4 mL solution of the crystalline material (5 mg) in a 1/3 (v/v) mixture of acetonitrile/diethyl ether. The ¹H NMR spectrum of the crystals dissolved in acetonitrile-*d*₃ was identical to that of the bulk product.

Monitoring the progress of the reaction of 1 with morpholine (5.3 μL) as described above indicated that no signals for 1 remained after 4 h.

Synthesis of [Re(CO)₃(6,6'-Me₂bipy)(HNC(CH₃)N(CH₂CH₂)₂CH₂)]BF₄ (8). The general treatment of 2 with piperidine (59 μL, 0.60 mmol) yielded 35 mg (88%) of yellow crystalline material. ¹H NMR signals (ppm) in acetonitrile-*d*₃: 8.19 (d, $J = 8.1$ Hz, 2H, H3/3'), 8.06 (t, $J = 7.9$ Hz, 2H, H4/4'), 7.62 (d, $J = 7.9$ Hz, 2H, H5/5'), 5.14 (b, 1H, NH), 3.06 (s, 6H,

6/6'-2CH₃), 3.03 (overlapped m, 4H, 2CH₂), 1.60 (s, 3H, CCH₃), 1.53 (m, 2H, CH₂), 1.29 (m, 4H, 2CH₂).

X-ray quality crystals of 8 (*E* isomer) formed upon slow evaporation of a 6 mL solution of the crystalline material (5 mg) in a 1/5 (v/v) mixture of acetonitrile/diethyl ether. The ¹H NMR spectrum of the crystals dissolved in acetonitrile-*d*₃ was identical to that of the bulk product.

Monitoring the progress of the reaction of 2 with piperidine (5.9 μL) as described above indicated that no signals for 2 remained after 3 min.

Synthesis of [Re(CO)₃(6,6'-Me₂bipy)(HNC(CH₃)N(CH₂CH₂)₂(CH₂)₂)]BF₄ (9). The general treatment of 2 with homopiperidine (60 μL, 0.60 mmol) yielded 32 mg (78%) of yellow crystalline material. ¹H NMR signals (ppm) in acetonitrile-*d*₃: 8.19 (d, *J* = 7.8 Hz, 2H, H3/3'), 8.06 (t, *J* = 7.9 Hz, 2H, H4/4'), 7.61 (d, *J* = 7.8 Hz, 2H, H5/5'), 4.90 (b, 1H, NH), 3.26 (b, m, 2H, CH₂), 3.07 (s, 6H, 6/6'-2CH₃), 3.04 (overlapped m, 2H, CH₂), 1.62 (s, 3H, CCH₃), 1.44 (b, m, 2H, CH₂), 1.38 (b, m, 2H, CH₂), 1.32 (b, m, 2H, CH₂), 1.11 (b, m, 2H, CH₂).

X-ray quality crystals of 9 (*E* isomer) grew upon slow evaporation of a 5 mL solution of the crystalline material (5 mg) in a 1/4 (v/v) mixture of acetonitrile/diethyl ether. The ¹H NMR spectrum of the crystals dissolved in acetonitrile-*d*₃ was identical to that of the bulk product.

Monitoring the progress of the reaction of 2 with homopiperidine (6 μL) as described above indicated that no signals for 2 remained after ~4.5 min.

Synthesis of [Re(CO)₃(6,6'-Me₂bipy)(HNC(CH₃)N(CH₂CH₂)₂(CH₂)₃)]BF₄ (10). The general treatment of 2 with heptamethyleneimine (76 μL, 0.60 mmol) afforded 15 mg (35%) of yellow crystalline material. ¹H NMR signals (ppm) in acetonitrile-*d*₃: 8.19 (d, *J* = 8.1 Hz, 2H, H3/3'), 8.07 (t, *J* = 7.9 Hz, 2H, H4/4'), 7.63 (d, *J* = 7.7 Hz, 2H, H5/5'), 4.82 (b, 1H, NH), 3.23 (b,

m, 2H, CH₂), 3.16 (b, m, 2H, CH₂), 3.07 (s, 6H, 6/6'-2CH₃), 1.66 (s, 3H, CCH₃), 1.49 (b, m, 2H, CH₂), 1.42 (b, m, 2H, CH₂), 1.32 (b, m, 2H, CH₂), 1.21 (b, m, 2H, CH₂), 0.92 (b, m, 2H, CH₂).

X-ray quality crystals of 10 (*E* isomer) formed upon slow evaporation of a solution of the crystalline material (5 mg/16 mL) in a 1/15 (v/v) mixture of acetonitrile/diethyl ether. The ¹H NMR spectrum of the crystals dissolved in acetonitrile-*d*₃ was identical to that of the bulk product.

Monitoring the progress of the reaction of 2 with heptamethyleneimine (7.6 μL) as described above indicated that no signals for 2 remained after 6 min.

Synthesis of [Re(CO)₃(6,6'-Me₂bipy)(HNC(CH₃)N(CH₂CH₂)₂NH)]BF₄ (11). The general treatment of 2 with piperazine (52 mg, 0.60 mmol) yielded 33 mg (83%) of yellow crystalline material. ¹H NMR signals (ppm) in acetonitrile-*d*₃: 8.19 (d, *J* = 8.0 Hz, 2H, H3/3'), 8.07 (t, *J* = 7.9 Hz, 2H, H4/4'), 7.62 (d, *J* = 7.7 Hz, 2H, H5/5'), 5.18 (b, 1H, NH), 3.05 (s, 6H, 6/6'-2CH₃), 2.96 (m, 4H, 2CH₂), 2.53 (m, 4H, 2CH₂), 1.63 (s, 3H, CCH₃).

X-ray quality crystals of 11 (*E* isomer) grew upon slow evaporation of a solution of the crystalline material (5 mg/5 mL) in a 1/4 (v/v) mixture of acetonitrile/diethyl ether. The ¹H NMR spectrum of the crystals dissolved in acetonitrile-*d*₃ was identical to that of the bulk product.

Monitoring the progress of the reaction of 2 with piperazine (5.1 mg) as described above indicated that no signals for 2 remained after 3 min.

Synthesis of [Re(CO)₃(6,6'-Me₂bipy)(HNC(CH₃)N(CH₂CH₂)₂O)]BF₄ (12). The general treatment of 2 with morpholine (53 μL, 0.60 mmol) (stirring time, 1 h) afforded 36 mg (90%) of yellow crystalline material. ¹H NMR signals (ppm) in acetonitrile-*d*₃: 8.19 (d, *J* = 7.9 Hz, 2H, H3/3'), 8.07 (t, *J* = 7.9 Hz, 2H, H4/4'), 7.62 (d, *J* = 7.7 Hz, 2H, H5/5'), 5.30 (b, 1H, NH), 3.45 (m, 4H, 2CH₂), 3.05 (s, 6H, 6/6'-2CH₃), 3.01 (m, 4H, 2CH₂), 1.66 (s, 3H, CCH₃).

X-ray quality crystals of 12 (*E* isomer) grew upon slow evaporation of a solution of the crystalline material (5 mg/4 mL) in a 1/3 (v/v) mixture of acetonitrile/diethyl ether. The ¹H NMR spectrum of the crystals dissolved in acetonitrile-*d*₃ was identical to that of the bulk product.

Monitoring the progress of the reaction of 2 with morpholine (5.3 μL) as described above indicated that no signals for 2 remained after 30 min.

Challenge Reactions. A 5 mM solution of [Re(CO)₃(5,5'-Me₂bipy)(HNC(CH₃)N(CH₂CH₂)₂CH₂)]BF₄ (3) in acetonitrile-*d*₃ (600 μL) was treated with a fivefold excess of 4-dimethylaminopyridine (2.0 mg, 25 mM), and the solution was monitored over time by ¹H NMR spectroscopy. A similar experiment was conducted in CDCl₃.

3.3 Results and Discussion

Synthesis. Treatment of [Re(CO)₃(L)(CH₃CN)]BF₄ (L = 5,5'-Me₂bipy (1), and 6,6'-Me₂bipy (2)) with heterocyclic amines in acetonitrile at room temperature afforded good yields (usually greater than 70%) of amidine complexes of the general formula, [Re(CO)₃(L)(HNC(CH₃)N(CH₂CH₂)₂Y)]BF₄ (L = 5,5'-Me₂bipy or 6,6'-Me₂bipy; Y = CH₂, (CH₂)₂, (CH₂)₃, NH, or O), as illustrated in Figure 3.2. ¹H NMR spectroscopic studies and structural characterization by single-crystal X-ray crystallography (see below) show that the reactions with cyclic amines form only one isomer (*E*) of the new amidine complexes. Reactions are often rapid at ambient temperature (≤3 min for complete reaction). Because the greater reactivity of [Re(CO)₃(6,6'-Me₂bipy)(CH₃CN)]BF₄ (2) than of [Re(CO)₃(5,5'-Me₂bipy)(CH₃CN)]BF₄ (1) with a given amine is best understood after a discussion of structural and spectroscopic results, we shall return to the topic of reaction times later.

Structural Results. Summarized in Tables 3.1 and 3.2 are the crystal data and details of the structural refinement for complexes **3-12**, having the general formula,

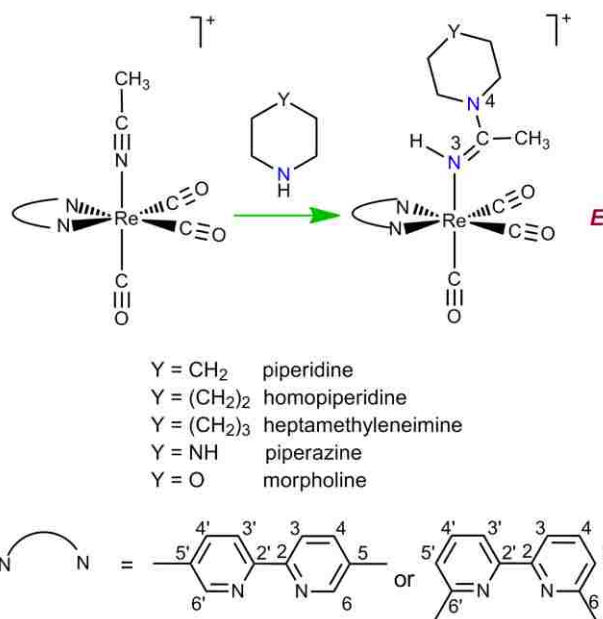


Figure 3.2. Reactions forming $[\text{Re}(\text{CO})_3(\text{L})(\text{HNC}(\text{CH}_3)\text{N}(\text{CH}_2\text{CH}_2)_2\text{Y})]^+$ complexes observed upon treatment of $[\text{Re}(\text{CO})_3(\text{L})(\text{CH}_3\text{CN})]^+$ complexes with heterocyclic amines $(\text{HN}(\text{CH}_2\text{CH}_2)_2\text{Y})$ in acetonitrile at 25 °C.

$[\text{Re}(\text{CO})_3(\text{L})(\text{HNC}(\text{CH}_3)\text{N}(\text{CH}_2\text{CH}_2)_2\text{Y})]\text{BF}_4$ (L = 5,5'-Me₂bipy or 6,6'-Me₂bipy, Y = CH₂, (CH₂)₂, (CH₂)₃, NH, or O). Figures 3.3 and 3.4 show the ORTEP plots of the cations in complexes **3-12**, together with the numbering scheme used to describe the solid-state data. All complexes have a pseudo octahedral structure, in which the three carbonyl ligands are coordinated facially. The remaining three coordination sites are occupied by the two nitrogen atoms of L and by one nitrogen atom of the neutral monodentate amidine ligand having the *E* configuration. Ni(II) amidine complexes formed upon addition of secondary amines to coordinated acetonitrile have the *E* configuration in the solid state.³⁸⁻³⁹

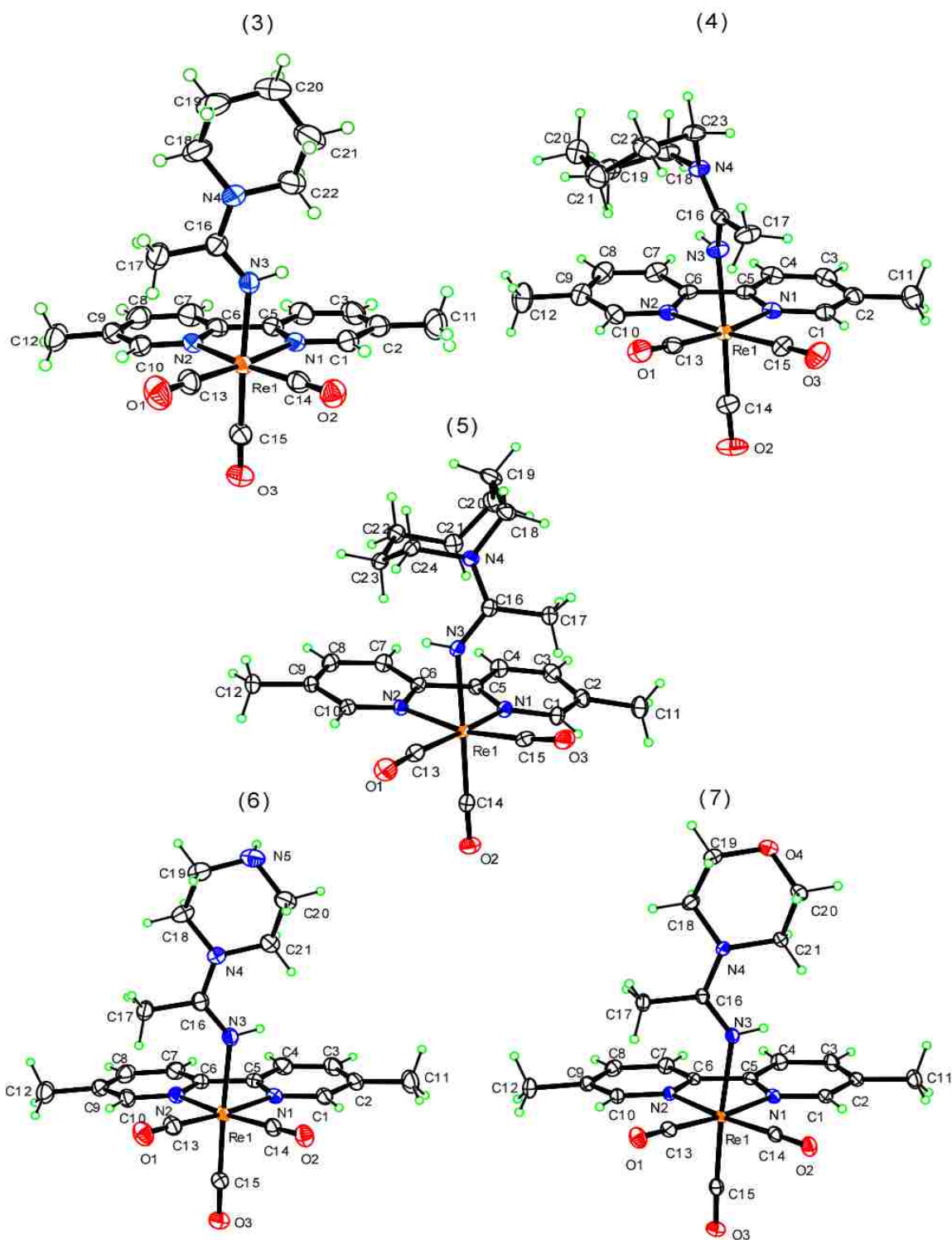


Figure 3.3. ORTEP plots of the cations in $[\text{Re}(\text{CO})_3(5,5'\text{-Me}_2\text{bipy})(\text{HNC}(\text{CH}_3)\text{N}(\text{CH}_2\text{CH}_2)_2\text{CH}_2)]\text{BF}_4$ (3), $[\text{Re}(\text{CO})_3(5,5'\text{-Me}_2\text{bipy})(\text{HNC}(\text{CH}_3)\text{N}(\text{CH}_2\text{CH}_2)_2(\text{CH}_2)_2)]\text{BF}_4$ (4), $[\text{Re}(\text{CO})_3(5,5'\text{-Me}_2\text{bipy})(\text{HNC}(\text{CH}_3)\text{N}(\text{CH}_2\text{CH}_2)_2(\text{CH}_2)_3)]\text{BF}_4$ (5), $[\text{Re}(\text{CO})_3(5,5'\text{-Me}_2\text{bipy})(\text{HNC}(\text{CH}_3)\text{N}(\text{CH}_2\text{CH}_2)_2\text{NH})]\text{BF}_4$ (6), and $[\text{Re}(\text{CO})_3(5,5'\text{-Me}_2\text{bipy})(\text{HNC}(\text{CH}_3)\text{N}(\text{CH}_2\text{CH}_2)_2\text{O})]\text{BF}_4$ (7). Thermal ellipsoids are drawn with 50% probability.

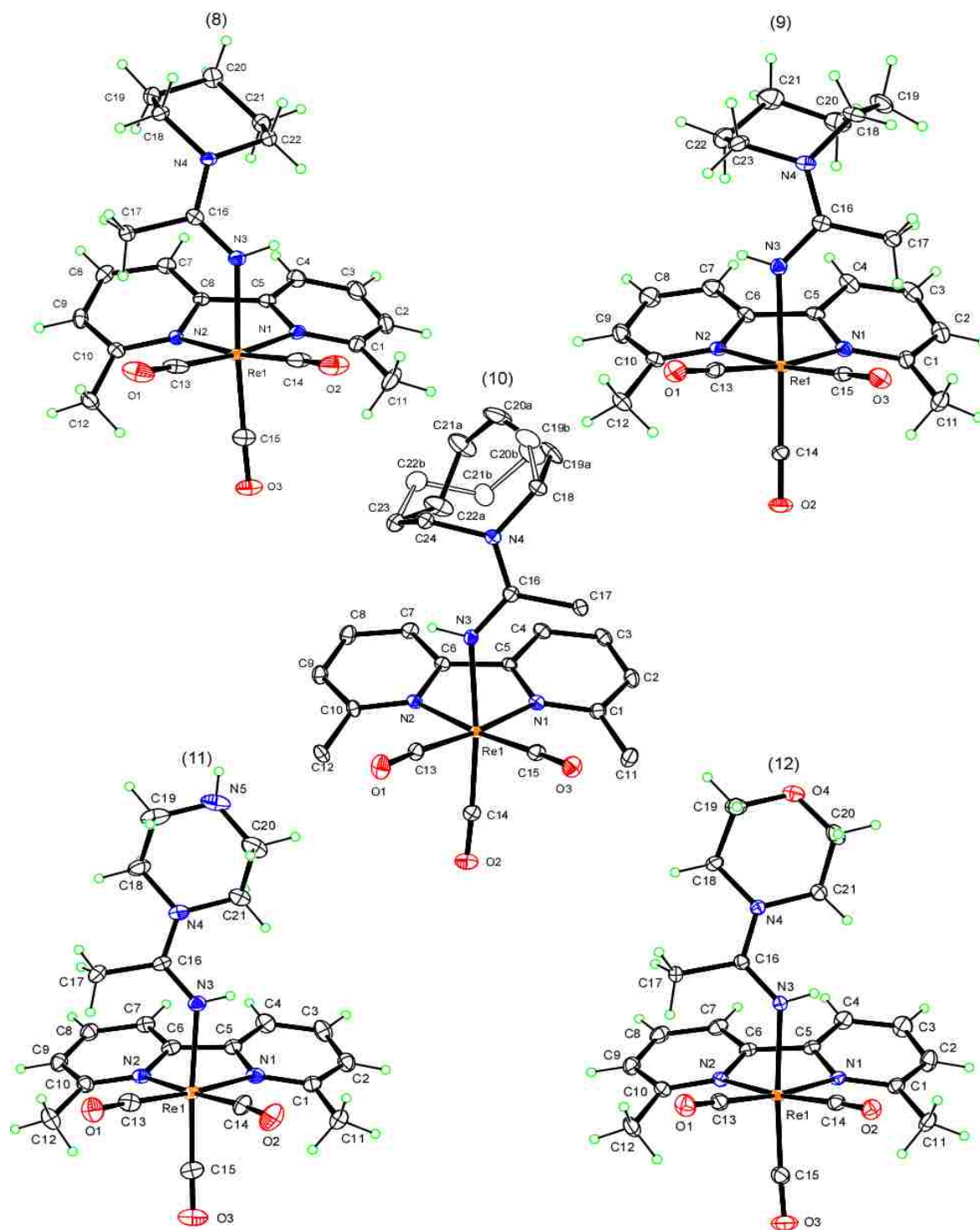


Figure 3.4. ORTEP plots of the cations in $[\text{Re}(\text{CO})_3(6,6'\text{-Me}_2\text{bipy})(\text{HNC}(\text{CH}_3)\text{N}(\text{CH}_2\text{CH}_2)_2\text{CH}_2)]\text{BF}_4$ (8), $[\text{Re}(\text{CO})_3(6,6'\text{-Me}_2\text{bipy})(\text{HNC}(\text{CH}_3)\text{N}(\text{CH}_2\text{CH}_2)_2(\text{CH}_2)_2)]\text{BF}_4$ (9), $[\text{Re}(\text{CO})_3(6,6'\text{-Me}_2\text{bipy})(\text{HNC}(\text{CH}_3)\text{N}(\text{CH}_2\text{CH}_2)_2(\text{CH}_2)_3)]\text{BF}_4$ (10), $[\text{Re}(\text{CO})_3(6,6'\text{-Me}_2\text{bipy})(\text{HNC}(\text{CH}_3)\text{N}(\text{CH}_2\text{CH}_2)_2\text{NH})]\text{BF}_4$ (11), and $[\text{Re}(\text{CO})_3(6,6'\text{-Me}_2\text{bipy})(\text{HNC}(\text{CH}_3)\text{N}(\text{CH}_2\text{CH}_2)_2\text{O})]\text{BF}_4$ (12). Thermal ellipsoids are drawn with 50% probability. For 10, both conformations of the disordered 8-membered ring are shown, and H atoms are not illustrated, except for N-H.

The Re–C bond distances (not shown) of the two CO groups cis to the amidine ligand are generally not significantly different from the one trans to it in all complexes (3-12). All of the $[\text{Re}(\text{CO})_3(5,5'\text{-Me}_2\text{bipy})(\text{HNC}(\text{CH}_3)\text{N}(\text{CH}_2\text{CH}_2)_2\text{Y})]\text{BF}_4$ complexes (3-7) show Re–N bond lengths (Table 3.3) comparable to the typical Re sp^2 nitrogen bond length, typically ranging from 2.14 to 2.18 Å.²² This result is consistent with the structural results for the recent monodentate amidine complexes of Re^{I} with primary amines.²⁵ As found for the iminoether complexes, in which the Re–N3 bond lengths found for $[\text{Re}(\text{CO})_3(5,5'\text{-Me}_2\text{bipy})(\text{HNC}(\text{CH}_3)\text{OCH}_3)]\text{BF}_4$ (2.1860(18) Å) and $[\text{Re}(\text{CO})_3(6,6'\text{-Me}_2\text{bipy})(\text{HNC}(\text{CH}_3)\text{OCH}_3)]\text{BF}_4$ (2.175(3) Å) were not significantly different,²³ the Re–N3 bond lengths are quite similar for complexes 3-12. These bond lengths appear to be very slightly longer for the 6,6'-Me₂bipy complexes (range 2.1848(18) - 2.193(2), mean 2.190 Å) than for the 5,5'-Me₂bipy complexes (range 2.178(3) - 2.1806(18), mean 2.179 Å).

The recent study of *fac*- $[\text{Re}(\text{CO})_3(\text{L})(\text{HNC}(\text{CH}_3)\text{OCH}_3)]\text{BF}_4$ complexes revealed that the Re–N bond lengths in the equatorial plane were significantly longer for L = 6,6'-Me₂bipy than for L = 5,5'-Me₂bipy.²³ These examples of a slight Re–N bond lengthening were attributed to the distorted nature of the 6,6'-Me₂bipy ligand as a result of the close proximity of the two methyl substituents to the equatorial carbonyl groups. A comparison of the equatorial Re–N bond lengths (Tables 3.3 and 3.4) of all five $[\text{Re}(\text{CO})_3(6,6'\text{-Me}_2\text{bipy})(\text{HNC}(\text{CH}_3)\text{N}(\text{CH}_2\text{CH}_2)_2\text{Y})]\text{BF}_4$ complexes (8-12) with those of the corresponding five $[\text{Re}(\text{CO})_3(5,5'\text{-Me}_2\text{bipy})(\text{HNC}(\text{CH}_3)\text{N}(\text{CH}_2\text{CH}_2)_2\text{Y})]\text{BF}_4$ complexes (3-7) reveals that only some bonds in the 6,6'-Me₂bipy complexes are slightly longer by criteria of statistical significance. However, as for the Re–N3 axial distances, the equatorial Re–N(Me₂bipy) distances appear to be on average very slightly longer for the 6,6'-Me₂bipy complexes (range 2.194(2) - 2.213(2), mean 2.206 Å) than

for the 5,5'-Me₂bipy complexes (range 2.168(3) - 2.194(2), mean 2.179 Å). Thus, the more extensive solid-state results for complexes 3-12 now available indicate that the 6,6'-methyl groups in 8-12 affect the equatorial Re–N bond distances only slightly.

In all but one of the new complexes, the amidine ligand has a similar orientation (specified by the projection onto the equatorial plane of the amidine plane defined by the N3, C16 and N4 atoms). In this orientation, the amidine plane bisects the two N–Re–C angles in the equatorial plane. In [Re(CO)₃(5,5'-Me₂bipy)(HNC(CH₃)N(CH₂CH₂)₂(CH₂)₂)]BF₄ (4), the amidine plane orientation is different: it is rotated by about 65°, with the methyl group almost directly above one carbonyl ligand. However, in solution there is no evidence for this difference in orientation, as the ¹H NMR signals of 4 have chemical shifts similar to those of other [Re(CO)₃(5,5'-Me₂bipy(HNC(CH₃)N(CH₂CH₂)₂Y)]BF₄ complexes (3, 5, 6, 7). The different orientation in 4 is thus attributed to subtle packing effects. Furthermore, the structures of most of the complexes in this and previous studies lead us to conclude that the orientation of the amidine and iminoether ligands does not depend on the substitution pattern of the bipyridine ligands (L = 5,5'-Me₂bipy or L = 6,6'-Me₂bipy) present in the equatorial plane.^{23,25}

Tables 3.3 and 3.4 show that for complexes 3-12 the bond lengths from C_{am} (C16) to the rhenium-bound nitrogen atom (N3), and to the remote nitrogen atom (N4), are all closer to an average sp² C=N bond length (~1.28 Å), than to an average sp³ C–N bond length (~1.47 Å), as also reported for [Re(CO)₃(5,5'-Me₂bipy)(HNC(CH₃)NHR)]BF₄ complexes²⁵ and for Ni and Cu complexes.³⁷⁻³⁹ In addition to the C16–N3 and C16–N4 bond lengths, the values of the C16–N4–C18, C16–N4–C(n) and N3–C16–N4 angles, which are all close to 120° (Tables 3.3 and 3.4), also provide evidence for electron delocalization within the amidine group, as discussed in

previous reports.^{23, 37-40} Furthermore, the N3 hydrogen atoms in these complexes are all located in positions consistent with sp^2 rather than sp^3 hybridization for N3.

Table 3.3 Selected Bond Distances (Å) and Angles (deg) for Complexes Having the General Formula, $[\text{Re}(\text{CO})_3(5,5'\text{-Me}_2\text{bipy})(\text{HNC}(\text{CH}_3)\text{N}(\text{CH}_2\text{CH}_2)_2\text{Y})]\text{BF}_4$

Y =	CH ₂	(CH ₂) ₂	(CH ₂) ₃	NH	O
complex	3	4	5	6	7
bond distances					
Re–N1	2.168 (3)	2.172 (3)	2.1691 (18)	2.177 (2)	2.177 (2)
Re–N2	2.186 (3)	2.173 (3)	2.1823 (18)	2.190 (2)	2.194 (2)
Re–N3	2.178 (3)	2.179 (3)	2.1806 (18)	2.179 (2)	2.178 (2)
N3–C16	1.306 (4)	1.310 (5)	1.308 (3)	1.300 (4)	1.304 (3)
N4–C16	1.346 (5)	1.344 (5)	1.346 (3)	1.354 (4)	1.359 (3)
bond angles					
N1–Re–N2	75.06 (11)	74.58 (11)	74.82 (6)	75.08 (8)	75.16 (8)
N1–Re–N3	80.23 (11)	83.44 (11)	87.21 (6)	79.90 (9)	78.78 (8)
N2–Re–N3	86.41 (11)	79.02 (11)	79.34 (6)	86.11 (9)	86.30 (8)
Re–N3–H3N	113 (3)	111 (3)	106 (2)	110 (2)	110 (2)
Re–N3–C16	137.4 (2)	135.6 (3)	136.82 (15)	136.5 (2)	137.03 (18)
C16–N3–H3N	110 (3)	110 (3)	116 (2)	114 (2)	113 (2)
N3–C16–N4	123.6 (3)	122.9 (3)	122.47 (19)	123.3 (3)	122.5 (2)
N3–C16–C17	118.6 (3)	118.5 (3)	119.58 (19)	119.2 (3)	119.9 (2)
N4–C16–C17	117.8 (3)	118.7 (3)	117.95 (19)	117.4 (2)	117.7 (2)
C16–N4–C18	122.2 (3)	121.2 (3)	123.86 (18)	121.8 (2)	121.4 (2)
C16–N4–C(n) ^a	120.3 (3) ^b	122.7 (3) ^c	120.44 (18) ^d	120.7 (2) ^e	120.1 (2) ^f

^a n varies in number according to the R group. ^b n = 22. ^c n = 23. ^d n = 24. ^e n = 21. ^f n = 21.

Table 3.4. Selected Bond Distances (Å) and Angles (deg) for Complexes Having the General Formula, [Re(CO)₃(6,6'-Me₂bipy)(HNC(CH₃)N(CH₂CH₂)₂Y)]BF₄

Y =	CH ₂	(CH ₂) ₂	(CH ₂) ₃	NH	O
complex	8	9	10	11	12
bond distances					
Re–N1	2.213 (2)	2.203 (2)	2.211 (2)	2.212 (3)	2.2051 (19)
Re–N2	2.1984 (18)	2.194 (2)	2.211 (2)	2.202 (3)	2.2086 (19)
Re–N3	2.193 (2)	2.188 (2)	2.190 (2)	2.192 (3)	2.1848 (18)
N3–C16	1.307 (3)	1.309 (3)	1.308 (3)	1.307 (4)	1.307 (3)
N4–C16	1.356 (3)	1.350 (3)	1.347 (3)	1.350 (4)	1.356 (3)
bond angles					
N1–Re–N2	74.29 (7)	74.60 (8)	74.40 (8)	75.29 (11)	74.90 (7)
N1–Re–N3	80.26 (7)	82.12 (8)	83.41 (8)	79.19 (10)	79.35 (7)
N2–Re–N3	82.97 (7)	80.44 (8)	79.26 (8)	83.85 (10)	82.00 (7)
Re–N3–H3N	110 (2)	110 (2)	108 (2)	107 (3)	109 (2)
Re–N3–C16	136.66 (16)	135.62 (19)	136.74 (19)	135.4 (2)	137.12 (15)
C16–N3–H3N	113 (2)	115 (2)	115 (2)	115 (3)	114 (2)
N3–C16–N4	123.2 (2)	122.9 (2)	123.0 (2)	124.2 (3)	122.84 (19)
N3–C16–C17	119.5 (2)	119.8 (2)	119.2 (2)	118.4 (3)	119.85 (19)
N4–C16–C17	117.3 (2)	117.3 (2)	117.8 (2)	117.3 (3)	117.28 (19)
C16–N4–C18	122.62 (19)	122.4 (2)	123.2 (2)	124.2(3)	122.27(18)
C16–N4–C(n) ^a	122.93 (19) ^b	121.2 (2) ^c	121.0 (2) ^d	123.7 (3) ^e	121.29 (19) ^f

^a n varies in number according to the R group. ^b n = 22. ^c n = 23. ^d n = 24. ^e n = 21. ^f n = 21.

Distances that are slightly shorter for C16–N3 than for C16–N4 (Tables 3.3 and 3.4) indicate more double-bond character in the C16–N3 bond. For example, in [Re(CO)₃(5,5'-Me₂bipy)(HNC(CH₃)N(CH₂CH₂)₂CH₂)]BF₄ (3) the C16–N3 bond length is 1.306(4) Å and the C16–N4 bond length is 1.346(5) Å. Similar differences in the C16–N3 and C16–N4 bond distances reported previously for [Re(CO)₃(5,5'-Me₂bipy)(HNC(CH₃)NHR)]BF₄ complexes were attributed to greater double-bond character for the C16–N3 bond than for the C16–N4 bond.²⁵

In the solid state, [Re(CO)₃(5,5'-Me₂bipy)(HNC(CH₃)NHR)]BF₄ complexes exist as the *E'* isomer.²⁵ In solutions made with polar solvents such as acetonitrile, the *E'* isomer equilibrated to a mixture of the *E'* and *Z* isomers. This equilibration, involving sequential rotations around the C16–N4 bond (fast step forming the *E* isomer as an undetectable intermediate in polar solvents) and then around the C16–N3 bond (slow step), required several minutes.²⁵ The solution results are consistent with the X-ray data that indicate more double-bond character in the C16–N3 bond than in the C16–N4 bond. In solvents with low polarity, such as chloroform, abundant amounts of *E*, *E'* and *Z* isomers were found. Two-dimensional NMR data demonstrated that the *E'* to *E* interconversion, involving rotation around the C16–N4 bond (Figure 3.1), was fast. The similarity in the C16–N3 and C16–N4 bond distances in new and old amidine complexes indicates that *E* to *Z* isomer interconversion should be slow for the new amidine complexes (3-12) as well. Thus, the NMR evidence (see below) for the presence of only one isomer on dissolution of crystals containing only the *E* isomer indicates beyond doubt that this one isomer is the *E* isomer and that the *Z* isomer of the new [Re(CO)₃(L)(HNC(CH₃)N(CH₂CH₂)₂Y)]BF₄ complexes (3-12) is unstable. Preliminary data suggest that the rotation around the C16–N4 bond does occur and studies are planned to elucidate this process.

Steric Interaction of the Amidine Axial Ligand with the Equatorial Ligands. For amidine complexes 3-12, one of the bond angles from an equatorial N atom to the axial N3 atom (N1–Re–N3 or N2–Re–N3) is always significantly greater than the other such angle. For example, in complexes 3, 6, 7, 8, 11 and 12, the N2–Re–N3 angle is greater than the N1–Re–N3 angle, whereas in complexes 4, 5, 9 and 10 the N1–Re–N3 angle is the larger (cf. Tables 3.3 and 3.4). The smaller N–Re–N3 angle is always the one involving the equatorial N closest to the amidine N3H group. A similar relationship was also evident between the smaller equatorial N–Re–N3 bond angle and the orientation of the N3H group of previously studied primary amidine²⁵ and iminoether²³ complexes, when the axial ligand was oriented in the normal way. For the new complexes, this normal orientation is shown in Supporting Information. The reason that one N–Re–N3 bond angle is significantly larger than the other N–Re–N3 bond angle in complexes 3-12 is clearly because the larger angle leads to reduced repulsions between the amidine methyl group and the closest atoms of equatorial ligands.

When we began our investigations into reactions of coordinated acetonitrile in complexes with the *fac*-[M^I(CO)₃] core, one initial goal was to explore the effect of increasing the steric bulk near the metal center by using the 6,6'-Me₂bipy ligand. In the first such study (involving iminoether complexes), we found that, when the iminoether was oriented in the same way, the value of the larger N–Re–N3 angle in [Re(CO)₃(bipy)(HNC(CH₃)OCH₃)]BF₄ was greater than the corresponding larger N–Re–N3 value in [Re(CO)₃(6,6'-Me₂bipy)(HNC(CH₃)OCH₃)]BF₄.²³ We hypothesized that the distortion in the 6,6'-Me₂bipy complex decreases those interactions of the axial iminoether ligand with the equatorial ligands that cause one of the two N–Re–N3 angles to be larger.

In the new complexes, the size of the larger of the two N–Re–N3 bond angles in the 5,5'-Me₂bipy complexes is greater on average than the larger bond angles in the 6,6'-Me₂bipy complexes (Tables 3.3 and 3.4 and Supporting Information). This comparison supports the hypothesis that the distortion in the 6,6'-Me₂bipy complexes decreases those axial-equatorial ligand interactions that cause one of the two N–Re–N3 angles to be larger. This apparently counter-intuitive finding of smaller interactions in 6,6'-Me₂bipy complexes than in the related [Re(CO)₃(bipy)(HNC(CH₃)OCH₃)]BF₄ complexes can be understood by considering our structural results and those that have appeared during the course of our work.⁴¹ In the many structures now available, the clashes between the methyl groups of the 6,6'-Me₂bipy ligand and the two equatorial CO ligands distort the 6,6'-Me₂bipy ligand and force the 6,6'-methyl groups out of the equatorial plane (defined by the C13–Re–C14 atoms) toward the axial CO. These distortions of the Re(CO)₃(6,6'-Me₂bipy) moiety in [Re(CO)₃(6,6'-Me₂bipy)(HNC(CH₃)N(CH₂CH₂)₂Y)]BF₄ amidine complexes (8-12) (Figure 3.5 and Supporting Information) are very similar to those of the other complexes.^{23,41}

As can be seen in Figure 3.5, the distortion results in a tilted plane of the 6,6'-Me₂bipy ligand. To appreciate the effect of the tilting, it is convenient to view the two Me₂bipy ligands as having an interior or front side (atoms N1, C1, N2, C10) and an exterior or back side (atoms C3, C4, C7, C8), according to the numbering scheme in Figures 3.3 and 3.4. Although in the solid state the ligands are not fully symmetrical or fully planar, the front-side carbons 1 and 10 lie slightly below the equatorial plane in 6,6'-Me₂bipy complexes and lie in the equatorial plane in 5,5'-Me₂bipy complexes. To assess the space near the axial coordination site (trans to the axial CO), we measured some non-bonded distances from N3 (Supporting Information). For [Re(CO)₃(L)(HNC(CH₃)N(CH₂CH₂)₂Y)]BF₄ (Y = CH₂ or NH), the non-bonded distances from

N3 to C1 and C10 average ~ 0.15 Å longer in 6,6'-Me₂bipy than in 5,5'-Me₂bipy complexes. Properties (such as N–Re–N bond angles) affected by the interior structure have values (Tables 3.3 and 3.4) consistent with this additional space. On the other hand, for these same complexes the non-bonded distances from N3 to C4 and C7 average ~ 0.5 Å shorter in 6,6'-Me₂bipy than in 5,5'-Me₂bipy complexes. Other properties, such as some NMR shifts, are affected more by the exterior or peripheral structure (see below).

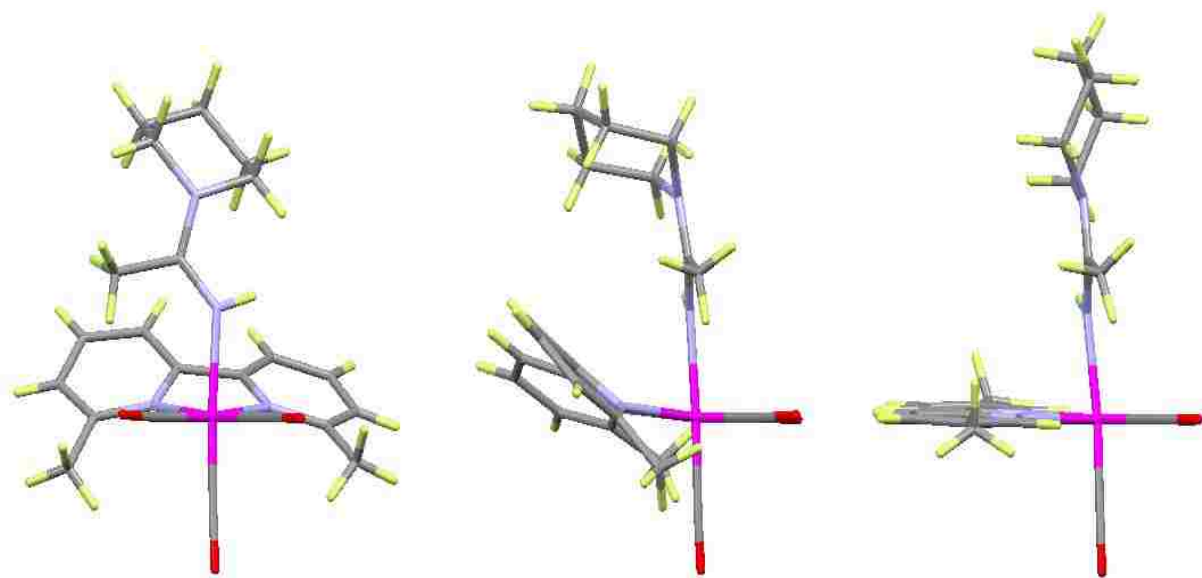


Figure 3.5. Views of piperidinylamidine complexes, $[\text{Re}(\text{CO})_3(\text{L})(\text{HNC}(\text{CH}_3)\text{N}(\text{CH}_2\text{CH}_2)_2\text{CH}_2)]\text{BF}_4$, depicted with the C13–Re–C14 equatorial plane perpendicular to the plane of the paper. Shown at *left* and *middle* are front and side views, respectively, of complex 8 with L = 6,6'-Me₂bipy. Pictured at *right* is a side view of complex 3 with L = 5,5'-Me₂bipy.

Furthermore, for some properties, the net effects of the differences in the bidentate ligand orientations may cancel. Indeed, regardless of whether the complex has L = 6,6'-Me₂bipy or 5,5'-Me₂bipy, the isomer distribution seems to be unaffected. Thus, for all the complexes in the

present study, the repulsions are large enough to favor the presence of only one isomer, namely the *E* isomer.

Our ranking of the expected effects of steric interactions on isomer stability for $[\text{Re}(\text{CO})_3(\text{Me}_2\text{bipy})(\text{HNC}(\text{CH}_3)\text{OCH}_3)]^+$, $[\text{Re}(\text{CO})_3(\text{L})\text{HNC}(\text{CH}_3)\text{NHR}]^+$, and $[\text{Re}(\text{CO})_3(\text{L})(\text{HNC}(\text{CH}_3)\text{N}(\text{CH}_2\text{CH}_2)_2\text{Y})]^+$ complexes is shown in Figure 3.6. This ranking

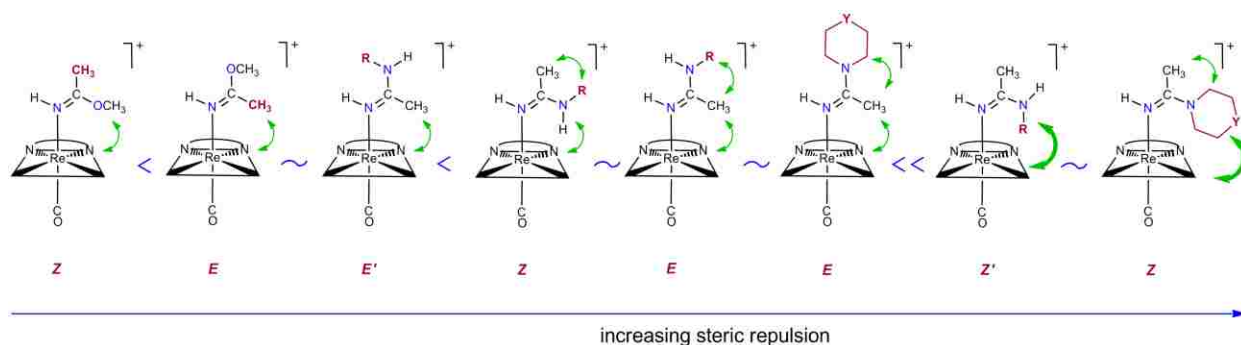


Figure 3.6. Ranking of increasingly unfavorable total steric repulsive interactions (each double-headed arrow indicates an interaction) in $[\text{Re}(\text{CO})_3(\text{Me}_2\text{bipy})(\text{HNC}(\text{CH}_3)\text{OCH}_3)]^+$, $[\text{Re}(\text{CO})_3(\text{L})\text{HNC}(\text{CH}_3)\text{NHR}]^+$, and $[\text{Re}(\text{CO})_3(\text{L})(\text{HNC}(\text{CH}_3)\text{N}(\text{CH}_2\text{CH}_2)_2\text{Y})]^+$ complexes [N–N denotes the 5,5'- or 6,6'-Me₂bipy ligands, and Y = CH₂, (CH₂)₂, (CH₂)₃, NH, or O].

summarizes our experimental observations of the relative isomer abundance of these complexes in this and previous studies.^{23,25} This ranking takes into account steric repulsions of the substituents on C_{am} or C_{ie} in the axial with the equatorial Me₂bipy and CO ligands and also the relative repulsions within the amidine ligand between the CH₃ and the NH or NR groups in $[\text{Re}(\text{CO})_3(\text{L})\text{HNC}(\text{CH}_3)\text{NHR}]^+$ complexes. As indicated for the two structures sketched at the far right of Figure 3.6, the repulsive interactions of the NR substituent with the equatorial ligands depicted in the respective *Z'* and *Z* sketches are expected to be the most severe. Thus, these interactions are shown with thicker double-headed arrows. The order of the *Z* and *E* isomers of

$[\text{Re}(\text{CO})_3(\text{L})\text{HNC}(\text{CH}_3)\text{NHR}]^+$ complexes (4th and 5th structures from left in Figure 3.6) reflects our suggestion that the N4H interaction with the equatorial ligands is less repulsive than the corresponding $\text{C}_{\text{am}}\text{CH}_3$ interaction with the equatorial ligands.

Repulsion between the CH_3 and NR groups is secondary and noticeably influences abundance mainly when the two isomers have the same interaction with the equatorial ligands, such as is the case with the E' and E isomers of $[\text{Re}(\text{CO})_3(\text{L})\text{HNC}(\text{CH}_3)\text{NHR}]^+$ complexes (3rd and 5th structures from left in Figure 3.6). For $[\text{Re}(\text{CO})_3(\text{L})\text{HNC}(\text{CH}_3)\text{NHR}]^+$ complexes,²⁵ clashes between the NR and the CH_3 amidine substituents destabilize the E isomer, which normally has low abundance. The abundance of the E' isomer increased as the steric bulk of the R substituent on C_{am} increased. In turn, the Z isomer of *fac*- $[\text{Re}(\text{CO})_3(5,5'$ - $\text{Me}_2\text{bipy})(\text{HNC}(\text{CH}_3)\text{NH}_2)]\text{BF}_4$ with similarly sized substituents (NH_2 and CH_3) on C_{am} was highly favored ($\sim 90\%$ abundant). We caution that the differences in electronic effects influencing the stability of the Z and E configurations are not known. Nevertheless, the ranking as illustrated in Figure 3.6 does provide a good guide for predicting the relative abundance of the isomers, especially in polar solvents.

NMR Spectroscopy. All complexes were characterized by ^1H NMR spectroscopy in acetonitrile- d_3 ; selected complexes were also studied in CDCl_3 and $\text{DMSO-}d_6$. ^1H NMR spectra were recorded within at least 6 min of dissolution. In contrast to the spectral data of the previously studied $[\text{Re}(\text{CO})_3(5,5'$ - $\text{Me}_2\text{bipy})(\text{HNC}(\text{CH}_3)\text{NHR})]\text{BF}_4$ complexes, all of the ^1H NMR spectra of the new $[\text{Re}(\text{CO})_3(\text{L})(\text{HNC}(\text{CH}_3)\text{N}(\text{CH}_2\text{CH}_2)_2\text{Y})]\text{BF}_4$ amidine complexes regardless of the solvent used consistently indicate the presence of only one isomer in solution. Moreover, the spectra of all of these complexes (3-12) showed no changes with time, even after several days.

The atom numbering system used in this NMR discussion is that shown in Figures 3.3 and 3.4. ^1H NMR signals of the bidentate ligand and of N3H were assigned by using the splitting pattern and integration, and by comparison to unambiguous assignments of spectra for previously reported analogous Re^{I} amidines and iminoether complexes.^{23,25}

We illustrate our findings by detailing our studies of compound **3**, $[\text{Re}(\text{CO})_3(5,5'\text{-Me}_2\text{bipy})(\text{HNC}(\text{CH}_3)\text{N}(\text{CH}_2\text{CH}_2)_2\text{CH}_2)]\text{BF}_4$. When crystals of **3** were dissolved in three different solvents (acetonitrile- d_3 , CDCl_3 and $\text{DMSO-}d_6$), ^1H NMR spectra showed no evidence for more than one isomer: All peaks in all three solvents remained constant when solutions were monitored from 3 min after dissolution until two weeks. As indicated in our analysis of the C16–N3 bond lengths above, we believe that if the *Z* isomer were present, the interconversion rate would be slow and we would have detected signals for the *Z* isomer. Thus, we are absolutely confident that the *Z* isomer is unstable.

The N3H signal in the new complexes is easily assigned because the peak is a broad singlet integrating to one proton and because it disappeared gradually after the addition of D_2O . For **3**, this N3H signal has a more downfield shift in $\text{DMSO-}d_6$ (5.77 ppm) than in acetonitrile- d_3 (4.78 ppm) or CDCl_3 (4.60 ppm). The related values for **4** were 5.32, 4.52, and 4.32 ppm, respectively. A similar NMR dependence of the N3H shift on solvent was observed for $[\text{Re}(\text{CO})_3(5,5'\text{-Me}_2\text{bipy})(\text{HNC}(\text{CH}_3)\text{OCH}_3)]\text{BF}_4$; in a standard chloride titration experiment, the downfield shift in $\text{DMSO-}d_6$ was demonstrated to be caused by hydrogen bonding of N3H to $\text{DMSO-}d_6$.²³ In this iminoether complex, as for complexes **3** and **4**, N3H projects out toward the solvent, making this proton available for hydrogen bonding to $\text{DMSO-}d_6$. Such hydrogen bonding explains the solvent dependence found for **3** and **4**.

**Dependence on Y of the N3H NMR Signals of
[Re(CO)₃(L)(HNC(CH₃)N(CH₂CH₂)₂Y)]BF₄, for L = 5,5'-Me₂bipy and 6,6'-Me₂bipy.**

Selected ¹H NMR signals of the new amidine complexes (3-12) in acetonitrile-*d*₃ are compared in Table 3.5. For complexes with the amidines having six-membered N(CH₂CH₂)₂Y rings,

Table 3.5. ¹H NMR Shifts (ppm) for L, N3H, and C_{am}CH₃ in [Re(CO)₃(L)(HNC(CH₃)N(CH₂CH₂)₂Y)]BF₄ Complexes (Acetonitrile-*d*₃, 25 °C)

Y		H3/3'	H4/4'	H5/5'	H6/6'	L-CH ₃	N3H	C _{am} CH ₃
L = 5,5'-Me ₂ bipy								
CH ₂	(3)	8.26	8.04		8.85	2.48	4.78	2.10
(CH ₂) ₂	(4)	8.27	8.05		8.87	2.48	4.52	2.10
(CH ₂) ₃	(5)	8.27	8.04		8.87	2.48	4.49	2.12
NH	(6)	8.26	8.04		8.85	2.47	4.84	2.12
O	(7)	8.26	8.04		8.85	2.48	4.94	2.14
L = 6,6'-Me ₂ bipy								
CH ₂	(8)	8.19	8.06	7.62		3.06	5.14	1.60
(CH ₂) ₂	(9)	8.19	8.06	7.61		3.07	4.90	1.62
(CH ₂) ₃	(10)	8.19	8.07	7.63		3.07	4.82	1.66
NH	(11)	8.19	8.07	7.62		3.05	5.18	1.63
O	(12)	8.19	8.07	7.62		3.05	5.30	1.66

[Re(CO)₃(5,5'-Me₂bipy)(HNC(CH₃)N(CH₂CH₂)₂Y)]BF₄ (3, 6, and 7) and [Re(CO)₃(6,6'-Me₂bipy)(HNC(CH₃)N(CH₂CH₂)₂Y)]BF₄ (8, 11, and 12), the most downfield shift observed for the N3H signal is for the morpholine derivative (Y = O) in each series (4.94 ppm for 7 and 5.30 ppm for 12). The N3H signal is slightly upfield for piperazine derivatives (Y = NH) (4.84 ppm for 6 and 5.18 ppm for 11) and farther upfield for piperidine derivatives (Y = CH₂) (4.78 ppm for 3 and 5.14 ppm for 8). These data indicate that the remote O and N atoms of the morpholine and piperazine derivatives, respectively, exert electron-withdrawing effects on the amidine group, with the more electronegative O atom of the morpholine derivative having the greater downfield-

shifting effect on the N3H signal. In the two series, the N3H signal systematically shifted upfield as the size of the ring increased from six to seven to eight members. The most upfield N3H shift observed was for the heptamethyleneimine derivatives ($Y = (\text{CH}_2)_3$) with the eight-membered ring. The variations in NH shift as the ring size changes can be attributed to a combination of ring-strain, inductive, and solvation effects.

Dependence on L of the $\text{C}_{\text{am}}\text{CH}_3$ NMR Signals of $[\text{Re}(\text{CO})_3(\text{L})(\text{HNC}(\text{CH}_3)\text{N}(\text{CH}_2\text{CH}_2)_2\text{Y})]\text{BF}_4$, for $\text{L} = 5,5'$ -Me₂bipy and $6,6'$ -Me₂bipy. We can readily explain the differences in ¹H NMR shifts of the $\text{C}_{\text{am}}\text{CH}_3$ signal between the two series, $[\text{Re}(\text{CO})_3(5,5'\text{-Me}_2\text{bipy})(\text{HNC}(\text{CH}_3)\text{N}(\text{CH}_2\text{CH}_2)_2\text{Y})]\text{BF}_4$ (~2.1 ppm, 3-7) and $[\text{Re}(\text{CO})_3(6,6'\text{-Me}_2\text{bipy})(\text{HNC}(\text{CH}_3)\text{N}(\text{CH}_2\text{CH}_2)_2\text{Y})]\text{BF}_4$ (~1.6 ppm, 8-12). The shifts are very similar within each of the two series (Table 3.5). The more upfield shift (by ~0.5 ppm) of the $\text{C}_{\text{am}}\text{CH}_3$ signal for the $6,6'$ -Me₂bipy complexes (8-12) than for the $5,5'$ -Me₂bipy complexes (3-7) is clearly attributable to the anisotropic effect of the $6,6'$ -Me₂bipy aromatic ring system. Compared to the $[\text{Re}(\text{CO})_3(5,5'\text{-Me}_2\text{bipy})(\text{HNC}(\text{CH}_3)\text{N}(\text{CH}_2\text{CH}_2)_2\text{Y})]\text{BF}_4$ complexes (3-7), all of the $[\text{Re}(\text{CO})_3(6,6'\text{-Me}_2\text{bipy})(\text{HNC}(\text{CH}_3)\text{N}(\text{CH}_2\text{CH}_2)_2\text{Y})]\text{BF}_4$ complexes (8-12) have a shorter distance from the methyl carbon of the amidine ligand (C17) to the centroid of the closest bipyridine ring. This shorter distance results from the tilting in the $6,6'$ -Me₂bipy ligand, moving the back side of the ring up toward the amidine as discussed above. For example, these distances in $[\text{Re}(\text{CO})_3(5,5'\text{-Me}_2\text{bipy})(\text{HNC}(\text{CH}_3)\text{NC}_5\text{H}_{10})]\text{BF}_4$ (3) and $[\text{Re}(\text{CO})_3(6,6'\text{-Me}_2\text{bipy})(\text{HNC}(\text{CH}_3)\text{NC}_5\text{H}_{10})]\text{BF}_4$ (8) are 4.2 Å and 3.4 Å, respectively. Therefore, the anisotropic upfield-shifting effect of the bipyridine rings is greater on the $\text{C}_{\text{am}}\text{CH}_3$ methyl signal of $[\text{Re}(\text{CO})_3(6,6'\text{-Me}_2\text{bipy})(\text{HNC}(\text{CH}_3)\text{N}(\text{CH}_2\text{CH}_2)_2\text{Y})]\text{BF}_4$ complexes 8-12 than on the $\text{C}_{\text{am}}\text{CH}_3$ ¹H NMR signal for $[\text{Re}(\text{CO})_3(5,5'\text{-Me}_2\text{bipy})(\text{HNC}(\text{CH}_3)\text{N}(\text{CH}_2\text{CH}_2)_2\text{Y})]\text{BF}_4$ complexes 3-7.

The N3H shifts of $[\text{Re}(\text{CO})_3(\text{L})(\text{HNC}(\text{CH}_3)\text{N}(\text{CH}_2\text{CH}_2)_2\text{Y})]\text{BF}_4$ complexes for $\text{L} = 6,6'$ - Me_2bipy are downfield from the corresponding shifts of the $\text{L} = 5,5'$ - Me_2bipy analogues (Table 3.5). At this time, we cannot identify the reasons for this difference because as mentioned above, N3H shifts are influenced by a multiplicity of possible factors. In addition, as L is changed, any changes in the heavy-atom anisotropic or inductive effects of the Re will affect the shift.

Dependence of Reaction Times on the Me_2bipy Ligand and the Amine. For a given amine, reactions were relatively faster with $[\text{Re}(\text{CO})_3(6,6'\text{-Me}_2\text{bipy})(\text{CH}_3\text{CN})]\text{BF}_4$ (**2**) than with $[\text{Re}(\text{CO})_3(5,5'\text{-Me}_2\text{bipy})(\text{CH}_3\text{CN})]\text{BF}_4$ (**1**) (Table 3.6). For **1** and **2**, the time required for reaction, assessed by checking for reaction completion from time to time by NMR spectroscopy

Table 3.6. Times for Complete Reaction of $[\text{Re}(\text{CO})_3(\text{L})(\text{CH}_3\text{CN})]\text{BF}_4$ Complexes with Heterocyclic Amines ($\text{HN}(\text{CH}_2\text{CH}_2)_2\text{Y}$) to Form $[\text{Re}(\text{CO})_3(\text{L})(\text{HNC}(\text{CH}_3)\text{N}(\text{CH}_2\text{CH}_2)_2\text{Y})]\text{BF}_4$ Complexes^a

$\text{HN}(\text{CH}_2\text{CH}_2)_2\text{Y}$ (Y)	$\text{p}K_{\text{a}}$	$\text{L} = 6,6'\text{-Me}_2\text{bipy}$	$\text{L} = 5,5'\text{-Me}_2\text{bipy}$
piperidine (CH_2)	11.1	≤ 3 min	< 5 min
homopiperidine ($(\text{CH}_2)_2$)	10.9	~ 4.5 min	~ 8 min
heptamethyleneimine ($(\text{CH}_2)_3$)	10.8	~ 6 min	6 h
piperazine (NH)	10.2	≤ 3 min	20 min
morpholine (O)	8.5	30 min	4 h

^a Reaction monitored by NMR spectroscopy in acetonitrile- d_3 at 25 °C.

(Figure 3.7), varied with basicity and the ring size of the heterocyclic amine. The $\text{p}K_{\text{a}}$ values of the heterocyclic amines⁴² (Table 3.6) decrease in the order, piperidine (with the highest $\text{p}K_{\text{a}}$, 11.1) > homopiperidine > heptamethyleneimine > piperazine > morpholine.⁴² The reactions of

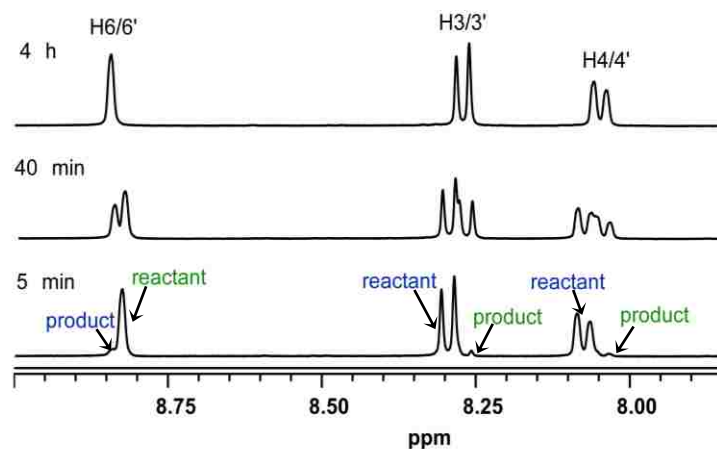


Figure 3.7. Aromatic region of the ^1H NMR spectra in acetonitrile at 25 °C of the reaction of $[\text{Re}(\text{CO})_3(5,5'\text{-Me}_2\text{bipy})(\text{CH}_3\text{CN})]\text{BF}_4$ (1) with morpholine to form $[\text{Re}(\text{CO})_3(5,5'\text{-Me}_2\text{bipy})(\text{HNC}(\text{CH}_3)\text{N}(\text{CH}_2\text{CH}_2)_2\text{O})]\text{BF}_4$ (7).

$[\text{Re}(\text{CO})_3(6,6'\text{-Me}_2\text{bipy})(\text{CH}_3\text{CN})]\text{BF}_4$ (2) with piperidine and piperazine were essentially complete before the first spectrum could be recorded (≤ 3 min). Morpholine, the other six-membered-ring amine, required a much longer reaction time (30 min) owing to its lower basicity ($\text{p}K_a = 8.5$). This same pattern as found for 2 was observed with these heterocyclic amines for 1. For example, morpholine had the longest reaction completion time (4 h) for the six-membered ring amines with 1 (Figure 3.7). These results indicate that greater heterocyclic amine basicity is associated with faster reactions, as would be expected. Piperazine has the second lowest $\text{p}K_a$ (10.2) compared to the other heterocyclic amines used here; however, the reactions of piperazine with 1 and 2 were relatively fast (≤ 3 min and 20 min, respectively). This relative reactivity can be attributed to the statistical reaction probability for each piperazine molecule (with two amine groups) being twice that of other amines used.

A comparison of reaction completion times for amines with no other heteroatoms in the ring (Table 3.6) is instructive. For both the $[\text{Re}(\text{CO})_3(5,5'\text{-Me}_2\text{bipy})(\text{HNC}(\text{CH}_3)\text{N}(\text{CH}_2\text{CH}_2)_2\text{Y})]\text{BF}_4$ and the $[\text{Re}(\text{CO})_3(6,6'\text{-$

Me₂bipy)(HNC(CH₃)N(CH₂CH₂)₂Y)]BF₄ series, the reaction times increase in the order, piperidine < homopiperidine < heptamethyleneimine (Table 3.6). This finding of longer reaction completion times as the number of amine methylene groups increases makes it clear that steric effects decrease amine reactivity. However, the effect of amine bulk on reaction time is highly pronounced only for heptamethyleneimine with the 5,5'-Me₂bipy complex 1. The effect is much less pronounced for the 6,6'-Me₂bipy complex 2 because of the greater interior space near the axial coordination site caused by the tilting of the 6,6'-Me₂bipy ligand (as described above).

Reactions of most cyclic secondary amines with [Re(CO)₃(5,5'-Me₂bipy)(CH₃CN)]BF₄ (1) reached completion in less than 1 h (Table 3.6). In contrast, more time was required for reactions of 1 with primary aliphatic amines, even though most of these previously studied amines have a basicity lying within the pK_a range in Table 3.6. For example, the reaction of [Re(CO)₃(5,5'-Me₂bipy)(CH₃CN)]BF₄ (1) required ~6 h for methylamine (pK_a⁴³ = 10.6) and ~4 days for *tert*-butylamine (pK_a⁴³ = 10.5).²⁵ Reaction times of [Re(CO)₃(5,5'-Me₂bipy)(CH₃CN)]BF₄ (1) and [Re(CO)₃(6,6'-Me₂bipy)(CH₃CN)]BF₄ (2) with isopropylamine (pK_a⁴³ = 10.6) are 28 h and 14 h, respectively.²⁴ These results are consistent with the expected lower nucleophilicity of primary amines as compared with that of the cyclic secondary amines studied here.

Robustness of the Piperidinylamidine Ligation. A fivefold excess of the relatively basic, strongly coordinating 4-dimethylaminopyridine ligand was added to [Re(CO)₃(5,5'-Me₂bipy)(HNC(CH₃)N(CH₂CH₂)₂CH₂)]BF₄ (3) in acetonitrile-*d*₃ or in CDCl₃. No changes in spectral features of 3 were observed for up to two months, indicating that the piperidinylamidine ligand is not readily replaced. The NMR signals for [Re(CO)₃(5,5'-Me₂bipy)(4-

dimethylaminopyridine)]BF₄,²⁵ synthesized as a control, did not change with time in either acetonitrile-*d*₃ or CDCl₃.

3.4 Conclusions

Unlike previously studied analogous amidine complexes derived from primary amines, all ten of the [Re(CO)₃(5,5'- or 6,6'-Me₂bipy)(HNC(CH₃)N(CH₂CH₂)₂Y)]BF₄ complexes formed from cyclic secondary amines studied here exist as only one isomer (the *E* isomer) in both the solid state and in solution. These findings are attributable to the combination of the high steric bulk and the *C*₂ symmetry of the amidine substituents. After dissolution and sufficient time for equilibrium to be established in solution, only the initial *E* isomer was detectable. Thus, the equilibrium between the *Z* and *E* isomers must lie far to the side of the *E* isomer. We conclude that steric repulsions between the N(CH₂CH₂)₂Y groups of the axial amidine ligands and the equatorial ligands preclude formation of any isomer other than *E* (Figures 2.2 and 2.6). Nevertheless, these repulsive interactions do not lead to a weakened Re–N₃ bond, as indicated by the length of this bond.

The 6,6'-methyl groups in [Re(CO)₃(6,6'-Me₂bipy)(HNC(CH₃)N(CH₂CH₂)₂Y)]BF₄ complexes (8-12) cause the 6,6'-Me₂bipy ligand to distort and tilt. Although the “front side” of the 6,6'-Me₂bipy ligand with the 6,6'-methyl groups projects down toward the axial CO group, the “back side” of the 6,6'-Me₂bipy ligand projects up. Thus the 6,6'-Me₂bipy ligand has a net steric footprint comparable to that of the untilted 5,5'-Me₂bipy ligand.

The [Re(CO)₃(5,5'-Me₂bipy)(HNC(CH₃)N(CH₂CH₂)₂CH₂)]BF₄ complex (3) in acetonitrile-*d*₃ or in CDCl₃ was robust when challenged with 4-dimethylaminopyridine, indicating that amidine ligands are strong donors. The heterocyclic amines employed here have a relatively high reactivity and form only amidines with the *E* configuration, indicating that

amidine complexes can be formed quickly and isomerically pure. All of these favorable properties cited here suggest that the strategy of using heterocyclic amines to create amidine links to the *fac*-[M(CO)₃]⁺ core (M = ^{99m}Tc and ^{186/188}Re radionuclides) may be a useful conjugation method for the development of targeted radiopharmaceuticals.

3.5 References

- (1) Alberto, R. *Eur. J. Nucl. Med. Mol. Imaging* **2003**, *30*, 1299-1302.
- (2) Schibli, R.; Schubiger, P. A. *Eur. J. Nucl. Med.* **2002**, *29*, 1529-1542.
- (3) Banerjee, S. R.; Maresca, K. P.; Francesconi, L.; Valliant, J.; Babich, J. W.; Zubieta, J. *Nucl. Med. Biol.* **2005**, *32*, 1-20.
- (4) Lipowska, M.; Marzilli, L. G.; Taylor, A. T. *J. Nucl. Med.* **2009**, *50*, 454-460.
- (5) Bartholomä, M.; Valliant, J.; Maresca, K. P.; Babich, J.; Zubieta, J. *Chem. Commun. (Cambridge, U.K.)* **2009**, 493-512.
- (6) Alberto, R. In *Technetium-99m radiopharmaceuticals : status and trends*; International Atomic Energy Agency: Vienna, **2009**, pp 19-40.
- (7) Wei, L.; Babich, J. W.; Ouellette, W.; Zubieta, J. *Inorg. Chem.* **2006**, *45*, 3057-3066.
- (8) Lipowska, M.; He, H.; Malveaux, E.; Xu, X.; Marzilli, L. G.; Taylor, A. T. *J. Nucl. Med.* **2006**, *47*, 1032-1040.
- (9) Taylor, A. T.; Lipowska, M.; Marzilli, L. G. *J. Nucl. Med.* **2010**, *51*, 391-396.
- (10) Desbouis, D.; Struthers, H.; Spiwok, V.; Küster, T.; Schibli, R. *J. Med. Chem.* **2008**, *51*, 6689-6698.
- (11) Abram, U.; Alberto, R. *J. Braz. Chem. Soc.* **2006**, *17*, 1486-1500.
- (12) Alberto, R.; Schibli, R.; Abram, U.; Egli, A.; Knapp, F. F.; Schubiger, P. A. *Radiochim. Acta* **1997**, *79*, 99-103.
- (13) Alberto, R.; Schibli, R.; Schubiger, A. P.; Abram, U.; Pietzsch, H. J.; Johannsen, B. *J. Am. Chem. Soc.* **1999**, *121*, 6076-6077.
- (14) Murray, A.; Simms, M. S.; Scholfield, D. P.; Vincent, R. M.; Denton, G.; Bishop, M. C.; Price, M. R.; Perkins, A. C. *J. Nucl. Med.* **2001**, *42*, 726-732.

- (15) Schibli, R.; Schwarzbach, R.; Alberto, R.; Ortner, K.; Schmalle, H.; Dumas, C.; Egli, A.; Schubiger, P. A. *Bioconjugate Chem.* **2002**, *13*, 750-756.
- (16) Agorastos, N.; Borsig, L.; Renard, A.; Antoni, P.; Viola, G.; Springler, B.; Kurz, P.; Alberto, R. *Chem. Eur. J.* **2007**, *13*, 3842-3852.
- (17) Cyr, J. E.; Pearson, D. A.; Wilson, D. M.; Nelson, C. A.; Guaraldi, M.; Azure, M. T.; Lister-James, J.; Dinkelborg, L. M.; Dean, R. T. *J. Med. Chem.* **2007**, *50*, 1354-1364.
- (18) He, H. Y.; Lipowska, M.; Christoforou, A. M.; Marzilli, L. G.; Taylor, A. T. *Nucl. Med. Biol.* **2007**, *34*, 709-716.
- (19) He, H.; Lipowska, M.; Xu, X.; Taylor, A. T.; Marzilli, L. G. *Inorg. Chem.* **2007**, *46*, 3385-3394.
- (20) Lipowska, M.; He, H.; Xu, X.; Taylor, A. T.; Marzilli, P. A.; Marzilli, L. G. *Inorg. Chem.* **2010**, *49*, 3141-3151.
- (21) Alberto, R. *Eur. J. Inorg. Chem.* **2009**, 21-31.
- (22) He, H.; Lipowska, M.; Xu, X.; Taylor, A. T.; Carlone, M.; Marzilli, L. G. *Inorg. Chem.* **2005**, *44*, 5437-5446.
- (23) Perera, T.; Abhayawardhana, P.; Fronczek, F. R.; Marzilli, P. A.; Marzilli, L. G. *Eur. J. Inorg. Chem.* **2012**, 616-627.
- (24) Perera, T.; Abhayawardhana, P.; Marzilli, P. A.; Fronczek, F. R.; Marzilli, L. G., Manuscript in Preparation.
- (25) Perera, T.; Fronczek, F. R.; Marzilli, P. A.; Marzilli, L. G. *Inorg. Chem.* **2010**, *49*, 7035-7045.
- (26) Wald, J.; Alberto, R.; Ortner, K.; Candreia, L. *Angew. Chem. Int. Ed.* **2001**, *40*, 3062-3066.
- (27) Saidi, M.; Seifert, S.; Kretzschmar, M.; Bergmann, R.; Pietzsch, H. J. *J. Organomet. Chem.* **2004**, *689*, 4739-4744.
- (28) John, C. S.; Lim, B. B.; Geyer, B. C.; Vilner, B. J.; Bowen, W. D. *Bioconjugate Chem.* **1997**, *8*, 304-309.
- (29) Palma, E.; Correia, J. D. G.; Domingos, A.; Santos, I.; Alberto, R.; Spies, H. *J. Organomet. Chem.* **2004**, *689*, 4811-4819.
- (30) Seridi, A.; Wolff, M.; Boulay, A.; Saffon, N.; Coulais, Y.; Picard, C.; Machura, B.; Benoist, E. *Inorg. Chem. Commun.* **2011**, *14*, 238-242.

- (31) Eicher, T.; Hauptmann, S. *The Chemistry of Heterocycles*, 2nd ed., WILEY-VCH GmbH & Co. KGaA, Weinheim, **2003**.
- (32) Sun, H.; Scott, D. O. *ACS Med. Chem. Lett.* **2011**, 2 638–643.
- (33) Schmidt, S. P.; Trogler, W. C.; Basolo, F. *Inorg. Synth.* **1990**, 28, 160-165.
- (34) Edwards, D. A.; Marshalsea, J. J. *Organomet. Chem.* **1977**, 131, 73-91.
- (35) Otwinowski, Z.; Minor, W. *Macromolecular Crystallography, Part A, Methods in Enzymology*; New York Academic Press: New York, **1997**; Vol. 276, pp. 307-326.
- (36) Sheldrick, G. M. *Acta Crystallogr., Sect. A* **2008**, A64, 112-122.
- (37) Bao, X.; Holt, E. M. *Acta Crystallogr., Sect. C: Cryst. Struct. Commun.* **1992**, 48, 1655-1657.
- (38) Lefèvre, X.; Durieux, G.; Lesturgez, S.; Zargarian, D. *J. Mol. Catal. A: Chem.* **2011**, 335, 1-7.
- (39) Rozenel, S. S.; Kerr, J. B.; Arnold, J. *Dalton Trans.* **2011**, 40, 10397-10405.
- (40) Cini, R.; Caputo, P.; Intini, F. P.; Natile, G. *Inorg. Chem.* **1995**, 182, 1130-1137.
- (41) Liddle, B. J.; Lindeman, S. V.; Reger, D. L.; Gardinier, J. R. *Inorg. Chem.* **2007**, 46, 8484.
- (42) Frenna, V.; Vivona, N.; Consiglio, G.; Spinelli, D. *J. Chem. Soc. Perkin Trans. 2* **1985**, 1865-1868.
- (43) Hall, H. K. *J. Am. Chem. Soc.* **1957**, 79, 5441-5444.

CHAPTER 4

***fac*-[Re(CO)₃(5,5'- OR 6,6'-Me₂BIPYRIDINE)(HNC(R)N(CH₂)_x)]BF₄ COMPLEXES (R = CH₃ OR C₆H₅; X = 3 TO 5). FACILE SYNTHESIS OF *fac*-[Re(CO)₃(L)(AMIDINE)]⁺ COMPLEXES BY USING SMALL CYCLIC AMINES**

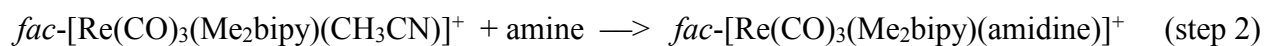
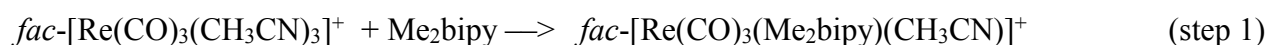
4.1 Introduction

The design of ligands for radiopharmaceuticals with the *fac*-M^I(CO)₃⁺ core (M = ^{99m}Tc, ^{186/188}Re) core having diagnostic and therapeutic properties continues to be an important endeavor.¹⁻⁶ Nonradioactive Re analogues are useful for understanding the chemistry of the radioactive ^{99m}Tc agents as well as for improving ligand design and for designing new linking chemistry for bioconjugation.^{7,8} The recently developed straightforward preparations of aqueous solutions of the nonradioactive *fac*-[Re(CO)₃(H₂O)₃]⁺ precursor^{7,9-12} have made possible the preparation of *fac*-[Re(CO)₃(L)] complexes under aqueous conditions simulating preparations of the clinically useful *fac*-[^{99m}Tc(CO)₃(L)] analogues from the *fac*-[^{99m}Tc(CO)₃(H₂O)₃]⁺ precursor; this clinically relevant precursor is produced in aqueous solutions by employing commercially available “kits”.^{2,13,14}

Whereas the use of aqueous conditions is necessary for medical applications, aqueous conditions limit full exploration of the synthetic chemistry of *fac*-[Re(CO)₃(L)] complexes because some ligands are not water soluble. Also, aqueous conditions can complicate the monitoring of reactions by NMR spectroscopy, TLC, etc. Finally, high pH conditions allowing basic ligands to coordinate can lead to oligomerization of *fac*-[Re(CO)₃(H₂O)₃]⁺ complexes.¹⁵ We have thus been exploring methods of synthesizing *fac*-[M(CO)₃L] complexes in organic solvents.¹⁶ Once the new chemistry is developed in organic solvents, modifications can be made to adapt the chemistry for radiopharmaceutical applications. For example, mixed aqueous-organic solvent conditions suitable for the use of the *fac*-[^{99m}Tc(CO)₃(H₂O)₃]⁺ precursor can be

employed. In addition, ligands not soluble in water can be modified to increase their hydrophilicity.

One approach for using organic solvents that we have recently explored employs the *fac*-[Re(CO)₃(CH₃CN)₃]X precursor (X = PF₆⁻ or BF₄⁻).¹⁶⁻¹⁹ We have investigated the use of this precursor for synthesizing *fac*-[Re(CO)₃(Me₂bipy)(CH₃CN)]⁺ complexes (Me₂bipy = dimethyl-2,2'-bipyridine) in organic solvents.¹⁷⁻¹⁹ In the present report, we refer to this reaction as step 1 of Method A. Step 2 of Method A is the reaction of *fac*-[Re(CO)₃(Me₂bipy)(CH₃CN)]⁺ in acetonitrile with an amine to form amidine complexes.



The first use of Method A involved the step 2 reaction of *fac*-[Re(CO)₃(5,5'-Me₂bipy)(CH₃CN)]⁺ with primary amines to form *fac*-[Re(CO)₃(5,5'-Me₂bipy)(HNC(CH₃)NHR)]⁺ amidine complexes (Figure 4.1).¹⁸ The sp carbon and sp nitrogen atoms of the acetonitrile nitrile group have been converted to an amidine sp² carbon (C_{am}) and a rhenium-bound sp² nitrogen (N3) (Figure 4.1).^{18,19} The partial double-bond character of the C_{am}-N3 and C_{am}-N4 bonds of these *fac*-[Re(CO)₃(5,5'-Me₂bipy)(HNC(CH₃)NHR)]⁺ complexes can lead to four configurations of the amidine ligand and hence four isomers in solution (Figure 4.1). The *fac*-[Re(CO)₃(5,5'-Me₂bipy)(HNC(CH₃)NHR)]⁺ complexes were found to exist as the *E'* isomer in the solid state; however, they equilibrated to mixtures of two isomers (*E'* and *Z*) in polar solvents such as CD₃CN and to three isomers (*E'*, *E*, and *Z*) in less polar solvents such as CDCl₃.¹⁸ The *E'* to *Z* equilibration upon crystal dissolution required ~15 min, indicating that rotation around the C_{am}-N3 bond is relatively slow, a finding consistent with the shorter distance reported for the C_{am}-N3 bond than for the C_{am}-N4 bond.¹⁸ In less polar solvents, in which the *E*

isomer exists in detectable abundance, the E' and E ^1H NMR signals were somewhat broad and connected by EXSY cross-peaks. Thus, although rotation around the $\text{C}_{\text{am}}\text{-N}_4$ bond is faster than rotation around the $\text{C}_{\text{am}}\text{-N}_3$ bond, rotation around the $\text{C}_{\text{am}}\text{-N}_4$ bond is slow enough to allow detection of separate E' and E ^1H NMR signals.¹⁸

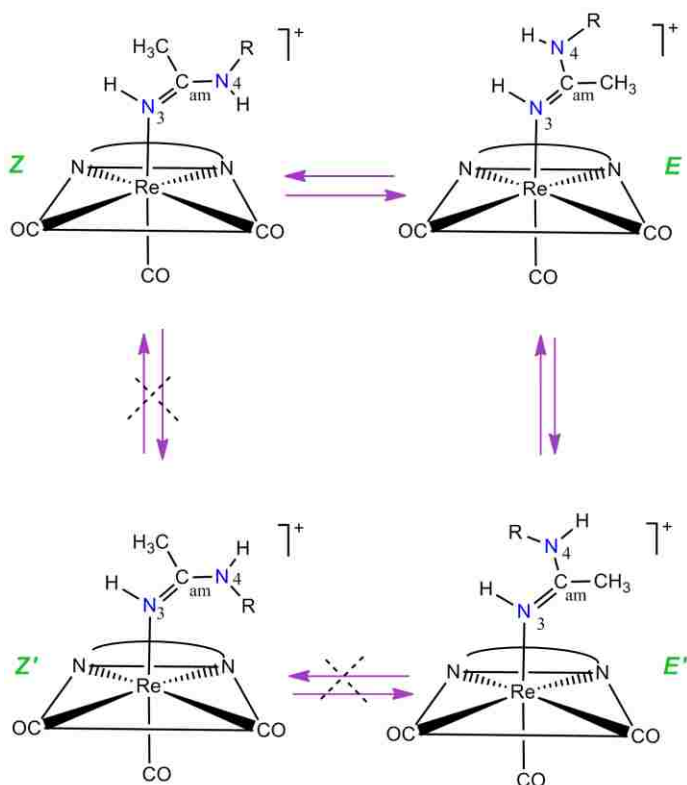


Figure 4.1. Four conceivable isomers of $\text{fac-}[\text{Re}(\text{CO})_3(5,5'\text{-Me}_2\text{bipy})(\text{HNC}(\text{CH}_3)\text{NHR})]^+$ N-N denotes a C_2 -symmetrical bidentate N-donor ligand. Note that the Z' isomer was not detected.¹⁸

We were encouraged by the finding that the monodentate axial amidine ligand is robustly attached to the metal and thus could be used as a means for bioconjugation of the $\text{fac-}M^{\text{I}}(\text{CO})_3^+$ core ($M = {}^{99\text{m}}\text{Tc}$, Re) core.¹⁸⁻²⁰ Our main goal became to identify a method of preparing exclusively a single isomer of amidine complexes because the presence of multiple isomers complicates the development of ideal agents for medical applications.¹⁹ The symmetry of C_2 -symmetrical secondary amines restricts the number of possible isomers to two, the E and Z isomers. By employing large 6-, 7-, and 8-membered ring C_2 -symmetrical, heterocyclic

secondary amines (HN(CH₂)₂Y, see Figure 4.2) instead of linear primary amines, we were able to synthesize isomerically pure and robust *E* isomers of *fac*-[Re(CO)₃(Me₂bipy)(HNC(CH₃)N(CH₂)₂Y)]BF₄ complexes.¹⁹ In these complexes, steric repulsions between the N-heterocyclic ring substituents, -N(CH₂)₂Y, of the axial amidine ligand and the ligands in the equatorial coordination plane (defined as the Me₂bipy and two trans CO ligands) greatly destabilize the only other possible isomer (*Z*) (Figure 4.3). Recently we utilized this concept to prepare a single isomer of analogues with a large 6-membered-ring cyclic amine moiety linking the *fac*-Re^I(CO)₃⁺ core to a B₁₂ model.²⁰

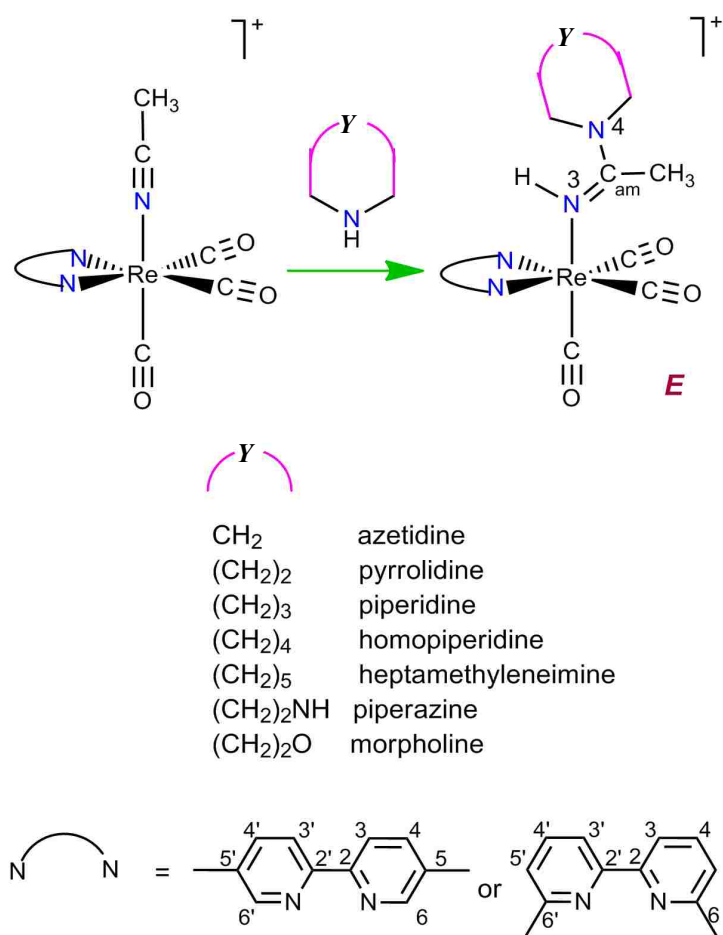


Figure 4.2. Synthetic scheme for *fac*-[Re(CO)₃(Me₂bipy)(HNC(CH₃)N(CH₂)₂Y)]BF₄ complexes,¹⁹ showing numbering system for discussion of NMR data (N–N denotes the Me₂bipy ligand).

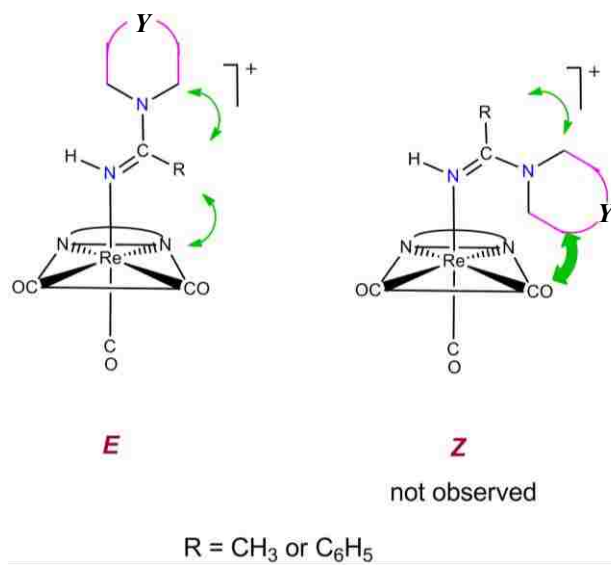


Figure 4.3. Conceivable isomers of *fac*-[Re(CO)₃(Me₂bipy)(HNC(R)N(CH₂)₂Y)]BF₄ complexes; R = CH₃ or C₆H₅. See Figures 4.2 and 4.4 for definition of Y. N–N = 5,5'-Me₂bipy or 6,6'-Me₂bipy ligand; double-headed arrows indicate steric interactions between groups, and arrow thickness reflects predicted qualitative severity of the steric repulsions.

Heterocyclic amines provide the added advantage of requiring less time than primary amines to form amidines.¹⁹ The smallest and most basic heterocyclic amines were most reactive. Greater reactivity is advantageous because smaller quantities of amines can be used. Consequently, in the present study we focus on the goal of further reducing reaction times for amidine formation by exploring the use of 4- and 5-membered cyclic amines in place of larger amines and of benzonitrile instead of acetonitrile. One important goal was to determine if smaller heterocyclic amines form amidine complexes having only a single isomer.

We determined in the present study that the use of 4- and 5-membered cyclic amines in step 2 of Method A quickly afforded amidine complexes having only the *E* isomer from either the *fac*-[Re(CO)₃(Me₂bipy)(CH₃CN)]BF₄ (Figures 4.2 and 4.4) or *fac*-[Re(CO)₃(Me₂bipy)(C₆H₅CN)]BF₄ (Figure 4.5) intermediates. However, synthesis of these *fac*-[Re(CO)₃(Me₂bipy)(RCN)]BF₄ intermediates starting from the *fac*-[Re(CO)₃(CH₃CN)₃]⁺

precursor in organic solvents required many hours (*cf.* Figure 4.4).¹⁷ A faster method is needed to make the amidine bioconjugation process more applicable to clinical studies.

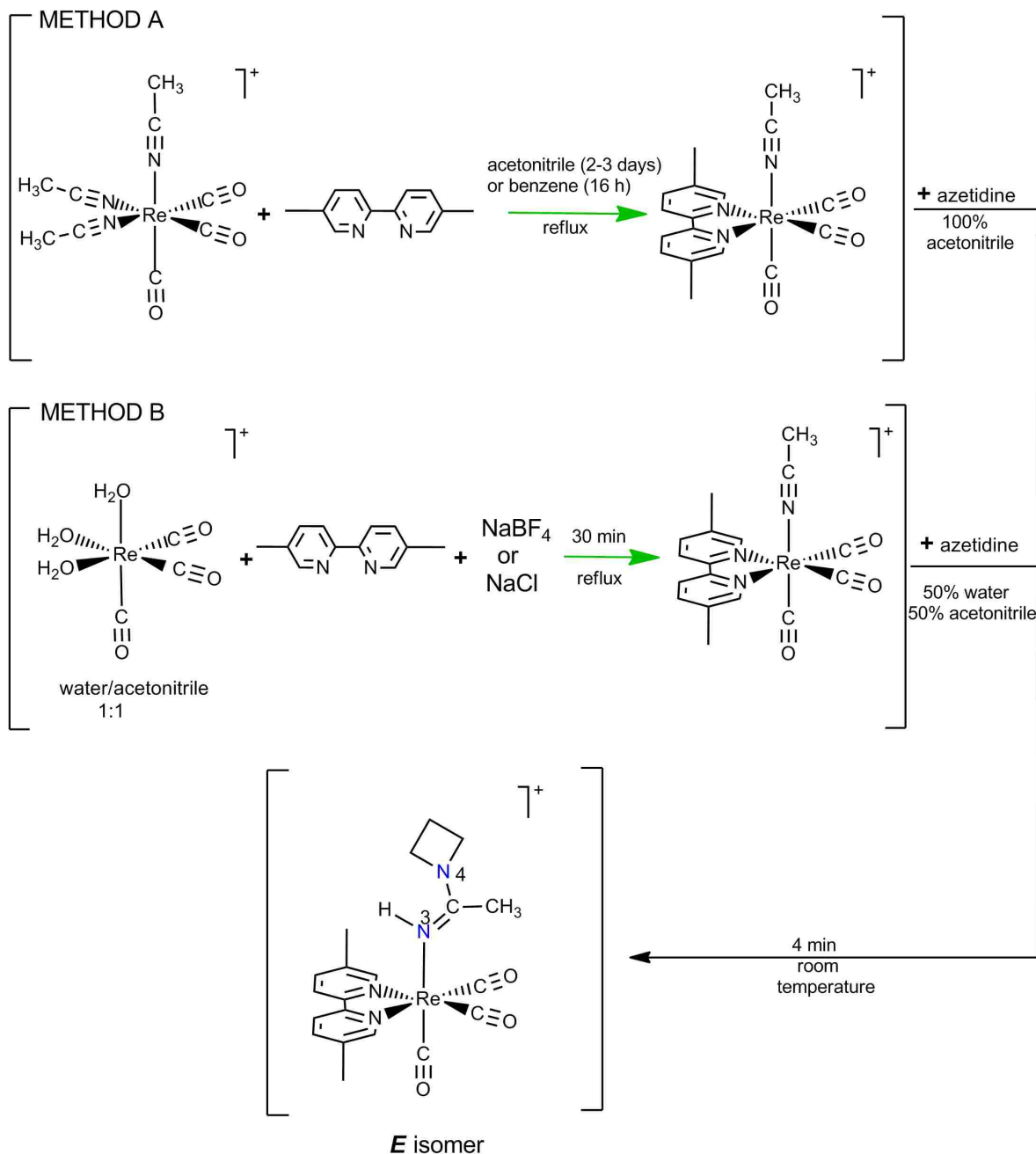


Figure 4.4. Comparisons of Methods A and B used to synthesize *fac*-[Re(CO)₃(5,5'-Me₂bipy)(HNC(CH₃)N(CH₂)₃)]BF₄, illustrated for azetidine.

In the present study we describe the use of the *fac*-[Re^I(CO)₃(H₂O)₃]⁺ precursor to synthesize *fac*-[Re(CO)₃(Me₂bipy)(HNC(CH₃)N(CH₂)_x)]⁺ complexes in partially aqueous conditions. The new method, Method B (Figure 4.4), requires much less time for step 1 and thus is superior to previous preparations in purely organic solvents. In addition, the conditions are consistent with employing the *fac*-[^{99m}Tc(CO)₃(H₂O)₃]⁺ precursor.

From this point onward, when discussing specific complexes, we omit the *fac*-designation because all of the new complexes and other similar complexes discussed below have the facial geometry. Whereas [Re(CO)₃(Me₂bipy)(HNC(R)N(CH₂)₂Y)]BF₄ is used to define more general cases in which *Y* may contain a heteroatom in addition to CH₂ groups (Figures 4.2, 4.3 and 4.5), numerical subscripts are used, as in [Re(CO)₃(Me₂bipy)(HNC(R)N(CH₂)₅₋₇)]BF₄ (R = CH₃ or C₆H₅), to designate complexes in which the heterocyclic ring substituent on the amidine carbon (C_{am}) contains a given number of methylene groups (5 to 7 in this case). (Note that in the present report, the atom-numbering scheme for crystallographic data uses C16 for C_{am}.)

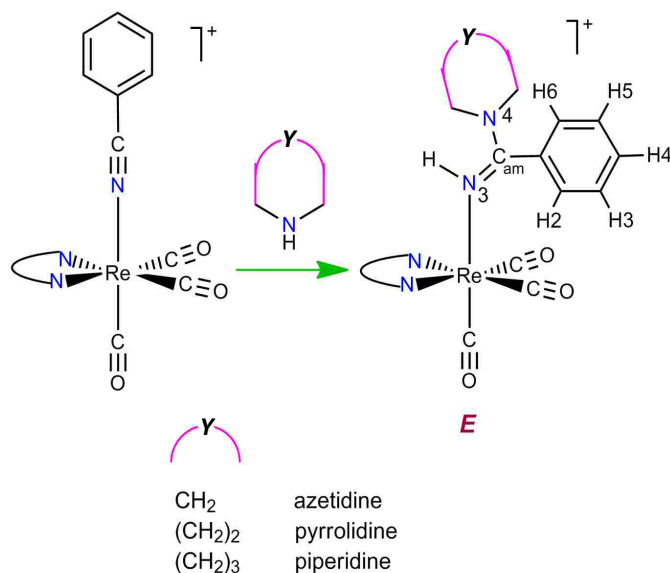


Figure 4.5. Synthesis of *fac*-[Re(CO)₃(Me₂bipy)(HNC(C₅H₆)N(CH₂)₂Y)]BF₄ complexes, showing the numbering system for discussing the phenyl ring NMR signals. N–N denotes the Me₂bipy ligand.

4.2 Experimental Section

Starting Materials. $\text{Re}(\text{CO})_5\text{Br}$ and previously reported $[\text{Re}(\text{CO})_3(\text{Me}_2\text{bipy})(\text{HNC}(\text{CH}_3)\text{N}(\text{CH}_2)_{5-7})]\text{BF}_4$ complexes were synthesized as described in the literature.^{19,21} $\text{Re}_2(\text{CO})_{10}$, 5,5'-dimethyl-2,2'-bipyridine (5,5'-Me₂bipy), 6,6'-dimethyl-2,2'-bipyridine (6,6'-Me₂bipy), benzonitrile, piperidine, piperazine, pyrrolidine, azetidine, and AgBF_4 were obtained from Aldrich. $[\text{Re}(\text{CO})_3(\text{CH}_3\text{CN})_3]\text{BF}_4$ (prepared by a slight modification of a known procedure²²) was used to prepare $[\text{Re}(\text{CO})_3(5,5'\text{- or }6,6'\text{-Me}_2\text{bipy})(\text{CH}_3\text{CN})]\text{BF}_4$.¹⁷ An aqueous stock solution (0.1 M) of $[\text{Re}(\text{CO})_3(\text{H}_2\text{O})_3]\text{OTf}$ (prepared as previously reported)⁹ was prepared and used as needed.

NMR Measurements. ^1H and ^{13}C NMR spectra were recorded on 400 MHz or 500 MHz Bruker spectrometers. Peak positions are relative to TMS or to solvent residual peak, with TMS as reference. All NMR data were processed with TopSpin and MestReNova software.

X-ray Data Collection and Structure Determination. Intensity data were collected at low temperature on a Bruker Kappa Apex-II DUO CCD diffractometer fitted with an Oxford Cryostream cooler and graphite-monochromated $\text{Mo K}\alpha$ ($\lambda = 0.71073 \text{ \AA}$) radiation. Data reduction included absorption corrections by the multiscan method, with SADABS.²³ All X-ray structures were determined by direct methods and difference Fourier techniques and refined by full-matrix least-squares methods by using SHELXL97.²⁴

Synthesis of $[\text{Re}(\text{CO})_3(\text{Me}_2\text{bipy})(\text{C}_6\text{H}_5\text{CN})]\text{BF}_4$ Complexes (Me₂bipy = 5,5'-Me₂bipy and 6,6'-Me₂bipy). A CHCl_3 solution (10 mL) of $[\text{Re}(\text{CO})_3(\text{Me}_2\text{bipy})(\text{CH}_3\text{CN})]\text{BF}_4$ (29 mg, 0.05 mmol) (Me₂bipy = 5,5'-Me₂bipy or 6,6'-Me₂bipy) was treated with benzonitrile (0.15 mL, 1.50 mmol), and the reaction mixture was stirred and heated at reflux. The volume was reduced to ~1 mL by rotary evaporation. Addition of diethyl ether to the point of cloudiness (~10–20

mL) produced a yellow crystalline material that was collected on a filter, washed with diethyl ether, and dried in air. ^1H NMR signals (ppm) in CDCl_3 for $[\text{Re}(\text{CO})_3(5,5'\text{-Me}_2\text{bipy})(\text{C}_6\text{H}_5\text{CN})]\text{BF}_4$: 8.73 (s, 2H, H6/6'), 8.70 (d, $J = 8.6$ Hz, 2H, H3/3'), 8.13 (d, $J = 7.8$ Hz, 2H, H4/4'), 7.66 (t, $J = 10.0$ Hz, 1H, H4), 7.58 (d, $J = 7.5$ Hz, 2H, H2/6), 7.49 (t, $J = 7.7$ Hz, 1H, H3/5), 2.54 (s, 6H, 5/5'-2CH₃). MALDI-TOF m/z: $[\text{M}^+]$ calcd for $\text{C}_{22}\text{H}_{17}\text{O}_3\text{N}_3\text{Re}$, 558.08; found, 558.139. ^1H NMR signals (ppm) in CDCl_3 for $[\text{Re}(\text{CO})_3(6,6'\text{-Me}_2\text{bipy})(\text{C}_6\text{H}_5\text{CN})]\text{BF}_4$: 8.80 (d, $J = 7.0$ Hz, 2H, H3/3'), 8.21 (t, $J = 7.6$ Hz, 2H, H4/4'), 7.62 (d, $J = 7.3$ Hz, 2H, H5/5'), 7.56 (t, $J = 7.8$ Hz, 1H, H4), 7.55 (d, $J = 8.6$ Hz, 2H, H2/6), 7.48 (t, $J = 7.8$ Hz, 2H, H3/4), 3.09 (s, 6H, 6/6'-2CH₃). MALDI-TOF m/z: $[\text{M}^+]$ calcd for $\text{C}_{22}\text{H}_{17}\text{O}_3\text{N}_3\text{Re}$, 558.08; found, 558.142.

General Procedure for the Synthesis and Isolation of $[\text{Re}(\text{CO})_3(\text{Me}_2\text{bipy})(\text{HNC}(\text{R})\text{N}(\text{CH}_2)_x)]\text{BF}_4$ Complexes (1–10). A reaction mixture consisting of 0.06 mmol $[\text{Re}(\text{CO})_3(\text{Me}_2\text{bipy})(\text{RCN})]\text{BF}_4$ ($\text{Me}_2\text{bipy} = 5,5'$ - or $6,6'$ - Me_2bipy ; $\text{R} = \text{CH}_3$ or C_6H_5) and 0.60 mmol of azetidine, pyrrolidine, or piperidine in CH_3CN ($\text{R} = \text{CH}_3$) or CHCl_3 ($\text{R} = \text{C}_6\text{H}_5$) solution (6 mL) was stirred at room temperature for ~30 to 60 min. The volume was reduced to ~1 mL by rotary evaporation. Addition of diethyl ether to the point of cloudiness (~10 mL) produced a yellow crystalline material that was collected on a filter, washed with diethyl ether, and dried in air. Ten new $[\text{Re}(\text{CO})_3(\text{Me}_2\text{bipy})(\text{HNC}(\text{R})\text{N}(\text{CH}_2)_x)]\text{BF}_4$ complexes (1–10) were prepared. For a given x , the five new $5,5'$ - Me_2bipy complexes are assigned an odd number (1, 3, 5, 7, and 9) and the five new $6,6'$ - Me_2bipy complexes are assigned an even number (2, 4, 6, 8, and 10).

All ^1H NMR spectra, recorded both immediately upon dissolution of the products (1–10) in CDCl_3 or CD_3CN and subsequently, showed signals for only one isomer (established to be the *E* isomer, Figure 4.3, by both solution and solid-state characterization). Also, when the progress

of the amidine formation reactions was monitored over time by ^1H NMR spectroscopy on a small scale in NMR tubes, the only signals observed for products were identical to those of the isolated products. ^1H and ^{13}C NMR data for 1–10 in CDCl_3 appear in Tables 4.1–4.4. ^1H NMR data for 1–4 in CD_3CN are given in Supporting Information.

Table 4.1. ^1H NMR Shifts (ppm) for $[\text{Re}(\text{CO})_3(\text{L})(\text{HNC}(\text{CH}_3)\text{N}(\text{CH}_2)_x)]\text{BF}_4$ Complexes (CDCl_3 , 27°C)

signal / x	3	4	5 ¹⁹	6 ¹⁹	7 ¹⁹	3	4	5 ¹⁹	6 ¹⁹
	L = 5,5'-Me ₂ bipy					L = 6,6'-Me ₂ bipy			
H6/6'	8.61	8.63	8.63	8.63	8.64				
H5/5'						7.48	7.50	7.51	7.53
H4/4'	7.97	8.01	8.02	8.05	8.04	8.04	8.08	8.07	8.10
H3/3'	8.36	8.47	8.48	8.55	8.57	8.37	8.44	8.40	8.44
L-CH ₃	2.50	2.50	2.50	2.50	2.50	3.03	3.05	3.04	3.06
N3H	4.27	4.10	4.58	4.25	4.21	4.31	4.26	4.92	4.60
C _{am} -CH ₃	2.08	2.30	2.32	2.33	2.34	1.66	1.83	1.88	1.87
N-CH ₂ <i>endo</i>	4.05	3.37	3.06 br	3.35	3.30	4.03	3.31	3.08 br	3.31
N-CH ₂ <i>exo</i>	3.68	2.78	3.06 br	2.88	3.03	3.67	2.80	3.08 br	2.96
CH ₂ signals	2.13	1.83	1.49	1.58	1.60	2.20	1.84	1.52	1.54
			1.43	1.43	1.52			1.43	1.43
				1.31	1.33				1.37
				1.25	1.10				1.37
					0.95				

Table 4.2. ¹H NMR Shifts (ppm) for [Re(CO)₃(L)(HNC(C₆H₅)N(CH₂)_x)]BF₄ Complexes in CDCl₃ at 27 °C

signal /x	3	4	5	3	4	5
	L = 5,5'-Me ₂ bipy			L = 6,6'-Me ₂ bipy		
H6/6'	8.37	8.38	8.42			
H5/5'				7.39	7.44	7.46
H4/4'	7.95	7.99	8.00	8.05	8.09	8.09
H3/3'	8.38	8.44	8.44	8.45	8.51	8.44
Ph ring H2/6	7.18	7.14	7.18	6.93	6.88	6.95
Ph ring H3/5	7.44	7.45	7.48	7.35	7.36	7.40
Ph ring H4	7.51	7.51	7.54	7.46	7.47	7.50
L-CH ₃	2.45	2.47	2.49	2.75	2.75	2.81
N3H	4.68	4.69	5.17	4.49	4.49	5.22
N-CH ₂ <i>endo</i>	3.63	2.88	br 2.87	3.63	2.87	br 2.84
N-CH ₂ <i>exo</i>	3.81	2.97	br 2.96	3.74	2.93	br 3.01
CH ₂ signals	2.13	1.92 (<i>exo</i>)	~1.56	2.18	1.96 (<i>exo</i>)	~1.57
		1.69 (<i>endo</i>)	1.52		1.71 (<i>endo</i>)	1.50

Table 4.3. ^{13}C NMR Shifts (ppm) for $[\text{Re}(\text{CO})_3(\text{L})(\text{HNC}(\text{CH}_3)\text{N}(\text{CH}_2)_x)]\text{BF}_4$ Complexes in CDCl_3 at 27 °C

signal /x	3	4	5 ¹⁹	6 ¹⁹	7 ¹⁹	3	4	5 ¹⁹	6 ¹⁹
	L = 5,5' -Me ₂ bipy					L = 6,6' -Me ₂ bipy			
C6/6'	152.22	152.28	152.35	152.24	152.25	162.52	162.33	162.68	162.64
C5/5'	138.21	138.39	138.47	138.50	138.54	127.00	127.12	127.36	127.36
C4/4'	141.09	141.44	141.51	141.67	141.69	140.44	140.87	140.86	141.02
C3/3'	124.74	125.13	125.08	125.36	125.39	123.06	123.59	123.03	123.27
C2/2'	153.88	153.53	153.48	153.41	153.98	157.69	157.73	157.67	157.63
L-CH ₃	18.77	18.74	18.72	18.74	18.72	29.68	30.03	29.90	30.02
C _{am}	167.23	166.14	167.13	167.52	167.03	166.89	165.79	166.48	166.04
C _{am} -CH ₃	18.77	22.63	22.52	21.96	22.07	16.81	21.03	20.91	20.40
N-CH ₂ <i>endo</i>	52.25	50.04	br 46.87	50.99	53.30	51.98	49.88	br 47.26	51.18
N-CH ₂ <i>exo</i>	49.37	46.27	br 46.87	48.02	47.96	48.72	46.22	br 47.26	48.14
CH ₂ signals	14.27	25.83	25.29	29.64	27.69	13.98	25.71	25.54	29.45
		24.77	23.55	26.77	27.37		24.74	23.63	26.78
				26.65	24.42				26.37
				25.03	24.25				25.38
					21.14				

Table 4.4. ^{13}C NMR Shifts (ppm) for $[\text{Re}(\text{CO})_3(\text{Me}_2\text{bipy})(\text{HNC}(\text{C}_6\text{H}_5)\text{N}(\text{CH}_2)_x)]\text{BF}_4$ Complexes in CDCl_3 at 27 °C

signal /x	3	4	5	3	4	5
	L = 5,5'-Me ₂ bipy			L = 6,6'-Me ₂ bipy		
C6/6'	152.26	152.21	152.23	162.53	162.553	162.75
C5/5'	138.13	138.22	138.26	127.07	127.12	127.36
C4/4'	140.96	141.18	141.21	140.45	140.64	140.66
C3/3'	124.63	124.78	124.90	123.63	123.79	123.30
C2/2'	153.66	153.53	153.68	157.91	157.91	157.82
L-CH ₃	18.76	18.75	18.79	29.93	29.93	29.93
C _{am}	169.20	167.86	170.05	169.09	167.77	169.71
Ph ring C1	131.90	135.27	134.95	131.09	134.69	134.22
Ph ring C2/6	127.81	127.45	128.25	127.59	127.22	127.86
Ph ring C3/5	129.12	129.24	129.34	129.13	129.28	129.38
Ph ring C4	130.59	130.23	130.63	130.81	130.39	130.81
N-CH ₂ <i>endo</i>	52.79	51.56	br 51.01	52.90	51.48	br 51.12
N-CH ₂ <i>exo</i>	49.34	46.20	br 45.73	49.15	46.17	br 45.68
CH ₂ signals	14.44	25.73 (<i>endo</i>)	br 29.96	14.38	25.69	br 30.15
		24.78 (<i>exo</i>)	br 27.72		(<i>endo</i>)	br 25.96
			23.76		24.77 (<i>exo</i>)	23.80

[Re(CO)₃(5,5'-Me₂bipy)(HNC(CH₃)N(CH₂)₃)]BF₄ (1). The use of the general procedure for the reaction of [Re(CO)₃(5,5'-Me₂bipy)(CH₃CN)]BF₄ (34.9 mg, 0.06 mmol) with azetidine (40.7 μL, 0.60 mmol) in acetonitrile afforded 20 mg (62% yield) of yellow crystalline material. Adding diethyl ether (19 mL) to a solution of this material in CH₃CN (5 mg/1 mL) and allowing the solvent mixture to evaporate slowly afforded X-ray quality crystals of the *E* isomer. Crystals of the *E* isomer of complexes 2–10 were obtained in a similar manner, as described below.

[Re(CO)₃(6,6'-Me₂bipy)(HNC(CH₃)N(CH₂)₃)]BF₄ (2). In the treatment of [Re(CO)₃(6,6'-Me₂bipy)(CH₃CN)]BF₄ (34.9 mg, 0.06 mmol) with azetidine (40.7 μL, 0.60 mmol) in CH₃CN, the general procedure afforded 29 mg (76% yield) of yellow crystalline material. X-ray quality crystals of 2 were obtained as described for 1 by the addition of 25 mL of diethyl ether.

[Re(CO)₃(5,5'-Me₂bipy)(HNC(CH₃)N(CH₂)₄)]BF₄ (3). The use of the general procedure for the reaction of [Re(CO)₃(5,5'-Me₂bipy)(CH₃CN)]BF₄ (34.9 mg, 0.06 mmol) with pyrrolidine (49.6 μL, 0.60 mmol) in CH₃CN afforded 30 mg (77% yield) of yellow crystalline material. X-ray quality crystals of 3 were obtained as described for 1 by adding diethyl ether (9 mL).

[Re(CO)₃(6,6'-Me₂bipy)(HNC(CH₃)N(CH₂)₄)]BF₄ (4). For the reaction of [Re(CO)₃(6,6'-Me₂bipy)(CH₃CN)]BF₄ (34.9 mg, 0.06 mmol) with pyrrolidine (49.6 μL, 0.60 mmol) in CH₃CN, the general procedure afforded 28 mg (71% yield) of yellow crystalline material. X-ray quality crystals of 4 were obtained as described for 1 by adding diethyl ether (15 mL).

[Re(CO)₃(5,5'-Me₂bipy)(HNC(C₆H₅)N(CH₂)₃)]BF₄ (5). The use of the general procedure in treating [Re(CO)₃(5,5'-Me₂bipy)(C₆H₅CN)]BF₄ (38.7 mg, 0.06 mmol) with azetidine (40.7 μL, 0.60 mmol) in CHCl₃ afforded 28 mg (67% yield) of yellow crystalline

material. X-ray quality crystals of **5** were obtained from a solution of this material in CHCl₃ (3.87 mg/600 μL) by adding diethyl ether (3 mL) and allowing the solvent mixture to evaporate slowly.

[Re(CO)₃(6,6'-Me₂bipy)(HNC(C₆H₅)N(CH₂)₃)]BF₄ (6). For the reaction of [Re(CO)₃(6,6'-Me₂bipy)(C₆H₅CN)]BF₄ (38.7 mg, 0.06 mmol) with azetidine (40.7 μL, 0.60 mmol) in CHCl₃, the general procedure afforded 26 mg (62% yield) of yellow crystalline material. X-ray quality crystals of **6** were obtained as described for **5** by adding diethyl ether (5 mL).

[Re(CO)₃(5,5'-Me₂bipy)(HNC(C₆H₅)N(CH₂)₄)]BF₄ (7). The use of the general procedure in the reaction of [Re(CO)₃(5,5'-Me₂bipy)(C₆H₅CN)]BF₄ (38.7 mg, 0.06 mmol) with pyrrolidine (49.6 μL, 0.60 mmol) in CHCl₃ afforded 30 mg (70% yield) of yellow crystalline material. X-ray quality crystals of **7** were obtained by recrystallization from CHCl₃ (15 mg/1 mL) after adding diethyl ether (~7 mL).

[Re(CO)₃(6,6'-Me₂bipy)(HNC(C₆H₅)N(CH₂)₄)]BF₄ (8). The use of the general procedure in the reaction of [Re(CO)₃(6,6'-Me₂bipy)(C₆H₅CN)]BF₄ (38.7 mg, 0.06 mmol) with pyrrolidine (49.6 μL, 0.60 mmol) in CHCl₃ afforded 32 mg (75% yield) of yellow crystalline material. X-ray quality crystals of **8** were obtained by recrystallization from CHCl₃ (21 mg/1 mL) after adding diethyl ether (~10 mL).

[Re(CO)₃(5,5'-Me₂bipy)(HNC(C₆H₅)N(CH₂)₅)]BF₄ (9). Reaction of [Re(CO)₃(5,5'-Me₂bipy)(C₆H₅CN)]BF₄ (38.7 mg, 0.06 mmol) with piperidine (59.2 μL, 0.60 mmol) in CHCl₃ by the general procedure afforded 38 mg (87% yield) of yellow crystalline material. X-ray quality crystals of **9** were obtained by recrystallization from CHCl₃ (5 mg/2 mL) after adding diethyl ether (7 mL).

[Re(CO)₃(6,6'-Me₂bipy)(HNC(C₆H₅)N(CH₂)₅)]BF₄ (10). Using the general procedure to treat [Re(CO)₃(6,6'-Me₂bipy)(C₆H₅CN)]BF₄ (38.7 mg, 0.06 mmol) with piperidine (59.2 μL, 0.60 mmol) in CHCl₃ afforded 36 mg (82% yield) of yellow crystalline material. X-ray quality crystals of 10 were obtained by recrystallization from CHCl₃ (18 mg/1 mL) after adding diethyl ether (~10 mL).

New Method of Synthesizing Amidine Complexes Starting with the *fac*-[Re(CO)₃(H₂O)₃]⁺ Precursor (Method B). Aqueous solutions of *fac*-[Re(CO)₃(H₂O)₃]⁺ (0.5 mL from the 0.1M stock solution, 0.05 mmol), (pH = 2.57) were treated with 5,5'-Me₂bipy (9.21 mg, 0.05 mmol), 0.5 mL of CH₃CN, and NaBF₄ (5.49 mg, 0.05 mmol). The reaction mixture (1:1 H₂O:CH₃CN), (pH = 5.87) was heated at reflux, and the reaction was monitored by ¹H NMR spectroscopy (Figure 4.6). The 5,5'-Me₂bipy ligand dissolved within 2–3 min in step 1 of the preparation. Aliquots (10 μL) of the reaction mixture were transferred to a vial and reduced to dryness by rotary evaporation. The residue was dissolved in CDCl₃ for ¹H NMR assessment. In the NaBF₄ preparations (recorded at 10 min, Figure 4.6), the first spectrum showed peaks arising from the [Re(CO)₃(5,5'-Me₂bipy)(CH₃CN)]⁺ product¹⁷ that were more intense than peaks from the reactant (5,5'-Me₂bipy). Product peaks continued to increase until no reactant peaks remained (~30 min, Figure 4.6). After 5 additional minutes, the solution was allowed to cool to room temperature to complete step 1 of the process.

In step 2, a 10:1 molar excess of piperidine (49.4 μL, 0.5 mmol) was added to the reaction mixture at room temperature, and the aliquot method described above was used to monitor the reaction by ¹H NMR spectroscopy (Figure 4.6). ¹H NMR spectra indicated complex formation of the expected amidine 30 min after the addition of piperidine. The reaction mixture was filtered and the dark yellow residue left in the vial after the solvent was removed by rotary evaporation

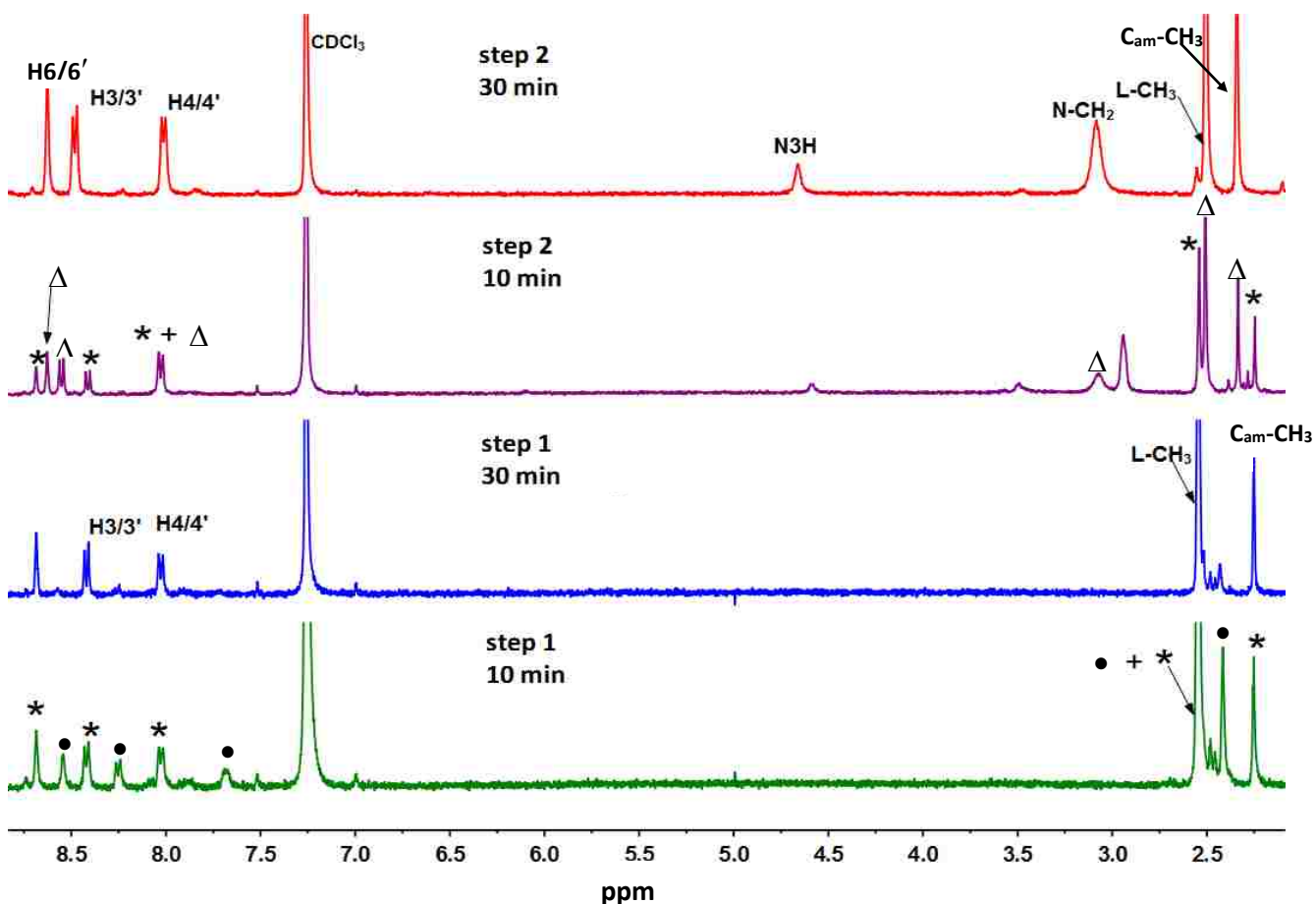


Figure 4.6. Stack plot of ¹H NMR spectra (CDCl₃, 27 °C) obtained to monitor steps 1 and 2 of Method B. Spectra chosen for the figure to illustrate the NMR data for Method B are from reaction of piperidine to form [Re(CO)₃(5,5'-Me₂bipy)(HNC(CH₃)N(CH₂)₅)]BF₄² because slow enough to obtain intermediate spectra for step 2. Also, the salt is NaBF₄ because crystals could be obtained. Signals of starting 5,5'-Me₂bipy are labeled with •. Signals for [Re(CO)₃(5,5'-Me₂bipy)(CH₃CN)]BF₄ are labeled with * in the 10-min step 1 and step 2 traces and with assignments in the step 1 30-min trace. Signals for the final [Re(CO)₃(5,5'-Me₂bipy)(HNC(CH₃)N(CH₂)₅)]BF₄ product are labeled with Δ in the step 2 10-min trace and with assignments in the step 2 30-min trace.

was collected on a filter, washed well with water, and air dried. This residue was then washed well with diethyl ether (~20 mL) and dissolved in CHCl₃ (5 mL). After filtration, the filtrate was taken to dryness (rotary evaporation), yielding 37 mg of product (91%); all yields in this section are based on the *fac*-[Re(CO)₃(H₂O)₃]⁺ precursor. The residue from this NaBF₄ preparation was dissolved in 0.5 mL of CH₃CN, and diethyl ether (~7 mL) was added to the point of cloudiness. Yellow crystals were obtained after 24 h. The ¹H NMR spectra in CD₃CN of the residue and of the crystals identically matched the ¹H NMR spectrum reported for [Re(CO)₃(5,5'-Me₂bipy)(HNC(CH₃)N(CH₂)₅)]BF₄.¹⁹

Furthermore, in step 2 the addition of azetidine (40.7 μL, 0.5 mmol) or pyrrolidine (49.6 μL, 0.5 mmol) to [Re(CO)₃(5,5'-Me₂bipy)(CH₃CN)]⁺ (generated in solution by Method B, 30 min) formed the expected products within 3 and 6 min, respectively. The ¹H NMR spectra in CDCl₃ of the crystalline precipitates, 1 (29 mg, 92% yield) and 3 (28 mg, 88% yield), were identical to those recorded for complexes 1 and 3 prepared by using Method A (Table 4.1).

Virtually identical results were obtained when NaCl (2.92 mg, 0.05 mol) was used in step 1 in place of the NaBF₄ in order to simulate the 0.1 M NaCl solution typically used in ^{99m}Tc radiolabeling. In step 2, with a 10:1 molar excess of either piperidine (49.4 μL, 0.5 mmol) or azetidine (40.7 μL, 0.5 mmol), ¹H NMR spectra indicated formation of the expected amidine complex within 20 min (piperidine) or 4 min (azetidine) in yields of 25 mg (85%) and 24 mg (80%), respectively.

Challenge Reactions. A 5 mM solution of [Re(CO)₃(5,5'-Me₂bipy)(HNC(CH₃)N(CH₂)₃)]BF₄ (1), [Re(CO)₃(5,5'-Me₂bipy)(HNC(CH₃)N(CH₂)₄)]BF₄ (3), [Re(CO)₃(5,5'-Me₂bipy)(HNC(C₆H₅)N(CH₂)₃)]BF₄ (5), and [Re(CO)₃(5,5'-Me₂bipy)(HNC(C₆H₅)N(CH₂)₄)]BF₄ (7) in CDCl₃ (600 μL) was treated with a 1:5 molar ratio of

4-dimethylaminopyridine (2.0 mg, 25 mM), and the solution was monitored over time by ^1H NMR spectroscopy.

4.3 Results and Discussion

Synthesis. Use of 100% Organic Solvents (Method A).

$[\text{Re}(\text{CO})_3(\text{Me}_2\text{bipy})(\text{CH}_3\text{CN})]\text{BF}_4$ ($\text{Me}_2\text{bipy} = 5,5'$ - or $6,6'$ - Me_2bipy) complexes prepared in organic solvents from the $[\text{Re}(\text{CO})_3(\text{CH}_3\text{CN})_3]\text{BF}_4$ precursor as described previously¹⁷ were used to prepare the new $[\text{Re}(\text{CO})_3(\text{Me}_2\text{bipy})(\text{C}_6\text{H}_5\text{CN})]\text{BF}_4$ ($\text{Me}_2\text{bipy} = 5,5'$ - or $6,6'$ - Me_2bipy) complexes in CHCl_3 (Experimental Section). Addition of heterocyclic secondary amines ($\text{HN}(\text{CH}_2)_x$) ($x = 3$ to 5) to $[\text{Re}(\text{CO})_3(\text{Me}_2\text{bipy})(\text{RCN})]\text{BF}_4$ ($\text{Me}_2\text{bipy} = 5,5'$ - or $6,6'$ - Me_2bipy ; $\text{R} = \text{CH}_3$ or C_6H_5) in CH_3CN ($\text{R} = \text{CH}_3$) or CHCl_3 ($\text{R} = \text{C}_6\text{H}_5$) in a 10:1 ratio produced good-to-high yields (~60% to 90%) of ten new $[\text{Re}(\text{CO})_3(\text{Me}_2\text{bipy})(\text{HNC}(\text{R})\text{N}(\text{CH}_2)_x)]\text{BF}_4$ complexes (1–10). For a given x , all new $5,5'$ - Me_2bipy complexes are assigned an odd number: [$\text{R} = \text{CH}_3$, $x = 3$ (1); $\text{R} = \text{CH}_3$, $x = 4$ (3); $\text{R} = \text{C}_6\text{H}_5$, $x = 3$ (5); $\text{R} = \text{C}_6\text{H}_5$, $x = 4$ (7); $\text{R} = \text{C}_6\text{H}_5$, $x = 5$ (9)] and all new $6,6'$ - Me_2bipy complexes are assigned an even number ($\text{R} = \text{CH}_3$, $x = 3$ (2); $\text{R} = \text{CH}_3$, $x = 4$ (4); $\text{R} = \text{C}_6\text{H}_5$, $x = 3$ (6); $\text{R} = \text{C}_6\text{H}_5$, $x = 4$ (8); $\text{R} = \text{C}_6\text{H}_5$, $x = 5$ (10)]. Both solution and solid-state characterizations establish that 1–10 exist only as the *E* isomer (Figure 4.3), as was found previously for the $[\text{Re}(\text{CO})_3(\text{Me}_2\text{bipy})(\text{HNC}(\text{CH}_3)\text{N}(\text{CH}_2)_5)]\text{BF}_4$ complexes ($\text{Me}_2\text{bipy} = 5,5'$ - or $6,6'$ - Me_2bipy).¹⁹

In a previous report,¹⁹ we found that the reactions of the same cyclic amine to form amidine complexes from $[\text{Re}(\text{CO})_3(\text{Me}_2\text{bipy})(\text{CH}_3\text{CN})]\text{BF}_4$ complexes in CD_3CN were complete in less time for $6,6'$ - Me_2bipy than for $5,5'$ - Me_2bipy complexes and that, for a given basicity of the amine, reactions of smaller-ring cyclic amines were faster than for the large-ring cyclic amines or for primary amines. Table 4.5 shows the time required for complete reaction, evaluated

Table 4.5. Times (min) for Complete Reaction of $[\text{Re}(\text{CO})_3(5,5'\text{-Me}_2\text{bipy})(\text{RCN})]\text{BF}_4$ Complexes with Amines to Form $[\text{Re}(\text{CO})_3(5,5'\text{-Me}_2\text{bipy})(\text{amidine})]\text{BF}_4$ Complexes

R	amine	CD_3CN	CDCl_3
CH_3	azetidine	< 3	< 4
CH_3	pyrrolidine	< 3	~ 32
CH_3	piperidine	< 5	~ 200
CH_3	piperazine	~20	~ 1320
C_6H_5	azetidine		< 4
C_6H_5	pyrrolidine		< 7
C_6H_5	piperidine		~ 60
C_6H_5	piperazine		~ 180

by monitoring a 10 mM solution of $[\text{Re}(\text{CO})_3(5,5'\text{-Me}_2\text{bipy})(\text{RCN})]\text{BF}_4$ in CDCl_3 or CD_3CN (600 μL) by ^1H NMR spectroscopy after the addition of a 1:10 molar excess of various amines (100 mM). All reactions of $[\text{Re}(\text{CO})_3(5,5'\text{-Me}_2\text{bipy})(\text{CH}_3\text{CN})]\text{BF}_4$ with 4-, 5-, or 6-membered ring heterocyclic amines in CD_3CN were significantly faster than the reactions of $[\text{Re}(\text{CO})_3(5,5'\text{-Me}_2\text{bipy})(\text{CH}_3\text{CN})]\text{BF}_4$ with primary amines.¹⁸ Reactions of azetidine or pyrrolidine with $[\text{Re}(\text{CO})_3(5,5'\text{- or }6,6'\text{-Me}_2\text{bipy})(\text{CH}_3\text{CN})]\text{BF}_4$ in 100% CD_3CN reached completion in under 3 min, even before the first spectrum could be recorded. The short reaction times of these amines with $[\text{Re}(\text{CO})_3(\text{Me}_2\text{bipy})(\text{CH}_3\text{CN})]\text{BF}_4$ in CD_3CN preclude comparison of the reactivity of azetidine or pyrrolidine with that of the larger cyclic secondary amines studied previously in CD_3CN .¹⁹ Therefore, the amidine formation reaction was monitored in CDCl_3 , in which slower

reaction times of $[\text{Re}(\text{CO})_3(5,5'\text{-Me}_2\text{bipy})(\text{CH}_3\text{CN})]\text{BF}_4$ with azetidine or pyrrolidine allowed us to estimate by ^1H NMR spectroscopy the time required for complete reaction. As shown in Table 4.5, the completion time in CDCl_3 with azetidine (<4 min) was significantly faster than the completion times with pyrrolidine (~32 min) or piperidine (~200 min). Decreasing the size of the heterocyclic amine to 4- and 5-membered rings decreased the completion time, a trend found earlier for 6-, 7-, and 8-membered cyclic amines.¹⁹

Moreover, although the times for the azetidine reactions were too short to assess by our method, the reactions with $[\text{Re}(\text{CO})_3(5,5'\text{-Me}_2\text{bipy})(\text{RCN})]\text{BF}_4$ in CDCl_3 for a given amine (pyrrolidine, piperidine, and piperazine) were relatively faster when $\text{R} = \text{C}_6\text{H}_5$ than when $\text{R} = \text{CH}_3$. This favorable reactivity in forming the $[\text{Re}(\text{CO})_3(5,5'\text{-Me}_2\text{bipy})(\text{HNC}(\text{C}_6\text{H}_5)\text{N}(\text{CH}_2)_2\text{Y})]\text{BF}_4$ complexes can be attributed to the electron-withdrawing ability of the phenyl ring, which facilitates addition of the amine to the coordinated nitrile group.

Use of 50% Water and 50% Acetonitrile Solvent Mixture (Method B). Formation of the $[\text{Re}(\text{CO})_3(5,5'\text{-Me}_2\text{bipy})(\text{CH}_3\text{CN})]^+$ complex from the organic solvent soluble $[\text{Re}(\text{CO})_3(\text{CH}_3\text{CN})_3]\text{BF}_4$ precursor needed for Method A requires 2-3 days in acetonitrile and 16 h in benzene.¹⁷ The time required to form the $[\text{Re}(\text{CO})_3(5,5'\text{-Me}_2\text{bipy})(\text{CH}_3\text{CN})]^+$ complex in the 50% water/50% acetonitrile solvent mixture is only 30 min (Figure 4.6). The final yields obtained from Method B are also higher (89%-92%, Experimental Section).¹⁹ Most importantly, the utilization of the aqueous solution of the *fac*- $[\text{Re}(\text{CO})_3(\text{H}_2\text{O})_3]^+$ precursor provides guidance for the use of the *fac*- $[\text{}^{99\text{m}}\text{Tc}(\text{CO})_3(\text{H}_2\text{O})_3]^+$ precursor. Knowledge of relevant amidine chemistry gained in earlier work¹⁷⁻²⁰ and in the present work can now potentially be adapted in utilizing this *fac*- $[\text{}^{99\text{m}}\text{Tc}(\text{CO})_3(\text{H}_2\text{O})_3]^+$ precursor for biomedical studies.

Structural Results. Recrystallization of the crystalline products isolated afforded X-ray

quality crystals for the ten new complexes (1–10). Tables 4.6 and 4.7 summarize the crystal data

Table 4.6. Crystal Data and Structural Refinement for [Re(CO)₃(5,5'-Me₂bipy)(HNC(CH₃)N(CH₂)₃)]BF₄ (1), [Re(CO)₃(6,6'-Me₂bipy)(HNC(CH₃)N(CH₂)₃)]BF₄ (2), [Re(CO)₃(5,5'-Me₂bipy)(HNC(CH₃)N(CH₂)₄)]BF₄ (3), and [Re(CO)₃(6,6'-Me₂bipy)(HNC(CH₃)N(CH₂)₄)]BF₄ (4)

complex	1	2	3	4
empirical formula	C ₂₀ H ₂₂ N ₄ O ₃ Re•0.8 4 (BF ₄)•0.16(Br)	C ₂₀ H ₂₂ N ₄ O ₃ Re•BF ₄	C ₂₁ H ₂₄ N ₄ O ₃ Re•0.97(BF ₄) •0.03(Br)	C ₂₁ H ₂₄ N ₄ O ₃ Re• BF ₄
<i>fw</i>	638.29	639.42	653.24	653.45
crystal system	triclinic	monoclinic	monoclinic	monoclinic
space group	<i>P</i> $\bar{1}$	<i>P</i> 2 ₁ / <i>n</i>	<i>P</i> 2 ₁ / <i>n</i>	<i>P</i> 2 ₁ / <i>n</i>
<i>a</i> (Å)	8.2743(4)	10.4580(2)	11.233(2)	8.9664(4)
<i>b</i> (Å)	10.3582(5)	11.7078(2)	13.582(2)	12.1161(4)
<i>c</i> (Å)	13.9310(7)	17.9573(4)	15.495(3)	21.9930(8)
β (deg)	78.234(2)	99.815(1)	100.307(17)	98.127(2)
<i>V</i> (Å ³)	1124.24(10)	2166.51(7)	2325.9 (7)	2365.28(16)
<i>T</i> (K)	100	90	90	180
<i>Z</i>	2	4	4	4
ρ_{calc} (Mg/m ³)	1.886	1.960	1.866	1.835
abs coeff (mm ⁻¹)	5.75	5.67	5.34	5.20
2 θ_{max} (°)	61.0	84.2	80.4	64.0
<i>R</i> [<i>I</i> > 2 σ (<i>I</i>)] ^a	0.026	0.026	0.017	0.026
<i>wR</i> ^{2b}	0.073	0.054	0.042	0.059
data/param	6737/309	15173/305	14590/317	8186/323

^a*R* = ($\sum||F_o| - |F_c||$)/ $\sum|F_o|$. ^b*wR*² = [$\sum[w(F_o^2 - F_c^2)^2]$]/ $\sum[w(F_o^2)^2]$]^{1/2}, in which *w* = 1/[$\sigma^2(F_o^2) + (dP)^2 + (eP)$] and *P* = (*F*_o² + 2*F*_c²)/3.

Table 4.7. Crystal Data and Structural Refinement for [Re(CO)₃(5,5'-Me₂bipy)(HNC(C₆H₅)N(CH₂)₃)]BF₄ (5), [Re(CO)₃(6,6'-Me₂bipy)(HNC(C₆H₅)N(CH₂)₃)]BF₄ (6), [Re(CO)₃(5,5'-Me₂bipy)(HNC(C₆H₅)N(CH₂)₄)]BF₄ (7), [Re(CO)₃(6,6'-Me₂bipy)(HNC(C₆H₅)N(CH₂)₄)]BF₄ (8), [Re(CO)₃(5,5'-Me₂bipy)(HNC(C₆H₅)N(CH₂)₅)]BF₄ (9), and [Re(CO)₃(6,6'-Me₂bipy)(HNC(C₆H₅)N(CH₂)₅)]BF₄ (10)

complex	5	6	7	8	9	10
empirical formula	C ₂₅ H ₂₄ N ₄ O ₃ Re•0.09(Br) •0.91(BF ₄)	C ₂₅ H ₂₄ N ₄ O ₃ Re•BF ₄	C ₂₆ H ₂₆ N ₄ O ₃ Re •0.911(BF ₄)• 0.089(Br)	C ₂₆ H ₂₆ N ₄ O ₃ Re •BF ₄	C ₂₇ H ₂₈ N ₄ O ₃ Re •BF ₄	5(C ₂₇ H ₂₈ N ₄ O ₃ Re•BF ₄)
<i>fw</i>	699.86	701.49	714.82	715.52	729.54	3647.71
crystal system	monoclinic	monoclinic	monoclinic	monoclinic	triclinic	trigonal
space group	<i>P2</i> ₁ / <i>c</i>	<i>Ia</i>	<i>P2</i> ₁ / <i>c</i>	<i>P2</i> ₁ / <i>c</i>	<i>P</i> $\bar{1}$	<i>R</i> $\bar{3}$: <i>R</i>
<i>a</i> (Å)	16.6697(12)	10.9466(4)	16.730(3)	10.6300(16)	9.0850(5)	27.6668(9)
<i>b</i> (Å)	11.1504(8)	16.3982(5)	11.0485(19)	47.473(7)	10.3191(6)	90
<i>c</i> (Å)	14.7196(10)	15.1842(6)	15.439(3)	15.928(2)	14.8996(8)	27.6668(9)
<i>α</i> (deg)	90	90	90	90	89.884(3)	83.540(1)
<i>β</i> (deg)	110.827(4)	109.033(1)	112.223(8)	102.985(7)	81.639(3)	90
<i>γ</i> (deg)	90	90	90	90	74.276(3)	90
<i>V</i> (Å ³)	2557.2(3)	2576.62(16)	2641.9(8)	7832(2)	1333.10(13)	20802(2)
<i>T</i> (K)	90	90	90	100	90	90
<i>Z</i>	4	4	4	12	2	6
<i>ρ</i> _{calc} (Mg/m ³)	1.818	1.808	1.797	1.820	1.817	1.747
abs coeff (mm ⁻¹)	4.95	4.78	4.79	4.72	4.62	4.44
2 <i>θ</i> _{max} (°)	84.2	75.4	91.2	67.2	61.2	63.0
<i>R</i> [<i>I</i> > 2σ(<i>I</i>)] ^a	0.030	0.020	0.030	0.0037	0.023	0.033

(Table 4.7 continued)

complex	5	6	7	8	9	10
wR^2 ^b	0.070	0.053	0.072	0.062	0.048	0.075
data/param	17947/346	8475/349	22180/367	26084/1116	8041/367	46238/1826

^a $R = (\sum||F_o| - |F_c||)/\sum|F_o|$. ^b $wR^2 = [\sum[w(F_o^2 - F_c^2)^2]/\sum[w(F_o^2)^2]]^{1/2}$, in which $w = 1/[\sigma^2(F_o^2) + (dP)^2 + (eP)]$ and $P = (F_o^2 + 2F_c^2)/3$.

and details of the structural refinement for complexes 1–4 and 5–10, respectively. ORTEP plots of the molecular structures showing the atom-numbering scheme used to describe the solid-state data are shown in Figure 4.7 for the cations of $[\text{Re}(\text{CO})_3(\text{Me}_2\text{bipy})(\text{HNC}(\text{CH}_3)\text{N}(\text{CH}_2)_3 \text{ or } 4)]\text{BF}_4$ (1–4), and in Figures 4.8 and 4.9 for the cations of $[\text{Re}(\text{CO})_3(\text{Me}_2\text{bipy})(\text{HNC}(\text{C}_6\text{H}_5)\text{N}(\text{CH}_2)_3\text{-}_5)]\text{BF}_4$ (5–10). Selected bond distances and angles for the $[\text{Re}(\text{CO})_3(\text{Me}_2\text{bipy})(\text{HNC}(\text{R})\text{N}(\text{CH}_2)_x)]\text{BF}_4$ complexes are listed in Tables 4.8 and 4.9.

Complexes 1–10 have a pseudo octahedral structure; three carbonyl groups occupy one face and the N1 and N2 atoms of the Me_2bipy ligand and the N3 atom of the amidine ligand having the *E* configuration (Figures 4.2 to 4.4) occupy the opposite face. The two carbonyl ligands trans to the N1 and N2 atoms and the bidentate Me_2bipy ligand are considered to define the equatorial coordination plane. The carbonyl trans to N3 and the monodentate amidine ligand are referred to as axial ligands. Unfavorable repulsive interactions between the 6-, 7-, or 8-membered heterocyclic ring moiety attached to C16 and the equatorial ligands believed to destabilize the *Z* isomer (Figure 4.3) were invoked to explain why the *E* isomer is favored for $[\text{Re}(\text{CO})_3(\text{Me}_2\text{bipy})(\text{HNC}(\text{CH}_3)\text{N}(\text{CH}_2)_2Y)]\text{BF}_4$ complexes with $Y = (\text{CH}_2)_3$, $(\text{CH}_2)_4$, $(\text{CH}_2)_5$, $(\text{CH}_2)_2\text{NH}$, and $(\text{CH}_2)_2\text{O}$.¹⁹

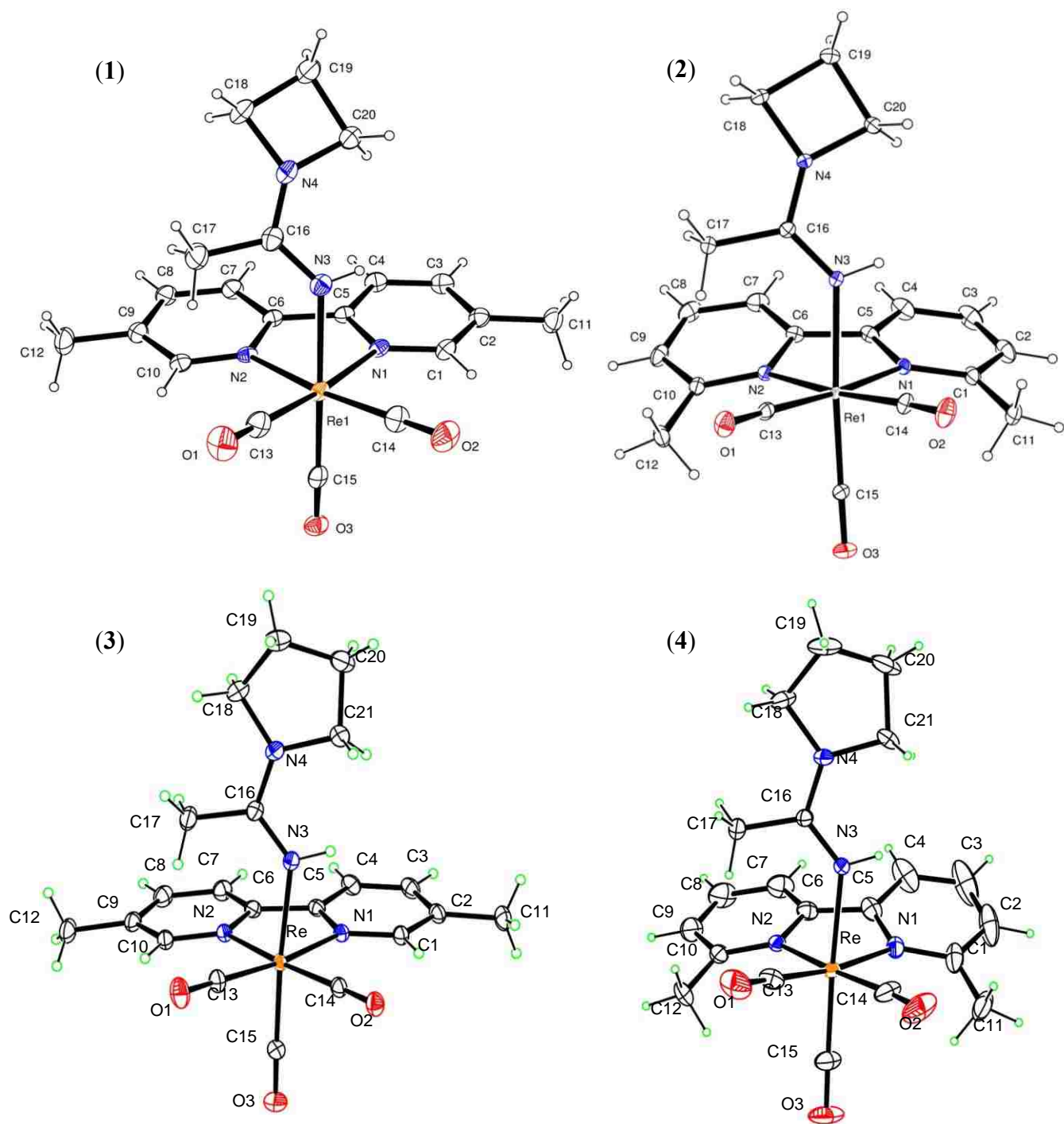


Figure 4.7. ORTEP plots of the cations of $[\text{Re}(\text{CO})_3(5,5'\text{-Me}_2\text{bipy})(\text{HNC}(\text{CH}_3)\text{N}(\text{CH}_2)_3)]\text{BF}_4$ (1), $[\text{Re}(\text{CO})_3(6,6'\text{-Me}_2\text{bipy})(\text{HNC}(\text{CH}_3)\text{N}(\text{CH}_2)_3)]\text{BF}_4$ (2), $[\text{Re}(\text{CO})_3(5,5'\text{-Me}_2\text{bipy})(\text{HNC}(\text{CH}_3)\text{N}(\text{CH}_2)_4)]\text{BF}_4$ (3), and $[\text{Re}(\text{CO})_3(6,6'\text{-Me}_2\text{bipy})(\text{HNC}(\text{CH}_3)\text{N}(\text{CH}_2)_4)]\text{BF}_4$ (4). Thermal ellipsoids are drawn with 50% probability.

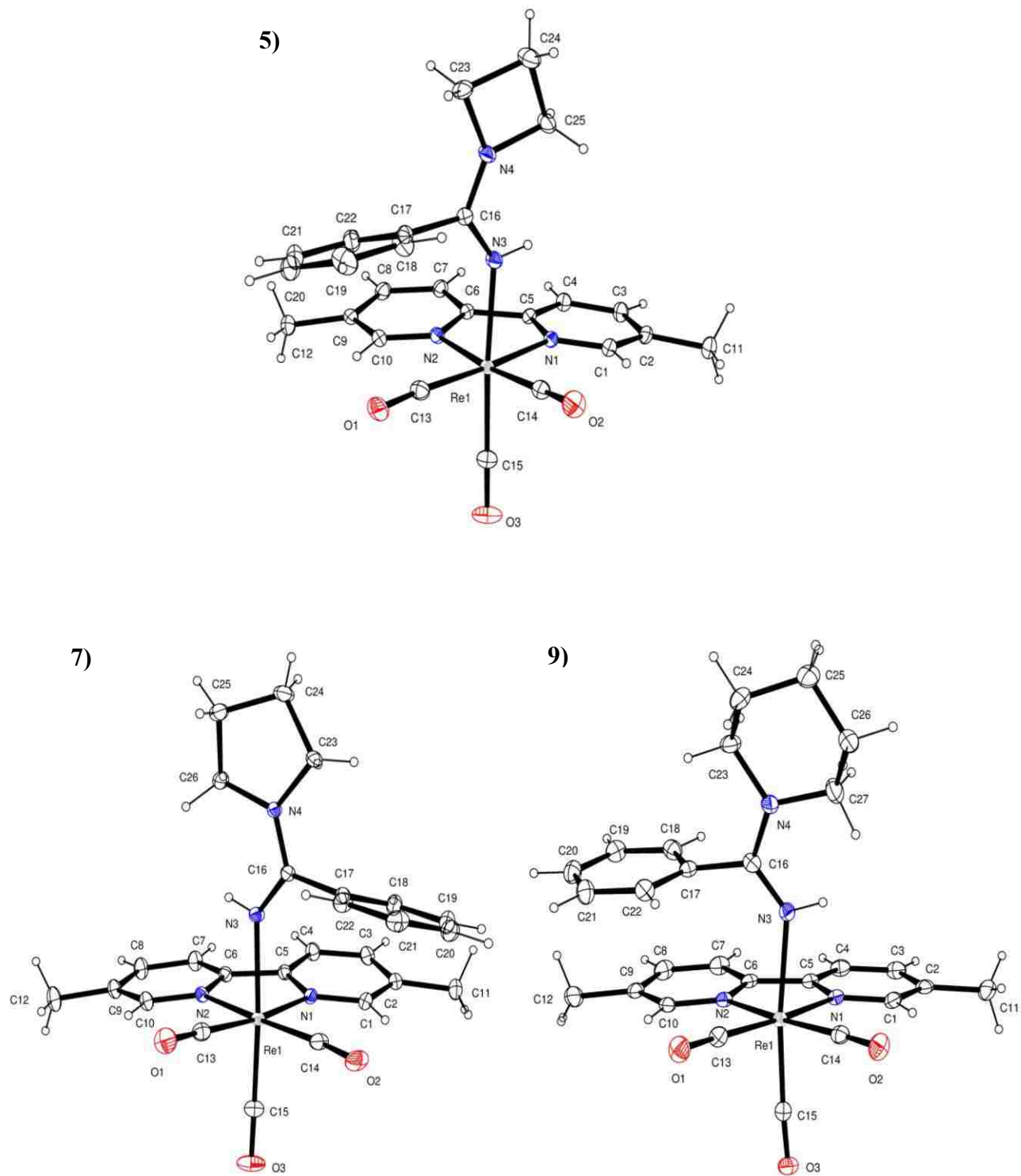


Figure 4.8. ORTEP plots of the cations of $[\text{Re}(\text{CO})_3(5,5'\text{-Me}_2\text{bipy})(\text{HNC}(\text{C}_6\text{H}_5)\text{N}(\text{CH}_2)_3)]\text{BF}_4$ (5), $[\text{Re}(\text{CO})_3(5,5'\text{-Me}_2\text{bipy})(\text{HNC}(\text{C}_6\text{H}_5)\text{N}(\text{CH}_2)_4)]\text{BF}_4$ (7), and $[\text{Re}(\text{CO})_3(5,5'\text{-Me}_2\text{bipy})(\text{HNC}(\text{C}_6\text{H}_5)\text{N}(\text{CH}_2)_5)]\text{BF}_4$ (9). Thermal ellipsoids are drawn with 50% probability.

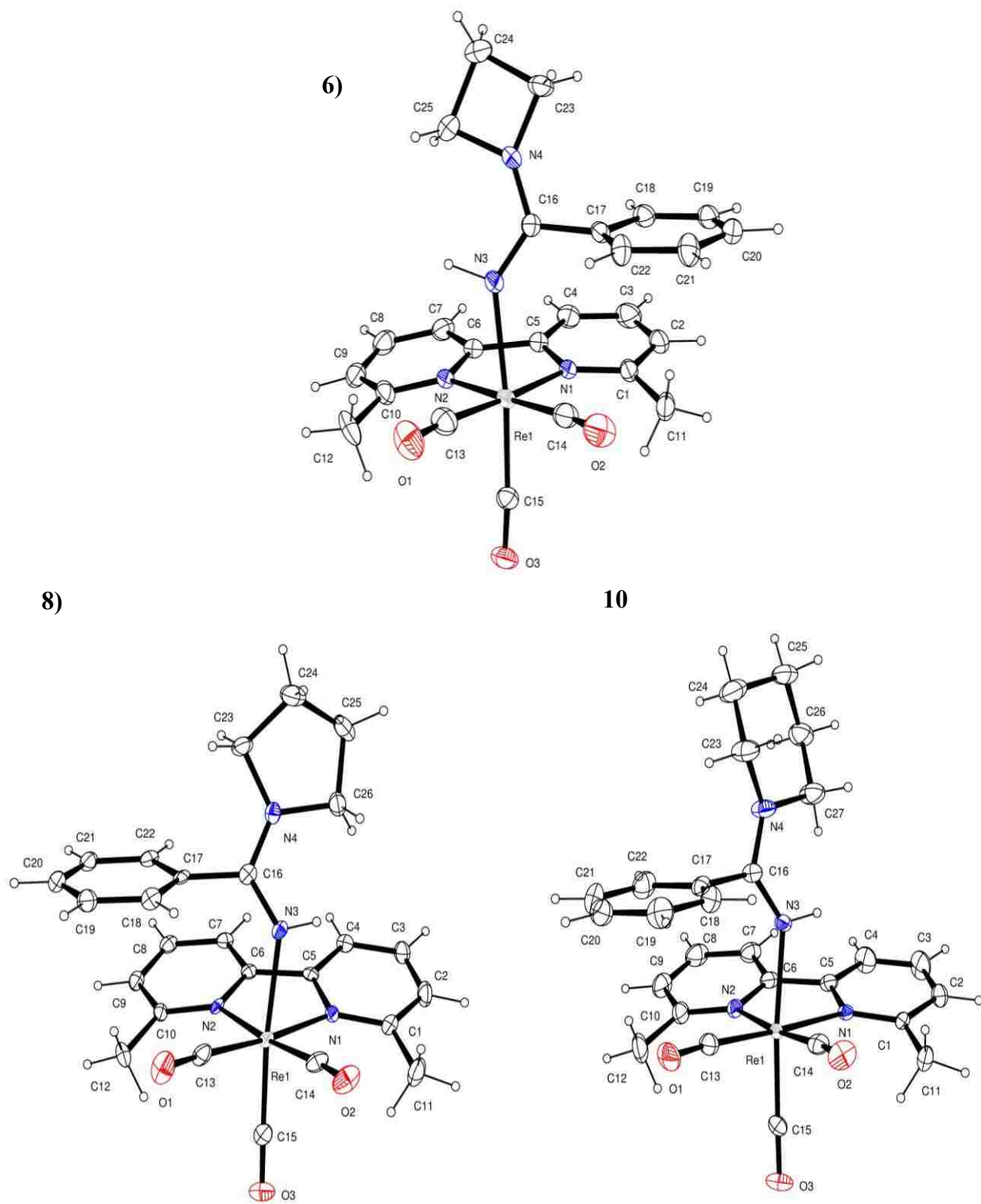


Figure 4.9. ORTEP plots of the cations of $[\text{Re}(\text{CO})_3(6,6'\text{-Me}_2\text{bipy})(\text{HNC}(\text{C}_6\text{H}_5)\text{N}(\text{CH}_2)_3)]\text{BF}_4$ (6), $[\text{Re}(\text{CO})_3(6,6'\text{-Me}_2\text{bipy})(\text{HNC}(\text{C}_6\text{H}_5)\text{N}(\text{CH}_2)_4)]\text{BF}_4$ (8), and $[\text{Re}(\text{CO})_3(6,6'\text{-Me}_2\text{bipy})(\text{HNC}(\text{C}_6\text{H}_5)\text{N}(\text{CH}_2)_5)]\text{BF}_4$ (10). Thermal ellipsoids are drawn with 50% probability.

Table 4.8. Selected Bond Distances (Å) and Angles (deg) for [Re(CO)₃(5,5'-Me₂bipy)(HNC(CH₃)N(CH₂)₃)]BF₄ (1), [Re(CO)₃(6,6'-Me₂bipy)(HNC(CH₃)N(CH₂)₃)]BF₄ (2), [Re(CO)₃(5,5'-Me₂bipy)(HNC(CH₃)N(CH₂)₄)]BF₄ (3), and [Re(CO)₃(6,6'-Me₂bipy)(HNC(CH₃)N(CH₂)₄)]BF₄ (4)

complex	1	2	3	4
Re–N1	2.178(2)	2.2050(12)	2.176(1)	2.198(2)
Re–N2	2.172(2)	2.1990(12)	2.186(1)	2.200(2)
Re–N3	2.184(3)	2.1704(11)	2.186(1)	2.181(2)
N3–C16	1.305(4)	1.3068(18)	1.311(1)	1.303(3)
N4–C16	1.331(4)	1.3313(17)	1.338(2)	1.334(3)
N4–C(<i>n</i>)	1.468(4) ^b	1.4667(18) ^b	1.471(2) ^c	1.460(4) ^c
N4–C18	1.477(4)	1.4708(18)	1.474(2)	1.480(3)
N1–Re–N2	75.28(9)	75.10(5)	74.85(3)	74.90(9)
N1–Re–N3	80.13(9)	80.15(5)	80.57(4)	80.14(8)
N2–Re–N3	82.84(9)	83.84(5)	85.19(4)	85.19(8)
Re–N3–H3	108(3)	111.3(16)	111(1)	111(2)
Re–N3–C16	133.6(2)	135.47(10)	135.44(8)	135.5(2)
C16–N3–H3	116(3)	113.2(17)	114(1)	113(2)
N3–C16–N4	121.4(3)	121.82(13)	122.8(1)	123.0(2)
N3–C16–C17	123.2(3)	122.88(12)	120.3(1)	120.1(2)
N4–C16–C17	115.4(3)	115.31(12)	116.9(1)	116.9(2)
C16–N4–C18	131.5(3)	131.78(12)	125.1(1)	124.6(2)
C16–N4–C(<i>n</i>) ^a	129.8(3) ^b	131.58(12) ^b	122.9(1) ^c	123.4(2) ^c
C18–N4–C(<i>n</i>) ^a	94.4(2) ^b	95.39(10) ^b	111.6(1) ^c	112.0(2) ^c

^a *n* varies in number according to the R group. ^b *n* = 20. ^c *n* = 21.

Table 4.9. Selected Bond Distances (Å) and Angles (deg) for [Re(CO)₃(5,5'-Me₂bipy)(HNC(C₆H₅)N(CH₂)₃)]BF₄ (5), [Re(CO)₃(6,6'-Me₂bipy)(HNC(C₆H₅)N(CH₂)₃)]BF₄ (6), [Re(CO)₃(5,5'-Me₂bipy)(HNC(C₆H₅)N(CH₂)₄)]BF₄ (7), [Re(CO)₃(6,6'-Me₂bipy)(HNC(C₆H₅)N(CH₂)₄)]BF₄ (8), [Re(CO)₃(5,5'-Me₂bipy)(HNC(C₆H₅)N(CH₂)₅)]BF₄ (9), and [Re(CO)₃(6,6'-Me₂bipy)(HNC(C₆H₅)N(CH₂)₅)]BF₄ (10)

complex	5	6	7	8	9	10
Re–N1	2.1797(14)	2.214(3)	2.1819(12)	2.211(2)	2.1726(19)	2.193(2)
Re–N2	2.1774(14)	2.201(4)	2.1773(11)	2.205(2)	2.1745(19)	2.218(3)
Re–N3	2.1785(13)	2.173(3)	2.1851(11)	2.183(2)	2.206(2)	2.178(2)
N3–C16	1.313(2)	1.307(5)	1.3121(16)	1.311(4)	1.301(3)	1.296(4)
N4–C16	1.327(2)	1.322(5)	1.3345(16)	1.339(4)	1.352(3)	1.362(4)
N4–C(<i>n</i>) ^a	1.469(2) ^d	1.467(5) ^d	1.4780(17) ^e	1.472(4) ^e	1.477(3) ^f	1.477(4) ^f
N4–C23	1.474(2)	1.479(5)	1.4680(17)	1.474(4)	1.480(3)	1.472(4)
N1–Re–N2	74.56(5)	75.74(12)	74.59(4)	75.01(9)	75.05(7)	75.48(9)
N1–Re–N3	81.10(5)	84.26(12)	84.10(4)	77.61(10)	82.63(7)	78.71(9)
N2–Re–N3	85.07(5)	80.85(13)	81.88(4)	87.15(9)	89.23(7)	82.36(10)
Re–N3–H3N	109.1(14)	115(2)	113.7(15)	111.233(4)	109.0(2)	107.0(3)
Re–N3–C16	134.03(11)	136.4(3)	133.16(9)	134.5(2)	137.04(17)	137.0(2)
C16–N3–H3N	115.2(14)	108(2)	112.7(15)	110.468(7)	111.0(2)	116.0(3)
N3–C16–N4	121.91(15)	123.5(4)	124.11(12)	122.4(3)	124.1(2)	123.1(3)
N3–C16–C17	122.27(14)	122.2(3)	120.68(11)	118.8(3)	119.1(2)	118.9(3)
N4–C16–C17	115.75(14)	114.3(3)	115.18(11)	118.7(3)	116.8(2)	117.9(3)
C16–N4–C23	134.71(15)	131.6(3)	124.41(11)	125.2(3)	121.7(2)	120.4(3)
C16–N4–C(<i>n</i>) ^a	130.72(14) ^d	132.6(4) ^d	123.92(11) ^e	122.1(3) ^e	120.6(2) ^f	121.1(3) ^f
C23–N4–C(<i>n</i>) ^a	94.57(12) ^d	94.6(3) ^d	111.62(10) ^e	111.41(2) ^e	115.3(2) ^f	113.4(3) ^f

^a *n* varies in number according to the R group. ^d *n* = 25. ^e *n* = 26. ^f *n* = 27.

Both crystallographic solid-state data and NMR solution data (see below) establish that $[\text{Re}(\text{CO})_3(\text{Me}_2\text{bipy})(\text{HNC}(\text{R})\text{N}(\text{CH}_2)_{3, 4, \text{ or } 5})]\text{BF}_4$ complexes 1–10 exist only as the *E* isomer. This finding strongly indicates that steric repulsions between the equatorial ligands and a substituent on the amidine carbon (C16) as small as a 4-membered ring can destabilize the *Z* isomer (Figure 4.3).

The characteristics of structures 1–10 (Tables 4.8 and 4.9) are similar to those typically found in structures reported for primary $[\text{Re}(\text{CO})_3(\text{Me}_2\text{bipy})(\text{HNC}(\text{CH}_3)\text{NHR})]\text{BF}_4$ ¹⁸ and secondary $[\text{Re}(\text{CO})_3(\text{Me}_2\text{bipy})(\text{HNC}(\text{CH}_3)\text{N}(\text{CH}_2)_2\text{Y})]\text{BF}_4$ amidine¹⁹ complexes and even of iminoether $[\text{Re}(\text{CO})_3(\text{Me}_2\text{bipy})(\text{HNC}(\text{CH}_3)\text{OCH}_3)]\text{BF}_4$ complexes.¹⁷ We attribute the similarity in structure of these complexes to the fact that the NHR (*E'* isomer) or $\text{N}(\text{CH}_2)_2\text{Y}$ (*E* isomer) substituent on the amidine carbon (C16) projects away from the equatorial plane, and thus the nature of the substituent has little influence on the structural features of the $\text{Re}(\text{CO})_3(\text{Me}_2\text{bipy})$, $\text{HNC}(\text{CH}_3)\text{N}$, and $\text{HNC}(\text{C}_6\text{H}_5)\text{N}$ moieties of the amidine complexes.

Structures 1–10 (Tables 4.8 and 4.9) all have Re–N bond lengths that are at the upper end or slightly longer than the typical $\text{Re}^{\text{L}}\text{--N}(\text{sp}^2)$ bond length (usually stated as ranging from 2.14–2.18 Å).⁹ The axial amidine ligand C17, C16, and N4 atoms usually are close to a *pseudo* "axial" plane which includes the axial CO, Re and N3 and which is equidistant from the two bound N atoms and the two bound C atoms of the equatorial ligands (Figure 4.10). In structures 1–10, the two $\text{N}_{\text{equatorial}}\text{--Re--N3}$ bond angles differ significantly from each other (Tables 4.8 and 4.9), a finding similar to those reported for related complexes.^{17–19} The larger of these two $\text{N}_{\text{equatorial}}\text{--Re--N3}$ angles involved the equatorial N closer to the amidine or imino ether methyl group, a finding consistent with a minimization of repulsions between the methyl group and the closest atoms of the equatorial plane.¹⁹ This explanation applies to 1–4 (Table 4.8) and to $[\text{Re}(\text{CO})_3(\text{Me}_2\text{bipy})(\text{HNC}(\text{C}_6\text{H}_5)\text{N}(\text{CH}_2)_{3-5})]\text{BF}_4$ complexes 5–10 in which the $\text{N}_{\text{equatorial}}\text{--Re--N3}$

angle involving the equatorial N closer to the amidine phenyl group is significantly larger than the other $N_{\text{equatorial}}\text{-Re-N3}$ (Table 4.9). This relationship holds true even for three of the $[\text{Re}(\text{CO})_3(\text{Me}_2\text{bipy})(\text{HNC}(\text{C}_6\text{H}_5)\text{N}(\text{CH}_2)_{3-4})]\text{BF}_4$ complexes (5, 7, and 10) in which the C_6H_5 group of complexes 5, 7, and 10 lie almost directly above one of the equatorial carbonyl groups and is thus not oriented close to the axial plane. As discussed in the next section, NMR spectroscopic evidence indicates this difference in orientation does not occur in solution.

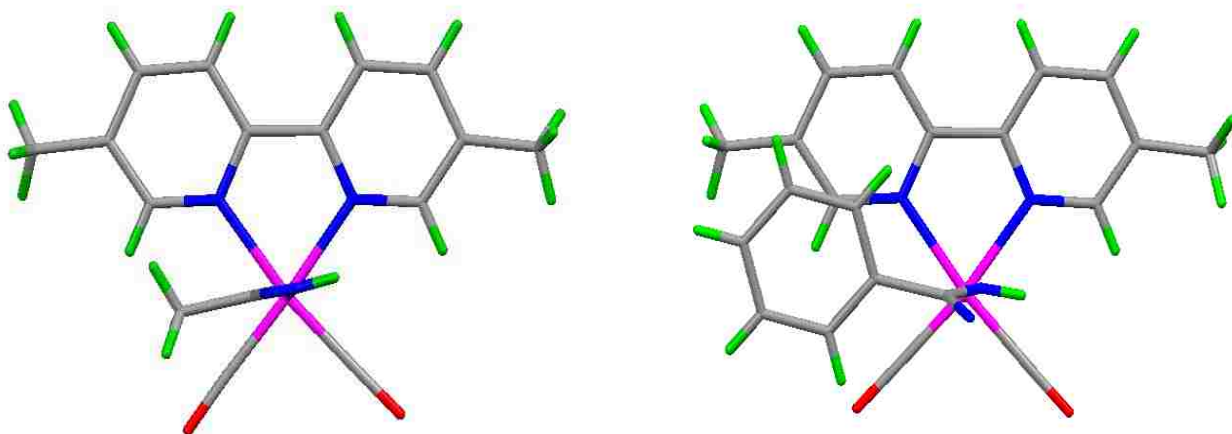


Figure 4.10. View from top of $[\text{Re}(\text{CO})_3(5,5'\text{-Me}_2\text{bipy})(\text{HNC}(\text{CH}_3)\text{N}(\text{CH}_2)_5)]\text{BF}_4^2$ (*left*) and $[\text{Re}(\text{CO})_3(5,5'\text{-Me}_2\text{bipy})(\text{HNC}(\text{C}_6\text{H}_5)\text{N}(\text{CH}_2)_5)]\text{BF}_4$ (*right*) complexes with the mean plane of the 5,5'- Me_2bipy rings oriented parallel to the plane of the paper. The heterocyclic CH_2 groups were deleted for clarity.

The N3-C16 and N4-C16 bond lengths for complexes **1–10**, ranging from 1.296 (3) Å to 1.362(4) Å (Tables 4.8 and 4.9), are closer to an average sp^2 $\text{C}=\text{N}$ bond length (~ 1.28 Å) than to an average sp^3 $\text{C}-\text{N}$ bond length (~ 1.47 Å).²⁵ All bond angles around C16 (close to 120°) indicate the presence of some electron delocalization. The N4-C16 bond distances in complexes **1–4**, with a 4- and a 5-membered ring, reported here are not statistically different from those of other $[\text{Re}(\text{CO})_3(\text{Me}_2\text{bipy})(\text{HNC}(\text{CH}_3)\text{N}(\text{CH}_2)_{5-7})]\text{BF}_4$ complexes having 6-, 7-, or 8-membered rings¹⁹ (Supporting Information) or from the N4-C16 bond distances in the

[Re(CO)₃(Me₂bipy)(HNC(C₆H₅)N(CH₂)₃₋₅)]BF₄ complexes (5-10) with the exception that this bond is very slightly but significantly longer in 9 and 10 (Table 4.9). The barrier to rotation around the N4–C16 bond created by its partial double-bond character gives rise to some interesting observations in the NMR studies, as discussed in the next section.

NMR Spectroscopy. General Considerations. The new [Re(CO)₃(Me₂bipy)(HNC(CH₃)(CH)_{2,3,4})]BF₄ complexes with 4- or 5-membered heterocyclic rings (1–4), the previously reported [Re(CO)₃(Me₂bipy)(HNC(CH₃)N(CH₂)₅₋₇)]BF₄ complexes with larger 6-, 7-, and 8-membered heterocyclic rings,¹⁹ and the new [Re(CO)₃(Me₂bipy)(HNC(C₆H₅)(CH)_{2,3-5})]BF₄ complexes with 4-, 5-, and 6-membered heterocyclic rings (5–10) were all characterized by ¹H and ¹³C NMR spectroscopy in CDCl₃ or CD₃CN (Tables 4.1–4.4 and Supporting Information). NMR signals were assigned by using 2D NMR data and by analyzing the splitting pattern and integration of signals in comparison to unambiguous assignments reported for [Re(CO)₃(Me₂bipy)(HNC(CH₃)N(CH₂)₂Y)]BF₄¹⁹ and [Re(CO)₃(5,5'-Me₂bipy)(HNC(CH₃)NHR)]BF₄ complexes.¹⁸

The atom-numbering systems used for NMR signals are shown in Figures 4.2 and 4.5. Also, in order to distinguish between types of methyl signals, the Me₂bipy signals are labeled as L-CH₃ and amidine methyl signals are labeled as C_{am}-CH₃. Furthermore, when rotation about the C_{am}–N4 bond is slow, the two N–CH₂ signals observed are designated as *endo* and *exo* (Figure 4.11).

All amidine complexes with heterocyclic ring substituents of the general class, [Re(CO)₃(Me₂bipy)(HNC(R)N(CH₂)₂Y)]BF₄, in the present study (R = CH₃ and C₆H₅) and a previous study (R = CH₃)¹⁹ show only one NMR signal for each type of proton. The ¹H NMR spectra of new complexes recorded within 5 min of dissolution in CDCl₃ or CD₃CN showed only

one signal for each type of proton (For examples, see spectra for 1 and 3 in Figure 4.12 and for 5, 7, and 9 in Figure 4.13). The ^1H NMR spectra in both solvents did not change with time. The finding of only one signal for each type of proton has two possible explanations: all complexes exist either as only one isomer, or else they exist as a mixture of isomers in rapid exchange. Complexes 1–10 all undoubtedly exist as only the *E* isomer in solution because this is the isomer found in the solid state, and isomerization between the *E* and *Z* isomers is slow enough for isomers to be detected easily by 1D NMR spectra.^{18,19}

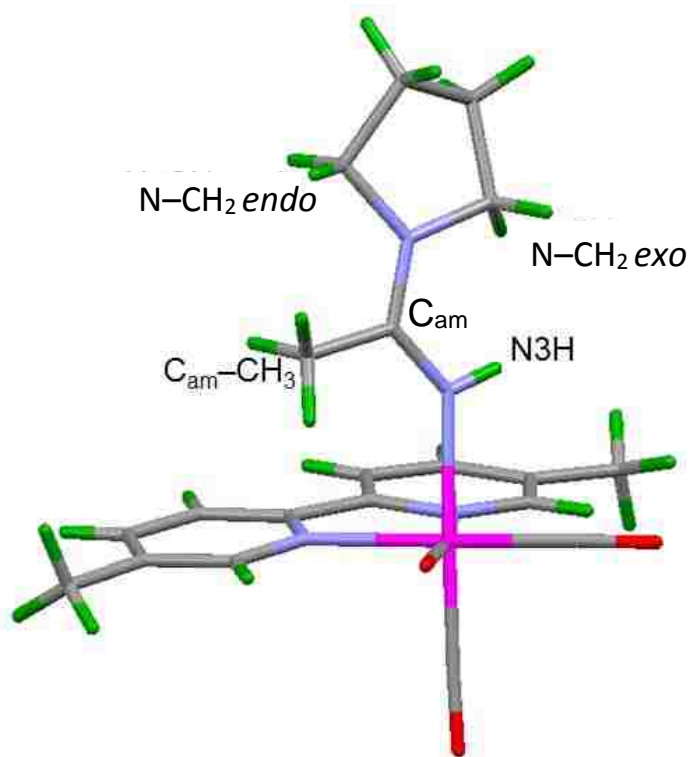


Figure 4.11. Designation of the N-CH_2 *endo* and N-CH_2 *exo* groups, illustrated for the structure of *fac*- $[\text{Re}(\text{CO})_3(5,5'\text{-Me}_2\text{bipy})(\text{HNC}(\text{CH}_3)\text{N}(\text{CH}_2)_4)]\text{BF}_4$ (3).

Sufficient precedent exists to permit assignment of the NMR signals by analysis of the shift, integral, and splitting patterns of the signals. Nevertheless, ROESY and HSQC data in CDCl_3 (for examples, see spectra in Figures 4.14–4.16 and Supporting Information) were used to

assign the ^1H NMR signals of all of the new $[\text{Re}(\text{CO})_3(5,5'\text{-Me}_2\text{bipy})(\text{HNC}(\text{R})\text{N}(\text{CH}_2)_x)]\text{BF}_4$ complexes (1, 3, 5, 7, and 9). The ^1H NMR signals of the $[\text{Re}(\text{CO})_3(6,6'\text{-Me}_2\text{bipy})(\text{HNC}(\text{R})\text{N}(\text{CH}_2)_x)]\text{BF}_4$ complexes were assigned by inspection because of the close parallels between the two series.

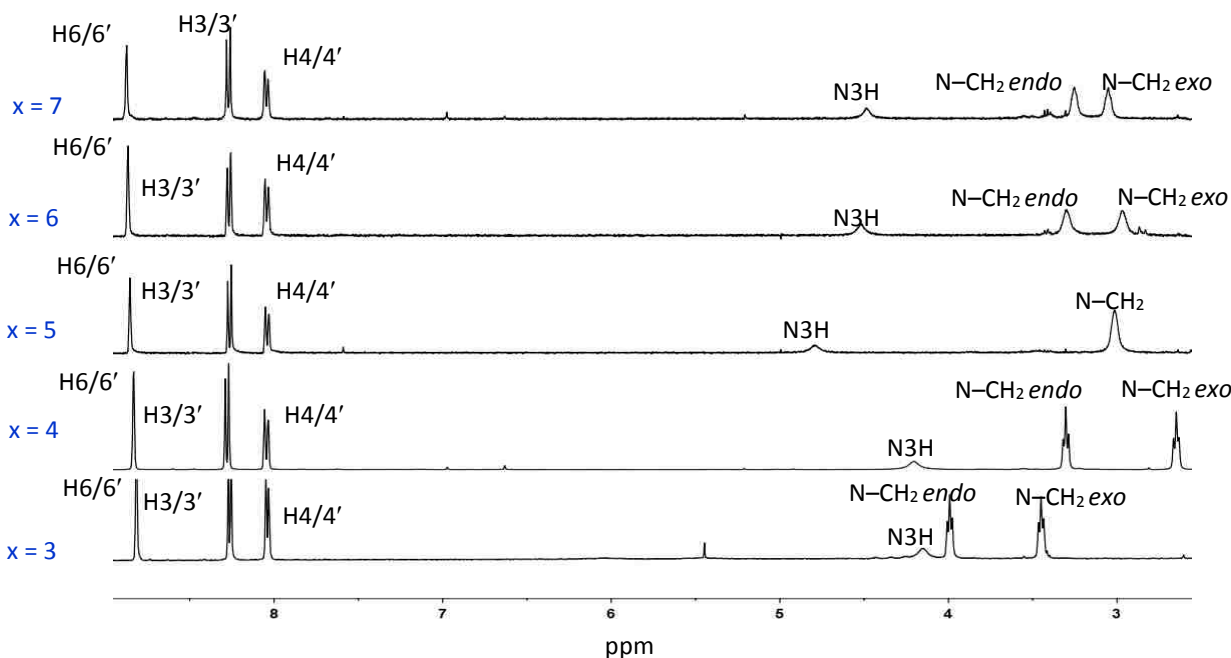


Figure 4.12. Stack plot of a selected region of the ^1H NMR spectra (CD_3CN , 27°C) of $[\text{Re}(\text{CO})_3(5,5'\text{-Me}_2\text{bipy})(\text{HNC}(\text{CH}_3)\text{N}(\text{CH}_2)_x)]\text{BF}_4$ complexes.¹⁹

For all $[\text{Re}(\text{CO})_3(\text{Me}_2\text{bipy})(\text{HNC}(\text{R})\text{N}(\text{CH}_2)_x)]\text{BF}_4$ complexes studied, the two protons in each methylene group of the C_2 -symmetrical heterocyclic ring moiety are magnetically equivalent because the puckered rings undergo rapid fluxional motion, creating a time-averaged planar amidine ligand. Because rotation about both $\text{C}_{\text{am}}\text{-N}$ bonds is slow (except for the special case of 6-membered rings; see end of the NMR discussion of amidine ligand signals), each ring methylene group of the amidine ligands is unique and gives rise to one signal.

Analysis of ^1H and ^{13}C NMR Data for Me_2bipy Ligands in Complexes 1–10. The presence of only one ^1H NMR signal per type of Me_2bipy proton (e.g., H4/4') for all of the

$[\text{Re}(\text{CO})_3(\text{Me}_2\text{bipy})(\text{HNC}(\text{R})\text{N}(\text{CH}_2)_x)]\text{BF}_4$ complexes studied here (Tables 4.1, 4.2, and Supporting Information, Figures 4.12 and 4.13) indicates, as expected, that rotation about the Re–N3 bond is fast. If rotation about the Re–N3 bond were slow, two ^1H NMR signals for each type of Me_2bipy proton would be observed when the amidine ligand is oriented as found in the molecular structures (Figures 4.7–4.9).

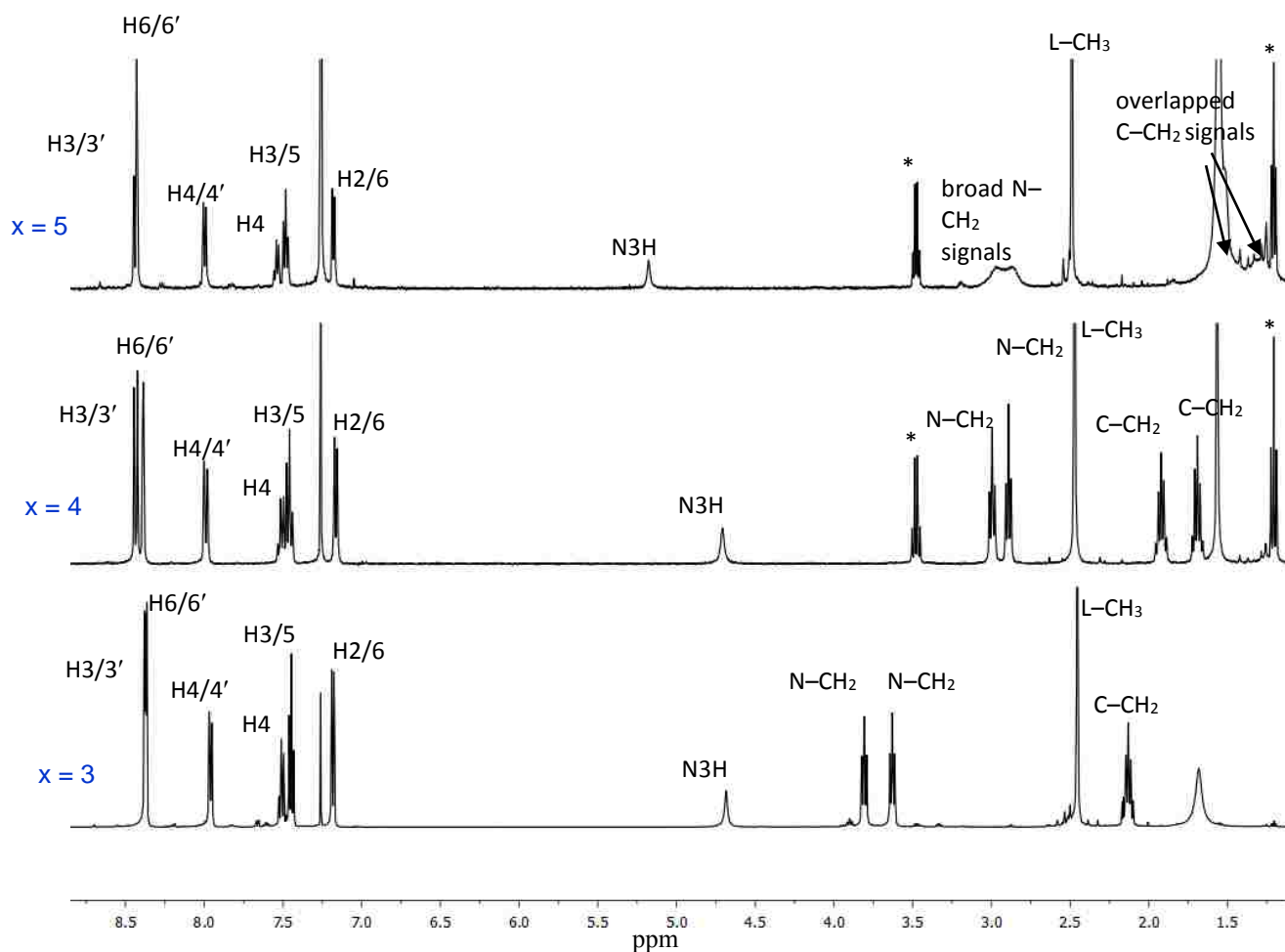


Figure 4.13. Stack plot of a selected region of the ^1H NMR spectra (CDCl_3 , 27 °C) of $[\text{Re}(\text{CO})_3(5,5'\text{-Me}_2\text{bipy})(\text{HNC}(\text{C}_6\text{H}_5)\text{N}(\text{CH}_2)_x)]\text{BF}_4$ complexes. Diethyl ether signals are marked with an asterisk.

For all $[\text{Re}(\text{CO})_3(5,5'\text{-Me}_2\text{bipy})(\text{HNC}(\text{CH}_3)\text{N}(\text{CH}_2)_x)]\text{BF}_4$ complexes studied here, the 5,5'- Me_2bipy H6/6' ^1H NMR signals have shifts falling in narrow ranges of ~8.63 ppm in CDCl_3

(Table 4.1 and ~8.85 in CD₃CN (Figure 4.12 and Supporting Information). These shifts agree well with the values reported for the *E'* and *E* isomers (Figure 4.1) of all [Re(CO)₃(5,5'-Me₂bipy)(HNC(CH₃)NHR)]BF₄ complexes studied in these solvents.¹⁸ In contrast, the values reported for the *Z* isomer of [Re(CO)₃(5,5'-Me₂bipy)(HNC(CH₃)NHR)]BF₄ complexes are consistently farther upfield. These results strongly indicate that the shift of the H6/6' signal is influenced by a through-space effect from the closest amidine substituent. Because for both [Re(CO)₃(5,5'-Me₂bipy)(HNC(CH₃)NHR)]BF₄ and [Re(CO)₃(5,5'-Me₂bipy)(HNC(CH₃)N(CH₂)_x)]BF₄ complexes the C_{am}-CH₃ methyl group is closest to H6/6' protons in the *E* or *E'* isomers, the similarity in H6/6' shifts noted above is consistent with the conclusion reached here and in our previous study¹⁹ that the *E* isomer is greatly favored when the amidine substituent is a heterocyclic ring.

For both series of [Re(CO)₃(Me₂bipy)(HNC(CH₃)(CH₂)_x)]BF₄ complexes, the Me₂bipy H4/4' ¹H NMR signals are independent of the differences in heterocyclic substituent (Table 4.1 and Supporting Information). Because the H4/4' protons are in the para position and remote from the axial amidine ligand, the H4/4' signal is subject to inductive effects but not to through-space effects from the axial ligand. Thus, the H4/4' shift is a good indicator of the relative electron-donor ability of the axial amidine ligand. The similarity in the H4/4' shifts and the independence of the H4/4' shifts on the axial ligand found in the present study both indicate that changes in the heterocyclic substituent do not significantly affect the donor ability of the axial ligand.

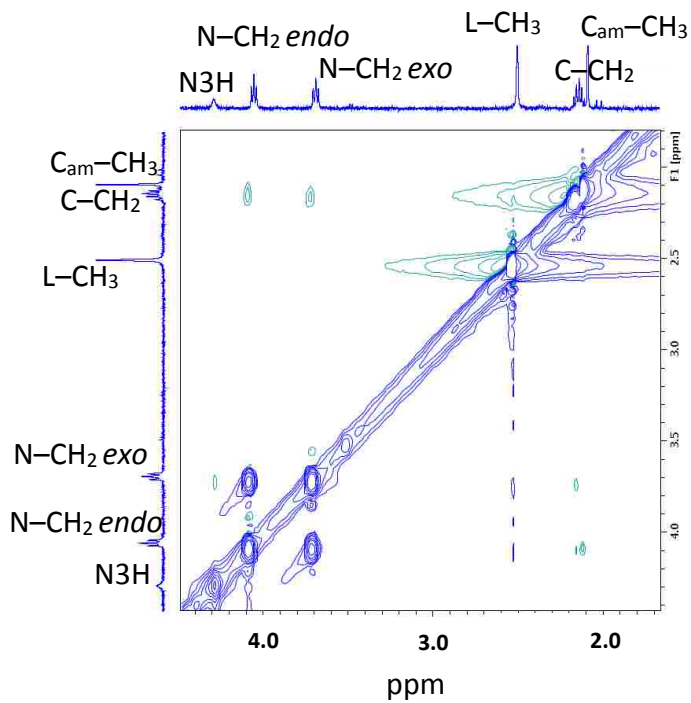


Figure 4.14. Selected region of the ROESY spectrum (CDCl_3 , 27 °C) of $\text{Re}(\text{CO})_3(5,5'\text{-Me}_2\text{bipy})(\text{HNC}(\text{CH}_3)\text{N}(\text{CH}_2)_3)]\text{BF}_4$ (1).

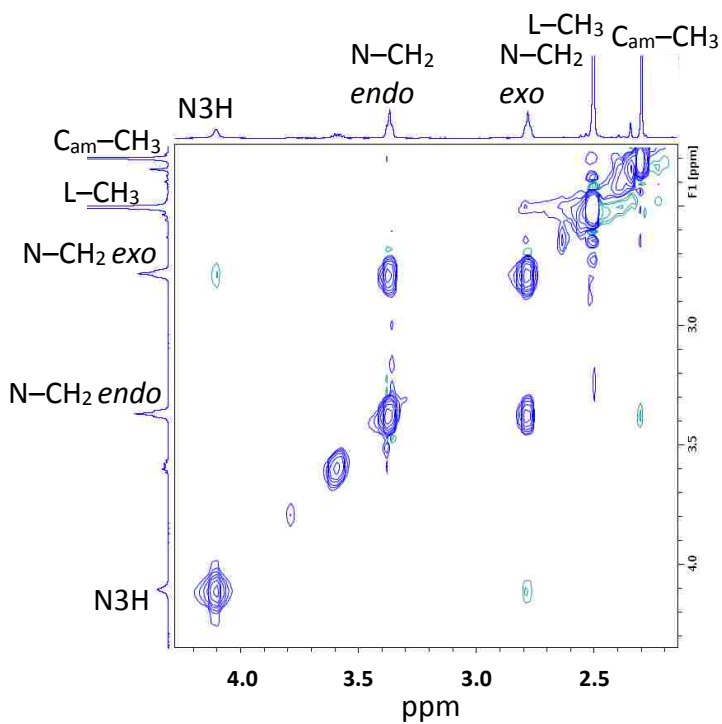


Figure 4.15. Selected region of the ROESY spectrum (CDCl_3 , 27 °C) of $\text{Re}(\text{CO})_3(5,5'\text{-Me}_2\text{bipy})(\text{HNC}(\text{CH}_3)\text{N}(\text{CH}_2)_4)]\text{BF}_4$ (3).

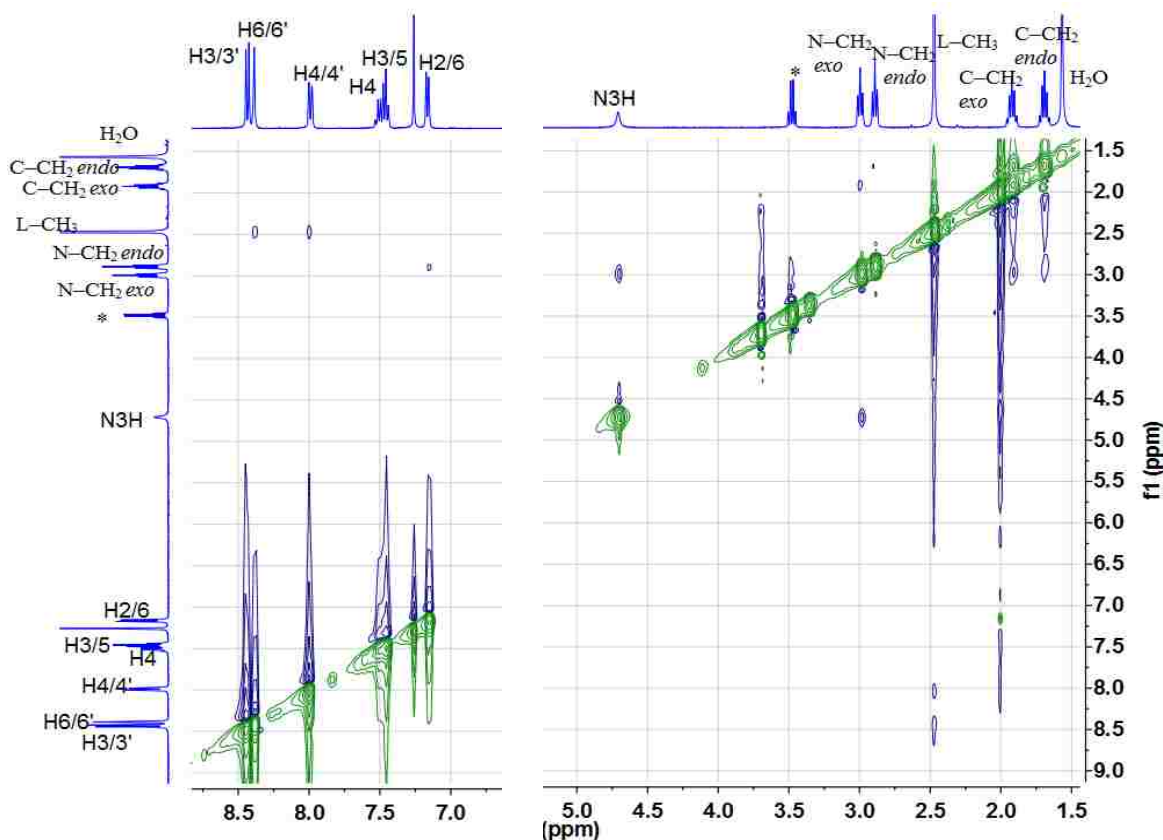


Figure 4.16. ROESY spectrum (CDCl_3 , 27°C) of $[\text{Re}(\text{CO})_3(5,5'\text{-Me}_2\text{bipy})(\text{HNC}(\text{C}_6\text{H}_5)\text{N}(\text{CH}_2)_4)]\text{BF}_4$ (7). Diethyl ether signals are marked with an asterisk.

^{13}C NMR data for complexes 1–4 in CDCl_3 are presented in Table 4.3 (along with new ^{13}C NMR data for related previously reported complexes).¹⁹ ^{13}C NMR signals for the free 5,5'- Me_2bipy and 6,6'- Me_2bipy ligands in CDCl_3 ¹⁷ are listed in Supporting Information. Although the shifts differ for the $[\text{Re}(\text{CO})_3(\text{Me}_2\text{bipy})(\text{HNC}(\text{CH}_3)(\text{CH}_2)_x)]\text{BF}_4$ complexes between the 5,5'- Me_2bipy and the 6,6'- Me_2bipy series of complexes, within each series the shifts of the L- CH_3 ^{13}C NMR signals do not vary much (Table 4.3), confirming the conclusion from the analysis of ^1H NMR signals that the nature of the heterocyclic ring moiety does not significantly change the amidine ligand's electron-donating ability. The same conclusion is reached from the ^{13}C NMR shifts of the Me_2bipy endocyclic carbons in the two series; shifts of signals for each type of endocyclic carbon fall into narrow ranges independent of changes in the amidine ligand.

For both series of $[\text{Re}(\text{CO})_3(\text{Me}_2\text{bipy})(\text{HNC}(\text{C}_6\text{H}_5)\text{N}(\text{CH}_2)_x)]\text{BF}_4$ complexes (5–10) the Me_2bipy H4/4' ^1H NMR signals are independent of the heterocyclic substituent (Table 4.2 and Figure 4.13). Furthermore, these H4/4' shifts for the two $\text{R} = \text{C}_6\text{H}_5$ series are very similar to those for the two $\text{R} = \text{CH}_3$ series. Thus, the donor ability of the axial amidine ligand is not significantly dependent on either the heterocyclic substituent or the R substituent in $[\text{Re}(\text{CO})_3(\text{Me}_2\text{bipy})(\text{HNC}(\text{R})\text{N}(\text{CH}_2)_x)]\text{BF}_4$ complexes. Consequently, differences in through-space effects between the two types of amidine R substituents, $\text{R} = \text{CH}_3$ and $\text{R} = \text{C}_6\text{H}_5$, will be the main factor affecting shifts of ^1H NMR signals of the Me_2bipy protons close to the axial amidine ligand.

In our previous studies, the majority of the molecular structures of $[\text{Re}(\text{CO})_3(\text{Me}_2\text{bipy})(\text{axial ligand})]\text{X}$ complexes with amidine ($\text{HNC}(\text{CH}_3)\text{NHR}$ or $\text{HNC}(\text{CH}_3)\text{N}(\text{CH}_2)_2\text{Y}$) or iminoether ($\text{HNC}(\text{CH}_3)\text{OCH}_3$) axial ligands had the same orientation of the axial ligand in the solid state.¹⁷⁻¹⁹ The common orientation is shown in Figure 4.10. Those few complexes with a differently oriented axial ligand, nevertheless, had very similar shifts for signals of protons of identical types, a result indicating that the axial ligands in these complexes had the same net orientation in solution regardless of the orientation in the solid state. However, the NMR data when R in the axial ligand is CH_3 did not provide clear evidence that the amidine orientation in solution was indeed the same as the common orientation in the solid. The analogues with $\text{R} = \text{C}_6\text{H}_5$ do provide such evidence. ^1H NMR signals of the 5,5'- Me_2bipy H6/6' protons for all $[\text{Re}(\text{CO})_3(5,5'\text{-Me}_2\text{bipy})(\text{HNC}(\text{C}_6\text{H}_5)\text{N}(\text{CH}_2)_x)]\text{BF}_4$ complexes (5, 7, and 9) fall in a narrow range of ~ 8.4 ppm in CDCl_3 (Table 4.2 and Figure 4.13). The shifts of the H6/6' signals, when $\text{R} = \text{C}_6\text{H}_5$, are ~ 0.2 ppm upfield compared to when $\text{R} = \text{CH}_3$ (Tables 4.1, 4.2, and Figure 4.17), a finding consistent with an axial amidine net orientation in solution very similar to

that in the solid (Figure 4.10). Likewise, whereas the signals of the relatively remote 5,5'-methyl groups have shifts that are independent of both the heterocyclic substituent or the R substituent in $[\text{Re}(\text{CO})_3(\text{Me}_2\text{bipy})(\text{HNC}(\text{R})\text{N}(\text{CH}_2)_x)]\text{BF}_4$ complexes, the close-in 6,6'-methyl groups have signals with shifts that are ~ 0.25 ppm more upfield for $\text{R} = \text{C}_6\text{H}_5$ than for $\text{R} = \text{CH}_3$ (Tables 4.1 and

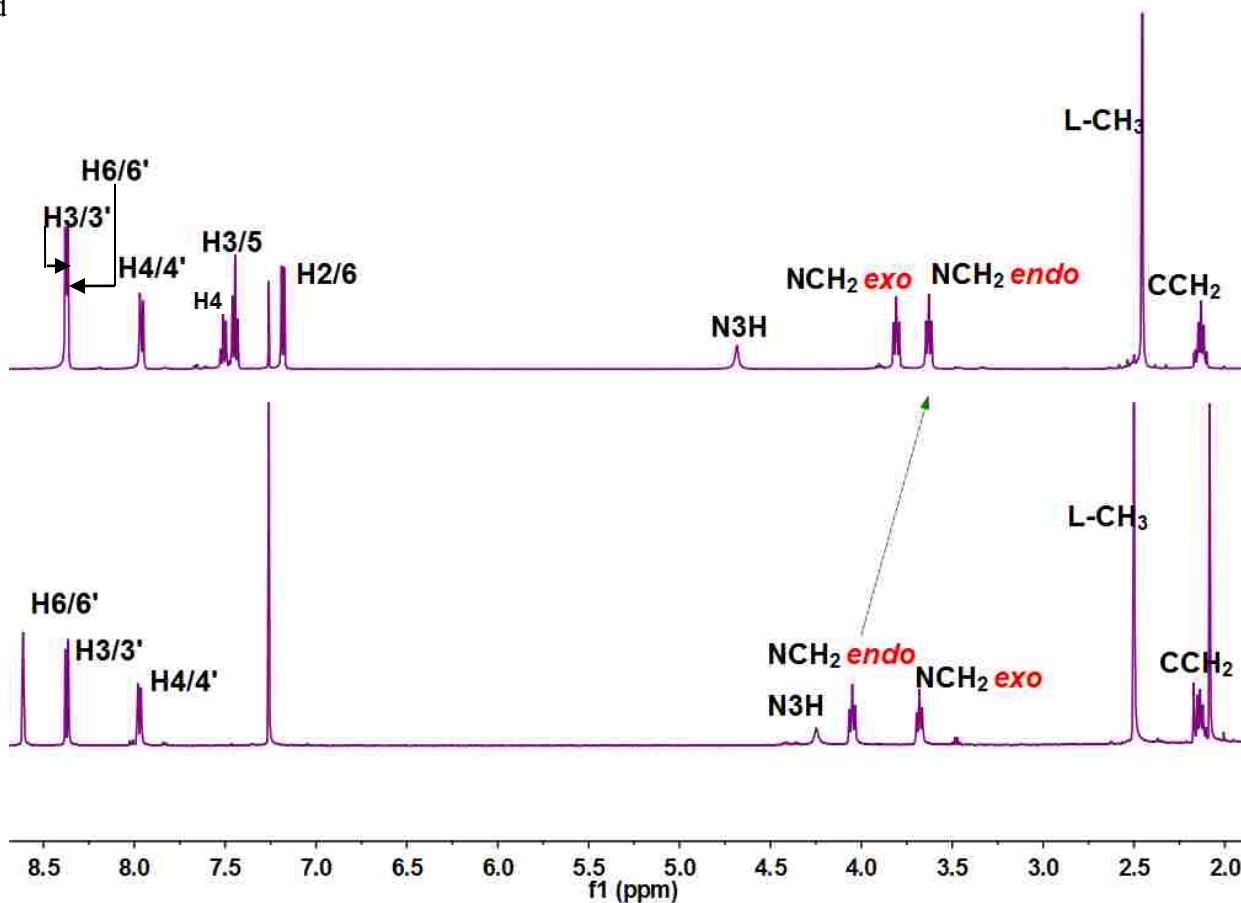


Figure 4.17. ^1H NMR stack plot of $[\text{Re}(\text{CO})_3(5,5'\text{-Me}_2\text{bipy})(\text{HNC}(\text{CH}_3)\text{N}(\text{CH}_2)_3)]\text{BF}_4$ (bottom) and $[\text{Re}(\text{CO})_3(5,5'\text{-Me}_2\text{bipy})(\text{HNC}(\text{C}_6\text{H}_5)\text{N}(\text{CH}_2)_3)]\text{BF}_4$ (top) in CDCl_3 at 27°C .

The narrow range observed for the ^{13}C NMR signals of the 5,5'- Me_2bipy carbons for all $[\text{Re}(\text{CO})_3(5,5'\text{-Me}_2\text{bipy})(\text{HNC}(\text{CH}_3)\text{N}(\text{CH}_2)_x)]\text{BF}_4$ complexes studied in CDCl_3 (Table 4.4) was also observed for the ^{13}C NMR signals of the 5,5'- Me_2bipy carbons for all of the $[\text{Re}(\text{CO})_3(5,5'\text{-Me}_2\text{bipy})(\text{HNC}(\text{C}_6\text{H}_5)\text{N}(\text{CH}_2)_x)]\text{BF}_4$ complexes (**5**, **7**, and **9**) in CDCl_3 . In addition, the shifts of

the 5,5'-Me₂bipy signals are very similar for R = C₆H₅ and R = CH₃ (Tables 4.3 and 4.4). Thus, for [Re(CO)₃(5,5'-Me₂bipy)(HNC(R)N(CH₂)_x)]BF₄ complexes in this study, the net electron-donating ability of the axial amidine ligands appears to be virtually independent of the identity of both R and N(CH₂)_x.

Analysis of ¹H and ¹³C NMR Data for Amidine Ligands in Complexes 1–10. In this section we will discuss the ¹H and ¹³C NMR data of the axial HNC(R)N(CH₂)_x ligands and relate the NMR information to the properties of the complexes. The section is arranged in the following order of NMR data: ¹H and ¹³C of R groups (CH₃ and C₆H₅); ¹H and ¹³C of N–CH₂ *endo* and N–CH₂ *exo* groups; ¹H of N₃H; and finally the special properties of 6-membered heterocyclic rings. Within the discussion of each of these NMR features, we will treat R = CH₃ before R = C₆H₅ complexes and ¹H NMR data before ¹³C NMR data, when possible. It should be noted that in addition to the new complexes, 1–10, for the present study we conducted additional NMR studies on previously reported compounds in CDCl₃, and the new NMR results for both new and reported complexes¹⁹ can be found in Tables 4.1–4.4 and Figures 4.12–4.16.

¹H and ¹³C NMR Signals of the R Groups of [Re(CO)₃(Me₂bipy)(HNC(R)N(CH₂)_x)]BF₄ Complexes. Comparing [Re(CO)₃(Me₂bipy)(HNC(CH₃)N(CH₂)_x)]BF₄ complexes, the 6,6'-Me₂bipy complexes 2 and 4 show a ~0.45 ppm upfield shifting of the C_{am}-CH₃ ¹H NMR signal relative to 5,5'-Me₂bipy complexes 1 and 3. In our previous work with [Re(CO)₃(Me₂bipy)(HNC(CH₃)N(CH₂)₂Y)]BF₄ complexes, we observed a similar upfield shift of the C_{am}-CH₃ ¹H NMR signal for the 6,6'-Me₂bipy complexes vs 5,5'-Me₂bipy complexes.¹⁹ We attributed such upfield shifts of the C_{am}-CH₃ ¹H NMR signal when the amidine ligand is in the *E* configuration in 6,6'-Me₂bipy complexes to the anisotropic effect of the aromatic rings of the tilted 6,6'-Me₂bipy ligand.¹⁹ In

these complexes, the *E* configuration of the amidine ligand places it close to the Me₂bipy ligands and the 6,6'-Me₂bipy tilting increases the shielding resulting from the anisotropic rings.

The previously studied [Re(CO)₃(Me₂bipy)(HNC(CH₃)N(CH₂)₂Y)]BF₄ complexes had very similar ¹H NMR shifts for the C_{am}-CH₃ methyl group within each Me₂bipy series.¹⁹ The shifts of the C_{am}-CH₃ ¹H NMR signal of the complexes with 5-membered rings (3 and 4) are similar in range to those of other [Re(CO)₃(Me₂bipy)(HNC(CH₃)N(CH₂)₅₋₇)] complexes for each Me₂bipy series (Table 4.1 and Supporting Information). In contrast, complexes with 4-membered rings (1 and 2) have very different C_{am}-CH₃ ¹H NMR chemical shifts as compared to complexes with larger rings within each Me₂bipy series. Complexes 1 and 2 have the most upfield C_{am}-CH₃ ¹H NMR signals in each Me₂bipy series. Moreover, in each of the two series of amidine complexes presented in Table 4.3, the C_{am}-CH₃ methyl ¹³C NMR signal is significantly more upfield in complexes 1 and 2 (with a 4-membered heterocyclic ring moiety), whereas the signal for complexes 3 and 4 (with a 5-membered heterocyclic ring moiety) has a shift that is similar to the shifts observed for complexes with larger-ring substituents in each series (Table 4.3). We attribute these effects to differences in the relative amounts of s and p character in the bonds of the heterocyclic ring moiety as the size of the ring changes from 4- to 5-membered. These changes in bond character of the rings in turn are transmitted through the N4-C_{am}-C(R group) bonds, and thus the changes affect the shifts of the R group NMR signals. Recall that the C18-N4-C(*n*) bond angles for complexes 1 and 2 (Table 4.8 and Supporting Information) are significantly more acute than in all of the other [Re(CO)₃(Me₂bipy)(HNC(CH₃)N(CH₂)₄₋₇)]BF₄ complexes studied here or previously.¹⁹

Comparing [Re(CO)₃(Me₂bipy)(HNC(C₆H₅)N(CH₂)_x)]BF₄ complexes, the 6,6'-Me₂bipy complexes (6, 8 and 10) show an ~0.25, ~0.1, and ~0.05 ppm upfield shifting of the phenyl H2/6,

H3/5, and H4 NMR signals, respectively, relative to 5,5'-Me₂bipy complexes 5, 7 and 9 (Table 4.2). The trend in decreasing size of the upfield shifts reflects the relative distance to the phenyl ring protons from the Me₂bipy rings. The upfield shifts can be attributed to the shorter distance from the phenyl protons to the 6,6'-Me₂bipy ligand resulting from the tilting of the anisotropic 6,6'-Me₂bipy ligand.

For each of the two series of [Re(CO)₃(Me₂bipy)(HNC(C₆H₅)N(CH₂)_x)]BF₄ complexes in Table 4.4, the phenyl C1 ¹³C NMR signal has a significant ~ 3 ppm upfield shift in complexes 5 and 6 (with the 4-membered heterocyclic ring moiety) as compared to the C1 ¹³C NMR signal for complexes 7, 8, 9, and 10 (with a 5- or 6-membered heterocyclic ring moiety). The relationship of these shifts to heterocyclic ring size can be attributed to differences in hybridization of the heterocyclic ring atoms as explained above.

¹H and ¹³C NMR Signals of the N-CH₂ Groups of [Re(CO)₃(Me₂bipy)(HNC(R)N(CH₂)_x)]BF₄ Complexes. For all complexes, because of relatively fast change in the ring pucker, each CH₂ group has only one ¹H NMR signal and one ¹³C NMR signal (Tables 4.1–4.4). Except for the four complexes with the 6-membered N(CH₂)₅ ring substituent studied by NMR methods in the present work, which are discussed below, the heterocyclic ring moiety of all other complexes undergoes relatively slow rotation around the C_{am}-N4 bond.

The [Re(CO)₃(Me₂bipy)(HNC(CH₃)N(CH₂)_{3,4})]BF₄ complexes (1–4) show two sharp N-CH₂ ¹H NMR signals in both CD₃CN and CDCl₃ (Figure 4.12), indicating slow rotation around the N4-C16 bond for the 4- and 5-membered heterocyclic ring moieties. Relative sizes of NOE cross-peaks allow the unambiguous assignment of the two heterocyclic ring N-CH₂ signals, as the N-CH₂ *endo* protons are closer to the C_{am}-CH₃ methyl group and the N-CH₂ *exo* protons are

closer to the N3H proton (Figure 4.11). As shown in ROESY spectra for complexes 1 and 3 (Figures 4.14 and 4.15), the downfield N–CH₂ signal of both 1 and 3 has a strong NOE cross-peak to the C_{am}-CH₃ methyl signal, thus assigning it to N–CH₂ *endo*. Similarly, the upfield N–CH₂ signal, which has a strong NOE cross-peak with the N3H signal, is assigned to the N–CH₂ *exo* protons. The similarity in the 1D NMR spectra of 2 and 4 to the spectra of 1 and 3 allowed us to assign the N–CH₂ *endo* and N–CH₂ *exo* signals for these [Re(CO)₃(6,6'-Me₂bipy)(HNC(CH₃)N(CH₂)_{3,4})]BF₄ analogues (2 and 4). Furthermore, the close similarity in these shifts for the 5,5'-Me₂bipy and 6,6'-Me₂bipy analogues establishes that even for the N–CH₂ *exo* protons, the closest ring protons to the equatorial ligand (Figure 4.11), the distance is too long (Figure 4.7) for detecting a shielding effect from the tilted 6,6'-Me₂bipy ligand. For all [Re(CO)₃(Me₂bipy)(HNC(CH₃)N(CH₂)_x)]BF₄ complexes (both in CDCl₃ and CD₃CN) with resolved N–CH₂ *endo* and N–CH₂ *exo* ¹H NMR signals, the N–CH₂ *endo* signal is downfield from the N–CH₂ *exo* signal regardless of the size of the heterocyclic ring (Figure 4.12, Table 4.1 and Supporting Information).

In ¹H NMR spectra of [Re(CO)₃(Me₂bipy)(HNC(CH₃)N(CH₂)_x)]BF₄ complexes 1–4, the N–CH₂ *endo* triplets are downfield of the N–CH₂ *exo* triplets by 0.45 to 0.65 ppm (Table 4.1). These differences in shift for the two N–CH₂ triplets cannot be attributed to the greater distance of the N–CH₂ *endo* group from the anisotropic bipyridine rings in the equatorial plane because even the closer-in N–CH₂ *exo* group is too distant to be affected by bipyridine anisotropy. Rather, as we discuss next, we believe that the difference in geometric relationship of the N–CH₂ *endo* and *exo* groups to the N3H and the C_{am}-CH₃ groups of [Re(CO)₃(Me₂bipy)(HNC(CH₃)N(CH₂)_x)]BF₄ complexes (Figure 4.11) can account for the difference in chemical shift between the N–CH₂ *endo* and the N–CH₂ *exo* signals.

For $[\text{Re}(\text{CO})_3(\text{Me}_2\text{bipy})(\text{HNC}(\text{CH}_3)\text{NHR})]\text{BF}_4$ complexes,¹⁸ the CH signals of the R group of the *E* isomer (having the same relationship to the N3H and the C_{am}-CH₃ groups as the N-CH₂ *endo* group) are typically downfield by ~0.4 ppm to the corresponding CH signals of the R groups of the *E'* isomer (having the same relationship to the N3H and the C_{am}-CH₃ groups as the N-CH₂ *exo* group). Thus, the relative downfield and upfield chemical shifts of the N-CH₂ *endo* and *exo* ¹H NMR signals result from differences in the environment of the N4-CH₂ protons with respect to the amidine ligand N3H and the C_{am}-CH₃ groups. The difference in relative chemical shifts is not a consequence of the different location of these methylene groups within the heterocyclic ring because the $[\text{Re}(\text{CO})_3(\text{Me}_2\text{bipy})(\text{HNC}(\text{CH}_3)\text{NHR})]\text{BF}_4$ complexes do not have any such ring. However, as discussed in the next paragraph, the size of the ring can have a significant effect on the chemical shifts of both types of N-CH₂ signals.

Both N-CH₂ ¹H NMR triplets (average shift ~ 3.85 ppm) for complexes 1 and 2, with a 4-membered heterocyclic ring, have significantly downfield chemical shifts in both CD₃CN and CDCl₃ compared to the N-CH₂ signals (average shift ~ 3.1 ppm) for all other $[\text{Re}(\text{CO})_3(\text{Me}_2\text{bipy})(\text{HNC}(\text{CH}_3)\text{N}(\text{CH}_2)_x)]\text{BF}_4$ complexes studied, including the N-CH₂ triplets of complexes 3 and 4 (Figure 4.12, Table 4.1 and Supporting Information). The ¹³C NMR signals of the two N-CH₂ carbon atoms of the heterocyclic ring moiety are well separated for complexes 1–4 and for complexes with a 7- or 8-membered heterocyclic ring, $[\text{Re}(\text{CO})_3(\text{Me}_2\text{bipy})(\text{HNC}(\text{CH}_3)\text{N}(\text{CH}_2)_{6,7})]\text{BF}_4$ (Table 4.3). The N-CH₂ ¹³C NMR signals for 1 and 2 are more downfield (average shift > 50 ppm) than for complexes with larger rings (average shift < 50 ppm). This finding of downfield ¹H and ¹³C NMR shifts of N-CH₂ signals for complexes 1 and 2 compared to the complexes with larger heterocyclic rings is again attributed to differences in hybridization of atoms in the 4-membered heterocyclic ring as compared to the larger rings.

The same strategy used for assigning the ^1H and ^{13}C NMR N-CH₂ *endo* and N-CH₂ *exo* signals of $[\text{Re}(\text{CO})_3(\text{Me}_2\text{bipy})(\text{HNC}(\text{CH}_3)\text{N}(\text{CH}_2)_x)]\text{BF}_4$ complexes was employed to assign these signals for the $[\text{Re}(\text{CO})_3(\text{Me}_2\text{bipy})(\text{HNC}(\text{C}_6\text{H}_5)\text{N}(\text{CH}_2)_x)]\text{BF}_4$ complexes (Tables 4.2 and 4.4). In ROESY spectra for these R = C₆H₅ complexes 5 (not shown) and 7 (Figure 4.16) used in the assignments of the N-CH₂ signals, strong NOE cross-peaks are present between the downfield N-CH₂ signal and the N3H signal and between the upfield N-CH₂ signal and the phenyl ring H2/6 signal, thus assigning these to N-CH₂ *exo* and N-CH₂ *endo* signals, respectively. Both the N-CH₂ *exo* signals and the N3H signals are ~0.1 to ~0.2 ppm downfield from the corresponding signals in the $[\text{Re}(\text{CO})_3(\text{Me}_2\text{bipy})(\text{HNC}(\text{CH}_3)\text{N}(\text{CH}_2)_x)]\text{BF}_4$ analogues, as might be expected from the electron-withdrawing nature of the phenyl group. In contrast, the N-CH₂ *endo* ^1H NMR signal for $[\text{Re}(\text{CO})_3(\text{Me}_2\text{bipy})(\text{HNC}(\text{C}_6\text{H}_5)\text{N}(\text{CH}_2)_{3,4})]\text{BF}_4$ complexes has been shifted ~0.4 ppm upfield by the anisotropic effect of the phenyl ring, relative to this signal for the $[\text{Re}(\text{CO})_3(\text{Me}_2\text{bipy})(\text{HNC}(\text{CH}_3)\text{N}(\text{CH}_2)_x)]\text{BF}_4$ analogues (Tables 4.1 and 4.2). This notable upfield shift has the result that the N-CH₂ *endo* signal is now slightly upfield (~0.1 ppm) to the N-CH₂ *exo* signal (Figures 4.12 and 4.17).

Relation of the Size of the Heterocyclic Ring Moiety to the Ease of its Rotation about the C_{am}-N4 Bond of $[\text{Re}(\text{CO})_3(\text{Me}_2\text{bipy})(\text{HNC}(\text{R})\text{N}(\text{CH}_2)_x)]\text{BF}_4$ Complexes. As mentioned above, restricted rotation of the N(CH₂)₂Y ring moiety around the amidine C_{am}-N4 bond occurs in $[\text{Re}(\text{CO})_3(\text{Me}_2\text{bipy})(\text{HNC}(\text{R})\text{N}(\text{CH}_2)_x)]\text{BF}_4$ complexes. $[\text{Re}(\text{CO})_3(5,5'$ -Me₂bipy)(HNC(CH₃)N(CH₂)_x)]BF₄ complexes with x = 3, 4, 6, and 7 exhibit NMR spectral features indicating restricted rotation around the C_{am}-N4 bond (Tables 4.1 and 4.3 and Figures 4.14, 15, and 16), and each heterocyclic ring CH₂ group has one ^{13}C NMR signal, one ^1H NMR signal, and one HSQC cross-peak in CDCl₃ (for examples, see spectra in Supporting Information when x = 3 and 4). This rotation around the C_{am}-N4 bond in these $[\text{Re}(\text{CO})_3(5,5'$ -

Me₂bipy)(HNC(CH₃)N(CH₂)_x)]BF₄ complexes can be qualitatively assessed from the ROESY spectra. As can be seen in Figures 4.14 and 4.15, the ROESY spectra for both complexes 1 and 3 in CDCl₃ show EXSY cross-peaks between the two well-separated N–CH₂ *endo* and N–CH₂ *exo* signals, providing unambiguous evidence for rotation around the C_{am}–N4 bond.

In order to use the intensities of these EXSY cross-peaks to estimate roughly the relative ease of rotation around the C_{am}–N4 bond for complexes 1 and 3 as compared to [Re(CO)₃(5,5'-Me₂bipy)(HNC(CH₃)N(CH₂)_{6,7})]BF₄ complexes, we acquired ROESY spectra for these two previously reported complexes,¹⁹ under identical conditions in CDCl₃ as those used for 1 and 3. Next we compared the size of the EXSY cross-peaks for the four complexes. The ratios for N–CH₂ *endo* and N–CH₂ *exo* cross-peaks to N–CH₂ *endo* and N–CH₂ *exo* diagonal signals were computed by summing the intensities of the cross-peaks on both sides of the diagonal and dividing this sum by the sum of the diagonal peaks. The ratios obtained are as follows: 0.31 for x = 3 (1); 0.29 for x = 4 (3); 0.97 for x = 6; and 0.82 for x = 7. These ratios clearly indicate that rotation around the C_{am}–N4 bond is slower for complexes 1 and 3 than for the [Re(CO)₃(5,5'-Me₂bipy)(HNC(CH₃)N(CH₂)_{6,7})]BF₄ complexes with larger rings.

In addition to the EXSY cross-peaks, the NOE cross-peaks in the ROESY spectra of complexes 1 and 3 (Figures 4.14 and 4.15) also provide information on the relative ease of rotation in 1 and 3 versus the complexes with the larger rings. For both 1 and 3, the downfield N–CH₂ *endo* signal has a strong NOE cross-peak with the C_{am}–CH₃ methyl signal, and the upfield N–CH₂ *exo* has a strong NOE cross-peak with the N3H signal. In [Re(CO)₃(5,5'-Me₂bipy)(HNC(CH₃)N(CH₂)_{6,7})]BF₄ complexes (ROESY spectra not shown), however, both *endo* and *exo* N–CH₂ signals have NOE cross-peaks of equal intensity with the C_{am}–CH₃ methyl signal as well as with the N3H signal. The comparable NOE cross-peak intensity exhibited by the

complexes with larger rings arises from rotation fast enough to allow a phenomenon we have called "exchange-NOE peaks".²⁶ This observation also indicates that rotation around the C_{am}-N4 bond in these two complexes with larger rings is faster than in complexes 1 and 3.

In contrast to complexes with both smaller and larger heterocyclic rings, when $x = 5$ ([Re(CO)₃(5,5'-Me₂bipy)(HNC(CH₃)N(CH₂)₅)]BF₄), instead of two N-CH₂ signals, only one broad ¹H NMR signal integrating to four protons can be seen in CD₃CN or CDCl₃ (at ~3.0 ppm in CD₃CN and ~3.1 ppm in CDCl₃, Figures 4.12 and 4.18). The rest of the CH₂ protons in the piperidine-derived ring moiety give rise to two multiplets integrating to two and four protons in CD₃CN or CDCl₃. The larger C-CH₂ multiplet arises from time-averaging of the signals of the two β CH₂ groups.

For [Re(CO)₃(Me₂bipy)(HNC(CH₃)N(CH₂)₅)]BF₄ complexes with a 6-membered heterocyclic ring ($x = 5$), the two N-CH₂ ¹³C NMR signals are undetectably broad in the corresponding 1D ¹³C NMR spectrum at 27 °C (Supporting Information). The chemical shifts of the broad N-CH₂ signals in [Re(CO)₃(Me₂bipy)(HNC(CH₃)N(CH₂)₅)]BF₄ complexes were determined by using 2D HSQC experiments (for L = 5,5'-Me₂bipy, Figure in Supporting Information). A very weak HSQC ¹H-¹³C cross-peak between a broad ¹H NMR signal and very broad ¹³C NMR signal [at ~3.0 ppm to ~47 ppm for both 5,5'-Me₂bipy, (Supporting Information) and 6,6'-Me₂bipy complexes] allowed us to assign the ~47 ppm ¹³C NMR peak of the [Re(CO)₃(Me₂bipy)(HNC(CH₃)N(CH₂)₅)]BF₄ complexes to the N-CH₂ carbon atoms. At -13 °C, a solution of [Re(CO)₃(5,5'-Me₂bipy)(HNC(CH₃)N(CH₂)₅)]BF₄ in CDCl₃ showed two ¹H NMR signals (at 3.21 ppm and 2.80 ppm, Figure 4.18) and two ¹³C NMR signals (at 49.41 and 44.45 ppm, Supporting Information) for the *endo* and *exo* N-CH₂ groups, respectively, consistent with slower rotation around the C_{am}-N4 bond at lower temperature.

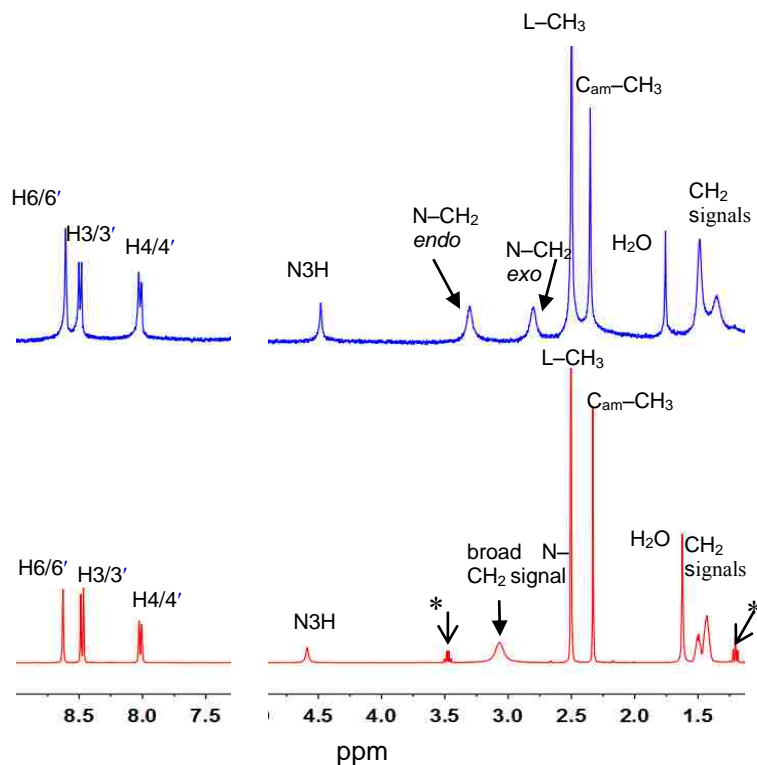


Figure 4.18. ^1H NMR stack plot of $[\text{Re}(\text{CO})_3(5,5'\text{-Me}_2\text{bipy})(\text{HNC}(\text{CH}_3)\text{N}(\text{CH}_2)_5)]\text{BF}_4^2$ in CDCl_3 at $-13\text{ }^\circ\text{C}$ (blue) and $27\text{ }^\circ\text{C}$ (red). Diethyl ether signals are marked with an asterisk.

The structure of the 6-membered heterocyclic ring is most probably responsible for the shallowness of the barrier to rotation around the $\text{C}_{\text{am}}\text{-N}_4$ bond in the $[\text{Re}(\text{CO})_3(5,5'\text{-Me}_2\text{bipy})(\text{HNC}(\text{CH}_3)\text{N}(\text{CH}_2)_5)]\text{BF}_4$ complex compared to this barrier in analogues with 3-, 4-, 6-, and 7-membered rings. As the rings rotate around the $\text{C}_{\text{am}}\text{-N}_4$ bond, this bond's character changes from partial double bond to single bond near the top of the rotation barrier. The hybridization of N_4 changes from sp^2 to sp^3 . In a 6-membered ring, all ring atoms can readily be pseudo tetrahedral because a 6-membered ring accommodates best to nearly ideal 109.5° bond angles at the ring atoms. Thus, the change in hybridization from sp^2 to sp^3 hybridization of the N ring atom is energetically more favorable than for the other rings, especially the smaller 4- and 5-membered rings.

4.4 Conclusions

The smaller heterocyclic amines employed here have a relatively high reactivity and form only $[\text{Re}(\text{CO})_3(5,5'\text{-Me}_2\text{bipy})(\text{HNC}(\text{R})\text{N}(\text{CH}_2)_{3,4})]\text{BF}_4$ amidine complexes with the *E* configuration, indicating that amidine complexes can be formed quickly and isomerically pure. We conclude that the bulk of the 4- and 5-membered rings is small enough to enhance the ease of attack of the amine onto the bound nitrile group but large enough to destabilize the *Z* isomer. The $[\text{Re}(\text{CO})_3(5,5'\text{-Me}_2\text{bipy})(\text{HNC}(\text{R})\text{N}(\text{CH}_2)_{3,4})]\text{BF}_4$ complexes were robust when challenged with 4-dimethylaminopyridine, indicating that amidine ligands are strong donors. The ^{13}C NMR shifts also indicate that amidine ligands with the smaller heterocyclic ring substituents have electron-donor ability to the Re similar to that of amidine ligands with larger rings. All of these favorable properties cited here suggest that the strategy of using heterocyclic amines to create amidine links to the *fac*- $\text{M}(\text{CO})_3^+$ core ($\text{M} = {}^{99\text{m}}\text{Tc}$ and ${}^{186/188}\text{Re}$ radionuclides) may be a useful conjugation method for the development of targeted radiopharmaceuticals. The feasibility of such an approach is further demonstrated by the new, convenient method of preparation of $[\text{Re}(\text{CO})_3(5,5'\text{-Me}_2\text{bipy})(\text{HNC}(\text{CH}_3)\text{N}(\text{CH}_2)_x)]\text{BF}_4$ complexes in a 1:1 water:acetonitrile mixture utilizing the *fac*- $[\text{Re}(\text{CO})_3(\text{H}_2\text{O})_3]^+$ precursor. The present study has shown that rotation of the heterocyclic ring moiety around the $\text{C}_{\text{am}}\text{-N}_4$ bond is facile. Thus, heterocyclic amines based on the azetidine ring and bearing a targeting substituent at the 3-position would readily form amidine ligands without generating an asymmetric center; consequently, a conjugated targeting derivative could be designed by using this approach. Furthermore, although further studies are needed to find a solvent system compatible with preparing radiopharmaceuticals, our work has shown that the somewhat weaker donor benzonitrile can form complexes and that treatment of the resulting complex with heterocyclic amines preferentially creates amidine links instead of

replacing the weak benzonitrile donor ligand from the complex. The approach used is applicable to other nitriles, thus expanding the number of possible R substituents that could be used to develop targeting agents.

4.5 References

- (1) Alberto, R. *Eur. J. Nucl. Med. Mol. Imaging* **2003**, *30*, 1299-1302.
- (2) Schibli, R.; Schubiger, P. A. *Eur. J. Nucl. Med. Mol. Imaging* **2002**, *29*, 1529-1542.
- (3) Banerjee, S. R.; Maresca, K. P.; Francesconi, L.; Valliant, J.; Babich, J. W.; Zubieta, J. *Nucl. Med. Biol.* **2005**, *32*, 1-20.
- (4) Alberto, R. In *Technetium-99m radiopharmaceuticals : status and trends*; International Atomic Energy Agency: Vienna, 2009, p 19-40.
- (5) Lipowska, M.; Marzilli, L. G.; Taylor, A. T. *J. Nucl. Med.* **2009**, *50*, 454-460.
- (6) Bartholomä, M.; Valliant, J.; Maresca, K. P.; Babich, J.; Zubieta, J. *Chem. Commun. (Cambridge, U.K.)* **2009**, 493-512.
- (7) He, H.; Lipowska, M.; Xu, X.; Taylor, A. T.; Marzilli, L. G. *Inorg. Chem.* **2007**, *46*, 3385-3394.
- (8) He, H. Y.; Lipowska, M.; Christoforou, A. M.; Marzilli, L. G.; Taylor, A. T. *Nucl. Med. Biol.* **2007**, *34*, 709-716.
- (9) He, H.; Lipowska, M.; Xu, X.; Taylor, A. T.; Carlone, M.; Marzilli, L. G. *Inorg. Chem.* **2005**, *44*, 5437-5446.
- (10) Schibli, R.; Schwarzbach, R.; Alberto, R.; Ortner, K.; Schmalte, H.; Dumas, C.; Egli, A.; Schubiger, P. A. *Bioconjugate Chem.* **2002**, *13*, 750-756.
- (11) Lazarova, N.; Jamesa, S.; Babich, J.; Zubieta, J. *Inorg. Chem. Commun.* **2004**, *7*, 1023-1026.
- (12) Park, S. H.; Seifert, S.; Pietzsch, H. J. *Bioconjugate Chem.* **2006**, *17*, 223-225.
- (13) Alberto, R.; Ortner, K.; Wheatly, N.; Schibli, R.; Schubiger, A. P. *J. Am. Chem. Soc.* **2001**, *123*, 3135-3136.
- (14) Alberto, R.; Schibli, R.; Egli, A.; Schubiger, A. P.; Abram, U.; Kaden, T. A. *J. Am. Chem. Soc.* **1998**, *120*, 7987-7988.
- (15) Egli, A.; Hegetschweiler, K.; Alberto, R.; Abram, U.; Schibli, R.; Hedinger, R.; Gramlich, V.; Kissner, R.; Schubiger, P. A. *Organometallics* **1997**, *16*, 1833-1840.

- (16) Perera, T.; Marzilli, P. A.; Fronczek, F. R.; Marzilli, L. G. *Inorg. Chem.* **2010**, *49*, 2123-2131.
- (17) Perera, T.; Abhayawardhana, P.; Fronczek, F. R.; Marzilli, P. A.; Marzilli, L. G. *Eur. J. Inorg. Chem.* **2012**, 616-627.
- (18) Perera, T.; Fronczek, F. R.; Marzilli, P. A.; Marzilli, L. G. *Inorg. Chem.* **2010**, *49*, 7035-7045.
- (19) Abhayawardhana, P.; Marzilli, P. A.; Perera, T.; Fronczek, F. R.; Marzilli, L. G. *Inorg. Chem.* **2012**, *51*, 7271-7283.
- (20) Lewis, N. A.; Marzilli, P. A.; Fronczek, F. R.; Marzilli, L. G. *Inorg. Chem.* **2014**, *53* 11096-11107.
- (21) Schmidt, S. P.; Trogler, W. C.; Basolo, F. *Inorg. Synth.* **1990**, *28*, 160-165.
- (22) Edwards, D. A.; Marshalsea, J. *J. Organomet. Chem.* **1977**, *131*, 73-91.
- (23) Sheldrick, G. M. *SHELXL97, Program for Crystal Structure Solution and Refinement*, University of Gottingen: Gottingen, Germany, 1997.
- (24) Sheldrick, G. M. *Acta Crystallogr., Sect. A* **2008**, *A64*, 112-122.
- (25) Allen, F. H.; Kennard, O.; Watson, D. G.; Brammer, L.; Orpen, A. G.; Taylor, R. *J. Chem. Soc. Perkin Trans. 2* **1987**, S1-S19.
- (26) Alessio, E.; Hansen, L.; Iwamoto, M.; Marzilli, L. G. *J. Am. Chem. Soc.* **1996**, *118*, 7593-7600.

CHAPTER 5

CONCLUSIONS

In general, this dissertation research contributes toward the understanding of conjugation of the *fac*-[Re(CO)₃]⁺ core to make complexes of potential radiopharmaceutical utility. New *fac*-[Re(CO)₃L]⁺ complexes demonstrating two new approaches of possible bioconjugation of the *fac*-[Re(CO)₃]⁺ core via a tridentate sulfonamide ligand and a monodentate amidine ligand are studied in detail by ¹H NMR spectroscopy. The new complexes assist in exploring the chemistry of linking the *fac*-[Re(CO)₃]⁺ core.

The new conjugation approach presented through the synthesis of novel *N*(SO₂R)dien ligands and their Re complexes aids in achieving the goal of identify a robust, hydrophilic, and flexible chelate framework. Moreover, these *N*(SO₂R)dien ligands possess the ability of anchoring the *fac*-[Re(CO)₃]⁺ core with one sulfonamide nitrogen-to-metal bond having a normal length.

The chemistry related to the *fac*-[Re(CO)₃(L)(amidine)]⁺ complexes discovered in this work holds promise as providing suitable guidelines for preparing isomerically pure conjugates of *fac*-[M(CO)₃L]⁺ (M = ^{99m}Tc, ^{186/188}Re) radiopharmaceutical agents. In contrast to the formation of multiple isomers by previously reported *fac*-[Re(CO)₃(5,5'-Me₂bipy)(HNC(CH₃)NHR)]⁺ amidine complexes, formation of a single isomer of the *fac*-[Re(CO)₃(Me₂bipy)(HNC(CH₃)N(CH₂)₂Y)]BF₄ complexes was achieved by utilizing C₂-symmetrical, saturated, heterocyclic secondary amines. The reason for the instability of other isomers is undoubtedly attributable to the unfavorable steric clashes between the equatorial ligands and the bulky the axial amidine ligand. The amidine formation reaction in organic

solvents could be made faster by replacing the methyl group of the amidine ligand with a phenyl group or by using a smaller heterocyclic amine.

The new method introduced in this work to synthesize fac -[Re(CO)₃(L)(amidine)]⁺ complexes utilizes a fewer number of steps making it faster and employs the fac -[Re(CO)₃(H₂O)₃]⁺ precursor in partially aqueous solvent conditions. This faster method and use of the fac -[Re(CO)₃(H₂O)₃]⁺ precursor, which more closely resembles the ^{99m}Tc precursor needed for the biomedical usage of radiopharmaceutical complexes, make the new amidine synthetic approach more applicable than the previous method to clinical studies. Utilization of this new synthetic strategy with smaller heterocyclic amines further reduced reaction times needed for amidine ligand formation, increasing the likely utility for the biomedical use of the new approach.

APPENDIX A

SUPPLEMENTARY MATERIAL FOR CHAPTER 2

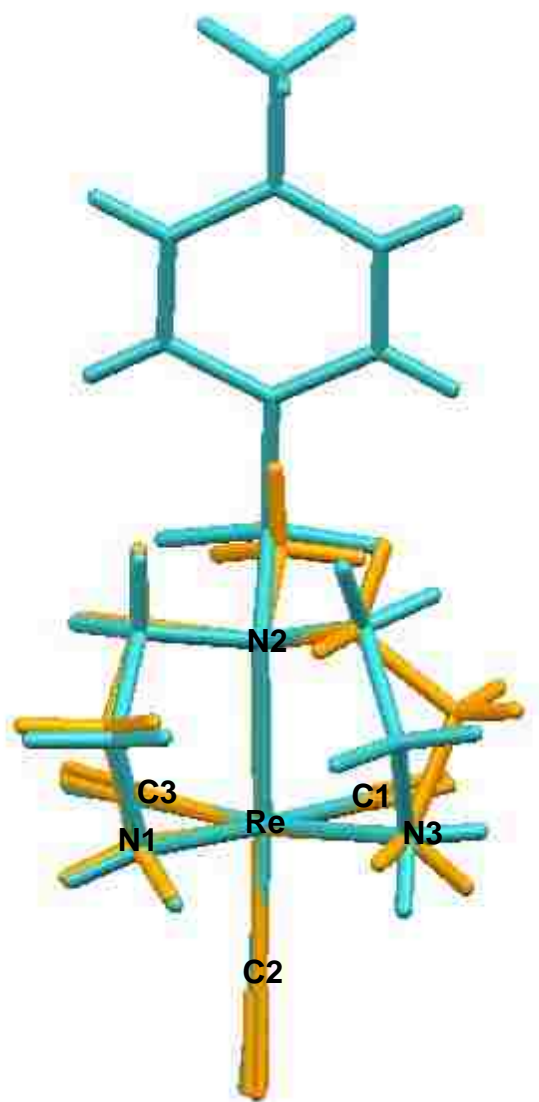


Figure A.1. Overlay of Re, C1, C2, and C3 atoms (C atoms of the carbonyl groups) of $[\text{Re}(\text{CO})_3(\text{N}(\text{SO}_2\text{tol})\text{dien})]\text{PF}_6$ (6) (blue) and $[\text{Re}(\text{CO})_3(\text{N}(\text{Me})\text{dien})]\text{PF}_6$ ⁴⁹ (yellow).

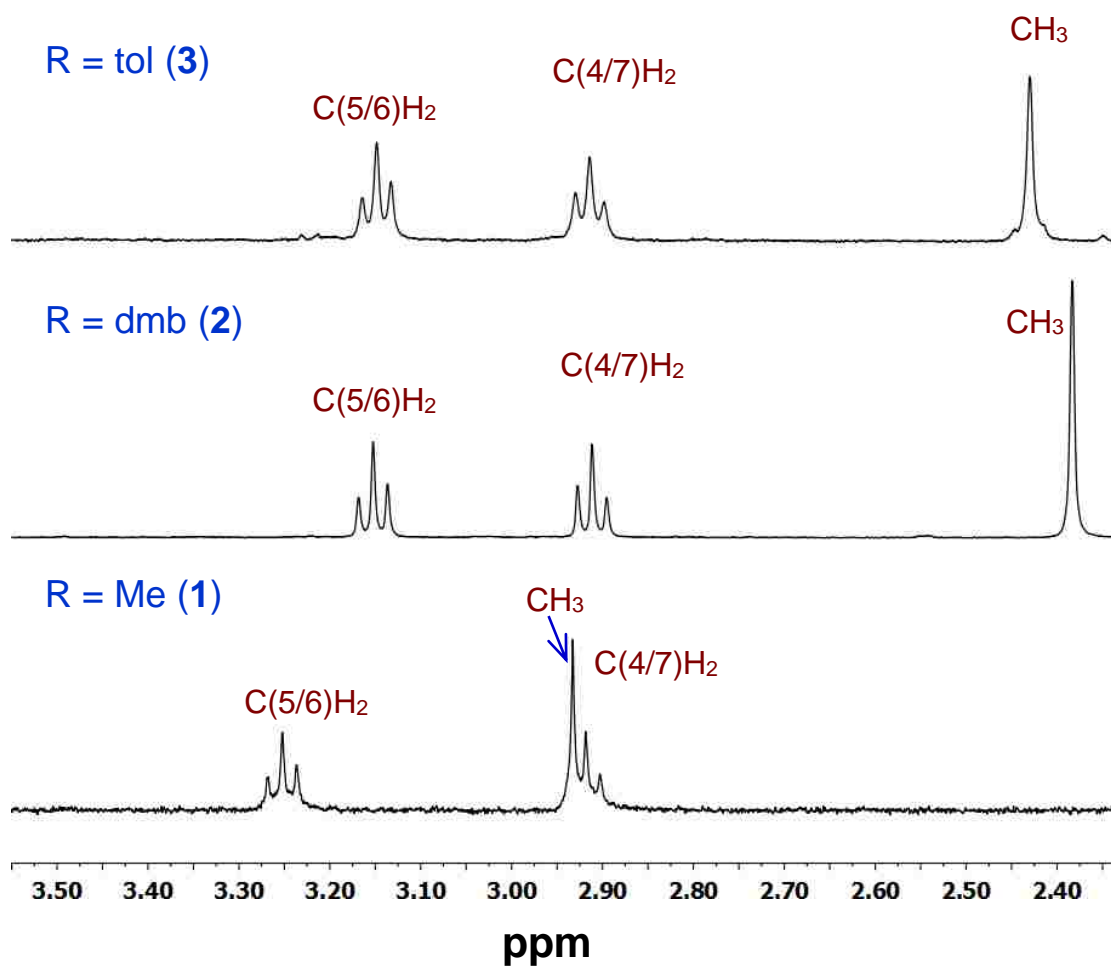


Figure A.1. Overlay of Re, C1, C2, and C3 atoms (C atoms of the carbonyl groups) of $[\text{Re}(\text{CO})_3(\text{N}(\text{SO}_2\text{tol})\text{dien})]\text{PF}_6$ (6) (*blue*) and $[\text{Re}(\text{CO})_3(\text{N}(\text{Me})\text{dien})]\text{PF}_6$ ⁴⁹ (*yellow*).

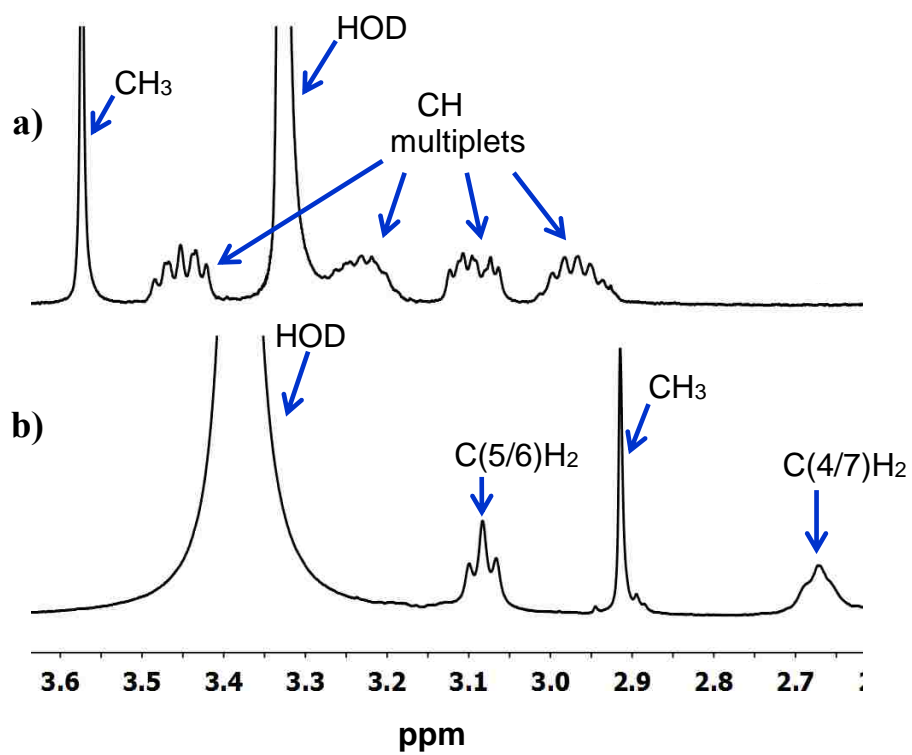


Figure A.2. Aliphatic region of the ¹H NMR spectra of *N*(SO₂R)dien ligands (1–3) in CDCl₃ at 25 °C.

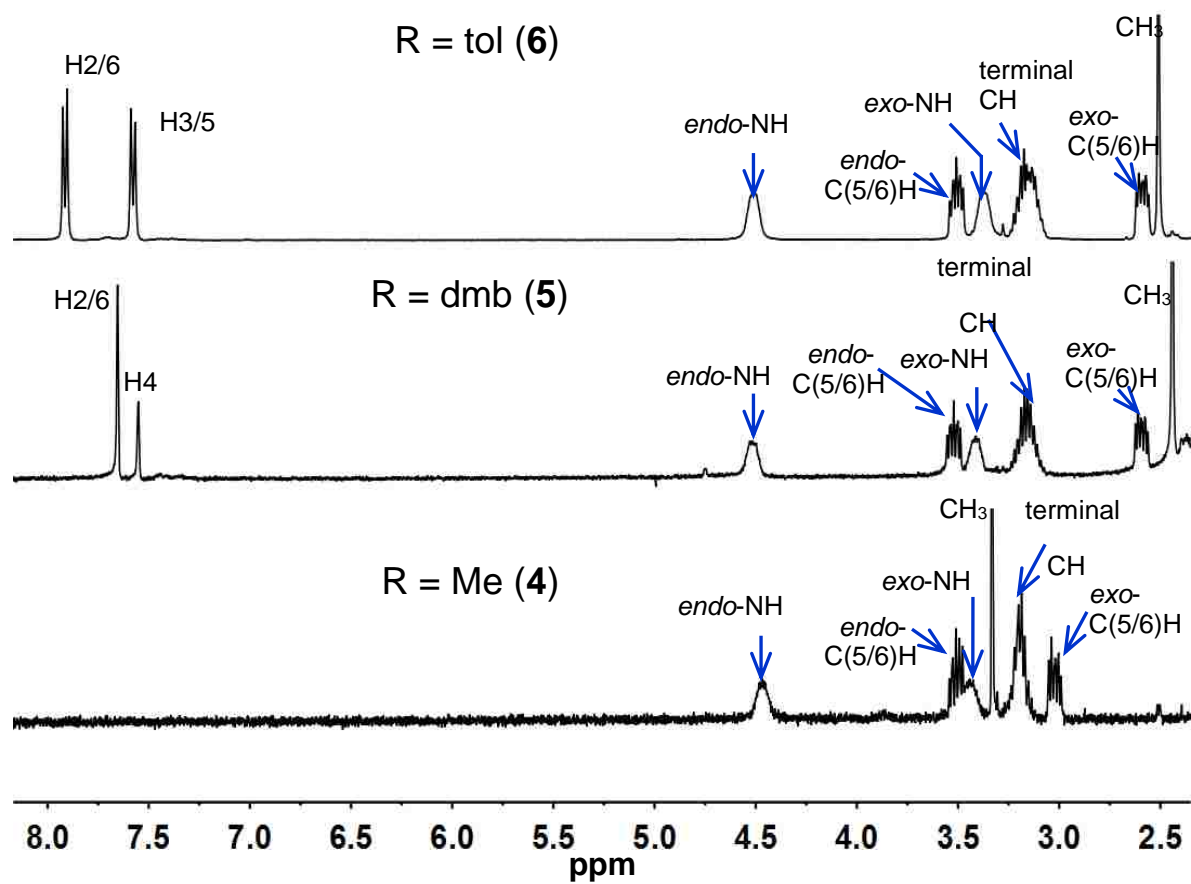


Figure A.4. ^1H NMR spectra of $[\text{Re}(\text{CO})_3(\text{N}(\text{SO}_2\text{R})\text{dien})]\text{PF}_6$ complexes (4–6) in acetonitrile- d_3 at 25 $^\circ\text{C}$.

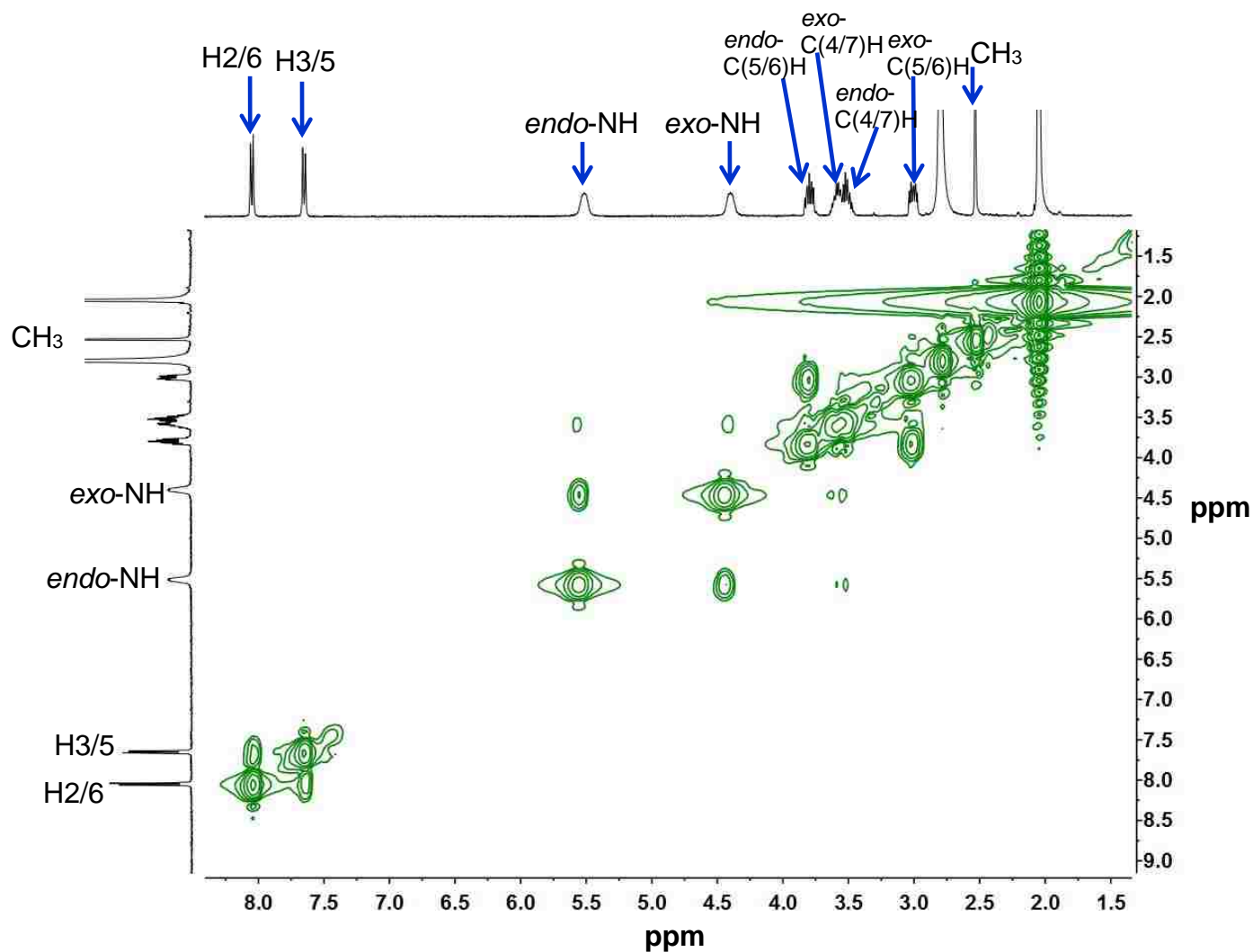


Figure A.5. COSY spectrum of $[\text{Re}(\text{CO})_3(\text{N}(\text{SO}_2\text{tol})\text{dien})]\text{PF}_6$ (**6**) in acetone- d_6 at 25 °C. The NH signals have weak COSY cross-peaks to multiplets at 3.55 ppm and 3.52 ppm, indicating that these are the two C(4/7)H₂ multiplets (C4/7 is the carbon attached to the terminal amines). The CH signals are connected by a strong COSY cross-peak, further confirming that the protons are attached to the same methylene carbon atom. The other two multiplets (for C(5/6)H₂) are connected by a COSY cross-peak, as expected. In the aromatic region, the tosyl H2/6 doublet at 8.05 ppm has a COSY cross-peak to the doublet at 7.65 ppm, unambiguously assigning it as the tosyl H3/5 signal.

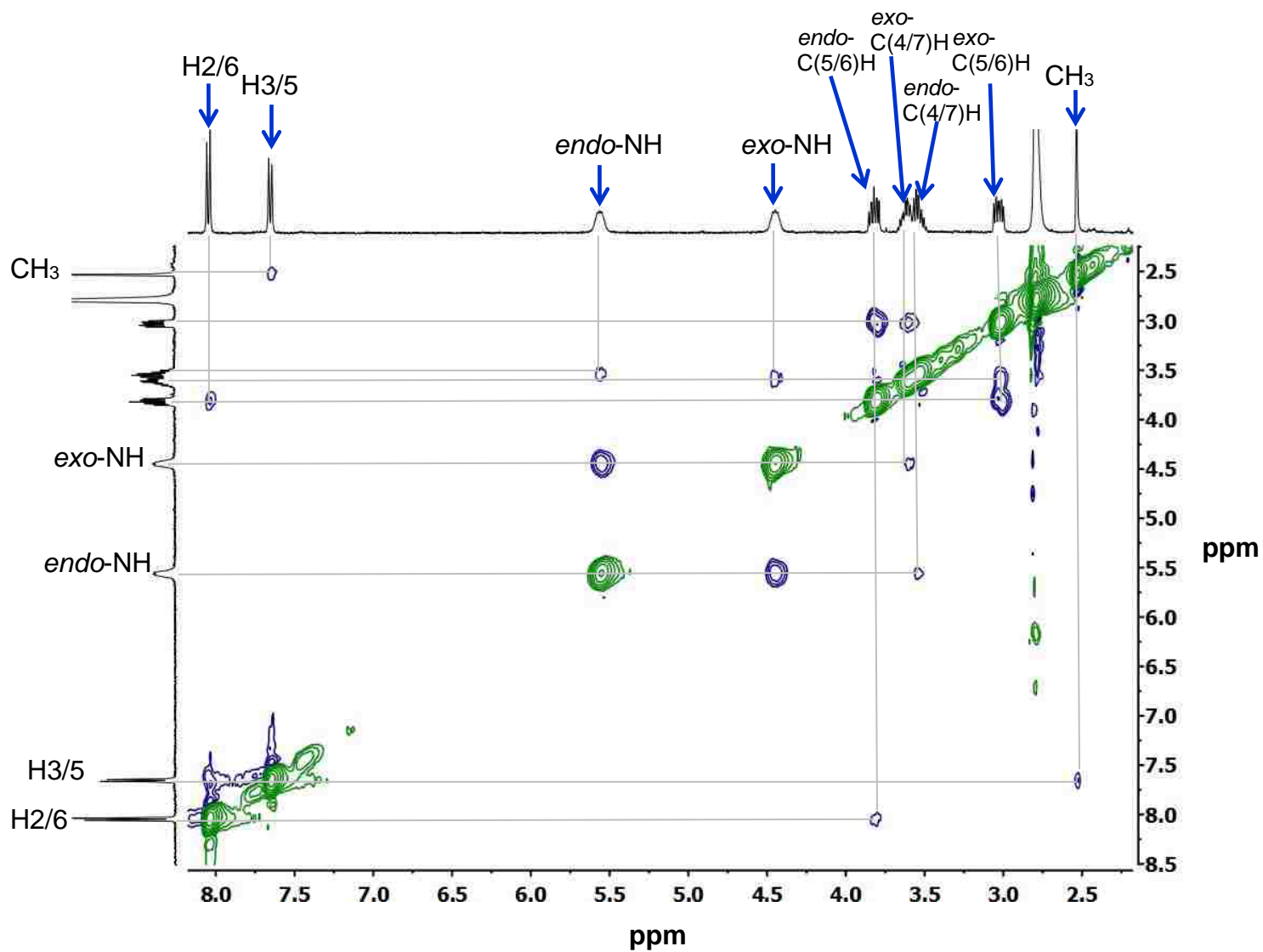


Figure A.6. ^1H - ^1H ROESY spectrum of $[\text{Re}(\text{CO})_3(\text{N}(\text{SO}_2\text{tol})\text{dien})]\text{PF}_6$ (6) in acetone- d_6 at 25 °C.

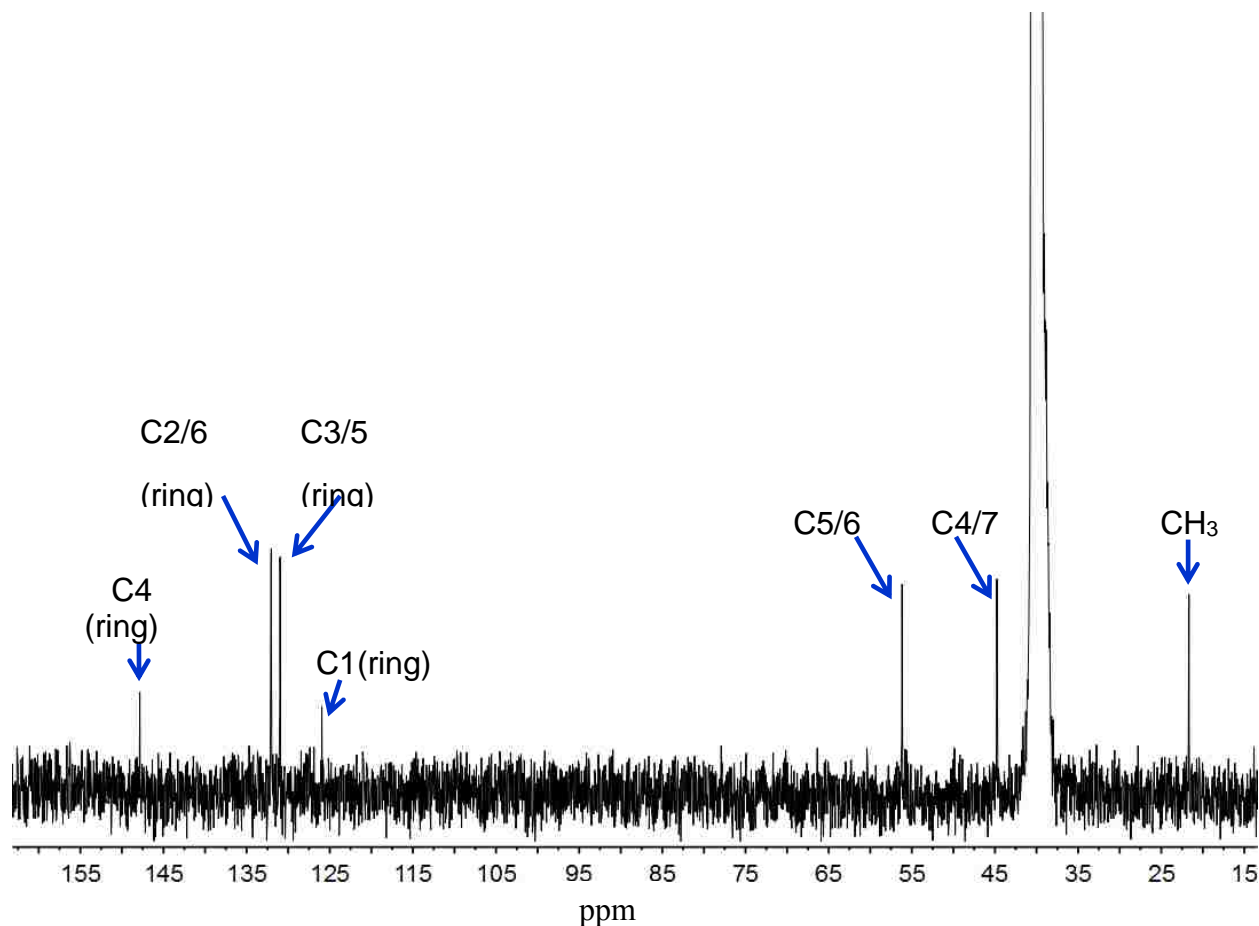


Figure A.7. ^{13}C NMR spectrum of $[\text{Re}(\text{CO})_3(\text{N}(\text{SO}_2\text{tol})\text{dien})]\text{PF}_6$ (**6**) in acetone- d_6 at 25 °C.

Assignment of ^{13}C NMR Signals of Complex **6 in Acetone- d_6 .** The seven ^{13}C NMR signals of $[\text{Re}(\text{CO})_3(\text{N}(\text{SO}_2\text{tol})\text{dien})]\text{PF}_6$ (**6**) shown in Figure S7 were assigned by considering HMBC (Figure S8) and ^1H - ^{13}C HSQC (Figure S9) spectral data. The HSQC cross-peak from the ^1H NMR CH_3 singlet (2.53 ppm) to the ^{13}C signal at 21.74 ppm assigns this signal beyond doubt to the methyl carbon of the tosyl ring. The HSQC spectrum of **6** also has two intense cross-peaks in the aromatic region involving the two aromatic ^1H NMR doublets (8.05/132.70 ppm and 7.65/131.59 ppm). These two cross-peaks thus arise from H2/6–C2/6 (aromatic ring) and H3/5–C3/5 (aromatic ring) coupling, respectively. The ^{13}C NMR signals at 148.88 ppm and 127.05

ppm lack HSQC cross-peaks, but do have HMBC cross-peaks (Figure S8) to the H2/6 and H3/5 doublets, respectively. The most downfield ^{13}C NMR signal (148.88 ppm) also shows an HMBC cross-peak to the tosyl CH_3 singlet at 2.53 ppm, allowing the assignment of the carbon signal to C4 in the tosyl ring. The remaining ^{13}C NMR signal at 127.05 ppm, which has an HMBC cross-peak to only the H3/5 doublet, is thus attributable to the tosyl ring quaternary C1 atom. Both multiplets of each methylene group have a strong HSQC cross-peak, allowing us to assign the ^{13}C NMR signal at 46.00 ppm to C4/7 and the signal at 56.94 ppm to C5/6.

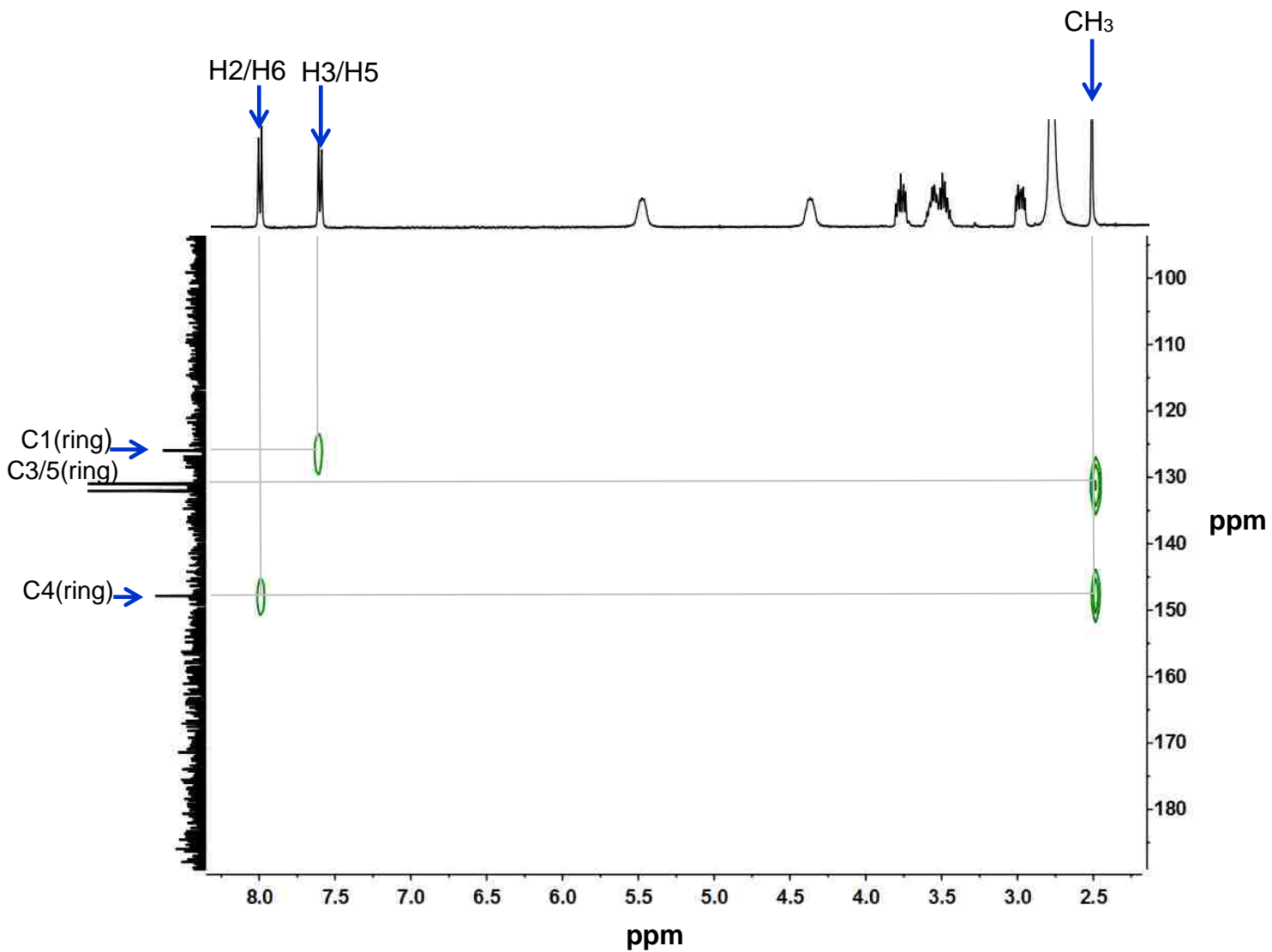


Figure A.8. Aromatic region of the HMBC spectrum of $[\text{Re}(\text{CO})_3(\text{N}(\text{SO}_2\text{tol})\text{dien})]\text{PF}_6$ (**6**) in acetone- d_6 at 25 °C.

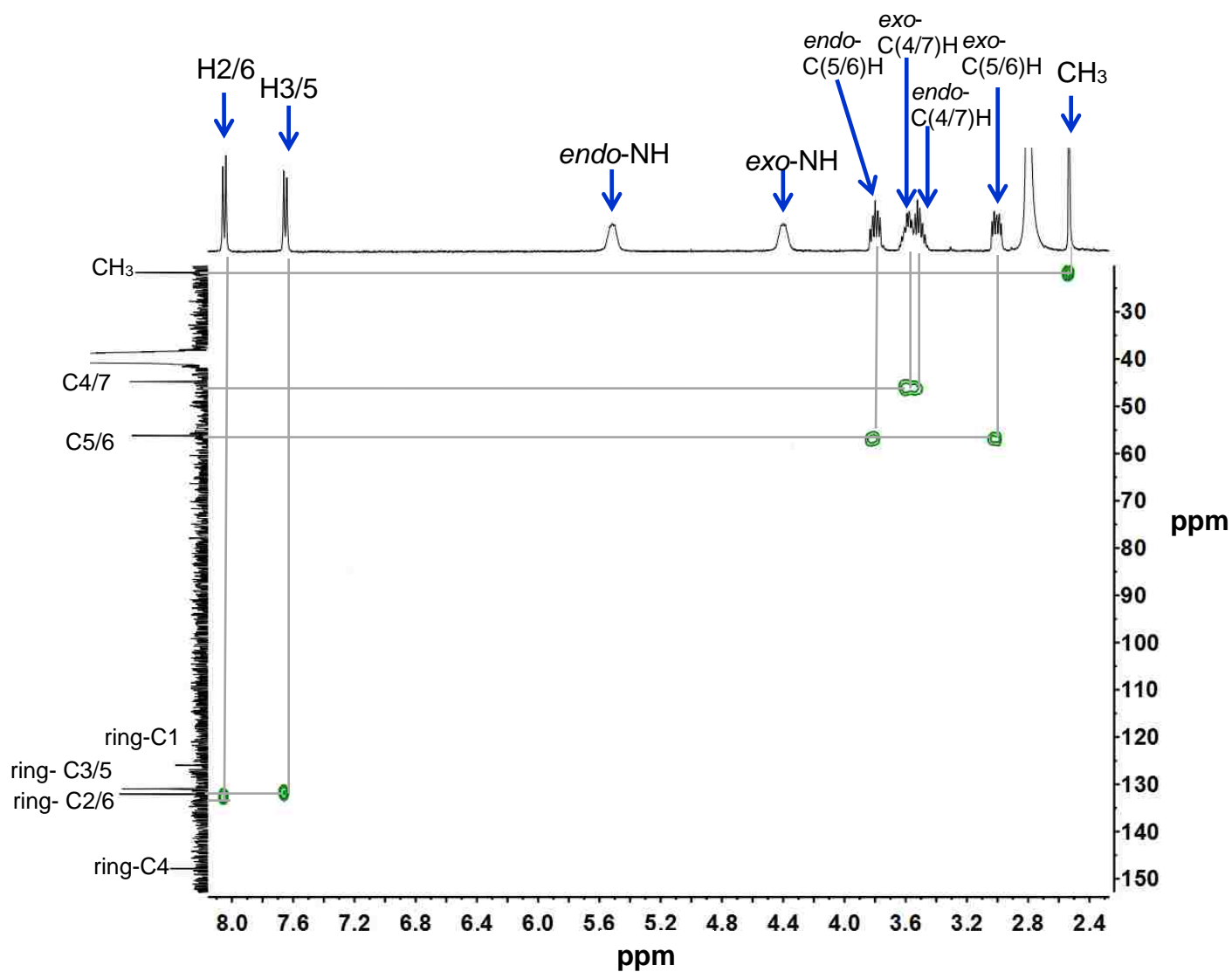


Figure A.9. HSQC spectrum of $[\text{Re}(\text{CO})_3(\text{N}(\text{SO}_2\text{tol})\text{dien})]\text{PF}_6$ (6) in acetone- d_6 at 25 °C.

Table A.1. Comparison of ^{13}C NMR Shifts (ppm) of $N(\text{SO}_2\text{R})\text{dien}$ Ligands and $[\text{Re}(\text{CO})_3(N(\text{SO}_2\text{R})\text{dien})]\text{PF}_6$ Complexes in Acetonitrile- d_3 at 25 °C

signal	$(N(\text{SO}_2\text{Me})\text{dien})$ (1)	$[\text{Re}(\text{CO})_3(N(\text{SO}_2\text{Me})\text{dien})]$ PF_6 (4)	$(N(\text{SO}_2\text{tol})\text{dien})$ (3)	$[\text{Re}(\text{CO})_3(N(\text{SO}_2\text{tol})\text{dien})]\text{PF}_6$ (6)
C4			145.04	149.40
ring C3/5			128.64	131.62
ring C2/6			130.71	132.67
C1			136.79	126.60
C5/6	52.65	56.29	51.50	56.76
C4/7	41.91	45.61	41.10	45.56
CH_3	37.87	33.02	21.03	21.87

The ^1H NMR signal assignments for the two triplets of the free ligands were confirmed by using values predicted by ChemBioDraw Ultra 12.0. ^{13}C NMR signals of the free $N(\text{SO}_2\text{tol})\text{dien}$ and $N(\text{SO}_2\text{Me})\text{dien}$ ligands (1 and 3, in acetonitrile- d_3) were assigned unambiguously (Experimental Section) by using ^1H - ^{13}C HSQC and HMBC cross peaks and were used for the shift comparison with the ^{13}C NMR signals of $[\text{Re}(\text{CO})_3(N(\text{SO}_2\text{Me})\text{dien})]\text{PF}_6$ (4) and $[\text{Re}(\text{CO})_3(N(\text{SO}_2\text{tol})\text{dien})]\text{PF}_6$ (6), for which the signals were also completely assigned by ^1H - ^{13}C HSQC and HMBC spectral data (in acetonitrile- d_3).

APPENDIX B

SUPPLEMENTARY MATERIAL FOR CHAPTER 3

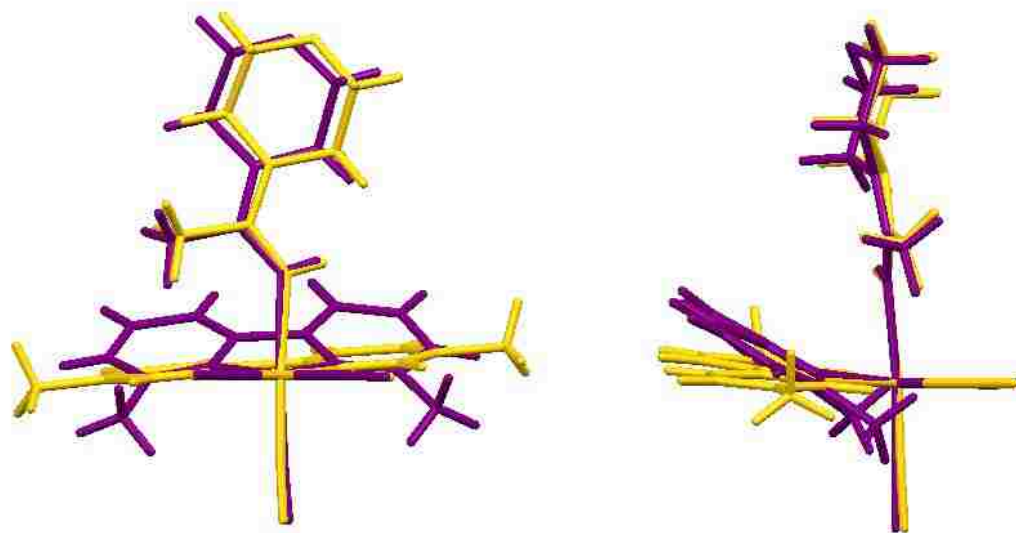


Figure B.1. Overlay of Re, O1, O2 and O3 atoms of carbonyl ligands of $[\text{Re}(\text{CO})_3(5,5'\text{-Me}_2\text{bipy})(\text{HNC}(\text{CH}_3)\text{N}(\text{CH}_2\text{CH}_2)_2\text{O})]\text{BF}_4$ (7) (gold) and $[\text{Re}(\text{CO})_3(6,6'\text{-Me}_2\text{bipy})(\text{HNC}(\text{CH}_3)\text{N}(\text{CH}_2\text{CH}_2)_2\text{O})]\text{BF}_4$ (12) (purple) depicted with the C13–Re–C14 equatorial plane perpendicular to the plane of the paper.

Table B.1. Selected Non-Bonded Distances (Å) for Complexes Having the General Formula, $[\text{Re}(\text{CO})_3(\text{L})(\text{HNC}(\text{CH}_3)\text{N}(\text{CH}_2\text{CH}_2)_2\text{Y})]\text{BF}_4$

bond distances	L = 5,5'-Me ₂ bipy	L = 6,6'-Me ₂ bipy	L = 5,5'-Me ₂ bipy	L = 6,6'-Me ₂ bipy
	Y = CH ₂	Y = CH ₂	Y = NH	Y = NH
N3 -N1	2.800 (4)	2.840 (3)	2.797 (3)	2.807 (4)
N3 -N2	2.987 (4)	2.909 (3)	2.983 (3)	2.935 (4)
N3- C1	3.517 (5)	3.867 (3)	3.528 (3)	3.748 (4)
N3-C10	3.859 (5)	3.913 (3)	3.871 (4)	3.938 (4)
N3- C4	4.541 (5)	4.146 (3)	4.452 (4)	4.057 (5)
N3-C7	4.689 (5)	3.848 (3)	4.667 (4)	4.171 (4)
N3-C3	5.030 (5)	4.935 (3)	4.954 (4)	4.764 (5)
N3-C8	5.288 (5)	4.606 (3)	5.293 (4)	4.935 (4)

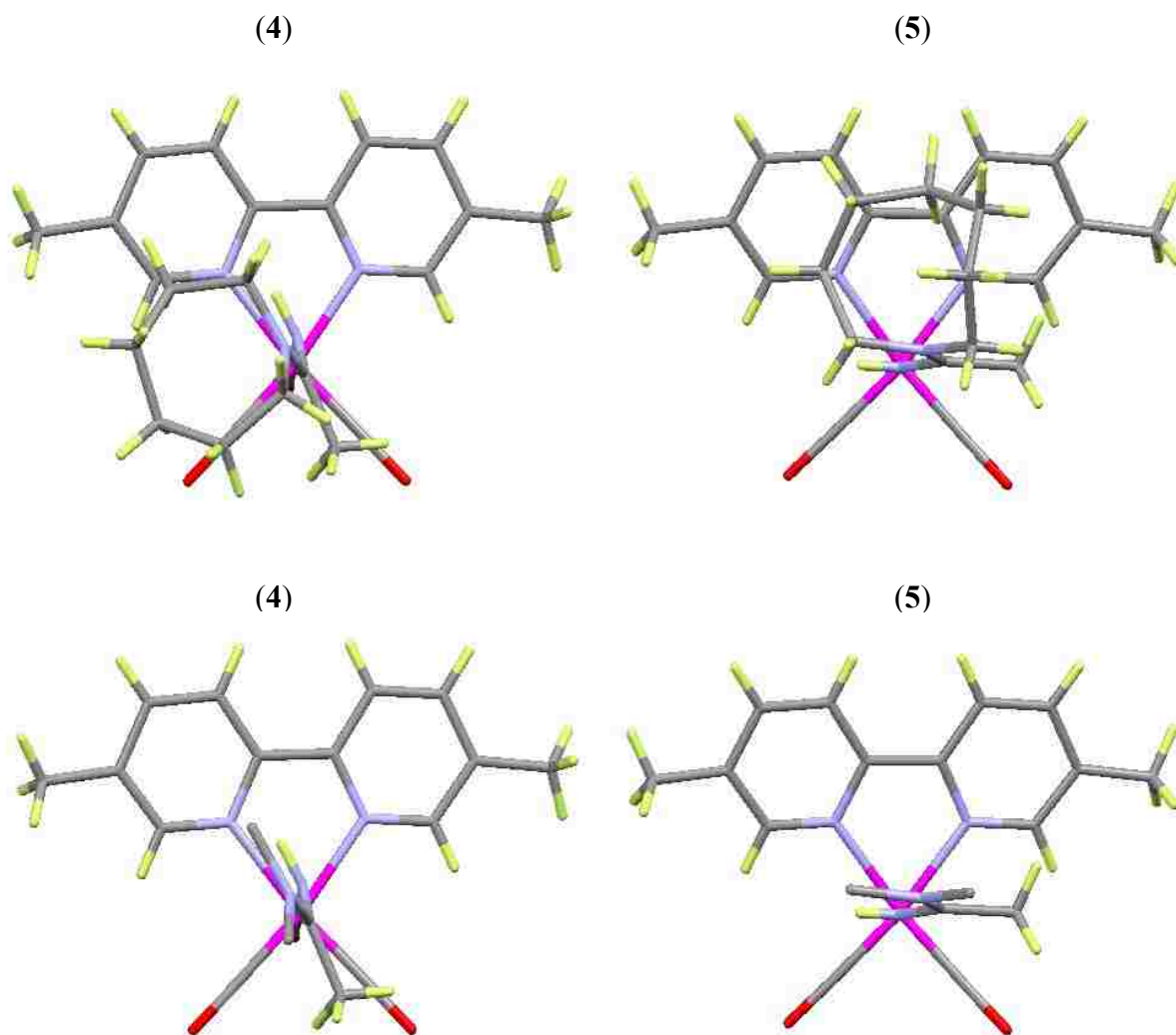


Figure B.2. Structures of $[\text{Re}(\text{CO})_3(5,5'\text{-Me}_2\text{bipy})(\text{HNC}(\text{CH}_3)\text{N}(\text{CH}_2\text{CH}_2)_2(\text{CH}_2)_2)]\text{BF}_4$ (4) and $[\text{Re}(\text{CO})_3(5,5'\text{-Me}_2\text{bipy})(\text{HNC}(\text{CH}_3)\text{N}(\text{CH}_2\text{CH}_2)_2(\text{CH}_2)_3)]\text{BF}_4$ (5) showing the orientation of the amidine ligand with the aromatic rings in the plane of the paper and amidine ligand projected toward the viewer. In the bottom two structures, selected atoms have been omitted in order to show the amidine group more clearly. All complexes in this work, except for 4, have the plane of the amidine group bisecting the N–Re–C angles in the equatorial plane as shown at the bottom right.

APPENDIX C

SUPPLEMENTARY MATERIAL FOR CHAPTER 4

Table C.1. ¹H NMR Shifts (ppm) for [Re(CO)₃(L)(HNC(CH₃)N(CH₂)_x)]BF₄ (CD₃CN, 25 °C)

signal / x	3	4	5 ¹	6 ¹	7 ¹	3	4	5 ¹	6 ¹	7 ¹
	L = 5,5'-Me ₂ bipy					L = 6,6'-Me ₂ bipy				
H6/6'	8.82	8.83	8.85	8.87	8.87					
H5/5'						7.61	7.61	7.62	7.61	7.63
H4/4'	8.04	8.04	8.04	8.05	8.04	8.06	8.07	8.06	8.06	8.07
H3/3'	8.26	8.28	8.26	8.26	8.27	8.19	8.19	8.19	8.19	8.19
L-CH ₃	2.48	2.48	2.48	2.48	2.48	3.03	3.05	3.06	3.07	3.07
N3H	4.15	4.21	4.78	4.52	4.49	4.59	4.62	5.14	4.90	4.82
C _{am} -CH ₃	1.90	2.13	2.10	2.10	2.12	1.49	1.71	1.60	1.62	1.66
N-CH ₂ <i>endo</i>	3.99	3.30	3.01 br	3.30	3.25	3.95	3.25	3.03 br	3.26	3.23
N-CH ₂ <i>exo</i>	3.45	2.65	3.01 br	2.96	3.05	3.50	2.71	3.03 br	3.04	3.16
CH ₂ signals	2.07	1.75	1.48	1.46	1.50	2.08	1.77	1.53	1.44	1.49
			1.28	1.31	1.39			1.29	1.38	1.42
				1.15	1.18				1.32	1.32
				0.96	0.96				1.11	1.21
					0.71					0.91

Table C.2. Selected Bond Distances and Angles for [Re(CO)₃(5,5'-Me₂bipy)(HNC(CH₃)N(CH₂)₂Y)]BF₄ Complexes

Y = complex	CH ₂ 1	(CH ₂) ₂ 3	(CH ₂) ₃ ¹	(CH ₂) ₄ ¹	(CH ₂) ₅ ¹	(CH ₂) ₂ NH ¹	(CH ₂) ₂ O ¹
bond distances (Å)							
Re–N1	2.178(2)	2.176(1)	2.168(3)	2.172(3)	2.1691(18)	2.177(2)	2.177(2)
Re–N2	2.172(2)	2.186(1)	2.186(3)	2.173(3)	2.1823(18)	2.190(2)	2.194(2)
Re–N3	2.184(3)	2.186(1)	2.178(3)	2.179(3)	2.1806(18)	2.179(2)	2.178(2)
N3–C16	1.305(4)	1.311(1)	1.306(4)	1.310(5)	1.308(3)	1.300(4)	1.304(3)
N4–C16	1.331(4)	1.338(2)	1.346(5)	1.344(5)	1.346(3)	1.354(4)	1.359(3)
bond angles (deg)							
N1–Re–N2	75.28(9)	74.85(3)	75.06(11)	74.58(11)	74.82(6)	75.08(8)	75.16(8)
N1–Re–N3	80.13(9)	80.57(4)	80.23(11)	83.44(11)	87.21(6)	79.90(9)	78.78(8)
N2–Re–N3	82.84(9)	85.19(4)	86.41(11)	79.02(11)	79.34(6)	86.11(9)	86.30(8)
Re–N3–H3N	108(3)	111(1)	113(3)	111(3)	106(2)	110(2)	110(2)
Re–N3–C16	133.6(2)	135.44(8)	137.4(2)	135.6(3)	136.82(15)	136.5(2)	137.03(18)
C16–N3–H3N	116(3)	114(1)	110(3)	110(3)	116(2)	114(2)	113(2)
N3–C16–N4	121.4(3)	122.8(1)	123.6(3)	122.9(3)	122.47(19)	123.3(3)	122.5(2)
N3–C16–C17	123.2(3)	120.3(1)	118.6(3)	118.5(3)	119.58(19)	119.2(3)	119.9(2)
N4–C16–C17	115.4(3)	116.9(1)	117.8(3)	118.7(3)	117.95(19)	117.4(2)	117.7(2)
C16–N4–C18	131.5(3)	125.1(1)	122.2(3)	121.2(3)	123.86(18)	121.8(2)	121.4(2)
C16–N4–C(n) ^a	129.8(3) ^b	122.9(1) ^c	120.3(3) ^d	122.7(3) ^e	120.44(18) ^f	120.7(2) ^c	120.1(2) ^c
C18–N4–C(n) ^a	94.4(2) ^b	111.6(1) ^c	113.3(3) ^d	114.3(3) ^e	115.7(2) ^f	112.6(2) ^c	112.3(2) ^c

^an varies in number according to the R group. ^bn = 20. ^cn = 21. ^dn = 22. ^en = 23. ^fn = 24.

Table C.3. Selected Bond Distances and Angles for [Re(CO)₃(6,6'-Me₂bipy)(HNC(CH₃)N(CH₂)₂Y)]BF₄ Complexes

Y = complex	CH ₂ 2	(CH ₂) ₂ 4	(CH ₂) ₃ ¹	(CH ₂) ₄ ¹	(CH ₂) ₅ ¹	(CH ₂) ₂ NH ¹	(CH ₂) ₂ O ¹
bond distances (Å)							
Re–N1	2.2050(12)	2.198(2)	2.213(2)	2.203(2)	2.211(2)	2.212(3)	2.2051(19)
Re–N2	2.1990(12)	2.200(2)	2.1984(18)	2.194(2)	2.211(2)	2.202(3)	2.2086(19)
Re–N3	2.1704(11)	2.181(2)	2.193(2)	2.188(2)	2.190(2)	2.192(3)	2.1848(18)
N3–C16	1.3068(18)	1.303(3)	1.307(3)	1.309(3)	1.308(3)	1.307(4)	1.307(3)
N4–C16	1.3313(17)	1.334(3)	1.356(3)	1.350(3)	1.347(3)	1.350(4)	1.356(3)
bond angles (deg)							
N1–Re–N2	75.10(5)	74.90(9)	74.29(7)	74.60(8)	74.40(8)	75.29(11)	74.90(7)
N1–Re–N3	80.15(5)	80.14(8)	80.26(7)	82.12(8)	83.41(8)	79.19(10)	79.35(7)
N2–Re–N3	83.84(5)	85.19(8)	82.97(7)	80.44(8)	79.26(8)	83.85(10)	82.00(7)
Re–N3–H3N	111.3(16)	111(2)	110(2)	110(2)	108(2)	107(3)	109(2)
Re–N3–C16	135.47(10)	135.5(2)	136.66(16)	135.62(19)	136.74(19)	135.4(2)	137.12(15)
C16–N3–H3N	113.2(17)	113(2)	113(2)	115(2)	115(2)	115(3)	114(2)
N3–C16–N4	121.82(13)	123.0(2)	123.2(2)	122.9(2)	123.0(2)	124.2(3)	122.84(19)
N3–C16–C17	122.88(12)	120.1(2)	119.5(2)	119.8(2)	119.2(2)	118.4(3)	119.85(19)
N4–C16–C17	115.31(12)	116.9(2)	117.3(2)	117.3(2)	117.8(2)	117.3(3)	117.28(19)
C16–N4–C18	131.58(12)	124.6(2)	122.62(19)	122.4(2)	123.2(2)	124.2(3)	122.27(18)
C16–N4–C(<i>n</i>) ^a	131.78(12) ^b	123.4(2) ^c	122.93(19) ^d	121.2(2) ^e	121.0(2) ^f	123.7(3) ^e	121.29(19) ^c
C18–N4–C(<i>n</i>) ^a	95.4(1) ^b	112.0(2)	111.3(2) ^d	114.8(2) ^e	115.8(2) ^f	111.8(3) ^c	112.5(2) ^c

^a*n* varies in number according to the R group. ^b*n* = 20. ^c*n* = 21. ^d*n* = 22. ^e*n* = 23. ^f*n* = 24.

Table C.4. ^{13}C NMR Shifts (ppm, 25 °C) of the Me₂bipy Ligands in CDCl₃²

signal	5,5'-Me ₂ bipy	6,6'-Me ₂ bipy
C6/6'	149.40	157.80
C5/5'	132.90	122.90
C4/4'	137.30	136.80
C3/3'	120.10	118.00
C2/2'	153.70	155.80
L-CH ₃	18.20	24.80

Table C.5. N3H ¹H NMR Shifts (ppm, 25 °C) of [Re(CO)₃(Me₂bipy)(HNC(CH₃)N(CH₂)_x)]BF₄ Complexes vs Non-bonded Distance (d) from the N3H Atom to the Closest CH Atom of the Heterocyclic Ring Moiety

x	d (Å)	5,5'-Me ₂ bipy complexes		d (Å)	6,6'-Me ₂ bipy complexes	
		CD ₃ CN	CDCl ₃		CD ₃ CN	CDCl ₃
3	2.55	4.15	4.27	2.54	4.59	4.31
4	2.15	4.21	4.10	2.21	4.62	4.26
5 ¹	1.82	4.78	4.58	1.89	5.14	4.92
6 ¹	1.88	4.52	4.23	1.96	4.90	4.60
7 ¹	2.14	4.49	4.21	2.09	4.82	

As stated in a previous report,^{1,3} factors influencing the N3H NMR signal shift are complex and difficult to explain. Within each Me₂bipy series of [Re(CO)₃(Me₂bipy)(HNC(CH₃)N(CH₂)₃₋₇)]BF₄ for new complexes and for previously reported complexes,¹ the N3H NMR signal has a more downfield shift when the non-bonded distance from N3H to the closest H atom of the heterocyclic ring moiety is relatively short (Table S5). The most upfield N3H signals in each series were observed for complexes with the smaller heterocyclic ring moiety (3- or 4-membered rings). The general trend suggests that through-space environmental effects of spatially close ring protons may be one of the factors influencing the shift of the N3H signal.

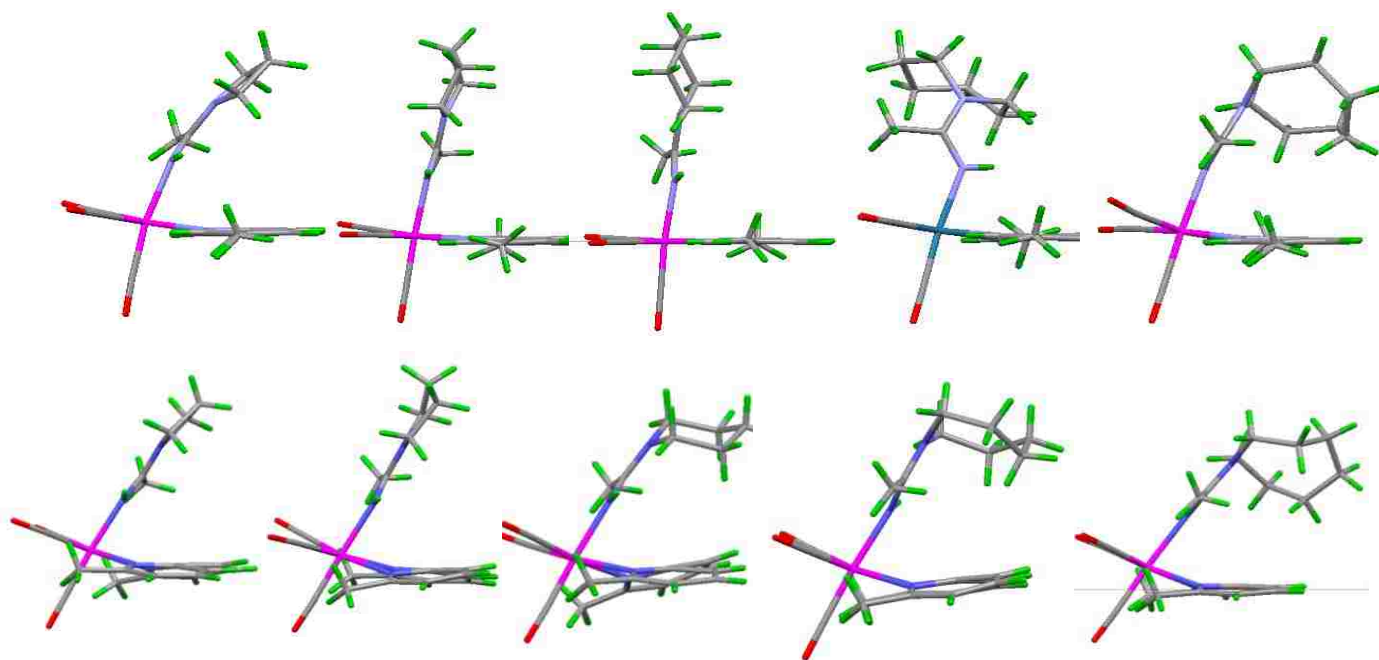


Figure C.1. As is evident from the molecular structures of $[\text{Re}(\text{CO})_3(\text{Me}_2\text{bipy})(\text{HNC}(\text{CH}_3)\text{N}(\text{CH}_2)_{3-7})]\text{BF}_4$ complexes,¹ the flexibility of the larger ring moieties appears in some cases to have allowed the large rings to lie over the equatorial Me_2bipy ligands in the solid. However, there is no evidence to support this relation of the heterocyclic rings to the Me_2bipy ligands in solution because the ^1H or ^{13}C NMR signals of the methylene groups of the ring moieties are not shifted significantly upfield in the bulkier rings in the 6,6'- Me_2bipy vs. 5,5'- Me_2bipy analogue.

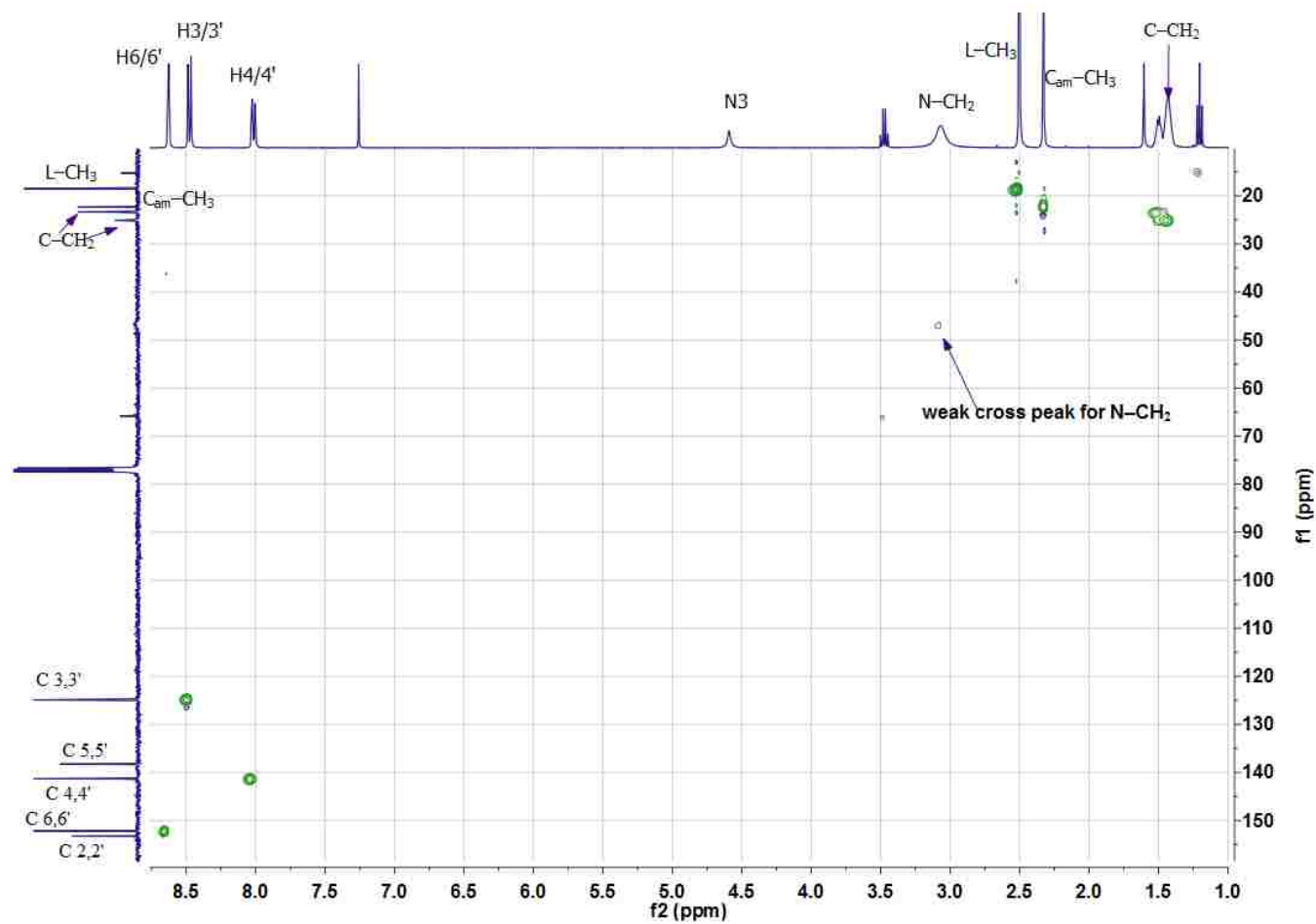


Figure C.2. HSQC spectrum (CDCl_3 , 27 °C) of $[\text{Re}(\text{CO})_3(5,5'\text{-Me}_2\text{bipy})(\text{HNC}(\text{CH}_3)\text{N}(\text{CH}_2)_5)]\text{BF}_4^1$.

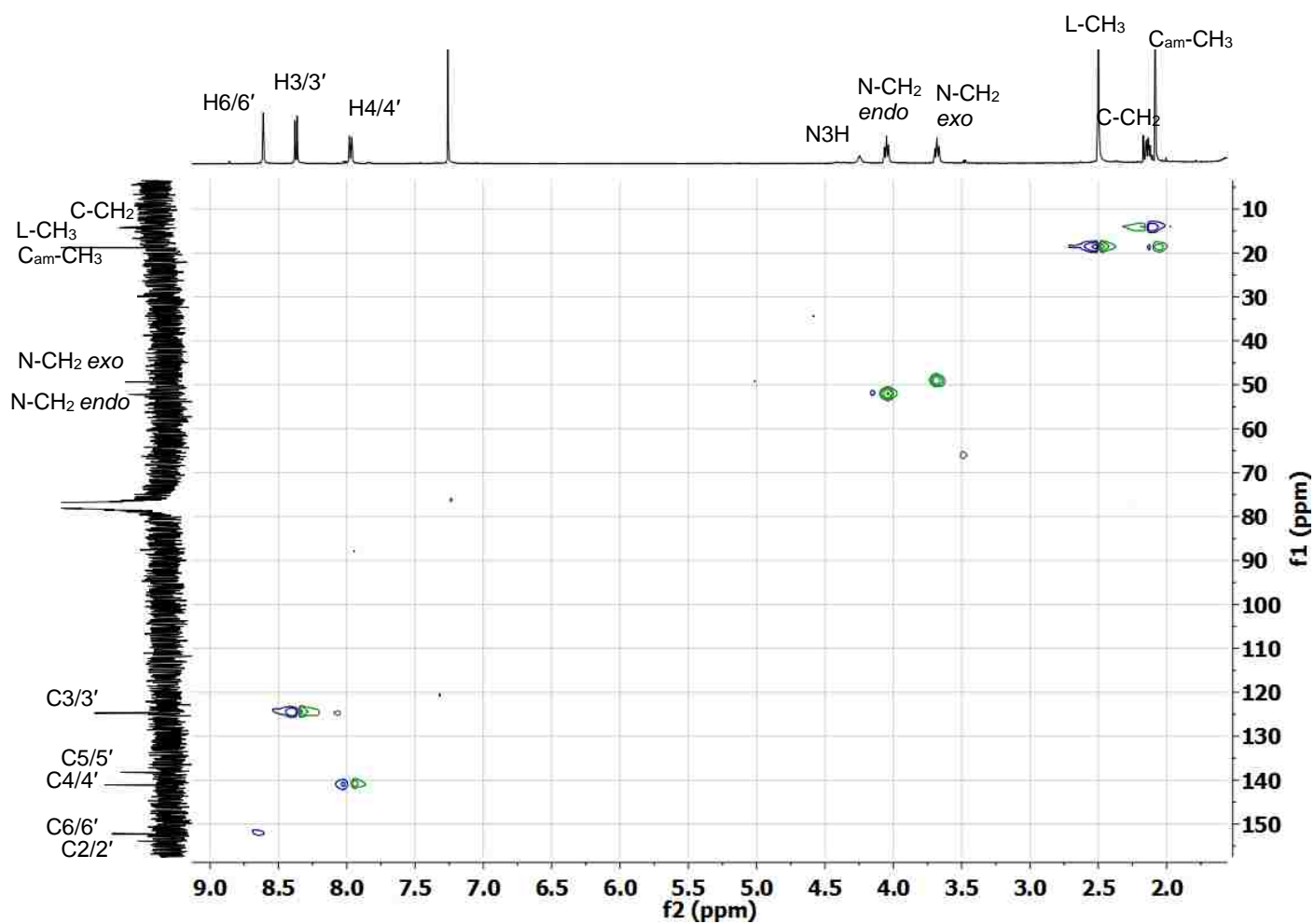


Figure C.3. HSQC spectrum (CDCl_3 , 27 °C) of $[\text{Re}(\text{CO})_3(5,5'\text{-Me}_2\text{bipy})(\text{HNC}(\text{CH}_3)\text{N}(\text{CH}_2)_3)]\text{BF}_4$ (1).

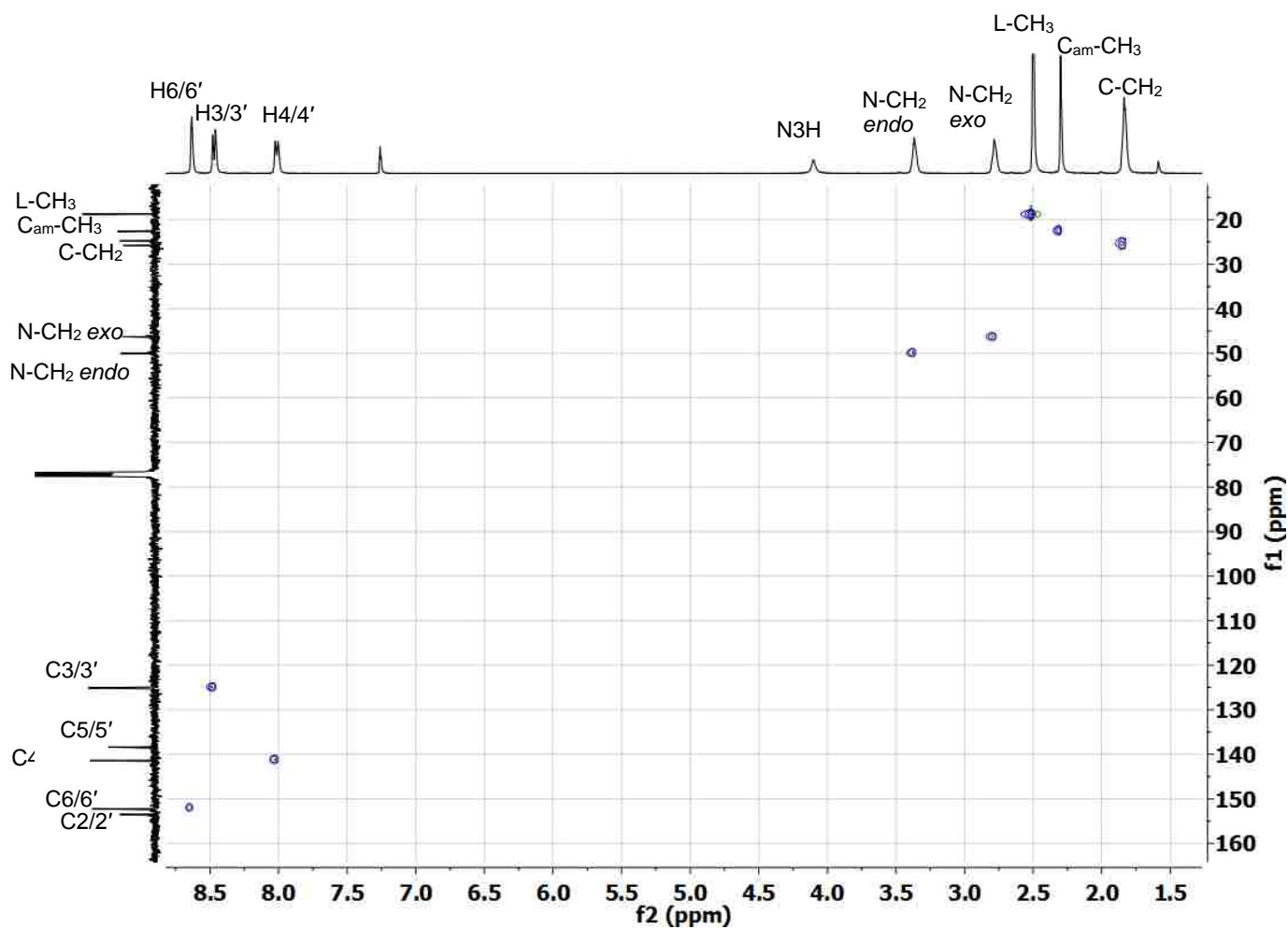


Figure C.4. HSQC spectrum (CDCl_3 , 27 $^\circ\text{C}$) of $[\text{Re}(\text{CO})_3(5,5'\text{-Me}_2\text{bipy})(\text{HNC}(\text{CH}_3)\text{N}(\text{CH}_2)_4)]\text{BF}_4$ (3).

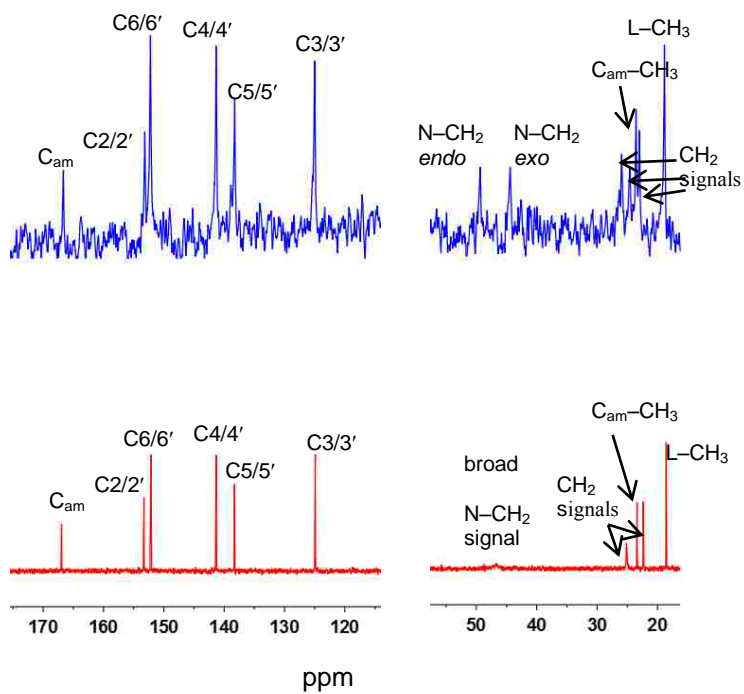





Figure C.5. ^{13}C NMR stack plots of $[\text{Re}(\text{CO})_3(5,5'\text{-Me}_2\text{bipy})(\text{HNC}(\text{CH}_3)\text{N}(\text{CH}_2)_5)]\text{BF}_4^1$ in CDCl_3 at $-13\text{ }^\circ\text{C}$ (blue) and $27\text{ }^\circ\text{C}$ (red).


Appendix C. References

- (1) Abhayawardhana, P.; Marzilli, P. A.; Perera, T.; Fronczek, F. R.; Marzilli, L. G. *Inorg. Chem.* **2012**, *51*, 7271-7283.
- (2) Perera, T.; Abhayawardhana, P.; Fronczek, F. R.; Marzilli, P. A.; Marzilli, L. G. *Eur. J. Inorg. Chem.* **2012**, 616-627.
- (3) Perera, T.; Fronczek, F. R.; Marzilli, P. A.; Marzilli, L. G. *Inorg. Chem.* **2010**, *49*, 7035-7045.

APPENDIX D

PERMISSION

HomeAccount InfoHelp

**ACS Publications**
Most Trusted. Most Cited. Most Read.

Title: Complexes Possessing Rare "Tertiary" Sulfonamide Nitrogen-to-Metal Bonds of Normal Length: fac-[Re(CO)₃(N(SO₂R)dien)]PF₆ Complexes with Hydrophilic Sulfonamide Ligands

Author: Pramuditha L. Abhayawardhana, Patricia A. Marzilli, Frank R. Fronczek, et al

Publication: Inorganic Chemistry

Publisher: American Chemical Society

Date: Jan 1, 2014

Copyright © 2014, American Chemical Society

Logged in as:
Pramuditha Abhayawardhana

[LOGOUT](#)

PERMISSION/LICENSE IS GRANTED FOR YOUR ORDER AT NO CHARGE

This type of permission/license, instead of the standard Terms & Conditions, is sent to you because no fee is being charged for your order. Please note the following:

- Permission is granted for your request in both print and electronic formats, and translations.
- If figures and/or tables were requested, they may be adapted or used in part.
- Please print this page for your records and send a copy of it to your publisher/graduate school.
- Appropriate credit for the requested material should be given as follows: "Reprinted (adapted) with permission from (COMPLETE REFERENCE CITATION). Copyright (YEAR) American Chemical Society." Insert appropriate information in place of the capitalized words.
- One-time permission is granted only for the use specified in your request. No additional uses are granted (such as derivative works or other editions). For any other uses, please submit a new request.

Title: New Monodentate Amidine
Superbasic Ligands with a Single
Configuration in fac-
[Re(CO)₃(5,5'- or 6,6'-
Me₂bipyridine)(amidine)]BF₄
Complexes

Author: Pramuditha Abhayawardhana,
Patricia A. Marzilli, Theshini
Perera, et al

Publication: Inorganic Chemistry

Publisher: American Chemical Society

Date: Jul 1, 2012

Copyright © 2012, American Chemical Society

Logged in as:
Pramuditha Abhayawardhana

[LOGOUT](#)

PERMISSION/LICENSE IS GRANTED FOR YOUR ORDER AT NO CHARGE

This type of permission/license, instead of the standard Terms & Conditions, is sent to you because no fee is being charged for your order. Please note the following:

- Permission is granted for your request in both print and electronic formats, and translations.
- If figures and/or tables were requested, they may be adapted or used in part.
- Please print this page for your records and send a copy of it to your publisher/graduate school.
- Appropriate credit for the requested material should be given as follows: "Reprinted (adapted) with permission from (COMPLETE REFERENCE CITATION). Copyright (YEAR) American Chemical Society." Insert appropriate information in place of the capitalized words.
- One-time permission is granted only for the use specified in your request. No additional uses are granted (such as derivative works or other editions). For any other uses, please submit a new request.

VITA

Pramuditha L. Abhayawardhana, daughter of Rani and Sunil Abhayawardhana, was born in 1981 in Colombo, Sri Lanka. She received her school education from Visakha Vidyalaya, Colombo. She entered the University of Colombo, in 2002 and graduated in 2006 with her Bachelor of Science degree majoring in Pharmacy. She enrolled in the doctoral program of chemistry at Louisiana State University and joined the laboratory of Prof. Luigi G. Marzilli in January 2009. In addition to the work presented in this dissertation, she has co-authored three more publications involving her work in Marzilli research group. Pramuditha was the recipient of the Kiran Allam international award awarded by the Department of Chemistry for outstanding research and teaching in chemistry in 2012, and a dissertation year fellowship award awarded by the Graduate School of Louisiana State University in 2015. She is a candidate for the degree of Doctor of Philosophy in the Fall Commencement of 2015.